FEB 7 1950

THE PHYSICAL REVIEW

VOLUME 77 *Second Series* NUMBER 3

FEBRUARY 1, 1950

Published for the

AMERICAN PHYSICAL SOCIETY

by the

AMERICAN INSTITUTE OF PHYSICS
Incorporated

LANCASTER, PA., AND NEW YORK, N. Y.

THE PHYSICAL REVIEW

A journal of experimental and theoretical physics established by E. L. Nichols in 1893

Published by the American Institute of Physics for the

AMERICAN PHYSICAL SOCIETY

Officers

President

F. W. LOOMIS
University of Illinois
Urbana, Illinois

Vice-President

I. I. RABI
Columbia University
New York, New York

Secretary

K. K. DARROW
Bell Telephone Laboratories
Office:
Columbia University
New York 27, New York

Treasurer

G. B. PEGRAM
Columbia University
New York 27, New York

Local Secretary for the Pacific Coast

J. KAPLAN
University of California at Los Angeles
Los Angeles, California

Managing Editor

JOHN T. TATE
University of Minnesota
Minneapolis, Minnesota

BOARD OF EDITORS

Editor

JOHN T. TATE

Assistant Editor

J. W. BUTTA

Associate Editors

H. A. BETHE — S. A. GOUDSMIT — W. E. LAMB, JR.
L. N. RIDENOUR — E. M. PURCELL — R. G. HERB
W. M. ZACHARIASEN — V. F. WEISSKOPF — J. BARDEEN

Manuscripts for publication should be submitted to John T. Tate, University of Minnesota, Minneapolis, Minnesota. The authors' institutions are requested to pay a publication charge of $8 per page which, if honored, entitles them to 100 free reprints. Instructions will be sent with galley proofs.

Proof and all correspondence concerning papers in the process of publication should be addressed to the Publication Manager, American Institute of Physics, 57 East 55 Street, New York 22, New York.

Subscription Price

United States and Canada.....$25.00
Elsewhere.....$27.00

Back Numbers[1]

Yearly back number rate when complete year is available:
Prior to 1949: $20.00
Thereafter: $27.00
Single copies: $2.00 each, prior to July, 1929;
$1.00 each, July, 1929–December, 1941;
$2.00 each, January, 1942–December, 1946;
$1.00 each, January, 1947–December, 1948;
$1.25 each, thereafter.
General index, 1893–1920: $4.00.

Subscriptions and orders for back numbers should be addressed to Prince and Lemon Streets, Lancaster, Pennsylvania, or to the American Institute of Physics, 57 East 55 Street, New York 22, New York.

Changes of address in the case of members of the American Physical Society should be addressed to the Treasurer; in the case of other subscribers to the Circulation Manager, American Institute of Physics.

[1] For Series 1 inquire of Physics Department, Cornell University, Ithaca, New York.

The Physical Review is published semi-monthly at Prince and Lemon Streets, Lancaster, Pennsylvania.

Entered as second-class matter March 6, 1917, at the Post Office at Lancaster, Pennsylvania, under the Act of March 3, 1879.

Acceptance for mailing at special rate of postage provided for in paragraph 4, section 538, P. L. & R., authorized January 27, 1925.

THE
PHYSICAL REVIEW

A journal of experimental and theoretical physics established by E. L. Nichols in 1893

SECOND SERIES, VOL. 77, NO. 3 FEBRUARY 1, 1950

Neutron Diffraction in Liquid Sulfur, Lead, and Bismuth

OWEN CHAMBERLAIN*
Department of Physics, University of Chicago, and Argonne National Laboratory, Chicago, Illinois
(Received September 29, 1949)

A new type of neutron diffraction instrument has been developed to minimize the disadvantage of the broad energy spectrum of available slow neutron sources. It has been used to study the neutron diffraction patterns of the elements sulfur, lead, and bismuth in the liquid state. The patterns have been interpreted in terms of the distribution in separation distance of neighboring pairs of atoms. The results are in reasonable agreement with x-ray diffraction of others. In liquid sulfur each atom has two nearest neighbors at 2.1A. In liquid lead there are 12 nearest neighbors at 3.4A. In liquid bismuth an atom has on the average eight neighbors within 4A, but the nearest neighbors are not well separated from those at greater distance.

INTRODUCTION

WITH the aid of the relatively large slow neutron flux densities available from piles, it has become possible to use neutron diffraction in the study of the structure of liquids. Presented here are neutron diffraction studies of liquid sulfur, lead, and bismuth, along with a new type of diffraction instrument developed especially to facilitate such studies.

Diffraction studies of liquids with x-rays have been extensive. Following the early work of Hewlett[1] and Keesom and de Smedt,[2] the theoretical analysis of Zernike and Prins[3] gave the detailed connection between the diffraction pattern and the arrangement of molecules within the liquid. The application to liquid mercury by Debye and Menke[4] has been followed by many others. A comprehensive review of x-ray diffraction studies of liquid elements has been given by Gingrich.[5]

The phase and amplitude of slow neutron scattering by various atomic species have been investigated by Fermi and Marshall,[6] using interference effects in solids and gases. Neutron diffraction in polycrystalline materials has been studied by Wollan and Shull[7] (who give a convenient list of references to earlier papers). Results of these and similar investigations have now been used in the determination of structures of solid matter.[8]

At the present time neutron diffraction studies are more difficult than x-ray diffraction studies for two principal reasons. First, the flux density of slow neutrons available from piles is still much smaller than the effective flux density of x-rays from existing x-ray tubes. By effective flux density of x-rays, we mean the actual flux density of photons times the efficiency for counting with a Geiger counter. It is hoped that higher flux piles may rather soon make neutron diffraction more attractive in this respect. Second, the slow neutrons have a broad energy spectrum (being essentially in thermal equilibrium), whereas much of the intensity from an x-ray tube is concentrated in the characteristic line spectrum of the target material. The design of the instrument used here represents a long step toward the removal of this disadvantage for neutron diffraction.

Neutron diffraction becomes an especially attractive tool in certain special cases in which x-ray diffraction is difficult. Hydrogen, though very difficult to observe in x-ray diffraction, is not much easier to observe in neutron diffraction because a small coherent scattering is masked by a large incoherent scattering. However,

* Present address: Department of Physics, University of California, Berkeley, California.

[1] C. W. Hewlett, Phys. Rev. **19**, 266 (1922).
[2] W. H. Keesom and J. de Smedt, Proc. Amst. Akad. Sci. **25**, 118 (1922); **26**, 112 (1923).
[3] F. Zernike and J. Prins, Zeits. f. Physik **41**, 184 (1927).
[4] P. Debye and H. Menke, Physik. Zeits. **31**, 797 (1930).
[5] N. S. Gingrich, Rev. Mod. Phys. **15**, 90 (1943). See also R. Glocker, Eng. der Exact. Naturw. **22**, 186 (1949).
[6] E. Fermi and L. Marshall, Phys. Rev. **71**, 666 (1947).
[7] E. O. Wollan and C. G. Shull, Phys. Rev. **73**, 830 (1948).
[8] Shull, Wollan, Morton, and Davidson, Phys. Rev. **73**, 842 (1948).

deuterium gives neutron scattering, mostly coherent, quite comparable to other elements, and offers promise of much information from deuterated hydrogenous substaces. Also, some heavy elements have reasonably small neutron capture cross sections, while their x-ray absorption coefficients are uniformly high. Elements of low absorption have been chosen in the present experiments.

Another advantage of the use of neutrons is that the incoherent scattering, which is a perturbing effect and must be subtracted, is under some circumstances large for x-rays and only approximately calculable; it is usually small for neutrons and very nearly spherically symmetric.

The design of the instrument used here is based on the fact (long known in the theory of x-ray diffraction) that the differential scattering cross section of an assembly of atoms is dependent primarily on the magnitude of the change of momentum of the scattered particle or photon. Except for a constant factor, the magnitude of the change of momentum is the same as the scattering parameter $\sin\theta/\lambda$ commonly used in x-ray diffraction. (Here θ is half the angle of deflection of the scattered particle and λ the wave-length.) The present instrument achieves increased intensity over conventional diffraction apparatus by using a fairly wide range of wave-lengths from the incident beam. The angle of deflection 2θ is a function of the wave-length, such that good resolution in the scattering parameter $\sin\theta/\lambda$ is obtained.

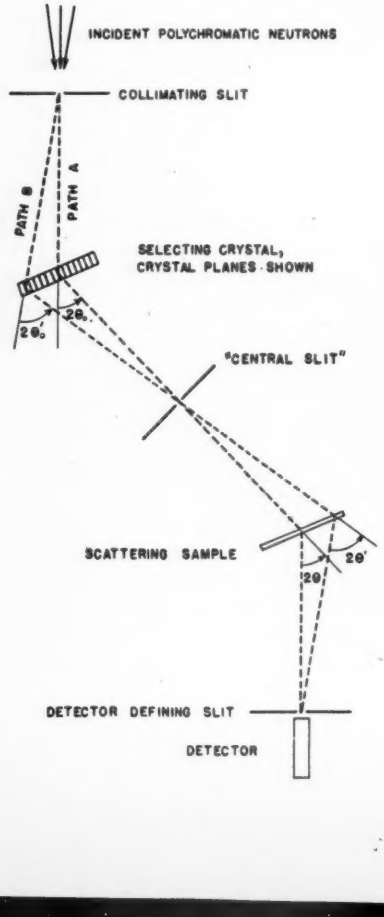

FIG. 1. Schematic diagram of the instrument for the special case $\sin\theta/\lambda = 1/2d$.

The results of the present experiments are to some extent summarized in Figs. 4–6 and 8–11. In liquid sulfur each sulfur atom has two nearest neighbors. In liquid lead each atom has 12 nearest neighbors. In liquid bismuth there is no well-defined group of atoms which can be called nearest neighbors to one atom, but there are eight atoms within a distance of 4.0A from one atom.

EXPERIMENTAL ARRANGEMENT

The new diffraction apparatus employed has some similarity to conventional diffraction apparatus, in that Bragg reflection from planes of a single crystal is used to select the proper neutrons from a polychromatic beam. It differs from the conventional apparatus in that the thermal neutron beam incident on the selecting crystal is not a parallel beam but a divergent beam collimated mostly by a single slit. The scattering sample is thin, but of large lateral dimensions. Neither θ nor λ separately, but only the quantity $\sin\theta/\lambda$ is well defined.

It has long been recognized that the factor by which the cross section of a single atom must be multiplied to obtain the cross section for a liquid is a function of $\sin\theta/\lambda$ only. This fact holds both for x-rays and neutrons; and in the latter case the scattering by a single nucleus is spherically symmetric.

Figure 1 shows a special case in which the angle of deflection at the crystal is equal to the angle of deflection at the scattering sample, so $\theta_0=\theta$. Due to the symmetry around the central slit, this is true for an arbitrary ray through the instrument, i.e., $\theta_0'=\theta'$. Applying the condition for first-order Bragg reflection $\lambda=2d\sin\theta, \sin\theta/\lambda=\sin\theta'/\lambda'=1/2d$. We describe this fact by saying that for all paths $\sin\theta/\lambda$ is the same. In a conventional type diffraction apparatus, all usable neutron paths would be very close to the central ray (path A). In this instrument we gain intensity by using other paths as well, such as the path B.

In the limit of a perfect crystal in the form of a thin slab, all neutrons which pass through the first (collimating) slit and are Bragg-reflected will pass through the central slit. There is thus a focusing of the Bragg reflected neutrons here. The existence of this focus point is important to the success of the instrument, for a rather good shield can be placed here to eliminate nearly all but the Bragg reflected neutrons.

Figure 2 shows the apparatus as used for scattering at another (larger) value of $\sin\theta/\lambda$. The collimating slit, the selecting crystal, and the first focus slit are unchanged in position, though they are drawn to a more realistic scale. The scattering sample is moved farther from the central slit and its orientation is changed. For neutrons which pass along the central ray of the instrument, we have the Bragg condition for first-order reflection, $\lambda=2d\sin\theta_0$, so

$$\sin\theta/\lambda=(\sin\theta/\sin\theta_0)(1/2d). \qquad (1)$$

Neutrons which pass through the instrument along

TABLE I. Spectrometer settings (when Bragg angle at crystal = 15°).

2θ (counter angle) in degrees	$\frac{\sin\theta}{\lambda}$	γ	φ in degrees
10	0.062	0 (−0.33)	0 (···)
12½	0.077	0 (−0.17)	0 (···)
15	0.093	0	undetermined
17½	0.108	0.18	5
20	0.124	0.35	7½
23⅓	0.144	0.55	10½
26⅔	0.164	0.80	13
30	0.184	1.00	15
33⅓	0.204	1.22	16½
36⅔	0.223	1.45	18
40	0.243	1.67	20
43⅓	0.262	1.89	22½
46⅔	0.281	2.10	26
50	0.300	2.23	30½
53⅓	0.318	2.33	35
56⅔	0.336	2.37	40
60	0.355	2.38	46
63⅓	0.373	2.39	51
66⅔	0.390	2.39	55
70	0.407	2.38	58½
73⅓	0.424	2.33	62
95	0.522	2.33 (···)	62 (···)
117	0.605	2.33 (···)	62 (···)

other rays may be made to have very accurately the same value of $\sin\theta/\lambda$ because there are two parameters of the instrument which may still be adjusted, φ and γ, defined in Fig. 2. These parameters are adjusted to the two conditions

$$(d\chi/d\alpha)_{\alpha=0}=0 \qquad (2a)$$

and

$$(d^2\chi/d\alpha^2)_{\alpha=0}=0, \qquad (2b)$$

where $\chi=\sin\theta/\lambda$.

Since the analytic forms of the expressions in Eqs. (2) are quite cumbersome, these equations are not solved analytically. Instead, a ray-tracing technique is used. The geometry is so adjusted that the central ray and the extreme ray on each side have the same value of the scattering parameter. Through most of the range of the instrument χ is then determined to one percent—thus better than the spread due to the slit widths. The values used in setting the apparatus are shown in Table I. Where the calculated values are different from the values used, they are shown in parentheses.

When γ is small, the scattering sample is close to the central slit and φ is essentially undetermined, though the resolution remains good in these cases. When solution of Eqs. (2) gives γ negative, the sample should be on the other side of the central slit—i.e., should have a convergent beam incident upon it. Attempts to realize this situation with cadmium vanes gave poor results due to large backgrounds from scattering off the vanes and incoherent scattering by the selecting crystal. Best practice was found to be to accept slightly poorer resolution by using $\gamma=0$.

The new apparatus described here is useful only when the source has a spectrum wide compared to the desired resolution, as the nearly Maxwellian distribution of slow neutrons from a graphite moderator. The apparatus would be useful for x-ray diffraction only in cases where such high resolution was sought that the characteristic x-ray line source appeared broad by comparison.

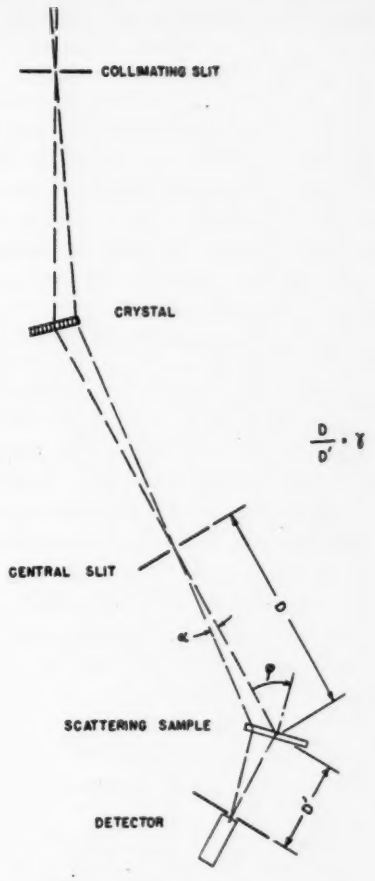

FIG. 2. Schematic diagram showing a typical setting of the instrument.

Figure 3 is a scale drawing of the apparatus. The collimating slit, 2 in. high, ⅞ in. wide, is placed within the shield of the heavy-water pile of the Argonne National Laboratory, at the graphite thermal column. The selecting crystal, placed just outside the shield, is actually four natural crystals of calcium fluoride arranged on a supporting stand for individual adjustment. The single crystals are ½ in. thick. The usable crystal area is 6 by 6 in. in all. The crystals are cut along the natural cube faces and arranged for reflection from the 200 planes. Lower intensity was given by other crystals tried, including natural calcite, artificially crystallized NaCl, PbS, mica (variety unknown), and another natural calcium fluoride crystal.

For the central ray the Bragg angle at the crystal is 15°, this being essentially the largest angle for which second-order reflection is negligible. (Measurement at 21° showed prohibitive (30 percent) second-order content.)

The central slit is 2 in. high, ¾ in. wide, surrounded on all sides by an extensive cadmium shield 0.030 in.

thick. The scattering sample and neutron counter are mounted on a rolling table which can be moved to adjust the distance D, the motion being parallel to the central ray incident on the scattering sample. The scattering sample can be rotated about a vertical axis and set at will to any desired value of φ. The neutron counter is mounted on an arm for rotation around the same vertical axis on the rolling table, the sample to counter distance D' being constant.

The usable part of the scattering sample is 6 in. high, 10 in. wide, thickness depending on the scattering material and adjusted for approximately 10 percent scattering in the sample for neutron beam incident normally. Liquid scattering materials are contained in "cells" with thin metal walls. Of several varieties of cell used, only the best will be described. The two sides of large area, through which the beam must pass, are of 0.040-in. aluminum (24S) sheet, welded to an aluminum frame on the side and bottom edges. Supports against bulging consist of 0.19-inch diameter aluminum rods which penetrate the liquid and are riveted at each end to the 0.040-in. sheet. These rods are placed through the sample on a 2-in. square lattice. Electric heaters are attached at side and bottom edges. Thermal insulation consists of asbestos around the heaters and 0.001-in. aluminum foil over the large sides. The aluminum foil acts as a radiation shield and to enclose a $\frac{1}{2}$-in. layer of air around the sample. The greatest temperature difference between two parts of the liquid sample is 10°C.

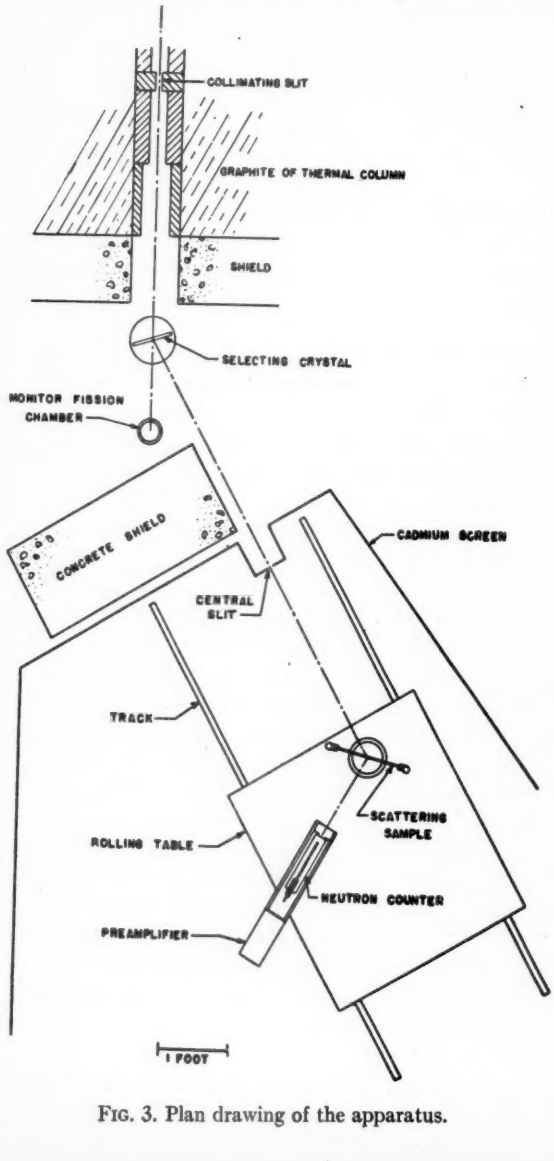

FIG. 3. Plan drawing of the apparatus.

The scattering by the cell is small (0.015) compared to the scattering by the material within the cell (0.10). Unfortunately, liquid bismuth dissolves some aluminum, approximately one percent by weight (seven percent by number of atoms).

The neutron detector is a pulse ionization chamber with pulse amplifier and scaling circuit. The chamber is of cylindrical construction, outside diameter 2 in., central electrode diameter 0.25 in., active length 8 in., filled with 1 atmos. boron trifluoride enriched in B^{10}. Neutrons are incident along the axis of symmetry. The operating voltage is 2000 v and the effective deadtime is 30 μsec. As is to be expected, no true plateau of counting rate *versus* amplifier gain is observed. However, the counting rate is quite insensitive to gain change in the operating region.

Shielding consists mainly of 0.03-in. cadmium sheet or 1-g/cm^2 boron carbide. Boron carbide is used around all sides of the pulse ion chamber except the front, where a cadmium defining slit is used. The central slit is of cadmium, surrounded by an extensive cadmium shield. Except for the scattering sample, the pulse ion chamber looks only at this cadmium shield. This condition is quite necessary to reduce the background from stray neutrons in the pile room.

For two reasons, the instrument must be calibrated before relative cross sections can be determined. First, the effective counting solid angle of the counter is not strictly a constant because different-sized areas of the scatterer are used at different settings of the instrument. Second, at some settings an additional cadmium diaphragm with fairly large aperture is placed in front of the scattering sample to make absolutely certain that no slow neutrons are scattered by the edges of the sample where there are heaters, supporting frame, etc. Both of these contingencies influence the counting rate in ways not easily calculable.

Calibration is effected by measuring the counting rates of one sample in both a wide beam instrument and a narrow beam instrument. Here the primary apparatus already described is referred to as the "wide beam instrument" whereas "narrow beam instrument" applies to the same apparatus when additional diaphragms with small apertures are added to restrict the beam to a narrow pencil surrounding the central ray. The narrow beam instrument, then, is a conventional diffraction apparatus in which the crystal reflection forms a narrow beam of well-defined wave-length λ and only

those neutrons count which are deflected through a well-defined angle 2θ at the scattering sample. Because the narrow beam instrument utilizes only a small area of the scattering sample, results obtained with it are easily interpretable.

In the comparison between narrow and wide beam instruments, a rather thick sample of Plexiglas has been used as scatterer. Its important properties are: (a) It is thick enough (transmission 0.5) to give large scattered intensity and (b) most of the scattering is due to hydrogen, so incoherent scattering predominates and one may be sure the scattering cross section is a slowly varying function of $\sin\theta/\lambda$. By using this sample one obtains a counting rate even in the narrow beam instrument sufficient to get good statistical accuracy.

The present instrument is thought to give about six times the intensity of the comparable narrow beam instrument. In instruments of higher resolution, the advantage of the new type instrument should become even greater.

For the determination of the scattered intensity at one angle, counting rates are measured when the sample position is occupied by (a) nothing (except air), (b) an empty cell, (c) an identical cell containing the scattering material (such as liquid sulfur), or (d) a piece of Plexiglas of standard thickness. For each case the counting rate is measured both with and without a cadmium shutter across the central slit. The inclusion of the standard thickness Plexiglas in each run affords some freedom from errors due to slight changes in total neutron flux, changes of the selecting crystal, long term changes in counter efficiency.

The counting rates for a typical sample and average pile level are as follows. Cadmium shutter open: no scatterer, 85 counts/min.; empty cell, 150 counts/min.; full cell (liquid lead), 720 counts/min.; Plexiglas, 2600 counts/min. Cadmium shutter closed; all counting rates between 60 and 120 counts/min. The full cell with shutter open is counted for 8 min., others 4 min. each, which gives the value of the lead scattering relative to the Plexiglass scattering to three percent.

RESULTS

The direct outcome of the measurements is a determination of the differential scattering cross sections of the materials studied as functions of $\sin\theta/\lambda$. More correctly, the differential scattering cross sections relative to the total cross sections are determined. The method of handling the data is outlined in this section.

Fast neutrons, which penetrate cadmium, are eliminated by using only the difference in counting rate, cadmium shutter open and closed. The correction for scattering from air surrounding the sample is accomplished by simple subtraction of the count obtained with nothing in the sample position. (This is adequate since the correction is small.) Correction for the variable solid angle of the counter is accomplished by multiplying the counts by the ratio of Plexiglas counts in narrow and wide beam instruments.

Since multiply scattered neutrons contribute a considerable fraction of the counting rate of the full cell, the counting rate is not a strictly linear function of the sample thickness. A correction for multiply scattered neutrons is therefore applied. It is applied separately to full cell and empty cell counting rates.

The counting rate of any sample is considered as

$$S=S'+S'', \tag{3}$$

where S' is the counting rate due to singly scattered neutrons and S'' is that due to multiply scattered neutrons. S' contains essentially the scattering in which we are interested. S'' is approximately calculable and is a smoothly varying function of θ. S'' averages about 20 percent of S'.

For the purpose of calculating S'', the samples are treated as homogeneous—with the material of the cell wall evenly distributed through the sample, and the atoms scattering isotropically. Furthermore, the approximation is used in which the scattered neutrons are considered as originating from the central plane of the sample. We omit details of the calculation.

The properties of the scattering material can conveniently be summarized in the quantity

$$s\equiv[\sigma_T]^{-1}(d\sigma/d\omega). \tag{4}$$

Here $d\sigma/d\omega$ is the cross section (per atom) for scattering into unit solid angle in a particular direction (the differential scattering cross section) and σ_T is the total cross section (per atom, absorption plus scattering). The relation between s and the counting rate due to singly scattered neutrons (S') may be given in the form

$$\eta s=(S'\cos\varphi/\Phi\Omega)\{\eta\sec[2\theta-\varphi]-\eta\sec\varphi\}/\{\exp(\eta\sec\varphi)-\exp(\eta\sec[2\theta-\varphi])\}, \tag{5}$$

where η is the negative logarithm of the transmission of the sample, Φ is the flux of neutrons through the central slit, and Ω is the effective counting solid angle of the neutron counter. From this we calculate the quantity (ηs) for full cell and empty cell.

Denoting the full cell by F, the empty cell by E, and the material of interest within the full cell by M, the scattering properties of M are obtained from

$$(\eta s)_M=(\eta s)_F-(\eta s)_E \tag{6}$$

and

$$(d\sigma/d\omega)_M=(\eta s)_M/N_M, \tag{7}$$

in which N_M is the number of atoms per cm^2 in the sample of scattering material and $(d\sigma/d\omega)_M$ is the differential scattering cross section per atom for the material of interest.

The differential scattering cross sections for (liquid) sulfur, lead, and bismuth are shown in Figs. 4–6. The observed differential scattering cross section of powdered graphite is shown in Fig. 7, as an indication that the resolution of the instrument is adequate for the present

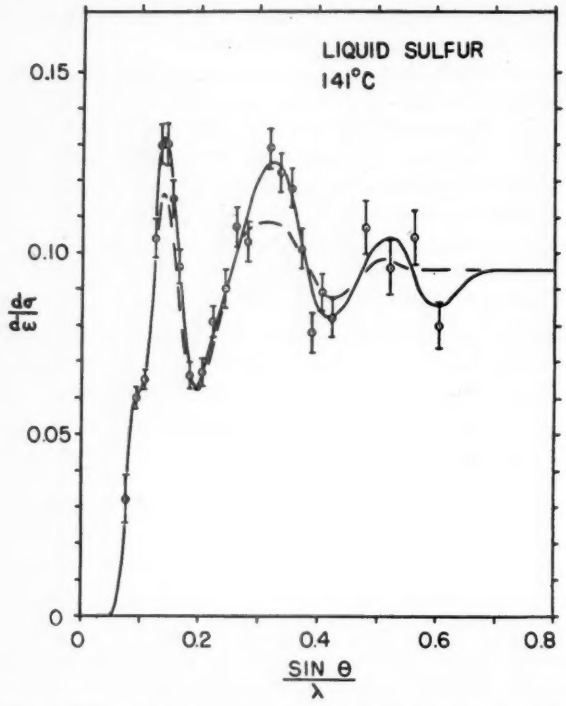

FIG. 4. Differential scattering cross section in barns per steradian as a function of the scattering parameter. The solid curve and the dashed curve show the results of two runs. Experimental points are shown for the solid curve only.

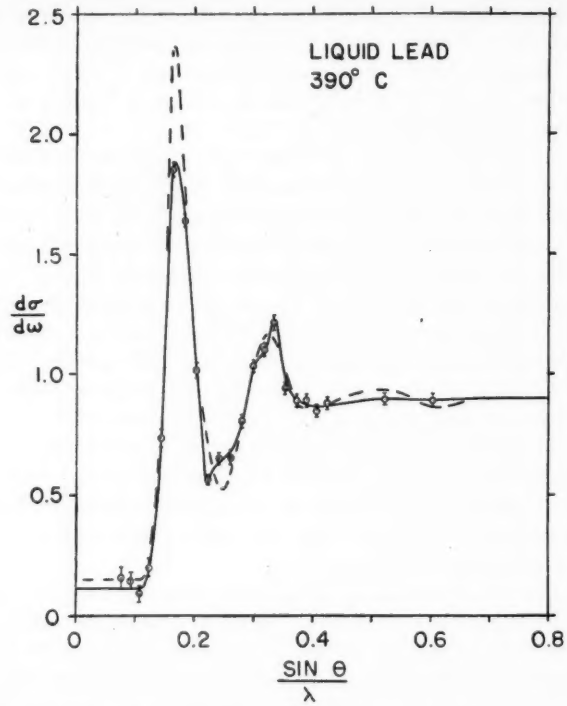

FIG. 5. Differential scattering cross section *vs.* scattering parameter. Each curve is the result of one run.

purpose. The observed resolution is in good agreement with that calculated from the geometry of the instrument.

Since the differential scattering cross section is a function only of $\sin\theta/\lambda$ the (total) scattering cross sections may be calculated. The two runs made with each substance give very closely the same total scattering cross sections. These results are shown in Fig. 8.

INTERPRETATION

Attempts to calculate the effects of thermal motion in the liquid on the scattering process have failed. We believe there should occur scattering from aggregates smaller than the typical aggregate involved in the elastic scattering. These scattering events should have a pattern with broader maxima than those of the elastic scattering pattern. In the limit in which one atom scatters independently a completely diffuse pattern will result. Presumably all except the independent scattering from single atoms will be hard to distinguish experimentally from the elastic scattering which already shows broad maxima due to the smallness of the distance over which there is coherence of positions of atoms. We believe these considerations to be in qualitative accord with the scattering phenomena in solids[9] and with a liquid model without potential energy (a closely packed gas of hard spheres).

The average atomic density ρ at distance R from any atom is calculated by the standard method of Zernike and Prins.[3] This is essentially the Born approximation in which the incident wave at any nucleus is taken as a plane wave to which neighboring nuclei contribute nothing. It may be remarked that coherence of position of atoms in the liquid extends only for a few atomic diameters and the amplitude of the wave scattered by one atom is, at a neighboring nucleus, smaller than the incident wave amplitude by a factor of 10^4. This guarantees the validity of the approximation.

The relation similar to that worked out by Zernike and Prins for x-rays between the distribution function (giving the average atomic density at various distances from one atom) and the differential scattering cross section may easily be derived for the case of neutron diffraction. The differential scattering cross section of an atom for neutrons is a constant independent of angle and nearly independent of wave-length (which is not the case for x-ray scattering). The scattered waves from a group of atoms may be added at great distance from the group. The absolute square of the resultant amplitude gives the scattering cross section for the group which contains a term for each pair of atoms in the group. Since the structure of the liquid is assumed to be repeated many times with random orientation, this is averaged over all orientations of the arrangement. This result depends only on the distance between pairs of atoms in the group. With the introduction of the distribution function, the sum over pairs of atoms may be transformed to an integral. (For details of this

[9] See W. H. Zachariasen, Phys. Rev. **57**, 597 (1940).

method as applied to x-ray scattering, see Gingrich, reference 5.)

The final result may be written

$$\chi\left(\frac{4\pi}{\sigma_s}\frac{d\sigma}{d\omega}-1\right)=\int_0^\infty dRR(\rho-\rho_0)\sin(4\pi\chi R), \quad (8)$$

where $\chi=\sin\theta/\lambda$. ρ_0 is the over-all average density of atoms in the liquid, ρ is the average density of atoms at a distance R from one atom, and σ_s is the scattering cross section of a (bound) atom. Notice this says that $\chi[(4\pi/\sigma_s)(d\sigma/d\omega)-1]$, which is a function of χ only, is essentially the Fourier transform of $R(\rho(R)-\rho_0)$ which is a function of R. The conjugate relation is then

$$R(\rho-\rho_0)=8\int_0^\infty d\chi\chi\left(\frac{4\pi}{\sigma_s}\frac{d\sigma}{d\omega}-1\right)\sin(4\pi\chi R). \quad (9)$$

These relations are derived on the assumption that all atoms of the liquid are identical, and that the spin of the neutron is unaffected in the scattering process. A somewhat more general derivation may take account of isotope and spin effects. The resulting relations are the same as those above, with the coherent scattering cross sections in place of total scattering cross sections.

Coherent differential scattering cross sections are obtained here by subtraction of the observed incoherent scattering from the total scattering. The incoherent cross section is taken to be that observed at very small angles, since the incoherent scattering is (very nearly) isotropic. In the present experiment slightly more incoherent scattering is observed in liquid lead and liquid bismuth than that reported by Fermi and Marshall in solid samples, presumably due to a small second-order content of the Bragg reflected beam used in the present experiment. Second-order reflection in the crystal gives scattered intensity at half the proper value of $\sin\theta/\lambda$. The difference in incoherent scattering observed here and that reported by Fermi and Marshall is considered negligible, both from the standpoint of experimental result and from the standpoint of the effect on the calculated distribution in R. In liquid sulfur the incoherent scattering could not be determined because measurements could not be made at sufficiently small values of $\sin\theta/\lambda$. No correction for incoherent scattering was made in this case.

Before proceeding with the Fourier analysis for the distribution in R, it is important to be sure of the normalization of the results for $(d\sigma/d\omega)/\sigma_s$. This quantity, if calculated directly, depends upon the factor $\sigma_T/\sigma_s\eta\Phi\Omega$, in which neither η nor $\Phi\Omega$ are known as accurately as the counting rates. An alternative procedure is used to establish proper normalization of $d\sigma/d\omega$, similar to the method common in x-ray diffraction. It is assumed that the density of atoms at distance R from one atom approaches zero as R approaches zero. The relations of Zernike and Prins then guarantee that

$$\int_0^\infty d\chi\chi^2\left(\frac{4\pi}{\sigma_s}\frac{d\sigma}{d\omega}-1\right)=-\frac{\rho_0}{32\pi}, \quad (10)$$

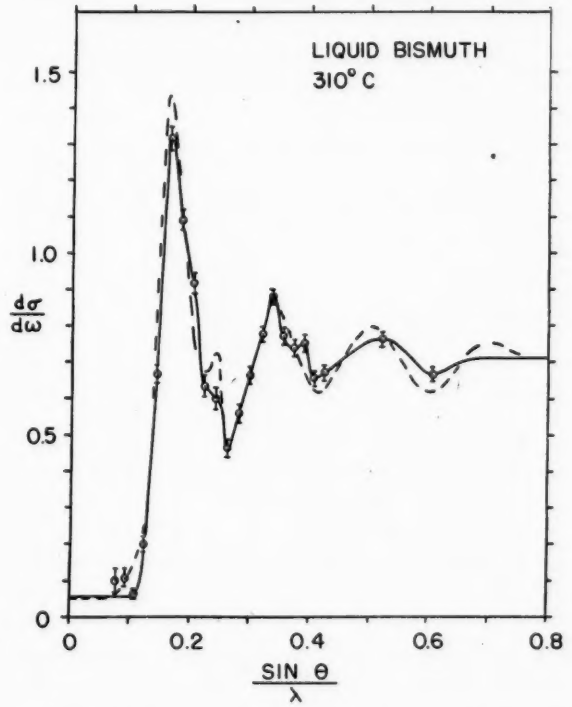

FIG. 6. Differential scattering cross section *vs.* scattering parameter. Each curve is the result of one run.

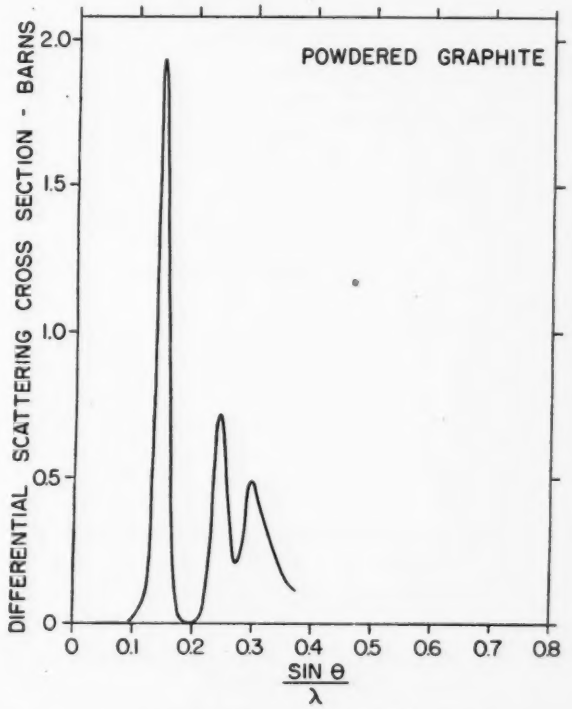

FIG. 7. Apparent differential scattering cross section of powdered graphite, used to indicate the resolution of the instrument.

where ρ_0 is the average numerical atomic density. Use of this relation establishes the normalization. It may be remarked that the less accurate but more straightforward normalization using η and $\Phi\Omega$ gives the same results to within a few percent.

Evaluation of the Fourier transform and hence of $\rho(R)$ is accomplished by the method of trigonometric interpolation, described in detail by Danielson and Lanczos.[10] Curves are drawn of the coherent differential scattering cross section *vs.* χ from which 32 values equally spaced (in χ) are taken. From these 32 points an equal number of values of the Fourier transform are obtained. Since it is difficult to specify the probable error of the values of the Fourier transform, the data for each material are divided into two groups corresponding to two runs and $\rho(R)$ separately evaluated. Only those features which both determinations have in common may be considered significant.

Results are shown in Figs. 9–11. The ordinate is $4\pi R^2\rho$; the abscissa is R, the distance from one atom. Also shown for comparison is $4\pi R^2\rho_0$.

Figure 9 for liquid sulfur requires special comment in that in one run the differential scattering cross section was not extended as far to large values of χ as the other. As a result, this run (shown with crosses in Fig. 9) gives poorer resolution in R, and less definite deviations from the curve representing the average density. The other curve (shown with circles) should be given greater weight, and agrees well with results of Gingrich.[11] Each atom has two nearest neighbors at about 2.1A with few or no other atoms at 2.6A. The density is greater than average from 4A to 5A and slightly less than average at 6A from one atom. This distribution function is consistent with, but does not prove, the existence of closed chains of eight atoms.

Figure 10 is a similar plot for liquid lead. The first maximum at 3.4A represents 12($\pm$1) nearest neighbors, not completely separated from other lead atoms. The curve shows a deficiency of atoms at 4.7A and 8A and an excess at 6.4A. Glocker and Hendus,[12] who have studied the x-ray diffraction of liquid lead, find eight neighbors with four more only slightly farther away. Only if the data were extended to much larger values of χ, could the present work be expected to resolve the two groups. Otherwise, the agreement with Glocker and Hendus is very close. Although the distribution function does not fit easily any picture of a loosely packed but solid-like structure, the hexagonal close-packed structure comes closest of any to fitting the observed distribution for lead.

Figure 11 shows the same data for liquid bismuth. In bismuth it is hard to count the nearest neighbors because they are not readily distinguishable from the atoms at greater distance. To 4A there are eight atoms. Significant excesses are found at 3.2A and 6.7A, and

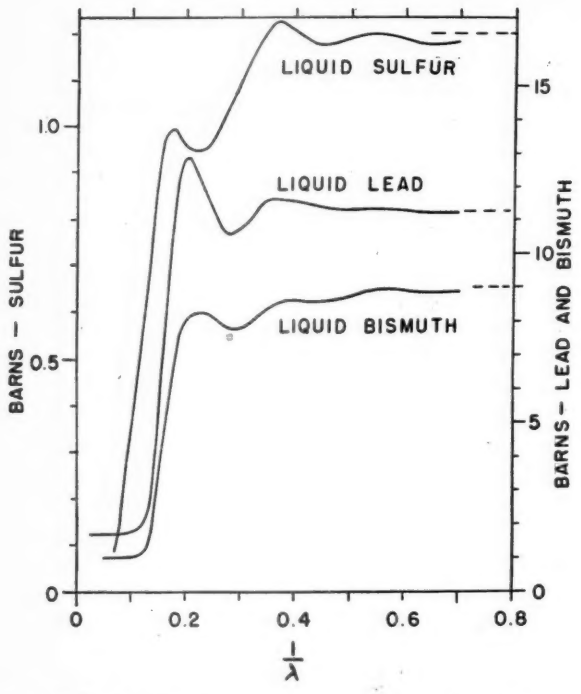

FIG. 8. Total scattering cross sections as functions of the inverse wave-length.

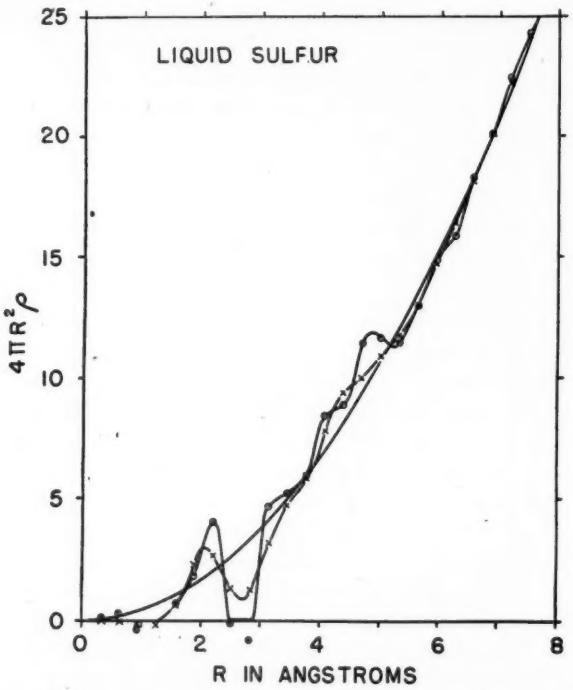

FIG. 9. The number of atoms per unit distance from one atom as a function of the distance. Results from two runs are shown.

[10] G. C. Danielson and C. Lanczos, J. Franklin Inst. **233**, 365 (1942); **233**, 435 (1942).

[11] N. S. Gingrich, J. Chem. Phys. **8**, 29 (1940).

[12] R. Glocker and H. Hendus, Ann. d. Physik **43**, 513 (1943).

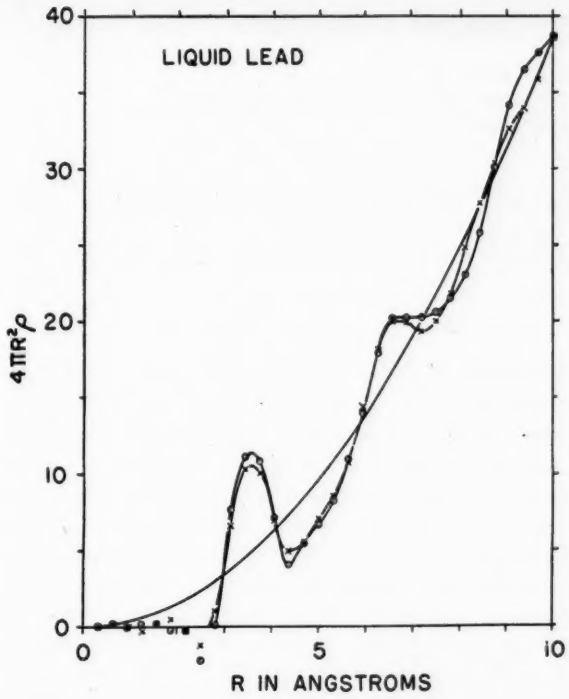

FIG. 10. The number of atoms per unit distance from one atom as a function of the distance. Results from two runs are shown. .

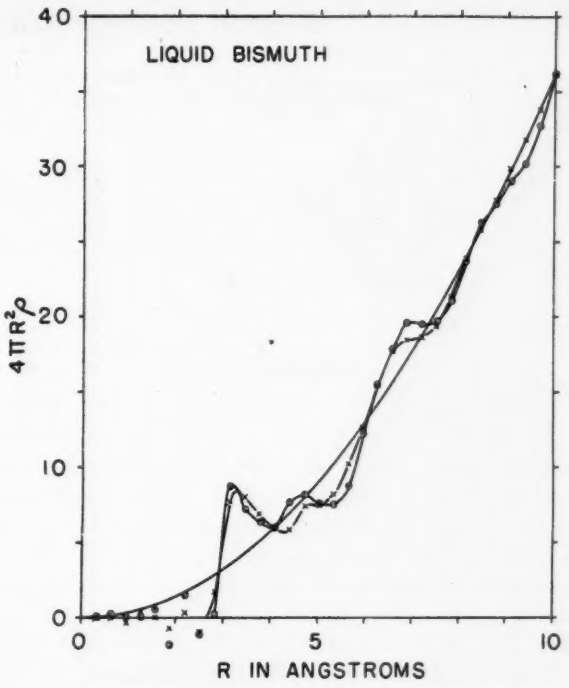

FIG. 11. The number of atoms per unit distance from one atom as a function of the distance. Results from two runs are shown.

deficiencies at 5.3A and 7.7A.† The liquid bismuth structure shows little similarity to simple solid structures.

The variation with energy of the total cross section of liquid lead given here may be compared with that given by Havens, Rabi, and Rainwater.[13] The results given here show less decrease in cross section with increasing wave-length, however, the error in the present result does not preclude the energy dependence given by Havens, Rabi, and Rainwater. One can only say that the two results are consistent.

The author wishes to express his gratitude to Professor E. Fermi for suggesting this subject for study and for advice during the investigation. Dr. A. Wattenberg of the Argonne National Laboratory has been of great assistance in making suggestions, in making available to him much of the equipment used, and in taking some of the data. The very essential aluminum fabrication and much of the construction of the instrument has been done by Mr. J. Dalman of the Argonne National Laboratory Staff.

† *Note added in proof:* The data of Fig. 11 are in close agreement with those of Hendus who has studied liquid bismuth using x-ray diffraction; H. Hendus, Zeits. f. Naturforschung **2A**, 505 (1947).

[13] Havens, Rabi, and Rainwater, Phys. Rev. **72**, 634 (1947).

Neutron Deficient Radioactive Isotopes of Rhenium

GEOFFREY WILKINSON AND HARRY G. HICKS*
Radiation Laboratory and Department of Chemistry, University of California, Berkeley, California
(Received August 16, 1949)

A study has been made of neutron deficient radioactive isotopes of rhenium. Using the 60-inch Crocker Laboratory cyclotron, bombardments have been made of tantalum with 38, 30, and 19 Mev α-particles, of wolfram with 10-Mev protons, and of rhenium with fast neutrons.

The radiation characteristics of four new radioactive isotopes and of the previously known 50-day Re^{184} isotope have been studied.

I. EXPERIMENTAL

TANTALUM was bombarded on the 60-inch Crocker Laboratory cyclotron as the spectroscopically pure metal foil. After bombardment, the foil was dissolved in hydrofluoric acid, with the addition of the minimum of strong nitric acid. Rhenium carrier was then added, and hydrogen sulfide passed into the boiling solution for fifteen minutes. The rhenium sulfide was dissolved in a solution of hydrogen peroxide and sodium hydroxide, which was then "scavenged" by ferric hydroxide precipitations. The rhenium was then reprecipitated from strong hydrochloric acid solution as the sulfide. While this procedure has been found to give radiochemically pure rhenium, the following additional chemistry was performed in early bombardments: Rhenium was distilled as the volatile chloride or oxide and recovered from the distillate by precipitation as sulfide. The latter was dissolved in a solution of hydrogen peroxide and sodium hydroxide and the rhenium then precipitated from the solution as nitron perrhenate by the well-known procedure. Similar chemical methods were used for neutron bombarded rhenium metal and for proton bombarded wolfram.

The radiation characteristics of radioactive isotopes have been obtained from aluminum and lead absorptions. The general procedure has been to measure the absorption of the gross radiations from a small thin source of active material mounted on thin mica in aluminum absorbers placed directly below the counter window; beryllium foil sufficient to remove electrons completely was then placed above the source and the aluminum absorption of soft electromagnetic radiation measured. A correction for reduction in intensity of the latter by the beryllium was made and a composite curve of total electromagnetic radiation constructed; subtraction of this curve from the measured absorption allowed resolution of electron radiations.

The ratios of the various components of the complex radiations usually observed in orbital electron capturing isotopes were obtained from lead and aluminum absorption data after correction for counting efficiencies, absorption in counter window and other absorbers, etc. The techniques and various assumptions made in interpreting results have been discussed in detail previously.[1,2]

II. RHENIUM ISOTOPES

Four new rhenium activities of half-lives 12.7 hours, 64.0 hours, ~240 days, and 2.2 days have been produced by α-particle bombardment of tantalum and have been allocated respectively to masses 182, 182, 183, and 184. The allocation of a previously reported 50-day rhenium

TABLE I. Production and properties of rhenium isotopes.

Isotope	Type of radiation	Half-life	Energy of radiation in Mev: Particles	Energy of radiation in Mev: γ-rays	Produced by
Re^{182}	K or I.T., e^-, γ	64.0±0.5 hours	0.11, 0,24(abs)	L, K x-rays 0.22, 1.5(abs)	Ta-α-3n W-p-n
Re^{182}	K or I.T., e^-, γ	12.7±0.2 hours	0.16, ~1(abs)	L, K x-rays 0.4, 1.6(abs)	Ta-α-3n W-p-n
Re^{183}	K, e^-, γ	~240 days	0.16(abs)	L, K x-rays 1.0 (abs)	Ta-α-2n W-p-n
Re^{184}	K, e^-, γ	50±2 days	0.2, ~0.7(abs)	L, K x-rays 0.17, 1.0(abs)	Ta-α-n W-p-n Re-n-2n
Re^{184}	K or I.T., e^-, γ	2.2±0.1 days	0.2, ~1(abs)	L, K x-rays	Ta-α-n W-p-n

* Present address: Chemical Research Section, General Electric Company, Hanford Engineer Works, Richland, Washington.
[1] G. Wilkinson, Phys. Rev. **75**, 1019 (1949).
[2] G. Wilkinson and H. G. Hicks, Phys. Rev. **75**, 1370 (1949).

activity to mass 184 has also been confirmed. The present data is summarized in Table I.

A. 64.0-hour Re^{182}; 12.7-hour Re^{182}

In the bombardment of tantalum with 38-Mev α-particles, two activities of half-lives 12.7 hours and 64.0 hours were observed, in addition to the longer-lived isotopes. The two short-lived isotopes were observed in the same ratio, but with greatly lowered intensities at 30 Mev, and not at all at 20-Mev bombarding energy. This observation is consistent with production by $\alpha,3n$ reaction. That the 12.7-hour activity cannot be Re^{181} produced by $\alpha,4n$ reaction is shown by the constancy of the 12.7-hour to 64-hour intensity ratio (Table II), and particularly by the production of the 12.7-hour activity by 9-Mev proton bombardment of tungsten where the $p,2n$ reaction does not occur. Further, the yield of the 140-day W^{181},[3] which would be produced as the daughter of any Re^{181} formed in an $\alpha,4n$ reaction of tantalum, agrees with that to be expected from the known deuteron contamination of the α-particle beam (<1 percent) and the measured cross section (5×10^{-2} barn) for the Ta-d-$2n$ reaction.

64.0±0.5-hour Re^{182}.

The gross decay of this activity, which comprises the bulk of the radioactivity in the 38-Mev α-particle bombardments of tantalum, has been followed through twelve half-lives to give a value of 64.0±0.5 hours for the half-life. The radiations consist of electrons, x-ray and hard γ-radiation, all of which have been separately followed and the same half-life obtained. The aluminum absorption of the radiations is shown in Fig. 1. The electromagnetic radiation contribution was obtained from aluminum absorption measurements after removal of the electrons by beryllium absorbers. Two electron components have been resolved, of ranges 16 mg/cm² (~110 kev), and 60 mg/cm² (0.24 Mev). The lead absorption curve shows complex hard electromagnetic radiation of half-thicknesses 137±5 mg/cm² (62 kev), 550 mg/cm² (220 kev) and 13.5 g/cm² lead (1.5 Mev) in addition to the soft radiation half-thickness 21±1 mg/cm² aluminum measured in the aluminum absorption; the two soft components agree well with the expected L and K x-radiation of wolfram or rhenium. No positrons were detected in a very active sample studied on a crude beta-ray spectrometer.

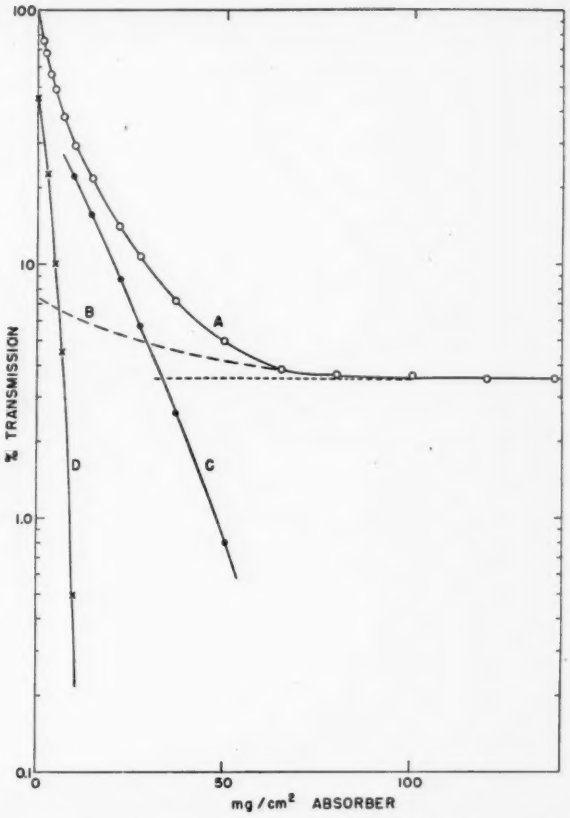

FIG. 1. Aluminum absorption of radiations of 64.0-hour Re^{182} activity (A). The contribution (B) of electromagnetic radiations was obtained from the aluminum absorption curve of this radiation measured after removal of electrons with a 100 mg/cm² beryllium foil; a correction was made for the absorption of the L x-rays in the beryllium and the curve B was constructed by addition of the intensity corrected L X-ray absorption curve to the K x-ray and γ-ray background. The electron lines C and D were resolved after subtraction of the electromagnetic contribution from the curve A.

From the aluminum absorption of the radiations from a "carrierless" rhenium sample mounted on very thin mica backing, the ratios of the two electrons and L x-radiations to the harder electromagnetic radiations were determined; corrections were made for absorption of the soft radiations in the air gap and counter window were made. The ratios of the hard electromagnetic radiations were obtained from the lead absorption. Counting efficiencies assumed were 2.5 percent for L x-radiation, 0.5 percent for K x-radiation and 220 kev γ-rays, and 1.5 percent for the 1.5 Mev γ-ray. Fluorescence yields of 0.8 and 0.5 were assumed for K and L x-rays, respectively. The following ratios were obtained:

110 kev e^- : 270 kev e^- : L x-rays : K x-rays : 220 kev γ : 1.5 Mev γ
= 1.4 : 0.2 : ~2 : 1 : 0.7 : 0.45 .

In view of the complex nature of the radiations it was thought that a shorter-lived lower isomer of the 64-hour activity might be present—possibly the 12.7-hour activity observed in the bombardments along with the 64-hour rhenium. An attempt was made to separate the nuclear isomers. A carrierless solution of rhenium was prepared by removal of tantalum from a bombarded target after solution in nitric and hydro-

[3] G. Wilkinson, Nature **160**, 864 (1947).

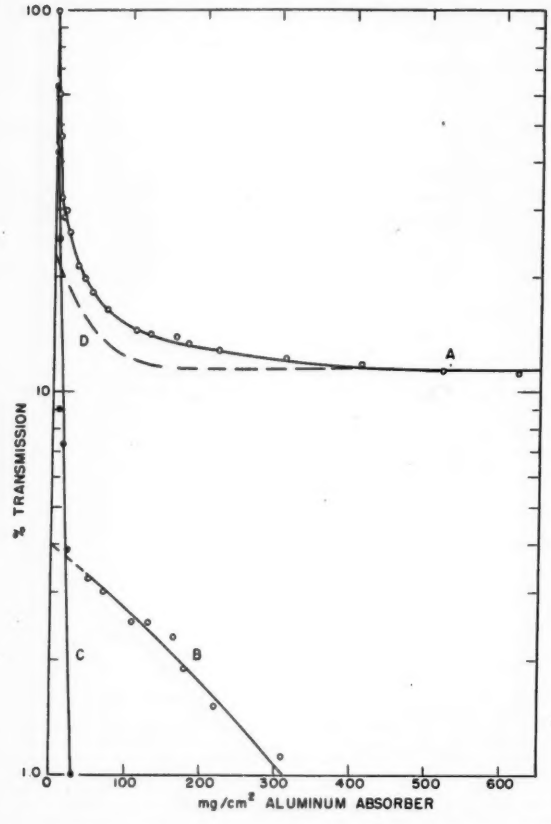

FIG. 2. Aluminum absorption (A) of 12.7-hour Re^{182} activity; electromagnetic contribution (D), ~1 Mev electrons (B), 0.16 Mev electron (C).

fluoric acids, by addition of boric acid followed by ammonia. The filtrate was evaporated with strong nitric acid and the solution, which should contain the radioactive rhenium as perrhenate, was diluted and neutralized with ammonia. If the 64-hour activity produced a lower isomeric daughter, part of the activity of the latter would be expected to remain in the III or IV oxidation states after decay of the parent. Any activity in the III or IV oxidation state could then be removed by scavenging the solution with ferric hydroxide. No evidence for such an isomer was observed, and it may be presumed that the very soft electrons of the 64-hour activity arise from conversion in γ-ray transitions from metastable levels in the daughter nucleus following orbital electron capture. It is somewhat difficult to decide what radiations constitute one disintegration, since x-rays can arise from conversion as well as from L or K orbital electron capture.

The relative yields for production of the 64-hour activity at the various energies of bombarding α-particles (Table II), can, however, be compared by taking the K x-rays as a reference.

12.7-hour Re^{182}

In bombardments of tantalum with α-particles, an activity of 12.7-hour half-life was found to accompany the 64-hour Re^{182}. The activity was found also in the bombardment of wolfram with 10-Mev protons. The decay of the gross and electromagnetic radiations from both Ta+α and W+p bombardments were followed through four and eight half-lives respectively to give a value of 12.7±0.2 hours for the half-life. The radiation characteristics were obtained by resolution of aluminum, beryllium and lead absorption curves, after the contribution of the longer-lived activities at the time of measurement had been subtracted. The aluminum (Fig. 2) and lead absorption curves for the 12.7-hour activity show the radiations to consist of electrons of ranges 35 mg/cm² (160 kev) and ~400 mg/cm² (~1 Mev), and electromagnetic radiations of half-thicknesses 20 mg/cm² aluminum (9.3 kev), 140 mg/cm² lead (62 kev), 3.0 g/cm² lead (400 kev) and 15 g/cm² (1.8 Mev). The two soft electromagnetic radiations correspond well with wolfram or rhenium L and K x-radiation. From the measurements, the following ratios were obtained:

160 kev e^- : ~1 Mev e^- : L x-rays : K x-rays : 0.4 Mev γ : 1.8 Mev γ
= 0.04 : 0.003 : 0.5 : 1 . 0.25 : 0.15 .

The isotope thus appears to decay by orbital electron capture, although partial decay by isomeric transition to the 64-hour activity is not excluded.

B. 50-day Re^{184}: ~240-day Re^{183}

After decay of the shorter lived periods in Ta+α and W+p bombardments, a complex long-lived activity remains in the rhenium fractions. This activity has been resolved into two components of half-lives 50±2 days and ~240 days, the measurements being carried through several half-lives. The 50-day activity has also been produced by fast neutron bombardment of rhenium. The radiation characteristics obtained by resolution of absorption (Fig. 3) and decay curves are the same in all bombardments, and agree well with those reported by other workers.[4] The approximate ratios of the various radiations of the 50-day activity are:

0.2 Mev e^- : 0.7 Mev e^- : L x-rays : K x-rays : ~1 Mev γ
0.35 : 0.004 : 0.35 : 1 : 0.2 .

In the rhenium fraction from Ta+α and W+p bombardments, an activity of ~240 days half-life has been observed after decay of the 50-day period. A pure intense source of this isotope was obtained from aged wolfram exit strips which had received deuterons,

[4] See G. T. Seaborg and I. Perlman, Rev. Mod. Phys. **20**, 585 (1948).

protons and α-particles from the 60-inch Crocker Laboratory cyclotron.

The aluminum absorption of an "infinitely thin" sample of the ~240-day activity mounted on thin mica and the lead absorption on a more active sample is shown in Fig. 4. The radiations consists of electrons, total range 35 mg/cm² (0.16 Mev) and electromagnetic radiations of half-thicknesses ~21 mg/cm² aluminum (9.4 kev), 140 mg/cm² lead (62 kev) and 10 g/cm² lead (1.0 Mev). On the crude beta-ray spectrograph only a single peak of very soft electrons of ~0.15 Mev energy were observed; no positrons were detected in a very active sample. The following ratios were obtained by the usual procedure.

0.16 Mev e^-: L x-rays: K x-rays: 1 Mev γ
= ~0.4 : ~1.1 : 1 : 0.1 .

The isotope thus appears to decay by orbital electron capture, with electrons arising from subsequent γ-ray transitions. The isotope has been allocated to mass 183 on the basis of yields in the α-particle bombardments.

C. 2.2-day Re^{184}

In the 19-Mev α-particle bombardment of tantalum, an activity of 2.2 days half-life has been observed in addition to the longer periods. The activity which was not observed in the higher energy bombardments because of the low yields and masking by other activities, is allocated to Re^{184} on the basis of its production by α,n reaction on tantalum. That the activity was not detected by other workers who studied the $n,2n$ reactions in rhenium and p,n reactions in wolfram is not surprising in view of the similarity in half-life to the 98.2-hour Re^{186} which would effectively mask the shorter half-life.

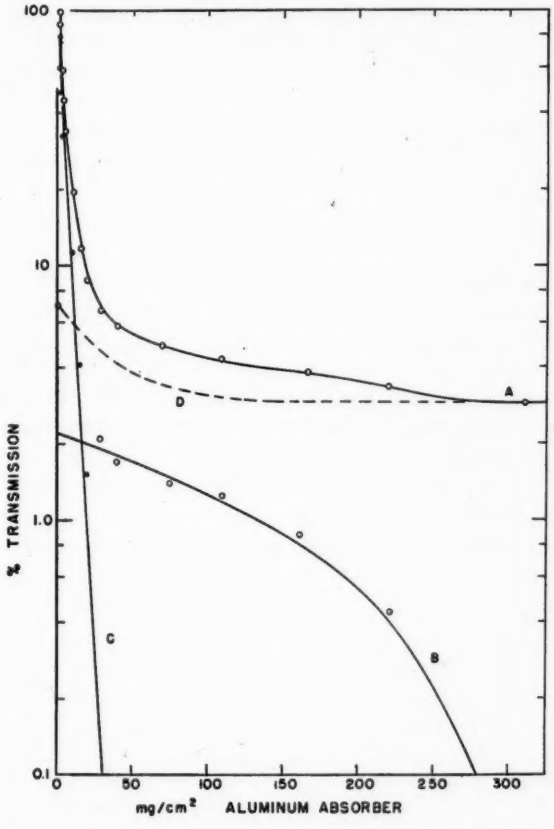

FIG. 3. Aluminum absorption (A) of 50-day Re^{184} activity; K electromagnetic radiation contribution (D), 0.7 Mev electron (B), and 0.2 Mev electron (C).

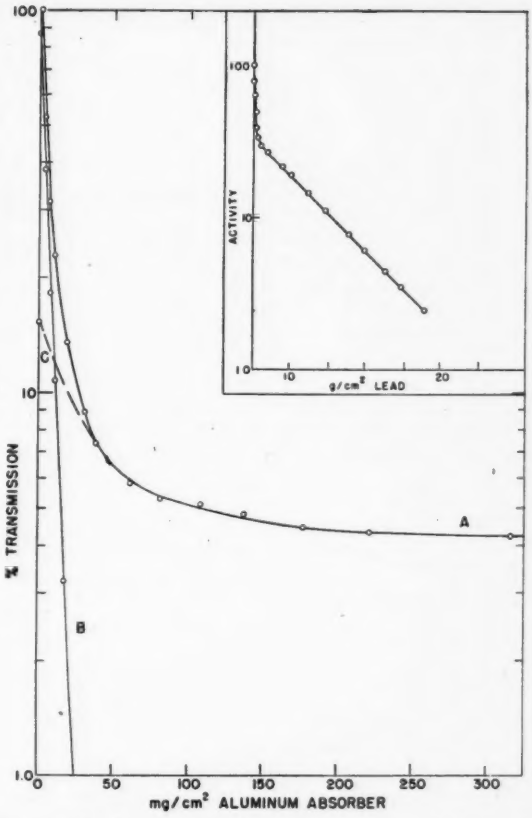

FIG. 4. Aluminum absorption curve (A) of ~240-day Re^{183} activity; curve C shows soft electromagnetic radiation contribution obtained after removal of electrons by beryllium. B is the electron contribution. The lead absorption curve shows K x-rays and 1.0 Mev γ-rays.

The half-life of the activity from Ta+α bombardment is 2.2±0.1 days measured through seven periods. The radiation characteristics were obtained by resolution of aluminum absorption (Fig. 5) and decay curves. The radiations consist of electrons of ranges 50 mg/cm² (0.2 Mev) and ~450 mg/cm² aluminum (1.1 Mev), soft electromagnetic radiation of half-thickness 21 mg/cm² (9.4 kev) and hard electromagnetic radiation. Lead absorptions were not taken because of insufficient activity. The following approximate ratios were calculated from the aluminum absorption:

0.2 Mev e^-: 1.1 Mev e^-: L x-rays: $K+\gamma$-rays
0.02 : 0.003 : 0.09 : 1 .

III. DISCUSSION

In order to clarify the status of the five rhenium activities, very active samples were prepared for study

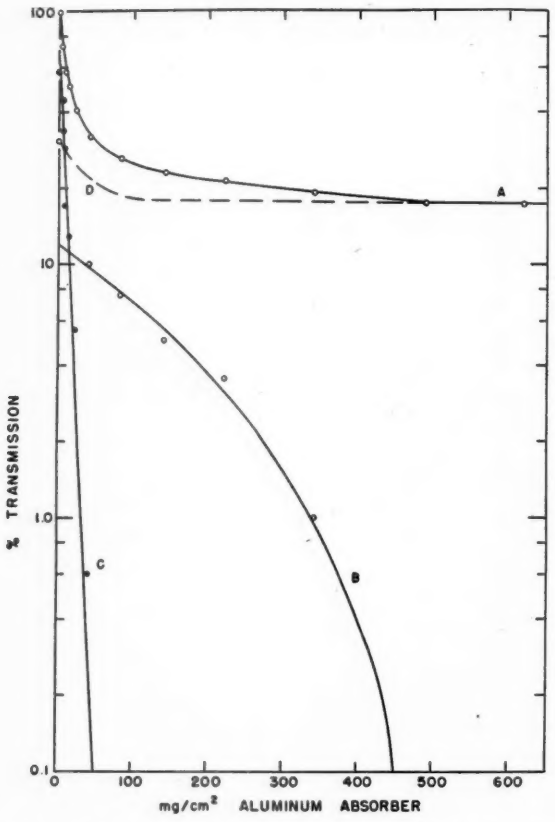

FIG. 5. Aluminum absorption curve (A) of 2.2-day Re^{184} activity; curve D gives the electromagnetic radiation contribution due to L and K x-rays and γ-rays; B and C are the electron contributions.

on a magnetic deflection beta-ray spectrometer, by Professor A. C. Helmholz and Mr. R. W. Hayward. The 64.0-hour and 12.7-hour activities appear to have identical radiations and since the isotopes have been allocated to Re^{182}, it is very probable that they are independent isomers decaying by orbital-electron capture to excited or metastable states of W^{182}. No evidence of beta-particle emission was found in any isotope and the suggestion of W. H. Sullivan[4] that the 50-day Re^{184} decays at least partially by beta-emission is not confirmed. The gamma-ray lines observed in the various isotopes are as follows:

64.0 hours, 12.7 hours: 0.110, 0.127, 0.250 (spec. conv.), 0.222, 0.346 (spec. and spec. conv.).

TABLE II. Relative yields of rhenium isotopes from α-particle bombardment of tantalum.

Activity	Energy of α-particles in Mev 38	30	19	Probable reaction	Mass assignment
12.7 hours	50	7	—	$\alpha,3n$	182
64.0 hours	100	14	—	$\alpha,3n$	182
~240 days	2	7	0.7	$\alpha,2n$	183
50 days	1	1	1	α,n	184
2.2 days	masked	masked	24	α,n	184

50 days: 0.043, 0.205, 0.285 (spec. conv.), 0.159 (spec. and spec. conv.).

~240 days: 0.081, 0.252 (spec. conv.).

2.2 days: 0.043 (spec. conv.), 0.159 (spec. and spec. conv.).

The mass assignments have been made according to measurements on cross sections for production of the isotopes by Ta-α,xn reactions at various bombarding energies. In view of the complex radiations in each case, it is impossible to determine even a rough disintegration scheme by the techniques used, and consequently, the measured K x-radiation is taken as a measure of one disintegration by orbital electron capture. In Table II, the various yields are given relative to those of the 50-day isotope which is unequivocally allocated to mass 184 on the basis of its production by Ta-α,n and Re-$n,2n$ reactions. The variations in yields of the isotopes at α-particle bombarding energies of 38, 30, and 19 Mev, then allow fairly certain mass allocations; the observed yield trends agree with those observed in bombardments of other elements.[2]

The present allocations are in agreement with the formation of the rhenium activities by proton bombardment of wolfram.

V. ACKNOWLEDGMENTS

We wish to thank Professor J. G. Hamilton, Messrs. T. Putnam and B. Rossi, and the crew of the 60-inch Crocker Laboratory cyclotron for their cooperation and assistance in making bombardments. We are grateful to Professor A. C. Helmholtz and Mr. R. W. Hayward for their helpful interest in making measurements on their beta-ray spectrometer. We are indebted to Professors G. T. Seaborg and I. Perlman for their continued encouragement and advice.

This work was performed under the auspices of the AEC.

On the Theory of Slow Neutron Scattering by Liquid Helium*

L. GOLDSTEIN, D. SWEENEY, AND M. GOLDSTEIN
Los Alamos Scientific Laboratory, Los Alamos, New Mexico
(Received September 12, 1949)

Using the extreme Bose-Einstein (B.E.) and Fermi-Dirac (F.D.) models of liquid He_4 and He_3, respectively, the theory of inelastic or incoherent slow neutron scattering by these liquids has been studied in this paper. It is, of course, fully realized that these liquids are not ideal symmetric or antisymmetric collections of atoms. Nevertheless, they might exhibit, in their behavior with respect to slow neutron scattering, such trends which could be interpreted as resulting from their respective statistical properties.

In liquid He_4, for neutrons of kinetic energy considerably larger than kT, k being Boltzmann's constant and T the liquid temperature, the incoherent differential cross section per atom is always larger, or at least equal to the free atom cross section exhibited by these atoms in the classical limit of vanishing degeneracy. At constant liquid temperatures, larger than the lambda-point temperature, i.e., in the He_4I region, the scattering has a maximum finite limit at vanishing scattering angles. This limit depends, at these small angles, on the liquid temperature only. The liquid cross section decreases with increasing scattering angle and tends asymptotically toward its free atom value. The latter is approached faster the larger the kinetic energy of the incident neutrons. At liquid temperatures near the lambda-point temperature, the vanishing small angle scattering cross section becomes very large and becomes some $N^{\frac{1}{3}}$ times the free atom value at the lambda-point.

In the liquid He_4II region the very small angle scattering cross section increases as Θ^{-2}, Θ denoting the scattering angle.

At constant scattering angles the scattering cross section varies as a function of the liquid temperature, in the following way. In the limit of high temperatures, or small degeneracy, the scattering cross section tends toward its asymptotic free atom value. As the liquid temperature decreases, or the degeneracy increases, the cross section increases. At the limit of the absolute zero temperature, perfect degeneracy, the distribution of the atoms being narrowed down to practically a single state, the scattering cross section is also classical, the fundamental symmetrical correlation having vanished because of the emptiness of the higher energy levels. The constant angle cross section curves thus exhibit a maximum as a function of the temperature.

In liquid He_3, treated here as a limiting ideal antisymmetric fluid, the differential cross section is always smaller, at small scattering angles, than the free atom cross section. The latter is reached asymptotically at large scattering angles from below, in contrast with the symmetric fluid. At sufficiently large scattering angles, the constant angle cross sections vary with temperature by exhibiting a minimum between the temperature of absolute zero and the limit of high temperatures or vanishing degeneracy. Again, in contrast with the symmetric fluid, the fluid cross section remains always finite and has no anomalies.

The preceding results correspond to those collision processes in which the incident neutron loses momentum and energy. Since however, in all practical cases, even the total loss of neutron kinetic energy to the target liquid He_4, over reasonable radiation times, cannot perturb the thermal equilibrium of the liquid, the inverse scattering processes have also been studied by using the principle of detailed balance. The resulting, direct plus inverse, liquid cross sections have also been evaluated both in He_4 and He_3. In the latter, however, the thermal equilibrium is far from being as well preserved as in liquid He_4, because of the large thermal neutron reaction cross section, $n(He_3, p)H_3$. This reaction appears to present serious difficulties for the eventual experimental investigation of the incoherent slow neutron scattering.

1. INTRODUCTION

IN view of the present status of the physics of liquid He_4, it appeared of interest to investigate some properties of this fluid which could be ascribed to it on the basis of either of the currently studied incomplete working models. One of these[1] is derived from the symmetrical character of liquid He_4, while the other results from an attempt to interpret quantum-mechanically the hydrodynamical picture of a liquid.[2] Among the fluid properties predicted by these models those which are experimentally accessible and which are different enough are the most interesting. One may add here that the interesting differentiating phenomena resulting from the theoretical liquid models are those which need the least amount of supplementary or intermediate assumptions regarding the interpretation of the experimental data representing the presumed behavior of the liquid.

It seems that as far as the Bose-Einstein (B.E.) fluid model is concerned, such a presumed behavior of liquid He_4 is present in the laws which govern the incoherent or inelastic slow neutron scattering phenomena exhibited by this fluid. By slow neutrons we mean those with kinetic energy substantially larger or much larger than the kinetic energy of thermal motion of the liquid. On the basis of this limitation of the neutron kinetic energy, the collision process of a neutron against a He atom will be described as if the atom were stationary. This approximation is, of course, better the higher the neutron kinetic energy is in comparison with kT, k being Boltzmann's constant and T the absolute temperature of the liquid.

It is interesting that the experimental investigation of the incoherent slow neutron scattering by liquid He_3 might equally yield information on the importance of the antisymmetrical character of this liquid. However, as it will be seen below, the technical difficulties in the neutron scattering experiments by liquid He_3 appear to be increased considerably over and above those present already in the case of liquid He_4.

We should like then, in what follows, to describe the theory of slow neutron inelastic scattering by liquid He_4I, He_4II and He_3 by assuming the rather extreme

* This document is based on work performed at Los Alamos Scientific Laboratory of the University of California under Government Contract W-7405-Eng-36.

[1] F. London, Phys. Rev. **54**, 947 (1938); L. Tisza, J. de phys. et rad. **1**, 165, 350 (1940) and Phys. Rev. **72**, 838 (1947).

[2] L. Landau, J. Phys. USSR **5**, 71 (1941).

ideal B.E. or F.D. fluid models as approximating the limiting behavior of these liquids. In doing so, however, we wish to emphasize that it is by no means our contention to consider these working models as describing satisfactorily these liquids. Evidently, none of these liquids are ideal, i.e., their atoms do exert forces upon each other in the ordinary sense. One may only expect that the present studies indicate clearly those possible trends in the inelastic slow neutron scattering by these liquids which could be recognized, if present, as due to their respective symmetries resulting from general statistical principles.

An inducement of a more academic type which could justify these investigations lies in the fact that the ideal B.E. or F.D. fluids form such systems of interacting particles whose formalism is complete and where the effect of the peculiar statistical interactions on the phenomenon of neutron scattering can be rigorously investigated.

It should be noted here that the coherent scattering of slow neutrons by these liquids would also be affected, possibly, by their respective statistical symmetry. The statistical correlation refers here essentially to its spatial residuum, in contrast with the incoherent neutron scattering which is directly affected by the fundamental correlation in phase space. Since the coordinate space correlations are obtained by averaging over the direct phase space interactions, one might, perhaps, expect a somewhat less pronounced statistical effect on the coherent neutron scattering than on the incoherent process.

2. THE INELASTIC SCATTERING OF SLOW NEUTRONS BY A COLLECTION OF ATOMS WITH SYMMETRICAL OR ANTISYMMETRICAL STATISTICS

Let us consider a neutron beam of intensity I, i.e., in which I neutrons cross per unit time a unit area perpendicular to the direction of motion of the neutrons. This beam falls on a scattering target containing N atoms so arranged that they are all exposed to the neutrons of the incident beam. The latter will be assumed monochromatic or monoenergetic. Assume further that the probability for a single neutron to undergo multiple collisions in the target is negligible. The collection of N atoms will now be assumed to be distributed, at some definite temperature T, according to statistical laws resulting from the application of general principles to this collection of atoms of known elementary characteristics. The absolute neutron kinetic energy will be taken to be large in comparison to kT, as mentioned above. Since the latter energy of thermal motion is of the same order of magnitude, in general, as the binding energy per atom in condensed systems, the energy condition is practically equivalent to that of the neutron kinetic energy being larger than the binding energy.

Let E_n denote the absolute kinetic energy of the neutrons. The condition $E_n > kT$ justifies our considering the target atoms as being practically stationary with respect to the much faster neutrons. Simultaneously, however, the distribution of the atoms in phase space, the target being at some fixed temperature T, will be fully taken into account. Let $n(\epsilon, T)d\epsilon$ be the number of atoms within the kinetic energy band $(\epsilon, \epsilon+d\epsilon)$, so that

$$\int_0^\infty n(\epsilon, T)d\epsilon = N(T). \tag{1}$$

We should like to consider first the limiting situation where the statistical symmetry or antisymmetry may be neglected in the description of the target atoms. It is to be remembered that the extremely low neutron density in the beam causes the latter to behave as a non-degenerate collection of particles. In this limit of vanishing quantum-statistical degeneracy, in a coordinate system in which the center of gravity of the incident neutron and the target atoms is at rest, the number of neutrons scattered per unit time and solid angle, in a direction θ to the direction of incidence, by atoms in the energy band $(\epsilon, \epsilon+d\epsilon)$, is given by

$$d\nu(E, \epsilon, \theta, T) = I\sigma(E, \theta)n(\epsilon, T)d\epsilon. \tag{2}$$

Here, $I\sigma n(\epsilon, T)$ is the number of collisions between the "ϵ" atoms and the neutrons, in unit time, according to our assumption of target atom arrangement mentioned above, while the proportionality constant $\sigma(E, \theta)$ determining the successful collisions is the differential cross section per unit solid angle, in the direction θ, for scattering processes associated with a single atom and the kinetic energy of relative motion E. The total number of neutrons appearing, per unit time, and per unit solid angle, in the direction θ, is, using the definition of $n(\epsilon, T)$, Eq. (1),

$$\nu(E, \theta, T) = IN(T)\sigma(E, \theta). \tag{3}$$

The preceding relations are merely the empirical definitions of the differential cross section per unit solid angle of a solitary free atom. They are based on the assumption that, within the target, there is no direct correlation between atoms in the band around ϵ and say those around $\epsilon' > \epsilon$, into which the first atoms are thrown as a result of the scattering process. An indirect correlation between the atoms is of course contained in the definition (1) of the distribution function $n(\epsilon, T)$.

In quantum statistics the definitions (1) and (2) have to be modified. This modification originates in the quantum-statistical collision numbers as obtained, for symmetrical statistics, from the fundamental researches on the statistical equilibrium between black-body radiation and matter or particles obeying the exclusion principle and matter.[3] Formally, one has instead of

[3] See A. Einstein, Physik. Zeits. **18**, 121 (1917), and W. Pauli, Zeits. f. Physik **18**, 272 (1923), for symmetrical statistics, and L. Brillouin, Ann. de physique **7**, 315 (1927) for anti-symmetrical statistics.

(2), E denoting the kinetic energy of relative motion,

$$d\nu_{\text{B.E.}}(E, \epsilon, \theta, T) = I\sigma(E, \theta)n_{\text{B.E.}}(\epsilon, T)(1+\bar{n}_{\text{B.E.}}(\epsilon', T))d\epsilon, \quad (4)$$

$$d\nu_{\text{F.D.}}(E, \epsilon, \theta, T) = I\sigma(E, \theta)n_{\text{F.D.}}(\epsilon, T)(1-\bar{n}_{\text{F.D.}}(\epsilon', T))d\epsilon, \quad (5)$$

where, $n_{\text{B.E.}}$ and $n_{\text{F.D.}}$ are the total number of atoms per unit energy range, around ϵ, at temperature T in a symmetrical (B.E.) or antisymmetrical (F.D.) collection of free atoms, while the $\bar{n}$'s are the average number of atoms, in the two systems, per state, in the band $(\epsilon', \epsilon'+d\epsilon')$. Here

$$\epsilon' = \epsilon + \Delta(E_n, \theta),$$

is the energy of the scattering atom after a collision resulting in the appearance of a particle in the direction θ, wherein the atom gained the energy $\Delta(E_n, \theta)$ from the scattered neutron, of incident energy E_n.

The fundamental formulas used in the present work are (4) and (5); they are based on the quantum statistical collision numbers included therein.[4] These numbers express in a striking way the remarkable attraction and repulsion, in phase space, between atoms of an ideal Bose-Einstein or Fermi-Dirac gas, respectively. It is seen also in formulas (4) and (5), remembering the form of the B.E. or F.D. distribution functions $n_{\text{B.E.}}$, $n_{\text{F.D.}}$, or the average number of particles per state $\bar{n}_{\text{B.E.}}$ and $\bar{n}_{\text{F.D.}}$, that the right-hand sides of (4) and (5) tend asymptotically, for large angle collisions or large energy exchanges Δ, and high temperatures, toward the classical expression (2).

It is also seen in (4) or (5), rewriting them in the following form:

$$\nu_{\text{B.E.}} = IN\sigma_{\text{B.E.}}, \quad (6)$$

$$\nu_{\text{F.D.}} = IN\sigma_{\text{F.D.}}, \quad (7)$$

with

$$\sigma_{\text{B.E.}}(E, \theta, T) = \frac{1}{N}\sigma(E, \theta)\int_0^\infty n_{\text{B.E.}}(\epsilon, T)(1+\bar{n}_{\text{B.E.}}(\epsilon', T))d\epsilon, \quad (8)$$

and

$$\sigma_{\text{F.D.}}(E, \theta, T) = \frac{1}{N}\sigma(E, \theta)\int_0^\infty n_{\text{F.D.}}(\epsilon, T)(1-\bar{n}(\epsilon', T))d\epsilon \quad (9)$$

that the B.E. and F.D. cross sections, associated with the direct scattering process in which the neutron loses energy and momentum, are always larger and smaller, respectively, than the free atom cross section $\sigma(E, \theta)$.

A formalism based on the theory of quantized symmetrical or antisymmetrical assemblies could be built up here, which, assuming the right interaction form between the neutrons and the heavy photons, i.e., symmetric and antisymmetric atoms, should yield the general formulas (4) and (5), or (8) and (9). Since, however, the physical content of this more complete formalism is already included in the statements of the general statistical principles expressing the fundamental collision numbers as depending on both the initial and final states of the heavy scattering particles, this formalism will not be developed here. The interaction form between the neutrons and the heavy atoms should include also the specific nuclear interaction between these, and this could only be a schematic one.

We will limit ourselves to mention here that the solitary free atom, slow neutron, center of gravity, scattering cross section $\sigma(E, \theta)$ should actually be independent of the energy of relative motion E, or kinetic energy of the incident neutron, and the scattering angle θ, in the neutron energy range investigated in this paper. The independence of energy is related to the assumption that in the slow neutron energy range it is not expected that the scattering due to the rather large nucleus-neutron interaction be affected by their slow relative motion. The independence of angle results essentially from the fact that the de Broglie wave-length in the relative or absolute motion being very large in comparison with nuclear dimensions only zero angular momentum, or s wave scattering, can be of importance, assuring thus spherical symmetry of the scattering process in the relative motion.

We should like to turn now to the study of the scattering processes as described by the fundamental formulas (8) and (9).

3. THE SCATTERING OF SLOW NEUTRONS BY LIQUID He_4I ACCORDING TO THE IDEAL B.E. FLUID MODEL

In the scattering process lifting a target atom from the energy band $(\epsilon, \epsilon+d\epsilon)$ into that of

$$\epsilon' = \epsilon + \Delta, \quad (\Delta \geq 0), \quad (10)$$

the energy gained by the atom, or lost by the neutron, is

$$\Delta = q^2/2M, \quad (11)$$

where

$$\mathbf{q} = \mathbf{p}_i - \mathbf{p}_f, \quad (12)$$

is the change in linear momentum, in the relative motion, and M is the mass of the scattering atom. Since, in the relative motion the scattering process is equivalent geometrically to a rotation of the vector $\mathbf{p}_i$ through the scattering angle θ, one obtains, with

$$|\mathbf{p}_i| = |\mathbf{p}_f| = p, \quad q^2 = 4p^2\sin^2(\theta/2). \quad (13)$$

The relative linear momentum $|\mathbf{p}|$ is $(2\mu E)$, μ denoting

[4] The generalization of the theory of transport processes to include the exclusion principle contained in the antisymmetrical collision number has been made first in the quantum theory of metals; see, for instance, L. Brillouin, *Les Statistiques quantiques* (Les Presses Universitaire, Paris, 1930). The general theory including both statistics is due to G. E. Uhlenbeck and E. A. Uehling, Phys. Rev. **43**, 552 (1933) and E. A. Uehling, Phys. Rev. **46**, 917 (1934).

the reduced mass of the neutron-scattering atom system or $(mM/(m+M))$, m being the neutron mass, and E the kinetic energy of relative motion. Then one obtains, at once,

$$\Delta=(4\mu^2/mM)E_n\sin^2(\theta/2). \tag{14}$$

The distribution function in an ideal B.E. fluid of N atoms of mass M, of zero spin angular momentum, occupying a volume V at temperature T will be written as:

$$n(\epsilon, T)d\epsilon=\bar{n}(\epsilon, T)\rho(\epsilon)d\epsilon, \tag{15}$$

where

$$\bar{n}(\epsilon, T)=[\exp[\alpha+\epsilon/kT]-1]^{-1}, \tag{16}$$

and

$$\rho(\epsilon)d\epsilon=(V/h^3)(2\pi MkT)^{\frac{3}{2}}[1/\Gamma(3/2)](\epsilon/kT)d(\epsilon/kT), \tag{17}$$

is the total number of free particle levels in the energy band $(\epsilon, \epsilon+d\epsilon)$ and $\Gamma(3/2)$ is $(\pi)^{\frac{1}{2}}/2$. The statistical parameter α, the ratio of the negative free energy per atom $(-\gamma)$ to kT, is determined by the total number of atoms, according to

$$N=\int_0^\infty n(\epsilon, T)d\epsilon=(V/h^3)(2\pi MkT)^{\frac{3}{2}}F(\alpha), \tag{18}$$

with

$$F(\alpha)=(1/\Gamma(3/2))\int_0^\infty(\exp[\alpha+x]-1)^{-1}x^{\frac{1}{2}}dx$$

$$=\sum_{n=1}^{\infty}e^{-n\alpha}/n^{\frac{3}{2}}, \quad F(0)=2.612. \tag{19}$$

From (18), according to Einstein,[5] the atomic concentration $(N/V)_0$ or n_0 at which condensation sets in, at temperature T, is

$$n_0=(2\pi MkT/h^2)^{\frac{3}{2}}F(0), \tag{20}$$

while the temperature T_0 at which condensation starts at a concentration n is

$$n=(2\pi MkT_0/h^2)^{\frac{3}{2}}F(0)$$
$$=(2\pi MkT/h^2)^{\frac{3}{2}}F(\alpha). \tag{21}$$

Hence,

$$F(\alpha)=(T_0/T)^{\frac{3}{2}}F(0)$$
$$=(n/n_0)F(0). \tag{22}$$

In the condensation region, $T<T_0$, a finite fraction of the N atoms is in the lowest state,[1] these are, possibly, the superfluid atoms

$$N_s/N=1-(T/T_0)^{\frac{3}{2}}, \tag{23}$$

while the rest of the atoms are in the excited states, distributed according to

$$n(\epsilon, T)d\epsilon=\bar{n}(\epsilon, T)\rho(\epsilon)d\epsilon$$
$$=\rho(\epsilon)d\epsilon[\exp(\epsilon/kT)-1]^{-1}, \tag{24}$$

since the parameter α is extremely small (of the order of N^{-1}).

[5] A. Einstein, Ber. d. Ber. Akad. p. 261 (1924) and p. 3 (1925).

With the scattering angle θ, defined by (13), associated with a process in which the scattering atom has been lifted from the energy band around ϵ into the one around $(\epsilon+\Delta(\theta))$, the corresponding B.E. cross section per unit solid angle is, according to (8),

$$\sigma_{\text{B.E.}}(E_n, \theta, T)$$

$$=\sigma\int_0^\infty\{1+[\exp(\alpha+(\epsilon+\Delta(\theta)/kT))-1]^{-1}\}$$

$$\times\rho(\epsilon)d(\epsilon)[\exp(\alpha+(\epsilon/kT))-1]^{-1}, \tag{25}$$

where σ stands, from now on, for the free atom differential cross section per unit solid angle. An elementary calculation yields, then,

$$r=\sigma_{\text{B.E.}}/\sigma=\frac{1-F(\alpha+\beta)/F(\alpha)}{1-e^{-\beta}}, \tag{26}$$

where

$$\beta=\Delta(E_n, \theta)/kT$$
$$=(E_n/kT_0)(T_0/T)(4\mu^2/mM)\sin^2(\theta/2)$$
$$=E_n'\tau f(\theta), \tag{27}$$

is the ratio of the energy exchange in the collision to the thermal energy kT. We shall henceforth measure the absolute neutron kinetic energy in units of kT_0; T_0 denotes the condensation temperature, E_n' is (E_n/kT_0), while τ is (T_0/T), with $f(\theta)$ standing for the last factor $(4\mu^2/mM)\sin^2(\theta/2)$ in (27). It is seen that the direct process cross section $\sigma_{\text{B.E.}}(E_n, \theta, T)$ is a universal function of the statistical parameter α and the energy exchange in the collision $\Delta(E_n, \theta)/kT$ measured in units of kT. We should like to discuss now the B.E. fluid cross-section formula (26).

It is of course, visible in the fundamental formulas (4) or (8) that the preferred collisions are those in which the scattering atom is lifted into well populated states. In such cases the statistical "attraction" term is the largest leading to a fluid cross section larger than the free atom cross section. It is evident that in those collisions which lead to a practically empty state, i.e., large angle scattering processes, the B.E. cross section differs but very little from that of the free atom.

Let us consider now the fluid kept at a constant temperature and study the scattering as a function of the scattering angle or the neutron kinetic energy. In a collision where the scattering atom gains energy according to Eqs. (10) and (14) or (27), the Einstein-Pauli induced scattering is larger the smaller Δ, the energy exchange. The maximum value of the induced scattering corresponds to the limit of vanishing Δ. Hence, at a constant liquid temperature and incident neutron kinetic energy, the scattering cross section should show a maximum in the forward direction and decrease toward larger angles. This behavior of $\sigma_{\text{B.E.}}(E_n, \theta, T)$ is described rigorously by the general formula (26), at $T>T_0$.

Here, $\alpha\sim 1$, and one sees that

$$\lim_{\beta\ll 1} r = \lim_{\beta\ll 1} \sigma_{\text{B.E.}}/\sigma$$
$$= -F'(\alpha)/F(\alpha), \quad F'(x)=dF/dx; \tag{28}$$

indicating that in the limit of very small scattering angles, the B.E. cross section becomes independent of the very small energy exchange and depends only on the liquid temperature and concentration through the parameter α. For increasing β, or θ, the cross section decreases monotonically and in the opposite limit of large β, essentially at large angles, since $E_n > kT$,

$$\lim_{\beta\gg 1} r = \lim_{\beta\gg 1} \sigma_{\text{B.E.}}/\sigma$$
$$= 1-e^{-(\alpha+\beta)}/F(\alpha)\sim 1. \tag{29}$$

In this limit $F(\alpha+\beta)$ reduces to its first term $e^{-(\alpha+\beta)}$ which is very small. A more complete numerical analysis of the cross-section formula (26) will be given below.

4. THE SLOW NEUTRON SCATTERING BY AN IDEAL B.E. FLUID IN THE CONDENSATION REGION (He II MODEL)

Below the transition temperature, the fluid may be said to be in the mixed phase region as mentioned briefly above in connection with Eqs. (23) and (24). The incoherent scattering will now be a superposition of the effects due to the condensed and excited phases. One finds after a simple calculation, using formulas (4) and (18),

$$\sigma_s(E_n, \theta, T) = \sigma/(1-e^{-\beta}) \tag{30}$$

for the cross section of the condensed or superfluid atoms, and

$$\sigma_n(E_n, \theta, T) = \sigma\frac{1-[F(\beta)/F(0)]}{1-e^{-\beta}}, \tag{31}$$

for the normal atom cross section. The resulting cross section becomes,

$$\sigma_{\text{B.E.}}(E_n, \theta, T\leq T_0) = (N_s\sigma_s + N_n\sigma_n)/N$$
$$= \sigma\frac{1-(T/T_0)^{\frac{3}{2}}F(\beta)/F(0)}{1-e^{-\beta}}. \tag{32}$$

Use has been made here of Eq. (23) giving (N_s/N) and its complement (N_n/N) or $(T/T_0)^{\frac{3}{2}}$. It will be observed, at once, that the preceding cross section reduces to the one obtained in the high temperature or single phase region, Eq. (26), as $T\to T_0$, i.e., at the condensation temperature. In other words, the liquid cross section is continuous at the transition point. This was to be expected on the basis of the smooth condensation process exhibited by the ideal B.E. fluid.[6]

[6] See L. Goldstein, J. Chem. Phys. 14, 276 (1946).

Let us consider again the scattering at a constant liquid temperature. In the limits of very small β or very small scattering angles, one obtains

$$\lim_{\beta\ll 1} \sigma_{\text{B.E.}}(E_n, \theta, T\leq T_0)$$
$$\cong\sigma\left\{\frac{1-(T/T_0)^{\frac{3}{2}}}{\beta} - \frac{(T/T_0)^{\frac{3}{2}}}{F(0)}\lim_{\beta\ll 1} F'(\beta)\right\}. \tag{33}$$

Using the explicit expression of β and the asymptotic value of $F'(\beta)$, $\beta\ll 1$, i.e.,

$$-F'(\beta) = \Gamma(\tfrac{1}{2})/\beta^{\frac{1}{2}};$$

one finds,

$$\lim_{\theta\to 0} \sigma_{\text{B.E.}}(E_n, \theta, T<T_0)$$
$$= \frac{\sigma}{N}\left\{\frac{N_s(mM)kT}{\mu^2 E_n\theta^2} + \frac{N_n\Gamma(\frac{1}{2})(mMkT)^{\frac{1}{2}}}{\mu E_n^{\frac{1}{2}}\theta}\right\}. \tag{34}$$

In the condensation region, in contrast with what occurs far above the transition temperature, the liquid cross section increases essentially as θ^{-2}, for very small scattering angles. It is seen that this very small angle scattering is due primarily to the condensed atoms N_s. It should be remembered, however, that these very small angle scattering processes may be more of an academic than practical interest. Indeed, it is questionable whether these processes could be observed with practical resolutions. In the opposite limit of $\beta\gg 1$, one obtains from (32) asymptotically the free atom cross section.

We are prepared now to discuss the neutron scattering process over the whole temperature range at constant scattering angles and constant incident neutron kinetic energies. Qualitatively, considering some finite scattering angle, the general behavior of symmetrical fluids makes one expect the following situation. The degeneracy vanishing at high temperatures, the B.E. cross section should become equal asymptotically to the free atom cross section. As the temperature decreases and the degeneracy increases, the fluid cross section has to increase above the free atom value because of the increasingly strong intervention of the induced scattering processes. In the limit of very low temperatures, the atoms have essentially collected in the condensed phase. With the very small population of the excited levels, the induced scattering process becomes less important and the whole scattering again becomes classical. Hence, for finite scattering angles, and constant incident neutron kinetic energies, the B.E. cross section should exhibit a maximum at some intermediate temperature. This is, of course, contained in the formulas (26) and (32).

The problem is less simple at small scattering angles near the transition point. We have seen that above the transition point, the small angle scattering cross section becomes independent of the scattering angle and the

neutron energy and depends only on the liquid temperature, Eq. (28). The latter gives,

$$\lim_{\substack{\beta\ll 1\\ \alpha\to 0}}(\sigma_{\text{B.E.}}/\sigma)=\lim_{\alpha\to 0}\left(\frac{-F'(\alpha)}{F(0)}\right). \tag{35}$$

Now the right-hand side diverges at $\alpha=0$; but actually α is not strictly zero but of order of N^{-1}, so that we may use the asymptotic value of $(-F'(\alpha))$ for very small α, which is

$$\lim_{\alpha\to 0}(-F'(\alpha))\cong\int_0^\infty \frac{e^{-n\alpha}}{n^{\frac{1}{2}}}dn$$

$$=\Gamma(\tfrac{1}{2})N^{\frac{1}{2}}.$$

Hence,

$$\lim_{\substack{\theta\to 0\\ T\to T_0}}\sigma_{\text{B.E.}}(E_n,\theta,T)\cong\sigma\Gamma(\tfrac{1}{2})N^{\frac{1}{2}}/F(0), \tag{36}$$

which is very large. Again the remark made above on the practical interest of the very small angle scattering processes should be remembered here. It should also be noted that the preceding result (36) can also be derived by approaching the transition temperature T_0 from the low temperature side, provided that one remembers the order of magnitude of α in the condensation region. The B.E. differential scattering cross section is strictly continuous, at all angles, across the transition point. The very large limit (36) of the transition point cross section is connected with the phase instability of the B.E. fluid in this region. The root-mean-square fluctuation in the number of excited atoms amounts, at the transition temperature, to $N^{\frac{1}{2}}$. The situation represented by the cross-section limit formula (36) resembles the one encountered in the application of the ideal B.E. fluid formalism to the coherent scattering of visible light near the transition line.[7] Since experimentally[8] no anomalous scattering could be detected in liquid helium with visible light it is unlikely that the very small angle neutron scattering anomaly indicated by (36) could be present in the actual behavior of the liquid. The inevitable transmission of a large portion of the incident beam in the forward direction would make quite difficult the experimental investigation of very small angle scattering processes.

5. THE SLOW NEUTRON SCATTERING BY AN IDEAL F.D. FLUID

Using the fundamental cross-section definitions (5) or (9), one obtains with the F.D. distribution functions, after a simple calculation:

$$\sigma_{\text{F.D.}}(E_n,\theta,T)$$

$$=\sigma[(1-\Phi(\alpha+\beta)/\Phi(\alpha))/(1-e^{-\beta})]\leq\sigma. \tag{37}$$

Here,

$$\Phi(x)=\sum_{n=1}^{\infty}(-)^{n+1}e^{-nx}/n^{\frac{1}{2}}.$$

The parameter α is positive at temperatures $T>T_0$, T_0 denoting the degeneration temperature:

$$T_0=(\hbar^2/2Mk)(3n/8\pi)^{\frac{1}{2}}, \tag{38}$$

for particles of spin angular momentum $\hbar/2$, at a concentration (N/V) or n, N being the total number of atoms of the fluid occupying volume V. The cross-section formula (37) is valid over the whole temperature range.

At some constant temperature it is easy to give limiting values of $\sigma_{\text{F.D.}}$. Since the condition $E_n>kT$ is adhered to here also, at moderate scattering angles, β is large, so that above the degeneration temperature

$$\Phi(\alpha+\beta)\sim e^{-(\alpha+\beta)},$$

and

$$\lim_{\beta\gg 1}\sigma_{\text{F.D.}}=\sigma[1-e^{-(\alpha+\beta)}/\phi(\alpha)]\sim\sigma, \tag{39}$$

as would be expected. In this case, the states of high energy into which the scattering atoms may be lifted, are practically unoccupied, so that the characteristic repulsion in phase space cannot operate fully, and the scattering cross section tends toward its free atom value. This result is similar to the one found in the B.E. case. However, the approach toward the free atom cross section is here opposite to the one in B.E. fluids, insofar as, in the present case, the cross section is always smaller than its asymptotic limit.

At $T>T_0$, in the limit of small scattering angles, β is small and

$$\lim_{\beta\ll 1}\sigma_{\text{F.D.}}=\sigma[-\Phi'(\alpha)/\Phi(\alpha)], \tag{40}$$

i.e., the cross section becomes independent of the scattering angle and the neutron kinetic energy, a situation similar to that of the B.E. case at $T>T_0$. The F.D. cross sections at small angles decrease with decreasing temperature. This is caused by the gradual filling up of the energy states. Since a small energy transfer to the scattering atom would lift it only into a neighboring higher situated level, which is practically full, the small angle scattering becomes increasingly prohibited with decreasing temperatures.

With

$$\Phi(\alpha)\underset{T\ll T_0}{\sim}\frac{2(-\alpha)^{\frac{1}{2}}}{3\Gamma(3/2)},\quad \alpha<0;\quad |\alpha|\gg 1,$$

one finds,

$$\lim_{\substack{\beta\ll 1\\ T\ll T_0}}\sigma_{\text{F.D.}}=\tfrac{3}{2}\sigma(-\alpha)^{-1}$$

$$=\tfrac{3}{2}\sigma(T/T_0), \tag{41}$$

[7] L. Goldstein, Phys. Rev. **57**, 241 (1940); A. D. Galanin, J. Exp. Theor. Phys. **10**, 1267 (1940).
[8] I. A. Jakovlev, J. Phys. USSR **7**, 307 (1943).

and, as expected, the forward scattering cross section vanishes at the temperature of absolute zero. At this temperature, only those atoms can contribute to the scattering process with an energy gain Δ, which are at the depth Δ below the top ϵ_0 of the distribution. One finds, at once,

$$\sigma_{\text{F.D.}}(\Delta, T=0)=\sigma\{1-[1-(\Delta/\epsilon_0)]^{\frac{1}{2}}\}; \quad \Delta<\epsilon_0. \quad (42)$$

The scattering becomes classical for $\Delta>\epsilon_0$, or for scattering angles θ larger than

$$\theta_0=2 \arcsin[(mM/4\mu^2)(\epsilon_0/E_n)]^{\frac{1}{2}},$$

where $E_n>\epsilon_0$. With respect to scattering angles larger than θ_0, one has then, as far as the temperature variation of the F.D. cross section is concerned, the following situation. The cross section is classical, i.e., it is the free atom cross section at the temperature of absolute zero. It becomes sub-classical as the temperature increases and then tends again asymptotically from the sub-classical values toward the free atom value at temperatures $T\gg T_0$. One clearly recognizes here, in the temperature variation of the F.D. cross sections a qualitatively opposite behavior from that of the B.E. cross sections. The former exhibit minima at constant scattering angles $\theta>\theta_0$ between the temperature of absolute zero and the high temperatures, the latter have maxima in the same temperature range.

While in He_3, at liquid densities, one might have an antisymmetric collection of atoms in a highly degenerate state, the experimental problem of investigating the slow neutron inelastic scattering on this liquid appears to be considerably more difficult than in liquid He_4. The origin of these difficulties lies in the very large absorption cross section of He_3 nuclei for thermal and subthermal neutrons.[9]

6. THE INVERSE SCATTERING PROCESSES

In the preceding sections we studied only the direct collision processes in which the neutron loses and the heavy atom gains energy and momentum. But the scattering fluids are and remain in thermal equilibrium even under the extreme assumption that all the neutrons of a thermal neutron beam available usually transfer their whole energy to the target liquids during practical irradiation times. This statement applies rigorously to liquid He_4, while in liquid He_3, because of the large energy release in the $n(He_3,p)H_3$ reaction, the equilibrium cannot be maintained to the same accuracy as in He_4, although it still remains conserved with fair accuracy. As a result, it is expected on the basis of the principle of detailed balance that all those direct processes in which the neutron loses energy and momentum to the liquid atoms have their counterpart in inverse processes due to those atoms which can, conservation theorems permitting, transfer energy and momentum to neutrons, scattering them out of their direction of incidence.

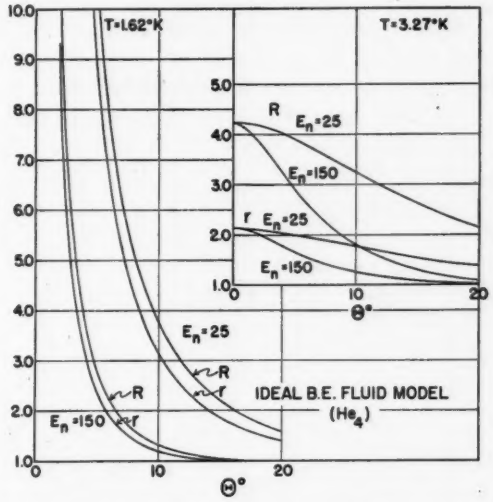

FIG. 1. Cross-section ratios *vs.* scattering angle for two neutron energies E_n, expressed in units of kT_λ.

One finds, to the approximation of the present studies, that the ratio

$$R_{\text{B.E.}}=[\sigma_{\text{B.E.}}(\text{direct})+\sigma_{\text{B.E.}}(\text{inverse})]/\sigma$$

associated with the energy exchange β, is given, in the center of gravity coordinate system, by

$$R_{\text{B.E.}}=\frac{\sigma_{\text{B.E.}\,th}}{\sigma}=\frac{\sigma_{\text{B.E.}}(\beta, T)}{\sigma}+\frac{1}{F(\alpha)}\frac{1}{\Gamma(3/2)}$$
$$\times\int_\beta^\infty\left\{1+\left[\exp\left(\alpha+\beta+\frac{\epsilon}{kT}\right)-1\right]^{-1}\right\}$$
$$\times\rho(\epsilon)\left[\exp\left(\alpha+\frac{\epsilon}{kT}\right)-1\right]^{-1}d\epsilon, \quad (43)$$

since only those atoms can lose energy and momentum, for the scattering in some direction, whose initial energy and momentum is at least equal to their eventual loss. One finds then, after a simple calculation, that

$$R_{\text{B.E.}}=\frac{\sigma_{\text{B.E.}\,th}}{\sigma}=2\frac{\sigma_{\text{B.E.}}}{\sigma}$$
$$-\frac{1}{F(\alpha)(1-e^{-\beta})}\sum_{n=1}^{\infty}\frac{e^{-n\alpha}}{n^{\frac{1}{2}}}(1-e^{-n\beta})\varphi(n\beta), \quad (44)$$

where

$$\varphi(n\beta)=\frac{1}{\Gamma(3/2)}\int_0^{n\beta}e^{-z}x^{\frac{1}{2}}dx.$$

In (44), $(\sigma_{\text{B.E.}}/\sigma)$ is given by Eq. (26), at temperatures T above the transition temperature T_0.

A similar reasoning leads, below the transition

[9] L. D. P. King and L. Goldstein, Phys. Rev. **75**, 1366 (1949); J. H. Coon and R. A. Nobles, Phys. Rev. **75**, 1358 (1949).

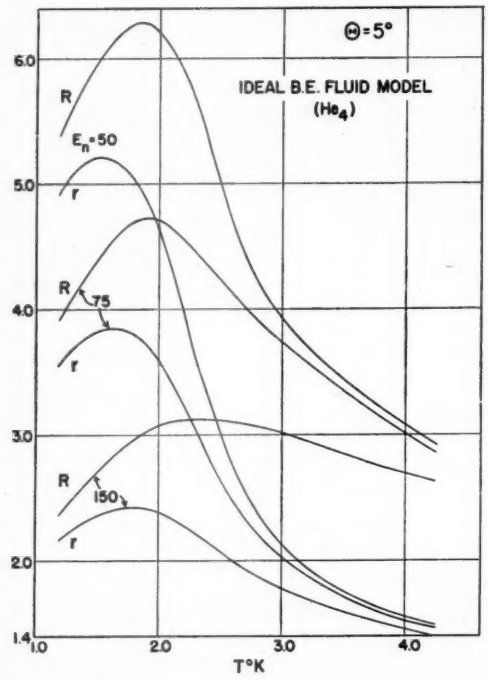

FIG. 2. Cross-section ratios *vs.* temperature, at the scattering angle of 5°, for three neutron energies E_n, expressed in units of kT_λ.

temperature, i.e., in the condensation region, to

$$R_{\text{B.E.}}=\frac{\sigma_{\text{B.E.}\,th}(T<T_0)}{\sigma}$$
$$=\frac{\sigma_{\text{B.E.}}(T<T_0)}{\sigma}+\frac{(N_n/N)}{1-e^{-\beta}}\left[1-\frac{F(\beta)}{F(0)}\right.$$
$$\left.-\left(\frac{1}{F(0)}\right)\sum_{n=1}^{\infty}\frac{(1-e^{-n\beta})}{n^{\frac{3}{2}}}\varphi(n\beta)\right]. \quad (45)$$

It is seen that below the transition temperature, only the excited or normal atoms take part in the inverse scattering processes. Evidently, the condensed atoms cannot lose energy and momentum.

A glance at the general relation (43) shows that the inverse processes are more important the smaller the energy exchange in terms of kT, i.e., the smaller β. This occurs, for large temperatures, and small scattering angles.

One finds similarly, after a simple calculation,

$$R_{\text{F.D.}}=\frac{\sigma_{\text{F.D.}\,th}(\beta,T)}{\sigma}=2\frac{\sigma_{\text{F.D.}}}{\sigma}-\frac{1}{\Phi(\alpha)(1-e^{-\beta})}$$
$$\times\sum_{n=1}^{\infty}(-)^{n-1}\frac{e^{-n\alpha}}{n^{\frac{3}{2}}}(1-e^{-n\beta})\varphi(n\beta). \quad (46)$$

Strictly speaking the numerical computations of $R_{\text{F.D.}}$ have been performed using the general formula (43) modified for F.D. statistics. Here $(\sigma_{\text{F.D.}}/\sigma)$ or $\sigma_{\text{F.D.}}$ is given by Eq. (37).

Clearly both in the B.E. and F.D. fluids the σ_{th}'s are larger than those associated with the direct collision processes only. For the sake of completeness, it is interesting that in a Maxwell-Boltzmann fluid, one would have

$$\frac{\sigma_{\text{M.B.}\,th}}{\sigma}=2\left(1-\frac{\varphi(\beta)}{2F_{\text{M.B.}}(\alpha)}\right),$$
$$\varphi(\beta)=\frac{1}{\Gamma(3/2)}\int_0^{\beta}e^{-x}x^{\frac{1}{2}}dx, \quad (47)$$

and $F_{\text{M.B.}}(\alpha)$ is the Maxwell-Boltzmann statistical function, which reduces to

$$F_{\text{M.B.}}(\alpha)=n/(2\pi MkT/h^2)^{\frac{3}{2}},$$

n standing for the atomic concentration; the function $F(\alpha)$ is the ratio of the number of atoms N to the number of states in phase space, whose momentum volume has the value $(2\pi MkT)^{\frac{3}{2}}$.

7. ANALYSIS OF THE INELASTIC SLOW NEUTRON SCATTERING PROCESSES IN B.E. AND F.D. FLUIDS

In order to facilitate any eventual comparison of future experimental data with the predictions of the limiting models studied here, the numerical analysis has been performed here in the laboratory coordinate system, i.e., the ratios r and R refer here to the laboratory differential cross sections.

The transition temperature T_0, in the B.E. case, has been taken to be the He_4 lambda-point temperature, while the degeneration temperatures of the F.D. fluid were computed using the approximate liquid He_3 density values obtained at Los Alamos.[10] The numerical results are given here in graphical form.

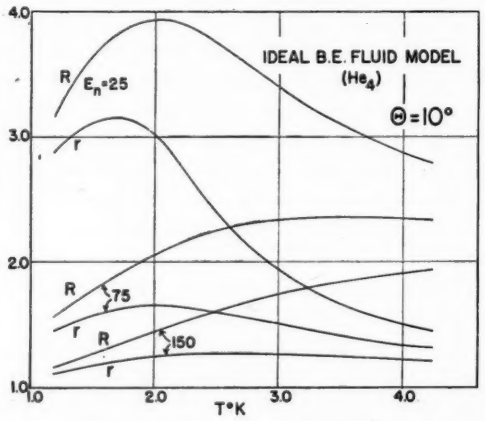

FIG. 3. Cross-section ratios *vs.* temperature, at the scattering angle of 10°, for three neutron energies E_n, expressed in units of kT_λ.

[10] Grilly, Hammel, and Sydoriak, Phys. Rev. **75**, 1103 (1949).

In Fig. 1 we give typical r and R ratio curves at 1.19°K ($T<T_0$) and 3.27°K ($T>T_0$) as a function of the laboratory scattering angle for two sets of neutron kinetic energies. The actual liquid cross sections could be gotten from these by multiplying the ordinates associated with an angle Θ by $\sigma(d\omega/d\Omega)$. Here σ the center of gravity free atom differential cross section per unit solid angle is[11] $(1.25/4\pi)\times10^{-24}$ cm^2, while the conservation theorems give

$$\frac{d\omega(\theta)}{d\Omega(\Theta)}=\frac{m(\cos\Theta+[(M/m)^2-\sin^2\Theta]^{\frac{1}{2}})^2}{M[(M/m)^2-\sin^2\Theta]^{\frac{1}{2}}},$$

m and M denoting the neutron and scattering atom masses respectively. It is to be recalled that

$$\beta(kT/E_n)=(4\mu^2/mM)\sin^2(\theta/2)$$
$$=1-(\mu/M)^2(\cos\Theta+[(M/m)^2-\sin^2\Theta]^{\frac{1}{2}})^2,$$

μ being the reduced mass. The free atom He_3 scattering cross section is unknown at present.[12]

Typical B.E. ratio curves, at constant scattering angles ($\Theta=5$ and 10 degrees) as a function of the liquid temperature T are given in Figs. 2 and 3 respectively.

These results indicate, as expected, that the smaller the neutron kinetic energy the more pronounced are the characteristic B.E. features of the scattering cross sections. It is remarkable that already with room temperature neutrons, the small angle scattering is affected by statistics to an extent which appears to be observable experimentally. At smaller neutron kinetic energies the effect becomes quite strong. The remarkable formation of the maximum in the ratio curves, at constant scattering angle, as a function of the fluid temperature is quite prominent. With the slow neutron beams available at the Enriched Uranium Pile of this Laboratory and the use of filtration technique,[9] it appears that the experimental investigation of slow neutron inelastic scattering by liquid helium could be undertaken starting first with broad, i.e., non-monochromatic neutron beams. With graphite filtration, however, the width of the spectral distribution of the beam is being automatically reduced, so that, if present, the characteristic features of the scattering phenomena appear to be observable.

We have to consider briefly at this juncture the inevitable presence, in the scattering experiments, of both incoherent and coherent processes. With some results available with x-rays,[13] the main coherent peak in liquid helium is to be expected at a scattering angle Θ, double that of the Bragg angle, such that

$$\sin(\Theta/2)=\lambda/2a,$$

λ denoting the radiation wave-length and a the average atomic separation in the liquid. According to Keesom,[13] a appears to be given in helium as well as in other monatomic liquids by the approximate separation computed from an assumed hexagonal close packing

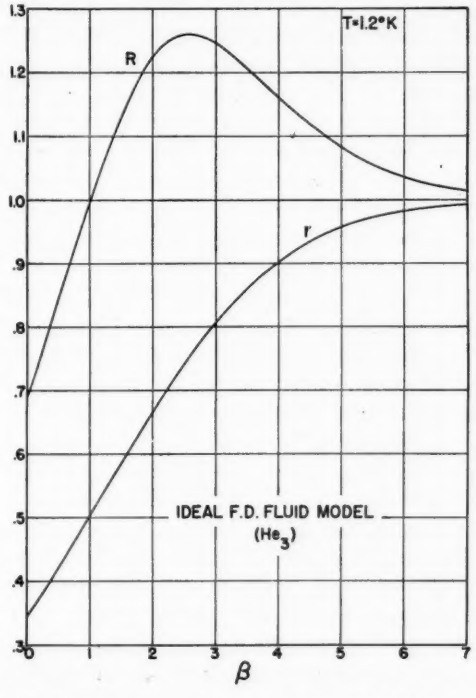

FIG. 4. Cross-section ratios *vs.* the energy exchange in the scattering process, expressed in units of kT.

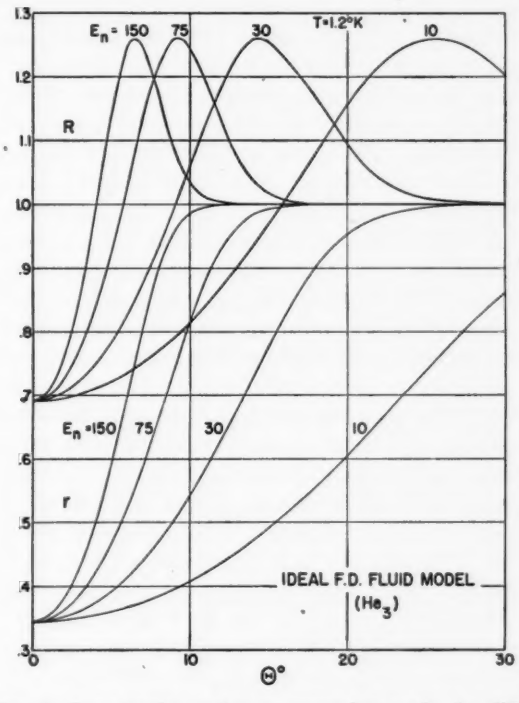

FIG. 5. Cross-section ratios *vs.* scattering angle, for different neutron energies E_n, expressed in units of kT_0, T_0 being the degeneration temperature.

[11] H. Carroll, Phys. Rev. **60**, 702 (1941).
[12] See, however, the first work quoted in reference 9.
[13] See the monograph of W. H. Keesom, *Helium* (Elsevier Publishing Company, Inc., Amsterdam, 1942), pp. 326–29.

of the atoms, axial ratio

$$c/a=2(2/3)^{\frac{1}{2}}, \quad a\cong 2^{1/6}(1.66M/\rho)^{\frac{1}{3}}\text{A}.$$

Here M is the atomic weight and ρ the liquid density. This gives $a\sim 4$A, so that the main coherent peak occurs at the scattering angles of about 26°, 31°, 45°, and 65° for neutrons of kinetic energy kT, at 293, 200, 100, and 50°K, respectively. Since the main B.E. effect appears to be limited to Θ values not exceeding 25–30°, it is seen that with smaller kinetic energy neutrons the statistical effect, if present, would appear without too great an overlap due to the broadened coherent neutron scattering peak. It should be remembered, however, that the transmitted beam in the forward direction, being itself broadened, tends to reduce the effective angular range where the statistical effects would appear.

Before turning to the presently more academic liquid He_3 case, we should like to mention the interesting studies by Akhiezer and Pomeranchuk[14] on the incoherent scattering of very low energy neutrons ($\lesssim 3.5$°K) using the continuum liquid He_4II model.[2] According to these workers the continuum model, at the neutron energies considered in this paper, would lead to incoherent scattering cross sections which should not differ much from the free atom cross section. Indeed, it should be remembered that the neutron kinetic energies involved here are considerably larger than both kT_D (T_D being some apparent Debye temperature of liquid He_4II) and the binding energy per atom in the liquid. These energies are, respectively, 10–15k, $T_D\sim 10$–15°K, and some 10^{-15} ergs/atom, at 0°K. Our lowest neutron kinetic energy is $25kT_\lambda$, or about 55k. Now the continuum liquid model may be said to correspond to a limiting solid model. In the latter, according to the investigations of Weinstock,[15] the inelastic differential cross section, although depending on the scattering angle, does not exhibit as critical a variation with angle as the B.E. fluid model, especially in the condensation region of the latter. The solid body incoherent neutron scattering results have but an approximate value in the case of He_4, because of the relatively large mass ratio (m/M). In the high neutron kinetic energy range, the application of the solid model leads to a situation which starts resembling that of diffuse incoherent x-ray scattering. The latter varies,[16] at constant solid temperature and wave-length, in such a way that the scattered intensity increases first with scattering angle reaches a maximum to decrease after with increasing scattering angles. This behavior is of course quite clear physically if one remembers that the incoherent diffuse scattering of x-rays by crystals is due to Compton-effect. For very small momentum and energy loss of the photon, the binding energy of the electrons reduces the scattering. At increasing scattering angles the scattering probability increases. At large scattering angles, where the energy transfer becomes larger, the scattering cross section should approach asymptotically some finite value.

Now, one may question here the physical plausibility of the finite and even large scattering cross sections resulting from the B.E. fluid model in the limit of vanishing scattering angles. Although in the actual liquid, the atoms are bound, it is not unlikely that inelastic collision processes may occur here at very small angles because of the possibility of transferring even very small momenta and energy to the liquid atoms. This question is of course closely related to the energy spectrum of the liquid atoms, and it is expected that the experimental investigation of slow neutron inelastic scattering processes should throw some light on this fundamental problem also. There does not seem to be any general justification in letting the binding energy of the individual atoms impose limitations on the small angle neutron scattering. One may say then that the continuum model of liquid He_4II appears to lead to predictions as to the inelastic neutron scattering, at the energies considered here, which appear to differ from those obtained in the application of the limiting B.E. fluid model to describe approximately liquid He_4.

In the F.D. case, we present in Fig. 4 laboratory differential cross-section ratios $r(T,\beta)$ and $R(T,\beta)$ at 1.2°K, as a function of β, the energy exchange in the collision in units of kT. These cross-section ratios have been obtained using the approximate liquid He_3 densities. The numerical calculations have been greatly helped here by the existence of tables of F.D. functions.[17] The universal character of these cross-section ratios manifests itself through their representation as a function of the laboratory scattering angles for different neutron kinetic energies, the latter are expressed in terms of the energy kT_0 associated with the liquid He_3 density at 1.2°K, Fig. 5. It is remarkable that these scattering curves resemble the "solid" type of incoherent scattering curves. The reason for this analogy is to be found in that the Fermi energy kT_0 does play a role which is similar to the finite electron binding energy in crystals. This is particularly so at the temperature of absolute zero, where the cross section (42) is almost similar to the one exhibited by a Fermi-Thomas atom.[18] The latter is essentially a collection of electrons at the temperature of absolute zero. It should again be noted that any experimental investigation of the inelastic slow neutron scattering by liquid He_3 presents major difficulties as we saw briefly above.

As to the total inelastic fluid cross sections, they differ only very little from the free atom total scattering

[14] A. Akhiezer and I. Pomeranchuk, J. Phys. USSR **9**, 461 (1945).

[15] R. Weinstock, Phys. Rev. **65**, 1 (1944). See also M. L. Goldberger and F. Seitz, AEC Report MDDC-1063 (1944).

[16] See A. H. Compton and S. K. Allison, *X-Rays in Theory and Experiment* (D. Van Nostrand Company, Inc., New York).

[17] See J. McDougall and E. C. Stoner, Phil. Trans. Roy. Soc., London **A237**, 67 (1938).

[18] See the incoherent scattering curve of such an atom on p. 143 of reference 16.

cross section. This is due to the rather reduced angular range of the statistical effects studied here.

We should like to conclude by again emphasizing that the scattering processes predicted by the models studied here could not represent but a qualitative description of these phenomena exhibited by liquid He_4 or liquid He_3, in the eventuality of an explicit effect of quantum statistics on neutron scattering. As mentioned briefly, the angular range in liquid He_4 where the statistical effects are prominent, if present, would be narrowed down by the broadening of the transmitted beam and the coherent beam. It would appear that the investigation of the scattering at some fixed intermediate angle as a function of the liquid temperature offers the most favorable way in which to look for the effect of statistics.[19]

[19] Dr. E. A. Long (University of Chicago) kindly informed the senior author (L.G.) of Dr. E. Fermi's independent suggestion of such experiments in 1948. He also briefly discussed this problem at the AEC Information meeting, Los Alamos, May 1949.

PHYSICAL REVIEW VOLUME 77, NUMBER 3 FEBRUARY 1, 1950

Experimental Photo-Fission Thresholds in $_{92}U^{235}$, $_{92}U^{238}$, $_{92}U^{233}$, $_{94}Pu^{239}$, and $_{90}Th^{232}$*

H. W. Koch,** J. McElhinney,** and E. L. Gasteiger***
Physics Department, University of Illinois, Urbana, Illinois

(Received September 26, 1949)

An investigation of the photo-fission thresholds in $_{92}U^{235}$, $_{92}U^{238}$, $_{92}U^{233}$, $_{94}Pu^{239}$, and $_{90}Th^{232}$ with a 20-Mev betatron is reported. A method of alpha-self-cancellation is described which permits the detection of fissions and the determination of threshold energies in the two highly alpha-active samples of $_{92}U^{233}$ and $_{94}Pu^{239}$. An investigation of the photo-neutron threshold in nitrogen and the energy calculation from mass data provided a check of the absolute energy scale obtained from voltage measurements on the betatron.

INTRODUCTION

THE production of high energy x-rays of adjustable energy by a betatron makes possible the study of the photo-fission thresholds in uranium. Previous work with monokinetic energy gamma-rays[1] could only be concerned with predictions of these threshold energies. A Japanese paper,[1] for example, predicted the $_{92}U^{238}$ photo-fission threshold to be at 3.0 Mev. This was based on their measured gamma-ray cross sections in uranium of 2.2×10^{-27} cm^2 at 6.3 Mev and of 16.7×10^{-27} cm^2 at 17 Mev and an assumed functional variation of cross section with energy.

A more reliable prediction can be made theoretically by making use of the liquid drop model of Bohr and Wheeler.[2] Frankel and Metropolis[3] from calculations on the Eniac found the values given in Table I for classical fission thresholds, that is for energy differences between the initial spherical equilibrium shape of the drop and the saddle point shape. Changes in the constants used for the nuclear radius and the surface tension would change the relations of these values only very slightly.

The first attempt to determine experimentally a uranium photo-fission threshold was done by Baldwin and Koch[4] with a 20-Mev betatron. Their use of a sample of ordinary uranium powder and the catcher method for studying the activity in the fission fragments showed that the threshold was less than 8 Mev. Threshold assignment was not possible due to the lack of fission intensity at the lower energies. More recently a University of Illinois thesis[5] described the use of the betatron's x-rays in conjunction with a fission ionization chamber and a linear amplifier. The determination of the fission pulse yield as a function of betatron energies gave a threshold for $_{92}U^{238}$ at 5.8 Mev and for $_{90}Th^{232}$ at 6.25 Mev.

These experiments were continued using the 20-Mev betatron at the University of Illinois when separated samples of the uranium isotopes were made available by the Manhattan Project. It was hoped that a definite check of the relative values of the predicted photo-

TABLE I. Theoretical threshold energies.

Nucleus	Fission threshold energies (Mev)
U^{238}	7.0
U^{235}	6.1
U^{233}	5.7
Pu^{239}	4.9

* This work was done under the auspices of the Metallurgical Laboratory at the University of Illinois under contract W-7401-37-121 in 1944 and 1945. The report as here presented was submitted on January 30, 1947 and declassified on August 29, 1949.

** Present address: X-Ray Section, National Bureau of Standards, Washington, D. C.

*** Present address: Department of Biophysics, University of Minnesota, Minneapolis, Minnesota.

[1] Arakatu, Uemura, Sonoda, Shimizu, Kimura, and Muraoka, Proc. Phys. Math. Soc. Japan **23**, 440 (1941); Haxby, Shoupp, Stephens, and Wells, Phys. Rev. **59**, 57 (1941).

[2] N. Bohr and J. A. Wheeler, Phys. Rev. **56**, 426 (1939).

[3] S. Frankel and N. Metropolis, Phys. Rev. **72**, 914 (1947).

[4] G. C. Baldwin and H. W. Koch, Phys. Rev. **67**, 1 (1945).

[5] H. W. Koch, thesis, University of Illinois (1944).

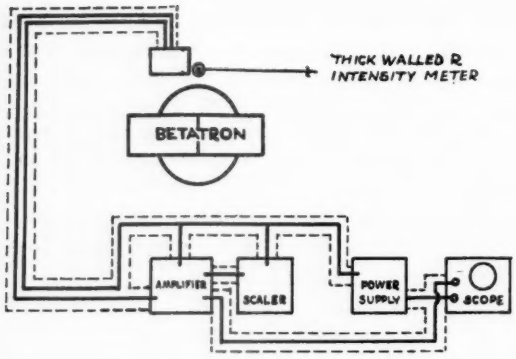

FIG. 1. Arrangement of apparatus.

fission thresholds could be determined with the betatron.

The work has proceeded along two lines: the improvement in the particular detection techniques required for handling the various uranium isotopes and the improvement of the absolute calibration of the betatron's x-rays. A new chamber principle was employed to reduce the alpha-background by self-cancellation in samples whose alpha-activity was so high that it would have masked the fission pulses in an ordinary chamber.

The first check of the energy calibration of the betatron which was obtained from voltage measurements was made with the photo-neutron threshold in nitrogen. Mass data allowed an accurate calculation of the nitrogen (γ, n) threshold.

APPARATUS

Figure 1 shows the general experimental arrangement in front of the 20-Mev betatron. The chamber containing the sample was placed directly in the cone-shaped x-ray beam which proceeds from the betatron. The half-angle of this cone is approximately $\theta = 171/E$, where θ is in degrees and E in Mev. Because of the width of the beam at the photo-fission thresholds at 5 Mev, the chamber and the Victoreen R-meter were completely covered with roughly the same x-ray intensity when placed at a distance of 70 centimeters from the target. The x-ray intensity at 5 Mev was 1 R/min. at the chamber position.

TABLE II. Summarized data for depleted uranium sample (Fig. 3).

Peak spectrum energy (Mev)	Total number of fission pulses	Total x-ray intensity R units	Total observation time (min.)	Fission counts per R	R.m.s.[a] deviation in counts/R
4.81	11	28.75	180	0.38	
4.88	9	36.70	210	0.25	
5.04	11	47.10	240	0.24	
5.20	78	54.05	255	1.44	
5.35	161	53.25	240	3.02	
5.51	390	66.40	270	5.87	
5.67	692	63.55	240	10.89	
5.84	1139	63.90	240	17.99	
6.00	1086	44.55	150	24.40	
6.16	1447	48.25	150	29.99	
6.33	1605	40.15	120	40.01	
6.49	2136	48.45	135	44.09	
6.66	2280	43.70	113	52.08	
6.82	2390	37.60	90	63.57	

[a] The data books containing the information for column 6 were not available at the time of this writing.

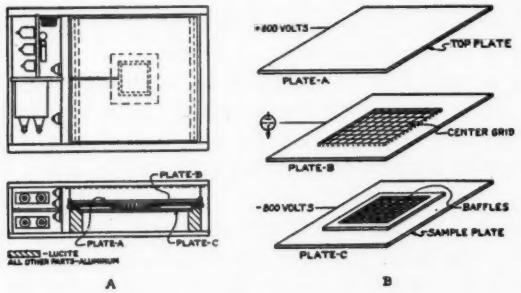

FIG. 2. Cancellation chamber. The alpha-particles from the sample of plate C are caused by proper collimation to traverse both chambers and to produce self-cancelling voltage pulses. Ideally, no alpha-particle voltage pulse is transmitted to the amplifier grid connected to plate B. On the other hand, the shorter range fission fragments produce voltage pulses across plates B and C and are registered by the linear amplifier-scaler counting circuits.

The chamber with a built-in preamplifier was connected by means of a 50-foot shielded cable to a fast amplifier, a discriminator and a Higginbotham type of scaling circuit. The amplification of the amplifier was comparatively constant at roughly 105 up to a high frequency cut-off at 700 kilocycles per second.[6] The input time constant was 5 microseconds. Although low frequency pick-ups from sources such as the betatron power frequency of 180 cycle per second were entirely eliminated, a high frequency signal disturbance was observed due to the betatron electron injection pulse whose fundamental frequency was about 10^5 cycles per second. A grounded Faraday screen shield between the injection circuit and the chamber almost entirely eliminated this stray effect.

The preliminary work for the investigation was done

TABLE III. Summarized data for enriched uranium sample (Fig. 4).

Peak spectrum energy (Mev)	Total number of fission pulses	Total x-ray intensity R units	Total observation time (min.)	Fission counts per R	R.m.s.[a] deviation in counts/R
4.99	6	28.70	135	0.21	
5.07	5	36.67	178	0.13	
5.16	8	42.26	195	0.19	
5.25	8	39.93	180	0.20	
5.32	29	44.85	193	0.65	
5.41	49	42.60	190	1.15	
5.49	71	47.96	195	1.48	
5.64	134	45.98	180	2.92	
5.81	270	47.90	179	5.64	
5.98	353	45.45	160	7.74	
6.44	536	31.44	100	16.99	
6.93	1253	38.06	110	32.94	
7.43	1790	37.09	100	47.26	
8.48	3644	33.23	70	109.42	

[a] The data books containing the information for column 6 were not available at the time of this writing.

[6] Mr. T. Brill designed the amplifier circuits used in this work, and a great indebtedness is owed him for his suggestions.

with both a fast and a slow amplifier using an ordinary parallel plate ionization chamber. The fissionable material was coated on both inner sides of the chamber plates. Fission pulses as well as alpha-particle pulses could be detected by means of a linear amplifier and an oscilloscope when 1000 volts d.c. was applied to the chamber plates. The fission pulse height was at least 4 times the pulse heights due to alpha-particles obtained from an ordinary uranium sample. However, from a highly alpha-active source, many alpha-particles are emitted into the chamber simultaneously; thus they pile up and make fission pulses undetectable with the high alpha-background. Two of the isotopes used in our experiment, $_{94}Pu^{239}$ and $_{92}U^{233}$, have a high alpha-decay rate. In order to allow the use of ordinary surface densities of these two isotopes and thereby maintain a given sensitivity, a special chamber was developed which reduced the alpha-pulse heights by self-cancellation.

This chamber schematically shown in Fig. 2 consisted of three plates, *A*, *B*, and *C*, where *A* and *C* were run at positive and negative 800 volts respectively, while *B* was connected to the grid of the first amplifier stage. Air was used in the chamber at a pressure suitable for the given investigation. The samples to be irradiated were coated on the top of plate *C* facing into the bottom chamber volume. Plate *B* was a wire mesh grid. With the addition of a baffle placed over the sample on plate *C* (see Fig. 2) all those alphas whose paths formed too small an angle with the plates of the chamber were removed. The dimensions of the baffles were so determined that most alphas which did not ionize in both chambers and which, therefore, did not produce opposing voltage pulses for self-cancellation were eliminated.

The possibility of applying the chamber to photo-fission work is due to the fact that fission ranges in general are approximately one-half the alpha-ranges for any particular isotope. Thus alphas can be partially self-cancelled with a minimum in the reduction of the fission pulse size. Special care was taken to prevent the loss of any of the fission pulses, since the pulses of fission particles entering the chamber were initially reduced in height by the baffles. The baffles were directly over the sample and were $\frac{7}{32}''$ thick, while the chamber depth, which was adjusted to equal approximately the fission range, was $\frac{13}{32}''$. Therefore, since the baffles were at the same potential as the sample plate, the first $\frac{7}{32}''$ of the fission range was below the plane of the baffle surface and was lost. This represents about $\frac{1}{3}$ of the total fission ionization produced in the chamber.

The cancellation chamber was also effective in balancing out the background x-ray burst from the betatron which is $\frac{1}{2}$ microsecond wide. The x-ray pulses occurring in the two bucked chambers are canceled as are the alpha-pulses while the fission pulses in one chamber are registered.

Plates 13×13 inches in area were first used to give as large a practical chamber as possible. Alpha-particles could be detected in spite of this large capacity. However, because of definite limitations to the available sample supplies, a 3×3 inch center plate was used and the chamber volume was limited by Lucite walls. (See Fig. 2.) A desirable increase in the signal-to-noise ratio, a reduction in microphonics, and a standardization in sample data resulted from the use of the smaller chamber.

METHOD

The preparations required for taking data with the five fissionable isotopes available differed because of the high alpha background which was present in only two of the isotopes, $_{92}U^{233}$ and $_{94}Pu^{239}$. In the experiments with $_{92}U^{235}$, $_{92}U^{238}$, and $_{90}Th^{232}$, it was possible to

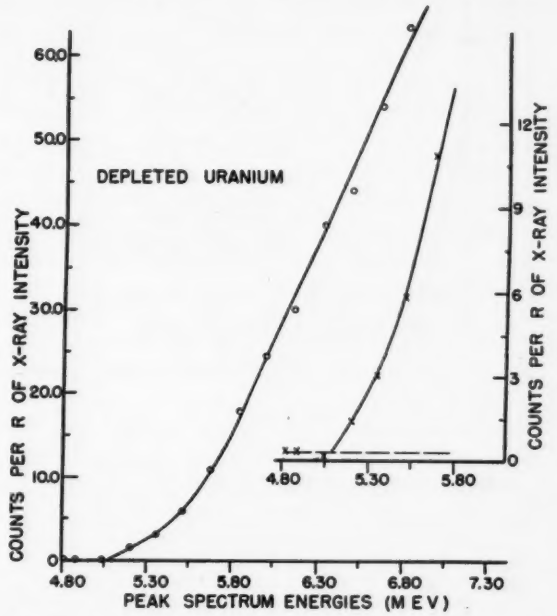

FIG. 3. $_{92}U^{238}$ experimental photo-fission threshold curve. The fission activities in terms of fission counts per *R* units of x-ray intensity are plotted as a function of the peak energy of the betatron x-ray spectrum. The background count level is shown by the dotted line.

disregard the alpha-cancellation technique and to replace the wire mesh grid of plate *B* in Fig. 2B by a solid plate. This permitted samples to be coated on both plates by forming the bottom chamber, i.e., plates *B* and *C*, and doubled the effective sample size, while still retaining the x-ray concellation.

The general arrangement as shown in Fig. 1 was to place the cancellation chamber containing the sample at a distance of approximately 75 centimeters from the betatron target and directly in the cone of x-rays issuing from the target. A Victoreen *R*-meter was placed in a 4 centimeter thick Bakelite container and was located close to the chamber in order to monitor the x-ray intensity. The procedure for taking data consisted in counting the number of fissions per roentgen

for each energy setting. The energy scale investigated was covered in successive steps resulting in sets of curves, which were averaged to give the completed data curves in Figs. 3–7.

No individual point was taken for more than a 30-minute period. Six or seven traversals of the energy scale were required to complete the data with a total x-ray intensity of approximately 40*R* at each energy setting. A given experimental arrangement was used for continuous running periods of three days or more, and a complete energy calibration was made for each three-day set of data.

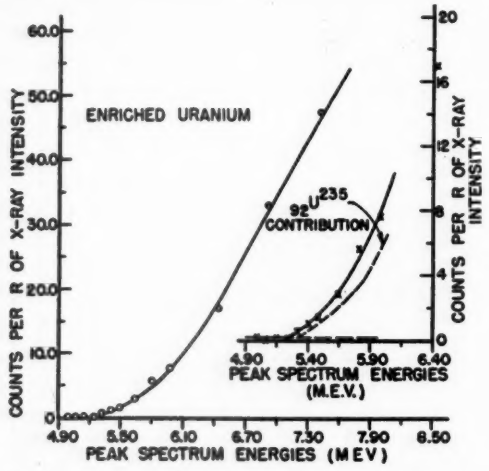
ENRICHED URANIUM
92U235 CONTRIBUTION
COUNTS PER R OF X-RAY INTENSITY
PEAK SPECTRUM ENERGIES (M.E.V.)
4.90 5.40 5.90 6.40
4.90 5.50 6.10 6.70 7.30 7.90 8.50

FIG. 4. $_{92}U^{235}$ experimental photo-fission threshold curve.

The only changes in procedure for the $_{94}Pu^{239}$ and $_{92}U^{233}$ concern the preparation of the chamber for alpha-cancellation. The general technique of observing fissions with these isotopes was facilitated by the use of a 100 milligram Ra-Be neutron source. By observing the ratio of fission pulse height to alpha-pulse height, it was possible to determine the optimum conditions for two of the variables—the chamber pressure and the amount of sample baffling. The best combination of chamber voltages and spacing, the only other variables, were determined from the tolerable degree of the residual alpha- and x-ray pulse heights after self-cancellation.

An air pressure of 30 centimeters of Hg was found to give the best fission height to alpha-noise ratio. Since the bottom chamber was 1.2 centimeters deep, these neutron data proved that much of the fission ionization was expended in the thickness of the sample and in the protective sample coatings.

Additional data taken with the neutron source showed the degree of baffling required by each sample. The $_{94}Pu^{239}$ sample required the most complete alpha-cancellation and hence the greatest reduction in the effective sample size. The transmission of the $_{94}Pu^{239}$ baffle was 0.006. This was determined by counting the number of fissions which occurred in the chamber with a $_{92}U^{235}$ sample exposed to neutrons. Runs were made with and without the sample baffle.

Similarly, neutron fission tests on $_{92}U^{233}$ showed that a smaller amount of baffling than required with $_{94}Pu^{239}$ could be used. The $_{92}U^{233}$ baffle produced a reduction in the effective sample weight to 1 percent of the actual weight.

A further decrease in the amount of baffling used on either sample gave an intolerable rise in the alpha-noise background. However, increased baffling produced little effect.

The x-ray cancellation data required that the distance between the top of the baffle and the center grid, as well as the top chamber distance, should be approximately similar and equal to 1.2 centimeters. With these interplate spacings, the baffles in the chamber and 30 centimeters of air pressure, tests were made on alpha-cancellation. Data on the alpha-background height were obtained by keeping the top chamber positive voltage fixed and varying the bottom chamber minus voltage. The cancelled alpha-noise height was then plotted as a function of the negative voltage and a minimum was observed. This minimum represented a reduction of 38 percent in the general alpha-level and was obtained with approximately 800 volts positive and negative on the two chambers. With a smoother control of the chamber spacings and, in general, a better chamber design, more complete alpha-cancellation should be possible.

RESULTS

The data in Tables II–VI were taken with each of the isotopes in turn. Emphasis was placed on an attempt to determine the relative values of the thresholds. Therefore, pairs of isotopes were run in quick succession with a given experimental set-up. This will be noted in the individual isotope discussions.

In the data tables are listed the number of fissions detected at each betatron energy setting normalized to a unit of x-ray intensity measured in *R*. These have been plotted in Figs. 3–7.

$_{92}U^{238}$ AND $_{92}U^{235}$

The $_{92}U^{238}$, or depleted sample, was depleted of $_{92}U^{235}$. It was coated on two plates[7] with a total area of 99 square centimeters.

The $_{92}U^{235}$, or enriched sample, was enriched in 235 with a 238/235 ratio of 1/4.95. Both the 238 and 235 samples had protective Zapon coating with a surface density of 0.1 mg/cm^2.

The data for $_{92}U^{238}$ and $_{92}U^{235}$ are given in Table II and III and are plotted in Figs. 3 and 4 as fission counts per *R* as a function of peak spectrum energies. Both sets of data were taken in succession with the same experimental set-up to assure a certainty in the relative energy values. On the plots are drawn the uncertainties

[7] The sample plates used in this experiment were coated by Mr. H. Hufford and Mr. D. C. Stewart of Dr. Cunningham's group at the Metallurgical Laboratory, University of Chicago. All the sample data were supplied by them.

in the experimental points. These uncertainties are the r.m.s. deviations listed in the last columns of Tables II–V. They were obtained from the actual spread in the experimental data obtained at each energy value. The statistical fluctuations were not calculated since the observed deviations should have included the statistical errors plus any other errors present. A dotted line has been drawn on the plots representing the natural background level, which was found experimentally. This background is due to counts produced by a coincidence of several alpha-pulses and also due to counts of the spontaneous fissions in the samples.

The thresholds as read from the curves in Figs. 3 and 4 are 5.08(±0.08) and 5.25(±0.10) for the depleted and enriched samples respectively. Note that the enriched sample threshold is well defined and does not show the presence of the $_{92}U^{238}$. This indicates some lack of definition. The estimated error represents the maximum possible reading error in the threshold and takes account of the uncertainties in the data for each energy value but does not include the errors in the energy scale. To the estimated reading errors must be added an r.m.s. error in the energy calibration.

Figure 4 shows a dotted curve obtained by subtracting 1/5.95 of the $_{92}U^{238}$ curve in Fig. 3 after a suitable correction for the difference in sample weights was made. The threshold obtained from the dotted curve is 5.31 Mev and this value is taken as the threshold for $_{92}U^{235}$.

Therefore, the threshold energies are:

$$E_t(_{92}U^{238}) = 5.08(\pm 0.15) \text{ Mev}$$
$$E_t(_{92}U^{235}) = 5.31(\pm 0.25) \text{ Mev.}$$

This shows that the $_{92}U^{235}$ threshold is 0.23 (±0.10) Mev higher than the $_{92}U^{238}$ value.

$_{94}Pu^{239}$

The $_{94}Pu^{239}$ sample was coated on an area of 58 square centimeters. The product was deposited in the form of $(NH_4)_2PuF_4$. A coating of Zapon protected the $_{94}Pu^{239}$ and had a density of 0.12 mg/cm².

The data for $_{94}Pu^{239}$ in Table IV are plotted in Fig. 5. A $_{92}U^{238}$ curve run in succession with the $_{94}Pu^{239}$ showed that the difference energy between the $_{94}Pu^{239}$ and $_{92}U^{238}$ thresholds is +0.23(±0.12) Mev. This fixed the $_{94}Pu^{239}$ threshold energy at 5.31(±0.27) Mev and determined the energy scale used in the plot of Fig. 5.

$_{92}U^{233}$

The $_{92}U^{233}$ sample was prepared in a like manner to the $_{94}Pu^{239}$. It was deposited as the ammonium fluoride. The protective Zapon coating had a surface density of 0.1 mg/cm².

Table V contains the $_{92}U^{233}$ photo-fission data. The plot of these values in Fig. 6 shows a threshold energy of 5.18(±0.27) Mev. The uncertainty in this energy was produced by the small number of experimental points and by the variable background. Time did not permit taking more complete data.

The difference energy found between the $_{92}U^{233}$ and a $_{92}U^{238}$ data curve taken in succession was +0.10(±0.12) Mev.

$_{90}Th^{232}$

The thorium sample was in the form of the oxide applied finely ground in an alcohol solution to the chamber plates. A thickness greater than the range of the fissions in the oxide was coated onto a total chamber area of 116 square centimeters.

The thorium data are listed in Table VI and plotted in Fig. 7. A set of $_{92}U^{238}$ data not shown, the $_{92}U^{233}$ data given above, and the thorium data were obtained in close succession. The threshold energy for $_{90}Th^{232}$ was found to be 5.40(±0.22) Mev. The $_{90}Th^{232}$ and $_{92}U^{238}$ threshold energy difference is +0.32(±0.07) Mev. This difference energy is to be compared with the value of +0.45 Mev obtained in 1944.[5]

A collection of the completed data of this photo-fission experiment, together with the thresholds predicted by Frankel and Metropolis[3] is shown in Table VII.

The errors associated with each difference energy of column 4 are the maximum limits to the errors in the experimental data and graphical plots. The errors assigned to the absolute energy values of column 2 are the sums of the errors in the $_{92}U^{238}$ calibration standard and of the errors in column 3. These errors again represent what are felt to be the maximum limits of the possible inaccuracies in the absolute photo-fission thresholds.

ENERGY CALIBRATION OF THE BETATRON

The spectrum of x-rays from the betatron is continuous up to a maximum energy determined by the accelerated electron energy at the time of the electron collisions with a target in the betatron. The calibration of this maximum spectrum energy as a function of betatron control panel settings permits the determina-

TABLE IV. Summarized data for $_{94}Pu^{239}$ (Fig. 5).

Peak spectrum energy (Mev)	Total number of fission pulses	Total x-ray intensity R units	Total observation time (min.)	Fission counts per R	R.m.s. deviation in counts/R
4.93	1	14.2	50	0.07	0.02
5.09	6	58.1	180	0.10	0.04
5.26	3	58.2	180	0.05	0.05
5.43	13	72.4	210	0.18	0.13
5.60	17	76.7	210	0.22	0.18
5.76	28	76.7	209	0.36	0.16
5.93	42	83.2	210	0.51	0.25
6.10	53	79.3	185	0.67	0.24
6.27	47	67.5	150	0.70	0.17
6.41	71	81.4	165	0.87	0.25
6.57	87	61.2	120	1.42	0.24
6.74	74	47.6	90	1.55	0.53
6.87	129	66.5	120	1.94	0.58
7.05	124	43.0	75	2.88	0.91
7.21	147	54.5	90	2.70	0.63

tion from excitation curves of threshold energies for gamma-processes.

The calibration has been accomplished by measuring directly the electron Hr values at the time of target collision and hence their kinetic energy by $T=3\times10^{-4}$ Hr-0.5 Mev. The magnetic field at the target position is measured by the difference voltage between two concentric coils which are placed accurately at radii 0.1 in. on either side of the target radius. The magnetic field, and from this the energy of the electrons, was determined as a function of betatron control panel settings.

The remaining portion of the calibration, aside from voltage measurements, concerns the selection of betatron energies, or the maximum spectrum energies. An energy selector originally designed by Dr. G. C. Baldwin was somewhat redesigned and completely rebuilt in order to increase the stability of an energy setting. The basis of the circuit is a trigger pair which fires at a predetermined input voltage. The electron collision with a target is timed by the output triggered pulse. Energy selections can be made in 100 kilovolt steps with a constancy accurate to at least ±20 kilovolts in the energy selector.

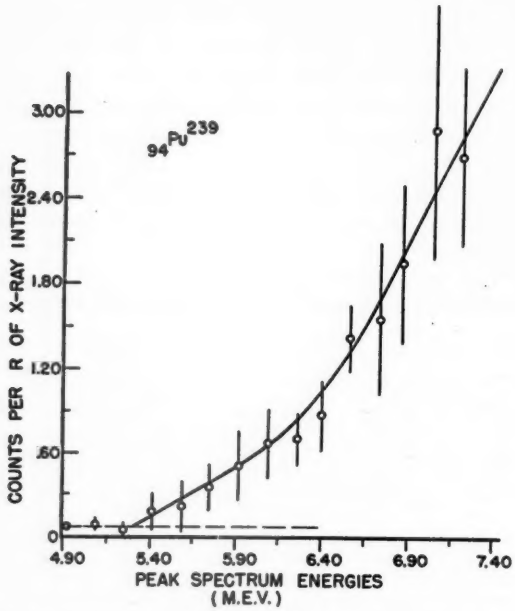

FIG. 5. $_{94}Pu^{239}$ experimental photo-fission threshold curve. The experimental r.m.s. deviations in the fission activities are plotted with each point.

An estimation of the maximum r.m.s. error to be expected in an energy value was made by considering the experimental r.m.s. deviations in each of the quantities appearing in the calibration. Errors other than that introduced by the difference voltage coils used for measuring the magnetic field lead to an estimated rms error of ±0.6 percent. This indicates the accuracy possible in the ability to reproduce energy setting; i.e., relative energy values should be accurate to ±0.6 percent.

TABLE V. Summarized data for $_{92}U^{233}$ sample (Fig. 6).

Peak spectrum energy (Mev)	Total number of fission pulses	Total x-ray intensity R units	Total observation time (min.)	Fission counts per R	R.m.s. deviation in counts/R
4.93	3	34.2	105	0.09	0.10
5.10	5	41.8	120	0.12	0.14
5.17	7	39.2	120	0.18	0.12
5.26	10	44.5	120	0.23	0.09
5.35	22	56.5	150	0.39	0.23
5.43	20	55.9	144	0.36	0.19
5.60	30	48.2	116	0.62	0.36
5.77	20	29.4	60	0.68	0.09
6.41	46	19.5	35	2.36	0.71

The absolute value of the energy readings are limited, however, by the skill with which the difference coils were machined and the care with which the measuring "coils" of silver paint were coated. The r.m.s. error here introduced to the absolute energy values will be less than 2 percent. Therefore, the total r.m.s. error in the absolute value of any energy setting has been estimated to be ±2.6 percent.

In a paper by Baldwin and Koch[4] it was suggested that the (γ, n) threshold in nitrogen could be used as a check on the betatron energy calibration obtained from voltage measurements. However, the positron intensities resulting from the photo-neutron processes were found at that time to be too small to give the desired accuracy.

Greater intensities by a factor of 17 were obtained in the present experiment. This was made possible by improved sample holders and positron counters, and by increased x-ray intensities at the sample position during irradiation.

The counter was a thin-walled aluminum counter. It was constructed at the Metallurgical Laboratory to have an aluminum cylindrical wall 0.011 centimeter

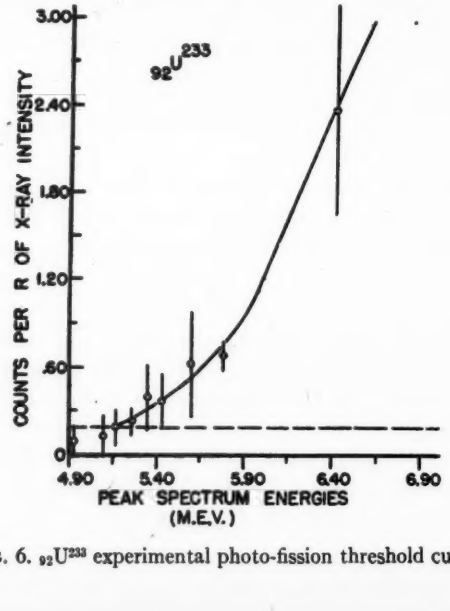

FIG. 6. $_{92}U^{233}$ experimental photo-fission threshold curve.

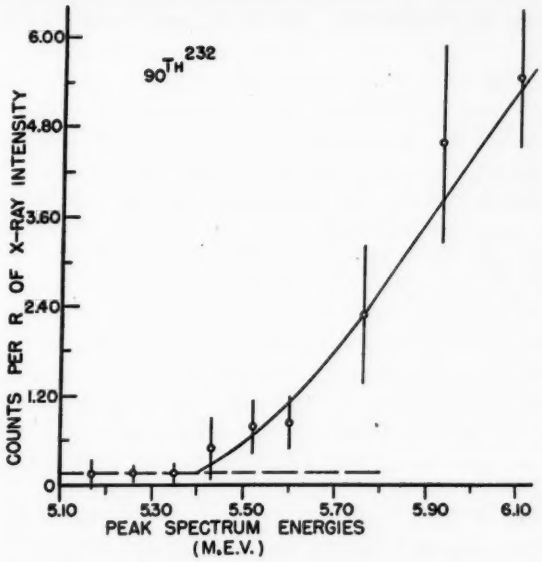

FIG. 7. $_{90}Th^{232}$ experimental photo-fission threshold curve.

thick, a 2.22-centimeter diameter, and a 12-centimeter length. A test with a 5-mg radium source proved the sensitive area to the 8 centimeters long.

The nitrogeneous material used was dicyandiamide ($C_2N_4H_4$). Approximately 60 grams of the powder filled the space between two concentric cylinders. The inner cylinder consisted of Cellophane, 0.025 centimeter thick, supported by Bakelite supports. The sample holder was 12 centimeters long and the annular section of $C_2N_4H_4$ was 0.72 centimeter thick. The material of which the sample holder was constructed was purposely made non-metallic so that it could be placed in the betatron alternating magnetic field and as close as 35 centimeters from the x-ray target. Three samples were prepared to allow alternate use, thus decreasing the possibility of residual activity.

The irradiation procedure was similar to that in the photo-neutron work.[4] A sample in its holder was irradiated in the x-ray beam for 10 minutes. Removal of the sample to a counter then followed, and the counting rates were studied. Data were obtained at successive betatron energies.

Figure 8 shows a decay curve of activity resulting from a 10-minute irradiation at a peak spectrum energy of 12.1 Mev. The half-life determined from Fig. 8 is 10.0(±0.3) minutes. This checks the half-life 9.93(±0.03) minutes found by Ward.[8] The decay curve shows no evidence of any other activity, which makes the comparatively low nitrogen threshold a satisfactory one for investigation.

TABLE VI. Summarized data for $_{90}Th^{232}$ sample (Fig. 7).

Peak spectrum energy (Mev)	Total number of fission pulses	Total x-ray intensity R units	Total observation time (min.)	Fission counts per R	R.m.s. deviation in counts/R
5.17	12	75.3	180	0.16	0.19
5.26	12	76.6	180	0.16	0.09
5.35	15	82.8	180	0.18	0.13
5.43	42	83.9	180	0.50	0.41
5.52	66	85.9	180	0.77	0.35
5.60	77	91.7	180	0.84	0.35
5.76	219	95.7	180	2.29	0.92
5.93	464	100.7	180	4.62	1.30
6.10	547	100.2	180	5.50	0.94

TABLE VII. Collection of data.

Sample	Photo-fission threshold (Mev)	Isotope threshold $-_{92}U^{238}$ threshold (difference energy) (Mev)	Theoretical[13] threshold energies (Mev)
$_{92}U^{238}$	5.08(±0.15)	0.00(±0.08)	7.0
$_{92}U^{235}$	5.31(±0.25)	+0.23(±0.10)	6.1
$_{94}Pu^{239}$	5.31(±0.27)	+0.23(±0.12)	4.9
$_{92}U^{233}$	5.18(±0.27)	+0.10(±0.12)	5.7
$_{90}Th^{232}$	5.40(±0.22)	+0.32(±0.07)	

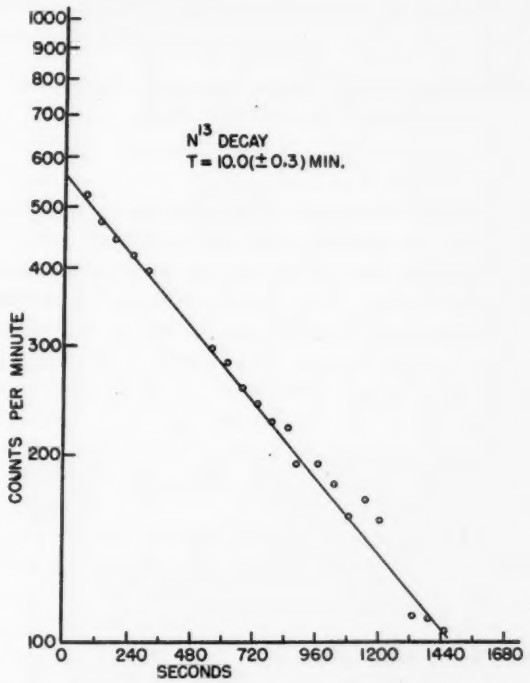

FIG. 8. Decay curve resulting from a 10-minute irradiation of a nitrogen sample at a peak betatron spectrum energy of 12.1 Mev.

In Fig. 9 is plotted the 10-minute counting totals corrected to an irradiation of 200R. The energy scale was calculated from voltage measurements. The threshold is seen to be 10.34(±0.25) Mev. The estimated error includes the graphical reading error added to the estimated r.m.s. error in the energy calibration.

For comparison, the (γ, n) threshold can be calculated from the following mass data:

$$M(_6C^{13}) = 13.00751 \pm 0.00010$$
$$M(_0n^1) = 1.00893 \pm 0.00003$$
$$2\ mc^2 = 0.00110$$
$$M(_7N^{14}) = 14.00751 \pm 0.00004$$
$$E_e^+ = 1.20 \pm 0.02\ \text{Mev}.$$

[8] A. G. Ward, Proc. Camb. Phil. Soc. **35**, 523 (1939).

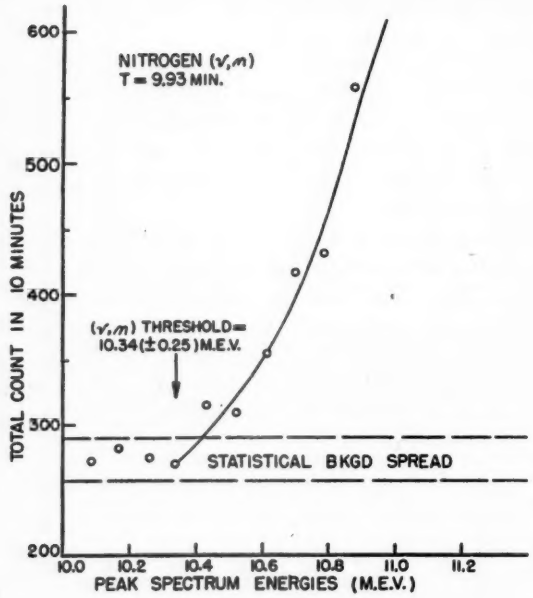

FIG. 9. $_7N^{14}(\gamma, n)$ threshold curve.

The expected photo-neutron threshold is 10.54(±0.06) Mev. Thus the voltage calibration method and the mass threshold calculation are in agreement within experimental error. The discrepancy of 1.9 percent which does exist is believed due to the error discussed above in the dimensions of the magnetic field measuring coils. It was thought justifiable to make this same percentage correction in the energy scale near the photo-fission threshold at 5 Mev. This procedure has been applied to all the energy values which have been reported in this paper.

The experimental thresholds determined are not in agreement with theory. From this investigation the photo-fission threshold values for $_{92}U^{238}$, $_{92}U^{235}$, $_{94}Pu^{239}$, and $_{92}U^{233}$ show a maximum difference or spread of 0.23 Mev, whereas the theory predicts a spread of 1.7 Mev. Also, the order of the experimental thresholds is not the same as the predicted order. Emphasis was placed on determining this order as accurately as was possible. For this reason, all the isotopes were referred to the $_{92}U^{238}$ threshold and were investigated in succession with $_{92}U^{238}$. The thresholds of $_{92}U^{235}$, $_{92}U^{238}$, and $_{90}Th^{232}$ were determined most accurately (see column 3 of Table VII). According to theory the $_{92}U^{238}$ threshold should be larger than the $_{92}U^{235}$ threshold by approximately 0.6 Mev. The experiment showed definitely that the order is reversed with the $_{92}U^{235}$ threshold the larger one by 0.23(±0.10) Mev. The orders of the experimental thresholds for $_{94}Pu^{239}$ and $_{92}U^{233}$ are also not in agreement with theory.

The fact that the thresholds are spread over such a small energy band raised the question of the influence of fissions induced by neutrons. The evidence found was not discussed because the data books containing specific data were not available at the time of this writing. However, general comments can be made. The number of fission counts at a particular betatron energy setting was determined as a function of different experimental conditions. The tests made were:

(1) Ionization chamber containing a fission sample was surrounded by 5 in. of paraffin.
(2) Same as (1) with $\frac{1}{32}$ in. of cadmium sheet interposed between chamber and paraffin.
(3) Ionization chamber was placed at the 0° and 15° positions with respect to the axis of the x-ray beam.

Neither the paraffin nor the paraffin plus cadmium appreciably changed the number of fissions counted. Also, the number of fissions was reduced in test number 3 by moving from the 0° position to the 15° position, but this fall-off can be explained by the decrease in the x-ray intensity at the 15° position. Because of these three tests it was concluded that the fissions counted in this experiment were principally produced by x-rays and not by neutrons.

ACKNOWLEDGMENT

The authors take pleasure in thanking Dr. Sidney Dancoff for his kind interest and invaluable assistance. They are also indebted to the members of the Chicago Metallurgical Laboratory for their cooperation.

Multiple Production of Mesons

PHYLLIS FREIER AND E. P. NEY
Physics Department, University of Minnesota, Minneapolis, Minnesota
(Received October 13, 1949)

Cloud-chamber photographs and photographic emulsion events have been obtained which are interpreted in terms of multiple meson production. In some cases it can be shown by charge conservation and penetration of lead that a large number of the particles in hard showers are not nucleons or electrons. The results are compared with the predictions of Heisenberg and Leprince-Ringuet. By comparing the interactions in carbon and lead one is led to the conclusion that mesons are made at 55° geomagnetic latitude with an average multiplicity of about five by protons of average energy about 8 Bev.

THE generation of penetrating showers in lead was first observed by Fussel[1] and later reported by a number of other observers. In some cases it has been possible to show that one or more of the particles produced in such showers are mesons.[2,3] Recently photographic emulsion experiments[4,5*] have shown that, in energetic nuclear interactions, forward direction showers are produced and the particles in these showers are believed to be mesons. In one case,[5] the number of particles was great enough to make certain that at least several of the particles were either mesons or electrons. In cloud-chamber experiments, it is difficult to determine the number of mesons because the showers usually take place in lead and, consequently, the particles could all be nucleons (in the absence of mass determinations of individual particles). In the photographic emulsion, the difficulty of observing multiplication of electrons together with the uncertainty about the absorbing nucleus has made the results ambiguous.

An example of a shower containing penetrating particles is shown in Fig. 1. It was obtained in a balloon flight at a geomagnetic latitude of 55°. The residual pressure at which the cloud-chamber picture was taken was 1.7 cm of mercury. The top plate of the cloud chamber is $\frac{1}{4}$-in. carbon, the others are $\frac{1}{4}$-in. lead plates. The shower is associated with a star in the second (lead) plate and contains about 30 particles most of which penetrate the next lead plate. Two small electron showers originate in the plate below the one in which the interaction takes place. These showers seem to point to an origin in the gas between the plates and, although their energy and angle are consistent with neutral meson decay, turbulence in the cloud chamber makes this conclusion uncertain. The association of electrons with penetrating particles in nuclear interactions has been previously reported[6] and seems well established.

Figure 2 shows a photograph of a particle entering the carbon plate (top plate) and producing an interaction in which 13 charged particles come out. The ionization of the incident particle is estimated to be between 1.5 and 3 times minimum. It could not, therefore, be an incident α-particle. The charge of the incident particle plus the atomic number of carbon is seven, so at least six of the emerging particles must be

TABLE I. Multiplicity and average angle of hard showers.

Material	Average number of particles emerging	Average projected angle within which all of the particles are contained	Average projected angle within which half of the particles are contained
Carbon	6.8±2.0	56°	24°
Lucite	5.5±2.0	38°	15°
Lead	10.1±1.7	52°	16°

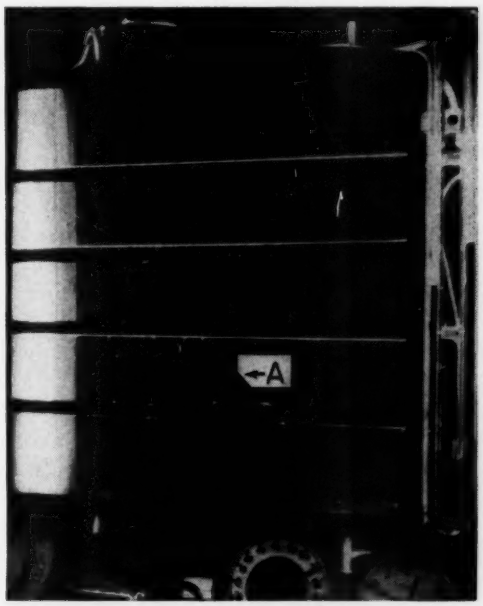

FIG. 1. A penetrating shower produced at a residual pressure of 1.7 cm mercury. This event has associated electrons and star particles. The ionization and scattering of particle *A* led us to believe that it is a meson.

[1] Reported by H. Euler and W. Heisenberg, Ergeb. d. exak. Naturwiss. **17**, 1 (1938).
[2] Rochester, Butler, and Runcorn, Nature **159**, 227 (1947).
[3] W. M. Powell, Phys. Rev. **69**, 385 (1946).
[4] J. Hornbostel and E. O. Salant, Phys. Rev. **76**, 859 (1949).
[5] Leprince-Ringuet, Bousser, Tchang-Fong, Jauneau, and Morellet, Comptes Rendus **229**, 163 (1949).
* It has just come to our attention that Kaplon, Peters, and Bradt have also obtained photographic emulsion data bearing on this question.
[6] W. B. Fretter, Phys. Rev. **73**, 41 (1948).

mesons or electrons. Although all of the particles cannot be followed through the next lead plate, of the nine that can be followed, none produce electron showers. The conclusion can be drawn that at least three and probably more than six of the particles emerging are mesons. It is interesting to note that the particles come out in groups which may be the result of several nucleon-nucleon interactions. The fact that the ionization of the incident particle is above minimum is believed to be due to the relativistic increase of energy loss at very high energies. Two carbon and two Lucite

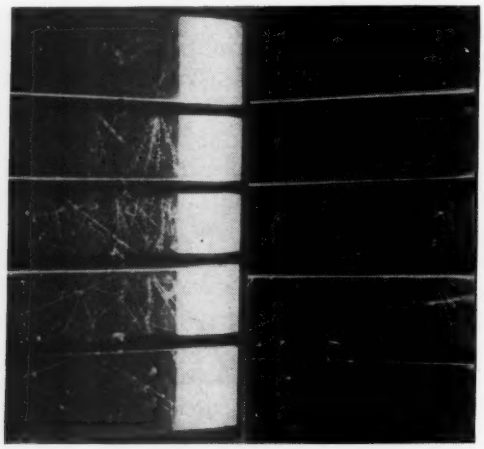

FIG. 2. Right and left stereophotographs of a carbon interaction in which a particle enters the carbon plate and 13 charged particles come out of the interaction. The electron shower which crosses in front at an angle of about 45° is unrelated to the event.

interactions have been observed giving rise to at least 13, 11, 7, and 10 particles, respectively. No cascade multiplication was observed in any of these cases. The Lucite interactions took place in the top of the cloud chamber which is constructed of plastic.

Because the carbon interactions demonstrate that mesons can be made in groups, the cloud-chamber interactions in which narrow groups of particles come out were compared in lead, Lucite, and carbon. Table I shows the results, based on six carbon, four Lucite, and 32 lead interactions.

Because of the difficulty of deciding which events to include and because of the rather poor statistics, these figures should be considered tentative.

Leprince-Ringuet[7] and Heisenberg[8] have considered the dynamics of meson production. Leprince-Ringuet considers the case in which the mesons are all emitted with the same energy in the center-of-mass system of the nucleons, and Heisenberg has assumed an energy spectrum of emitted mesons in the center-of-mass system of the form

$$dI = a dK_0/K_0, \qquad (1)$$

where dI is the number of mesons emitted with energies

[7] Peyrou, d'Espagnat, and Leprince-Ringuet, Comptes Rendus 228, 1777 (1949).
[8] W. Heisenberg, Nature 164, 67 (1949).

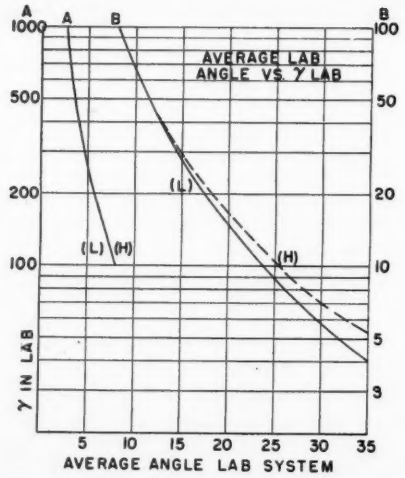

FIG. 3. The average proton γ_L for production of mesons with the indicated average angle.

between K_0 and K_0+dK_0. Both theories assume that the mesons are emitted symmetrically in the center-of-mass system of the nucleons. We will use the following notation to present their theory for comparison with experiment. We will also assume that the mesons produced are π-mesons.

ψ = angle in the lab system of a given meson with respect to the direction of the incident nucleon.
ψ_{max} = maximum value of ψ.
$\bar{\psi}$ = angle within which half the mesons are contained.
β_1 = average v/c of the meson in the center-of-mass system.
n = total number of mesons produced.
$1/k$ = fraction of kinetic energy in the center-of-mass system used in making mesons.
$\beta = v/c$ of nucleon in the center-of-mass system.
$\gamma = (1-\beta^2)^{-\frac{1}{2}}$.
$\gamma_1 = (1-\beta_1^2)^{-\frac{1}{2}}$.
$\gamma_L = \gamma$ of the nucleon in the lab system.
r = ratio of rest mass energy of meson to rest mass energy of proton.

The two theories will be identified by (L) and (H).

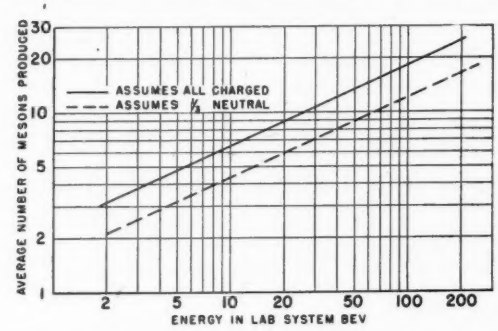

FIG. 4. The average number of mesons produced in a nucleon-nucleon encounter according to Heisenberg.

THE ANGULAR DISTRIBUTION OF MESONS

(L) $\tan\bar{\psi}=\beta_1/\beta\gamma$ (2a)

(L) $\sin\psi_{max}=\beta_1\gamma_1/\beta\gamma$ (2b)

(H) $\langle\cos\psi\rangle_{Av}=1-0.87/\gamma^2$. (2c)

For high energies of the primary nucleon and the emitted mesons, Eq. (2a) reduces to $\tan\bar{\psi}=1/\gamma$ and $\gamma_L\cong 2\gamma^2$. Hence, one should compare the following equations in the lab system.

(H) $\langle\cos\psi\rangle_{Av}=1-1.74/\gamma_L$ (3a)

(L) $\tan\bar{\psi}=1.41/\gamma_L{}^{\frac{1}{2}}$. (3b)

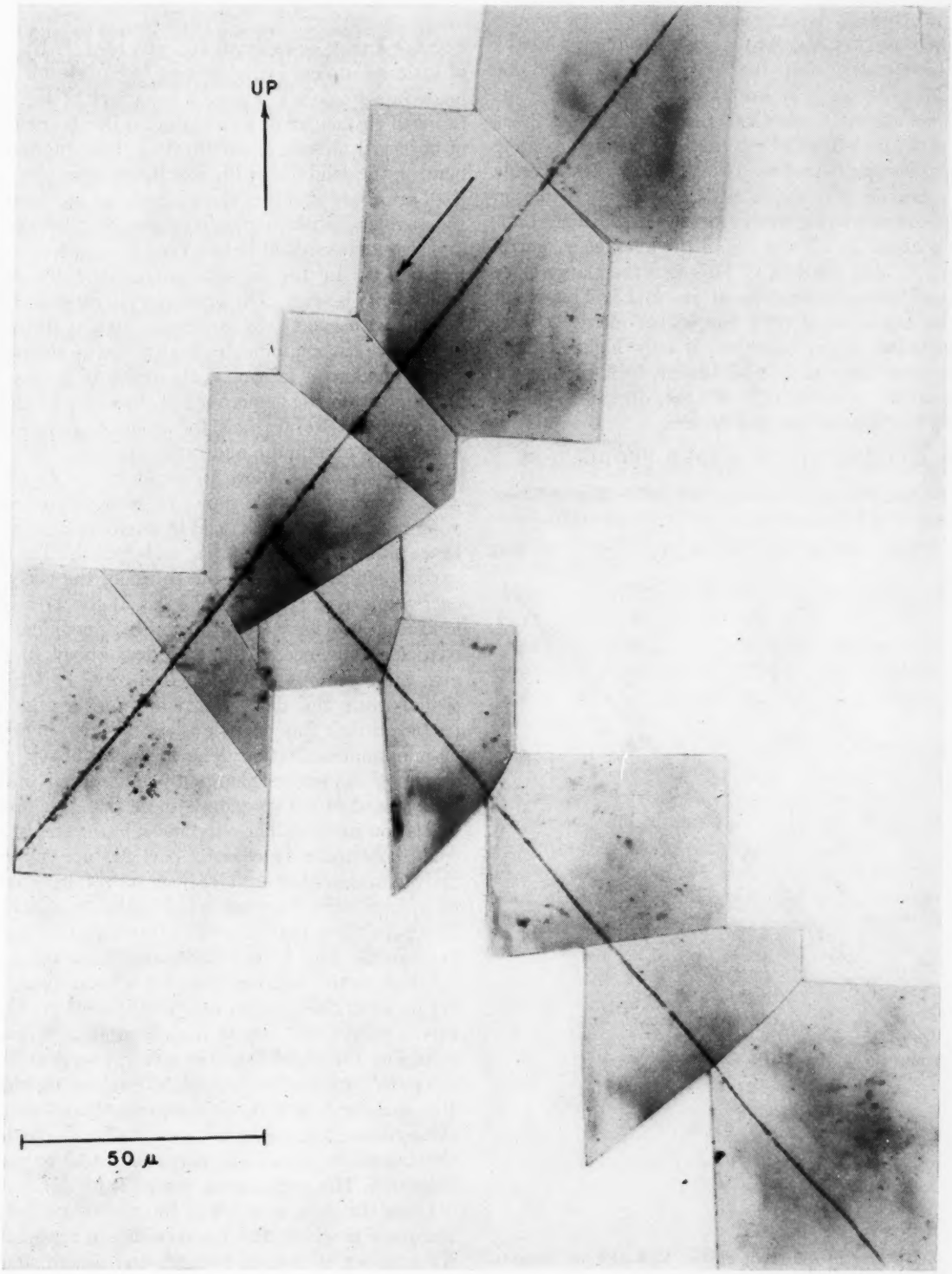

FIG. 5. Photo-micrograph of an event in which an incident carbon nucleus collides with an emulsion proton making mesons.

A graph of these functions is shown in Fig. 3 in which $\langle\cos\psi\rangle_{Av}$ is approximated by $\cos(\bar{\psi}/\sqrt{2})$. In spite of the quite different energy assumptions of (L) and (H), the angular distribution as a function of γ in both theories is essentially the same. It is probable then that the angular distribution depends to a first approximation only on the fact that the mesons are made, provided they are emitted with spherical symmetry in the center-of-mass system. The angles given in Table I vary considerably, but the average angles are not appreciably different in lead and carbon. This leads one to believe that the same fundamental process is going on with protons of essentially the same average energy in lead as in carbon. Using the data from Table I, we conclude that the average angle in the meson showers corresponding to the measured projected half-angles is about 25°. From Fig. 3 the average γ_L corresponding to this angle is 9. This is rather large since the cut-off γ at our latitude of 55° is 2.5. This result could be explained if only the higher energy events were included in our selection, if only higher energy protons make large groups of mesons, or if the mesons were emitted preferentially in the direction of the colliding nucleons in the rest system.

THE MULTIPLICITY OF MESON PRODUCTION

Heisenberg's theory predicts that the average number of mesons as a function of the energy is given by

$$\text{(H)} \quad n=[2(\gamma-1)/r]/\ln[2(\gamma-1)/r] \qquad (4a)$$

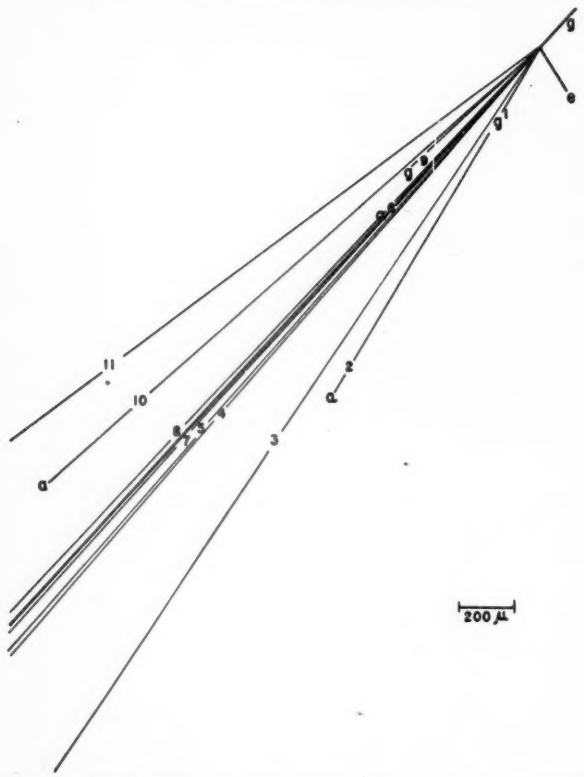

FIG. 6. Drawing of the event of Fig. 5. Angles are projected angles in the plane of the emulsion. The letters *g*, *a*, and *e* refer to the particles which leave the glass or air surface of the emulsion or end in the emulsion.

or as a function of the angle by

$$\text{(H)} \quad \langle\cos\psi\rangle_{Av}=1-8/n^2, \quad n>4. \qquad (4b)$$

According to (L), the number of mesons is directly related to the angle only when ψ is very large. For this case

$$\text{(L)} \quad \sin\psi_{max}=2/nkr. \qquad (4c)$$

Because k may be as small as 1 and $r\cong 1/7$, Eq. (4c) is of little use unless many mesons (greater than 14) are made in a single act. Figure 4 is a graph of Eq. (4a) in terms of γ_L instead of γ. The dotted line is the number of observed mesons if one-third of those produced are neutral, the solid line is the number of observed mesons if all are charged. From the γ estimated on the basis of the angular distribution, one can see that between four and six mesons should be observed in a nucleon-nucleon interaction. In the carbon interactions the average multiplicity is seven. The average of 10 mesons observed in lead with essentially the same angular distribution as those in carbon indicates that in heavy elements the larger number of mesons is the result of several interactions within the same nucleus. In order to check up on this point we are now flying cloud chambers with many lead, aluminum, and carbon plates.

Figures 5 and 6 show an event in the emulsion in which a heavy particle comes in, is associated with 11 minimum ionization particles in a narrow cone and one slow proton, and goes on undeflected. The heavy particle ionizes less after the collision, the δ-ray count decreasing by a factor of 1.5 ± 0.3. If the 11 minimum ionization tracks were protons, the incoming heavy particle would necessarily have lost about 10 Bev to give these protons the required energy. This is inconsistent with the decreased ionization of the heavy particle unless this particle is on the high energy side of minimum ionization. The incoming heavy particle does not change its charge by more than one, and, therefore, does not contribute more than one minimum ionization particle. The only nuclei in the emulsion that could contribute 11 charged particles are Ag and Br, and no stars definitely identified as resulting from Ag or Br have been observed to have only one slow particle. The possibility that there are 11 protons is, therefore, very small. The 11 minimum ionization particles are followed in this one emulsion for a total distance of 4 cm or 16 g/cm^2 without any multiplication. Although this is only about two-thirds of a radiation length in emulsion, the cloud-chamber pictures seem to rule out the possibility that such particles as these are electrons. Because the heavy particle travels almost parallel to the emulsion, the angles between the heavy particle and the minimum ionization particles could be carefully measured. The angles are given in Table II.

Using the angle in which all the mesons are contained, the angle in which half the mesons are contained, and the number of mesons formed, and assuming that in the center-of-mass system monoenergetic π-mesons are produced with angular symmetry, one can determine

TABLE II. Angles between the heavy particle and the minimum ionization particles.

1. 12° 20′	5. 55′	9. 4° 50′
2. 12° 15′	6. 8°	10. 8° 50′
3. 8° 10′	7. 20′	11. 13° 25′
4. 1° 10′	8. 20′	

the velocity of the emitted mesons, the velocity of the incoming particle, and the fraction of the kinetic energy which is used in the meson production. Such an analysis leads to the following tentative interpretation of this event.

A relativistic carbon nucleus with 60 Bev/nucleon in the lab system enters at an angle of 39° from the vertical. Its ionization is 1.3 times that of carbon at minimum ionization. One proton in the carbon collides with a hydrogen nucleus in the emulsion and they rebound after collision 180° apart in the center-of-mass system. The incoming proton of the carbon is the 5.2-Mev proton ejected after collision at 102° 30′ in the lab system. The knock-on proton is computed to be at 6′ from the heavy particle. Particle No. 8 is in the right plane but makes an angle of 20′ with the heavy particle. Ten charged mesons are produced in the collision. The remainder of the carbon nucleus goes on as B_5^{11} and can be followed for 6 g/cm² after the collision. If 10 mesons are produced in this one collision, the incoming proton loses one-third of its energy measured in the center-of-mass system.

Figure 7 shows a cloud-chamber picture in which 11 particles arise in a carbon interaction. It can be seen that this case of a proton colliding with a carbon nucleus is very similar to the angular distribution of the emitted particles to the emulsion example of an *incident carbon* nucleus colliding with a proton. In the emulsion case, of course, the residual nucleus continues in the forward direction.

CONCLUSIONS

Evidence is presented which indicates that at 55° geomagnetic latitude and 1 cm residual pressure the average multiplicity of meson production in nucleon-nucleon encounters is about five. In single nucleon-nucleon interactions as many as 10 mesons can be produced. Because hard showers produced in lead have a higher multiplicity but essentially the same angular distribution as in carbon, the larger average number of particles produced in heavy nuclei should probably be interpreted as caused by successive interactions in the same nucleus. At present the data are not detailed enough to decide about the energy distribution and angular distribution in the rest system of the mesons produced.

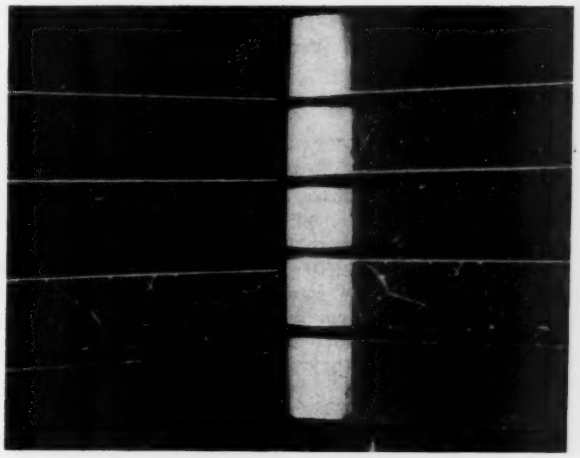

FIG. 7. Right and left stereos of a cloud-chamber photograph very similar to the emulsion event of Fig. 5 except that the carbon nucleus at rest is struck by an incident proton. The angular distribution of the mesons is quite similar to that in Figs. 5 and 6.

We wish to express our sincere appreciation to Professors C. L. Critchfield and J. T. Tate for many helpful discussions. Dr. John Nafe observed the photographic emulsion event of Figs. 5 and 6. Miss Sophie Oleksa was very helpful in examining cloud-chamber pictures.

This research was done under the partial support of the joint program of the ONR and the AEC, Contract N6onr-246. It was also materially assisted by the University of Minnesota Technical Research Fund subscribed to by General Mills, Inc., the Minneapolis Honeywell Regulator Company, the Minneapolis Star Journal and Tribune Company, the Minnesota Mining and Manufacturing Company, and the Northern States Power Company.

A Cloud-Chamber Study of Cosmic-Ray Nuclear Interactions at 3260 Meters Elevation

W. W. BROWN* AND A. S. MCKAY†
Cornell University, Ithaca, New York
(Received September 14, 1949)

In 4949 photographs of cosmic-ray phenomena, not associated with dense air showers, occurring in a counter controlled cloud chamber surrounded by lead, the numbers of nuclear interactions in which secondaries were produced and observed to occur in and above the chamber were 182 and 223, respectively. The mean free path for nuclear interaction of the penetrating particles produced in these nuclear interactions is 316 ± 70 g/cm² of lead, while for nuclear scattering (large angle scattering without the production of secondaries) it is at least 4 or 5 times this value. The projected zenith angular distributions of the secondaries from these interactions are given. The lightly ionizing secondaries going in the forward direction have an angular distribution $\sim\cos^3\theta$, while those in the backward direction from nuclear interactions occurring in the chamber have a uniform distribution.

1. INTRODUCTION

DURING the summer of 1948 a series of cloud-chamber pictures of cosmic-ray phenomena were taken at Echo Lake, Colorado (elevation 3260 meters). The various types of Geiger counter coincidences employed in the selection of these phenomena provided a means of dividing them into two main classes: (*a*) those associated with extensive air showers, and (*b*) those not associated with extensive air showers. The former class has been described in an earlier paper[1] and the latter class is the subject of the present analysis.

2. EXPERIMENTAL

The geometrical disposition of Geiger counters and absorber about the cloud chamber‡ are shown to scale in the two perpendicular sections of Fig. 1. The roof and wall thicknesses are 6 inches and 3 inches of lead respectively. The counters at X, Y, and Z, some of which are connected in pairs as indicated, have effective dimensions $\frac{1}{2}$ inch$\times$10 inches, 1 inch$\times$2.75 inches, and 1 inch$\times$16 inches, respectively. Four neon bulbs situated at S, P, C, and A indicate the type of counter coincidence causing each particular expansion and were photographed simultaneously with the cloud chamber. The photographs were non-stereoscopic.

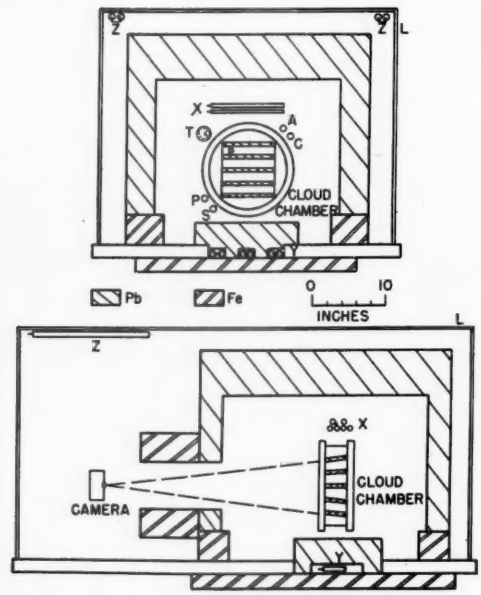

FIG. 1. Two perpendicular sections showing the disposition of absorber and counters about the cloud chamber. The chamber is triggered by various coincidences in the counters at X, Y, and Z.

The expansion of the chamber was triggered whenever a master pulse was generated by one of the following events:

(*a*) A sixfold coincidence of the counters at X, indicated by the lighting of neon bulb S, and referred to hereafter as an S-event.
(*b*) A threefold coincidence of any one of the counters at X with any two of the pairs at Y, indicated by neon bulb P and referred to hereafter as a P-event.

The simultaneous lighting of neon bulb A with either of the above coincidences indicated the presence of an accompanying extensive air shower of sufficient density to cause coincident pulses in the trays at Z, and simultaneous lighting of C indicated that an accompanying air shower had caused coincidences in some more distant counters. All events of this kind have been discussed in detail in reference 1. In the present analysis of the events (*a*) and (*b*), not associated with dense air showers, it is only important to note the absence of

Table I. The number of times counter coincidences not associated with extensive air showers triggered the cloud chamber in 871 hours under the lead shield (Fig. 1) and the number of nuclear interactions observed which satisfy the criteria of the present analysis.

Type of triggering coincidence	Number of triggering coincidences	Number of pictures in which nuclear interactions were observed: Origin above chamber	Origin within chamber: By charged particles	Origin within chamber: By uncharged particles	Origin within chamber: By particles of undetermined nature
S	3551	135	40	32	14
SP	153	29	12	5	12
P	1245	59	39	19	9

* Now at Duke University, Durham, North Carolina.
† Now with the Texas Company, Bellaire, Texas.
[1] W. W. Brown and A. S. McKay, Phys. Rev. **76**, 1034 (1949).
‡ Operational details are given in reference 1.

coincidences in the air shower counters. The numbers of S-, P-, and coincident SP-events recorded in the 871 hours of operation are given in Table I.

The efficiency of the Z counters for detecting air showers of density Δ-particles per unit area is $(1-e^{-A\Delta})^2$ where $A=200$ cm² is the Z-counter area. The median angle of ejection of the lightly ionizing secondaries (mostly mesons) with reference to the primary is in agreement with that predicted by the symmetric pseudoscalar meson theory. For the nuclear interactions occurring in the chamber, the ratio of the forward moving to backward moving heavily ionizing secondaries is 3.7, while the ratio for lightly ionizing ones is between 5 and 11, a result which shows the increase in the asymmetry of the angular distribution with the energy of the secondaries. The relative number of charged to neutral penetrating secondaries from the nuclear interactions occurring above the chamber is 1.5 ± 0.4—a result deduced from the relative number of nuclear interactions these secondaries had in the chamber and assuming the charged and neutral particles to have equal mean free paths. Cascades of 5 or more particles at their maximum development were generated at the origins of 12 percent of the nuclear interactions which occurred in the chamber. The heavily ionizing secondaries from nuclear interactions occurring in the chamber show an exponential absorption in the lead plates in which they are produced with absorption coefficients 0.20 ± 0.02 and 0.24 ± 0.04 per g/cm² of lead for the forward and backward ejected particles, respectively. In these same interactions a ratio of number of protons to mesons of about 0.3 is observed for particles in the ionization region 2–4 times minimum—while among particles of ionization less than twice minimum, 12 were identified as mesons and 5 as protons. Five huge cascades, of energy greater than 10 Bev, and not associated with large air showers were recorded. This efficiency rapidly approaches 1 for $\Delta>50$ particles per square meter, but is small for showers of lower density. As described in reference 1, the air shower signals "C" also indicated, in general, showers of rather high particle density. The exclusion, in the present paper, of events associated with A or C signals essentially excludes, therefore, only those events occurring in air showers of more than about 50 particles per square meter. The S, SP, and P coincidences occurring simultaneously with A or C signals were only 136 as compared with 4949 not associated with such dense air showers.

The various phenomena observed in these 4949 pictures included many like the examples of cascades, penetrating showers, mixed showers, and nuclear disintegrations shown in the accompanying photographs.

TABLE II. The mean free path for nuclear interaction of the ionizing penetrating secondaries of nuclear interactions.

Triggering coincidence	g/cm² Pb traversed in chamber by penetrating secondaries of nuclear interactions		Number of nuclear interactions of the ionizing penetrating secondaries of nuclear interactions		m.f.p. for nuclear interaction g/cm² Pb
	Observed	Corrected	Observed	Corrected	
S, SP	19700	21500	39	68	316 ± 70
P	8800	9620	26	46	209 ± 50

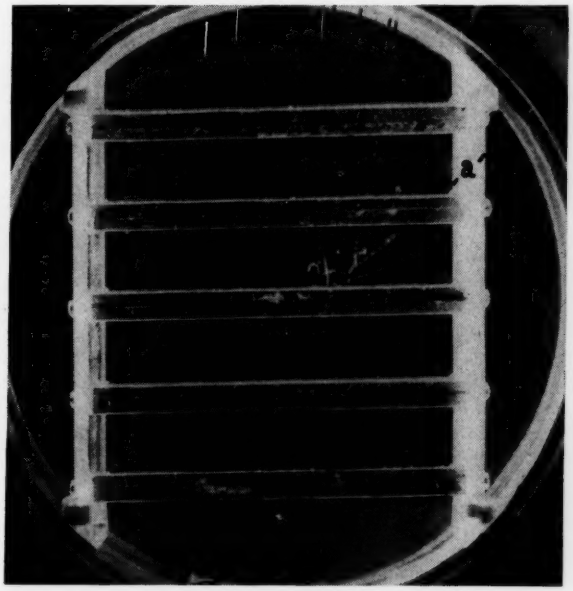

FIG. 2(A). A four-particle penetrating shower seen with a P trigger, originating two inches above the bottom of the lead roof. One of the shower particles undergoes a secondary nuclear interaction in which it produces five secondaries in the upper third of the third plate. One of the backward ejected secondaries, (a) penetrates the second plate and appears in the compartment to the right of the Lucite wall.

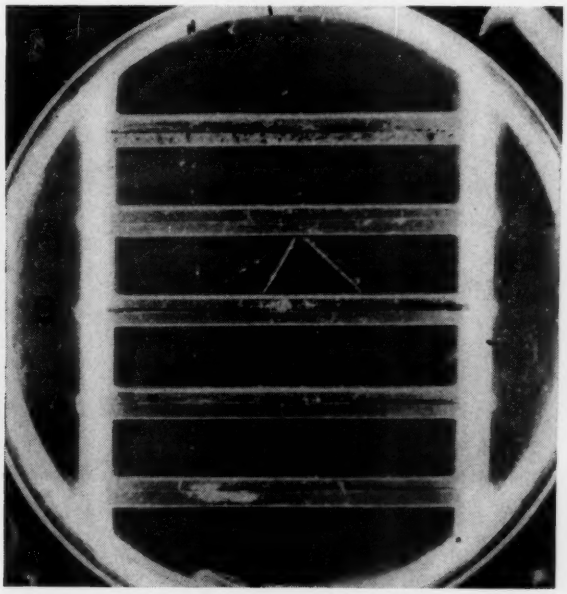

FIG. 2(B). A three-particle penetrating shower seen with an S trigger, originating about one inch above the bottom of of the lead roof. One of the shower particles undergoes a secondary nuclear interaction in which it produces three lightly ionizing and two heavily ionizing secondaries in the lower third of the second plate.

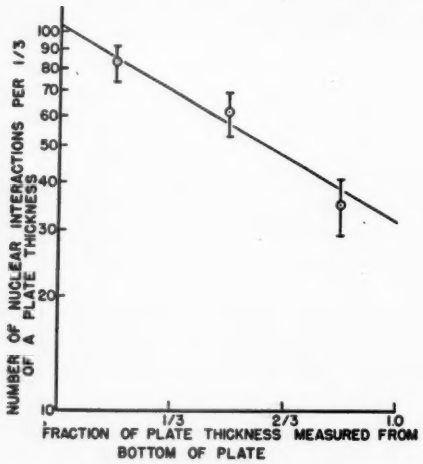

FIG. 3. The frequency of nuclear interactions occurring in the lead plates of the chamber *vs.* the point of origin of the interactions measured from the bottom of the plate in units of the plate thickness.

Similar events have been observed by others over the past few years.[2–7] In the present analysis some of the properties of these events and their secondaries are determined. For this purpose the following criteria, though not necessarily of fundamental significance, were useful for the classification of particles and nuclear interactions:

(1) Lightly ionizing particle—one which has a straight visible path and has less than 2 times minimum ionization.

(2) Heavily ionizing particle—one which has a straight visible path and has $\geqq 2$ times minimum ionization.

(3) Penetrating particle—a lightly ionizing particle which penetrates at least one lead plate without multiplication or a heavily ionizing particle which penetrates at least one plate.

(4) Penetrating shower—at least two penetrating particles which come from a common origin either above or in the chamber.

(5) Mixed shower—one or more penetrating particles and one or more cascades with common origins but different directions.

(6) Nuclear disintegration—minimum requirements are: either one penetrating particle plus one heavily ionizing particle, or one heavily plus one lightly ionizing particle, or two heavily ionizing particles which come from a common origin.

In the present article the general term "nuclear interaction" is used in referring to events which belong to any one of classes (4), (5), or (6). The term "nuclear disintegration" is employed in (6) rather than "star" since, in the present experiment, the average energy of events belonging to this group is considerably greater than that of the "stars" observed in photographic emulsions (see Section 9).

The numbers of nuclear interactions in *S*-, *SP*-, and *P*-events observed to occur above and in the chamber are given in Table I. Those occurring in the chamber are further subdivided in the table with regard to the nature of the initiating particle (charged, uncharged, or undetermined). Those made above the chamber con-

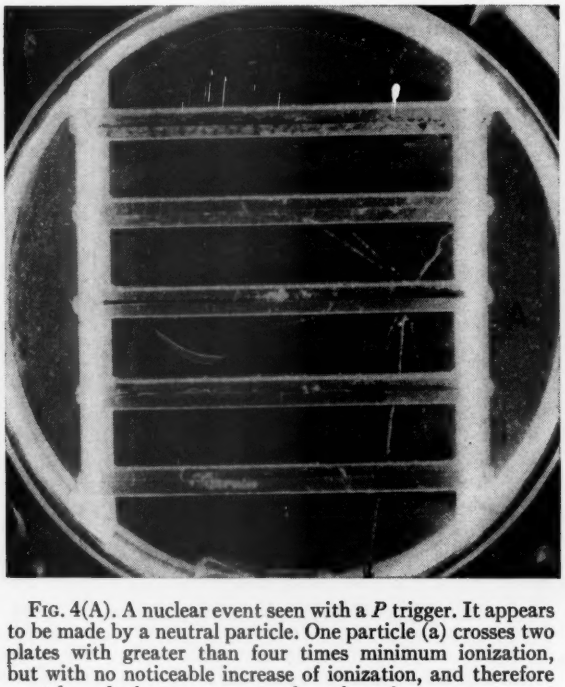

FIG. 4(A). A nuclear event seen with a *P* trigger. It appears to be made by a neutral particle. One particle (a) crosses two plates with greater than four times minimum ionization, but with no noticeable increase of ionization, and therefore must have had a mass greater than that of a proton.

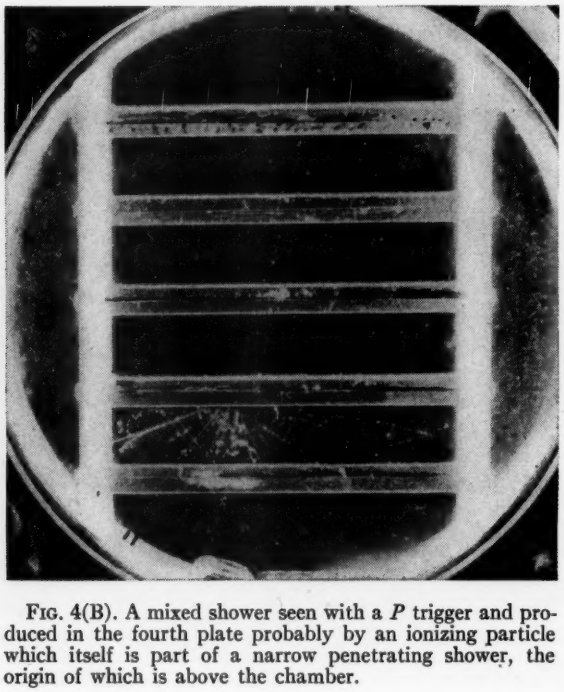

FIG. 4(B). A mixed shower seen with a *P* trigger and produced in the fourth plate probably by an ionizing particle which itself is part of a narrow penetrating shower, the origin of which is above the chamber.

[2] W. M. Powell, Phys. Rev. **69**, 385 (1946).
[3] W. B. Fretter, Phys. Rev. **73**, 41 (1948).
[4] H. Bridge and W. Hazen, Phys. Rev. **74**, 579 (1948).
[5] C. Y. Chao, Phys. Rev. **75**, 581 (1949).
[6] W. B. Fretter, Phys. Rev. **76**, 511 (1949).
[7] Lovati, Mura, Salvini, and Tagliaferri, Nature **163**, 1004 (1949).

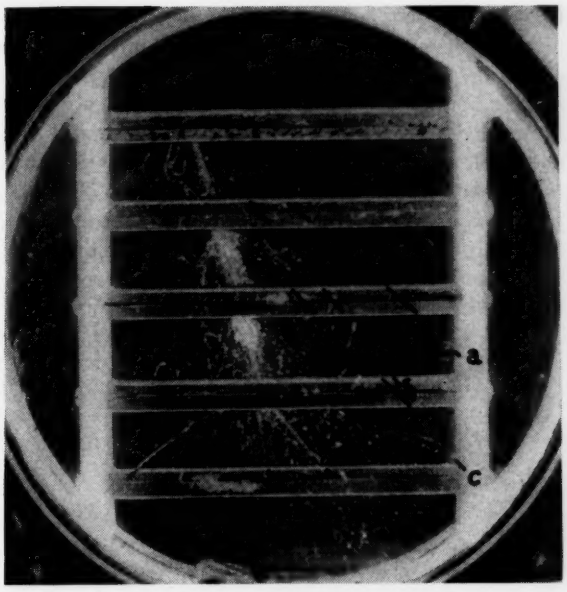

FIG. 5(A). A mixed shower seen with a *P* trigger. Nuclear interactions occur in plates 1, 2, and 4. There are three minimum ionizing penetrating particles at (a), (b), and (c). There are three heavily ionizing secondaries emerging from plate 4.

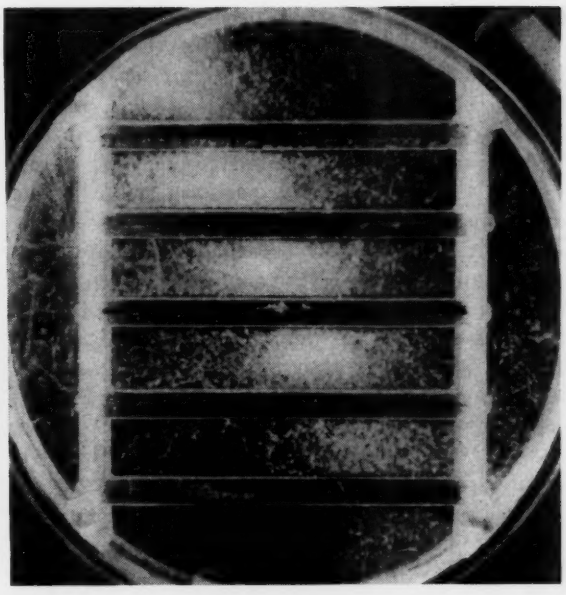

FIG. 5(B). A huge cascade with an *S* trigger. Altogether we saw five cascades of comparable size, none of which were accompanied by dense air showers or contained discernible penetrating particles.

sisted only of penetrating and mixed showers, while those in the chamber included nuclear disintegrations as well.

3. MEAN FREE PATH OF THE PENETRATING PARTICLES

The penetrating particles from nuclear interactions originating either above or in the chamber were observed to traverse a total projected path length of 28,500 g/cm² of lead in the chamber and there were 65 nuclear interactions produced by those ionizing particles (see for example Fig. 2). The distribution of total projected path length and number of nuclear interactions in *S*- and *SP*-events combined, and in *P*-events alone is given in Table II.

The observed path length is the projection of the true path length on a plane perpendicular to the line of sight of the camera. If $f(\theta)$ is the projected angular distribution of the penetrating particles from nuclear interactions, the ratio of the true path length to the projected path length is

$$\int_0^{\pi/2} f(\theta)\,\sec\theta d\theta \Big/ \int_0^{\pi/2} f(\theta)d\theta.$$

It is shown below in Sections 4a and 4b that the projected zenith angular distribution of the penetrating particles from nuclear interactions originating in and above the chamber respectively are both approximately of the form $\cos^3\theta$ for angles up to 60°. For $f(\theta)$ of this form the above ratio is 1.09. The corrected values of the path lengths are given in column 3 of Table II.

The points of origin of all nuclear interactions in the chamber, irrespective of the nature of the interacting particle, could, in all but three cases, be determined by

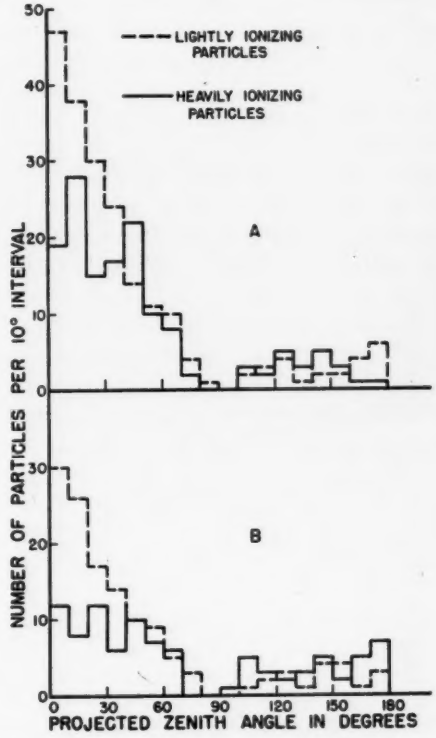

FIG. 6. The projected zenith angular distributions of the lightly and heavily ionizing secondaries of nuclear interactions occurring in the chamber. (A) Nuclear interactions of ionizing particles, (B) Nuclear interactions of neutral particles.

backward tracing of the paths of their ionizing secondaries. The frequency distribution of the points of origin, measured in each case with reference to the bottom surface of the plate, is shown in Fig. 3 plotted in intervals of $\frac{1}{3}$ of a plate. The predominance of nuclear interactions observed in the lower $\frac{2}{3}$ is a result of the asymmetry of ejection of the particles (more in the forward direction) and the strong absorption of the more heavily ionizing ones. These effects are discussed in more detail in Section 9. For the present purpose the distribution may be used to estimate the ratio of the actual number of nuclear interactions occurring in the lead to the number observed. Assuming the absorption to be of the form $n=n_0e^{-\mu t}$, application of the method of least squares gives $\mu=1.2\pm0.3$ per plate thickness (or 0.087 ± 0.022 per g/cm² of lead) and $n_0=104\pm14$ as the number per $\frac{1}{3}$ plate. Hence the desired ratio is

$$\frac{3n_0}{\text{observed number}}=\frac{312\pm42}{179\pm13}=1.75\pm0.27.$$

Since the nuclear interactions of ionizing particles are similar to those of neutral particles (see Sections 4a and 5a), it is reasonable to assume that the distributions of their points of origin in the lead plates are also similar. Hence a 75 percent correction must be added to the number of observed nuclear interactions of ionizing particles. The corrected numbers are given in column 5 of Table II and the resulting mean free paths for nuclear interaction in column 6.

It should be noted that a P coincidence is caused by two or more penetrating particles beneath the chamber and hence is more likely to occur when a shower has undergone further multiplication in the chamber than when it has not. Hence in P-selected events the probability for an interaction to be seen in the chamber is increased by the counter selection, and this is evident in the rather low mean free path given in Table II. On the other hand, an S coincidence demands multiplicity of particles only above the chamber. Since very few penetrating secondaries of nuclear interactions are ejected upward (see Section 9 and Table IV), the probability of an S coincidence is not appreciably influenced by whether or not an interaction has occurred in the chamber. Therefore the interaction mean free path deduced from the S- and SP-triggered pictures, 316 ± 70 g/cm² of lead, has not been significantly affected by the counter selection and may be considered as representing the mean free path for nuclear interaction of the penetrating particles from nuclear interactions. This is in agreement with the mean free path estimated by Lovati *et al.*,[7] but disagrees with Fretter's value of 750 g/cm².¶ Fretter made no correction for the "invisible" interactions occurring in the lead plates. Piccioni¶ also reports measurements which indicate a long range for the secondaries of penetrating showers (after filtering through large thickness of lead). He interprets this as indicating long mean free path for nuclear interaction. However, he would detect such interactions only if the primary and all its progeny were absorbed; not if an ionizing penetrating particle continued after the interaction. In the present experiment many nuclear interactions, in which there were penetrating secondaries, were observed (see for example Figs. 4B and 5A).

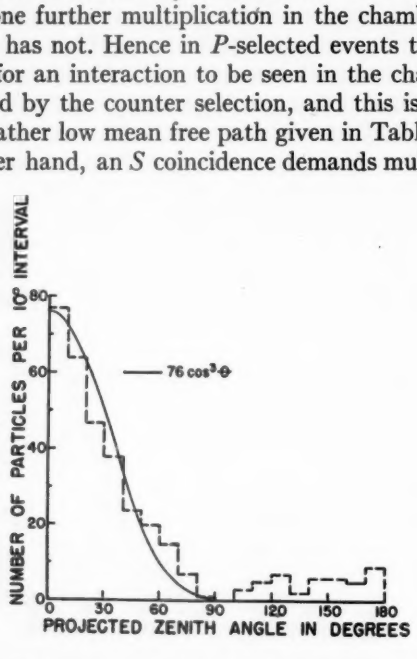

FIG. 7. The projected zenith angular distribution of all the lightly ionizing secondaries of nuclear interactions occurring in the chamber.

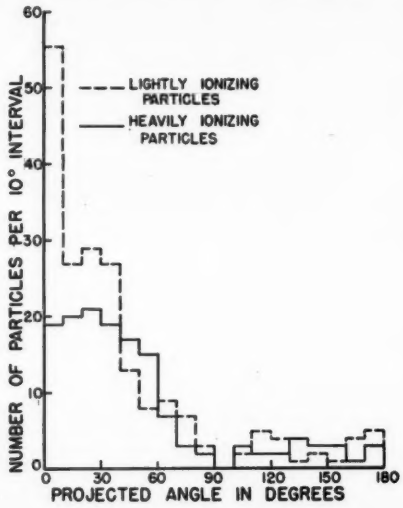

FIG. 8. The projected angular distributions of the lightly and heavily ionizing secondaries of the nuclear interactions of ionizing particles occurring in the chamber. The measured angles are those between the directions of the secondaries and that of the primary in each case.

4. ANGULAR DISTRIBUTIONS OF THE SECONDARIES

a. Nuclear Interactions in the Chamber

For nuclear interactions occurring in the cloud-chamber plates, the projected zenith angles of the

¶ Result given at Cosmic Ray Conference, Idaho Springs, Colorado, June 1949.

secondary particles that emerged from the plates could be measured in the full 0° to 180° interval, except in the region around 90° which was obscured by the plates. The zenith angular distributions of lightly ionizing (broken line histograms) and heavily ionizing secondaries (full line histograms) are given in Figs. 6A and 6B for the nuclear interactions of ionizing and neutral particles, respectively. The sum of the distributions of the lightly ionizing secondaries is given in Fig. 7. Up to 80° it may be represented by an empirical law of the

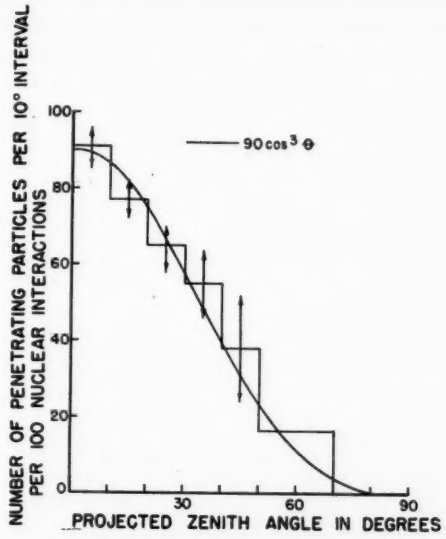
NUMBER OF PENETRATING PARTICLES PER 10° INTERVAL PER 100 NUCLEAR INTERACTIONS
90 cos³ θ
PROJECTED ZENITH ANGLE IN DEGREES

FIG. 9. The projected zenith angular distribution of the ionizing penetrating secondaries of nuclear interactions occurring above the chamber.

form $\cos^3\theta$, which has been used in Section 3 in connection with the mean free path.

For a nuclear interaction of an ionizing particle, the angles between the directions of the secondaries and the direction of the primary can be measured. The angular distribution of heavily and lightly ionizing particles about the primaries is given in Fig. 8. The median projected angle between a lightly ionizing secondary and its primary is 27°, corresponding to a median angle of 36°.

In the above angular distributions all nuclear interactions were counted irrespective of the method of counter selection since plotting of the distributions in $S+SP$- and P-events separately revealed no significant bias of secondaries in the P-events toward the vertical, either for the lightly or heavily ionizing particles. However, the ratios of the total number of lightly ionizing to heavily ionizing particles from the nuclear interactions in $S+SP$-, and P-events were 1.23 ± 0.18 and 1.70 ± 0.30, respectively. The P-event selection may thus exert some bias in favor of lightly ionizing particles without influencing the angular distribution very strongly. A bias of P-events in favor of lightly ionizing secondaries is understandable because a P coincidence requires at least two penetrating particles

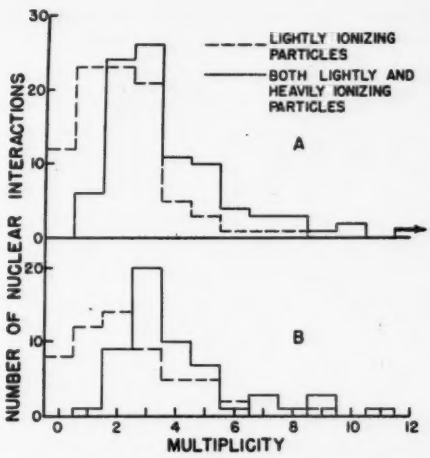

FIG. 10. The distributions of the total multiplicities and the multiplicities of the lightly ionizing secondaries of nuclear interactions occurring in the chamber (A) for the nuclear interactions of ionizing particles (B) for those of neutral particles. The occurrence of interactions of zero multiplicity of lightly ionizing secondaries merely means that these interactions were detected by the presence of the heavily ionizing secondaries only.

capable of traversing $3\frac{1}{2}$ inches of lead beneath the chamber. S coincidences, on the contrary, are not influenced by the nature of the secondaries created in the lead plates of the cloud chamber.

The projected zenith angular distributions of the secondaries of nuclear interactions of ionizing and netural particles (Figs. 6A and 6B) are similar, and the ratios of the numbers of lightly ionizing to heavily ionizing particles are 1.42 and 1.41, respectively. These two facts indicate that the neutral and ionizing particles experiencing these nuclear interactions are of about the same average energy.

b. Nuclear Interactions outside the Chamber

In all of these interactions the initiating particle is not observed and most of the heavily ionizing particles have been removed by absorbing layers between the point of origin and the cloud chamber; hence only the zenith angles of the penetrating particles were measured. For the angular distribution of these particles to have meaning some account had to be taken of the variations of the solid angle available for the detection of penetrating particles. To achieve this, the projection of the solid angle seen by the camera was divided into 10° intervals for each nuclear interaction. The number of cases where a given angular interval was visible and the number of penetrating particles in each of the intervals were recorded. Each interval and each penetrating particle was further weighted by the first power of the distance from the origin of the interaction to the nearest point in the sensitive volume of the chamber at which the particle could show its penetrating properties. Finally the ratio of the weighted numbers of penetrating particles to the weighted number of intervals was calculated and plotted as a function of zenith angle. The resulting histogram of Fig. 9 represents the prob-

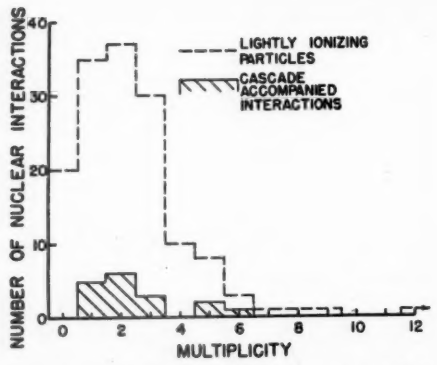

FIG. 11. The multiplicity distribution of the lightly ionizing secondaries of all nuclear interactions occurring in the chamber. The shaded portion gives the number of these interactions in which electrons or photons were generated with enough energy to make cascades in succeeding lead plates with 5 or more particles at their maximum development.

ability of a penetrating secondary particle lying in a given 10° projected zenith angular interval. The distribution follows an empirical law $\sim\cos^3\theta$, similar to that for the lightly ionizing particles ejected in the forward direction from the nuclear interactions occurring in the chamber.

5. MULTIPLICITY OF SECONDARIES AND CASCADE PRODUCTION

a. Nuclear Interactions in the Chamber

The multiplicities of the secondaries (not including those which were obviously electrons by virtue of their cascade production in Pb plates or scattering in the gas) from the nuclear interactions of ionizing and neutral particles in the lead plates of the chamber are given in the frequency histograms of Figs. 10A and 10B, respectively. Again all interactions irrespective of counter selection were counted. Broken lines represent the multiplicity of the lightly ionizing secondaries and the full lines the multiplicity of both lightly and heavily ionizing particles together. It is seen that the multiplicities of secondaries in interactions of neutral and charged particles have about the same distribution. The occurrence of nuclear interactions in which there were no lightly ionizing particles merely means that in these cases a nuclear interaction was detected by the presence of two or more heavily ionizing particles. The few cases in which there was a total of one particle were instances in which a nuclear interaction was detected by the presence of one heavy particle together with a cascade. The appearance of the distribution at these low multiplicities is thus a result of the selection criteria listed in Section 2.

The average multiplicity of lightly ionizing secondaries from the nuclear interactions of charged particles is 2.2, and for interactions of neutral particles is 2.4. Further division of these groups into $S+SP$-, and P-events still showed no significant difference in the average multiplicities, though the statistical uncertainties in these smaller groups are large. The results for the whole group ($S+SP+P$-events) are further

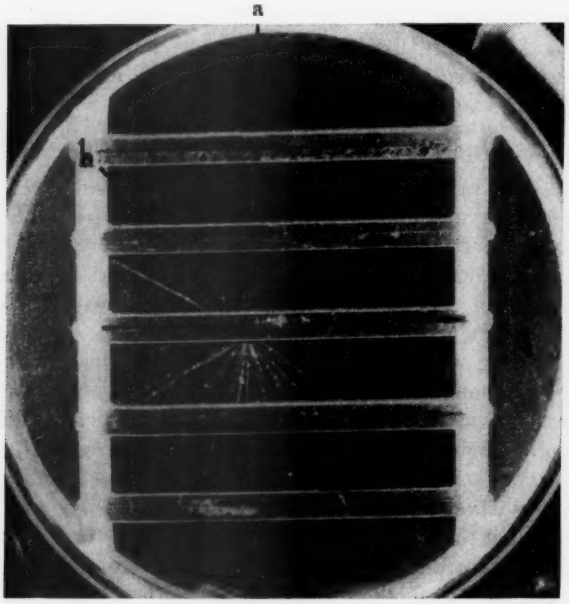

FIG. 12(A). A high energy nuclear interaction of a minimum ionizing particle (a) coming from above, in which there is no visible cascade radiation. The event is estimated to have had an energy of at least 8000 Mev. There are at least 26 secondaries coming from the common origin. One minimum ionizing particle (b) going in the backward direction penetrates the second plate. The chamber was triggered by a P coincidence, which indicates that at least two particles penetrated an additional 3.5 inches of lead.

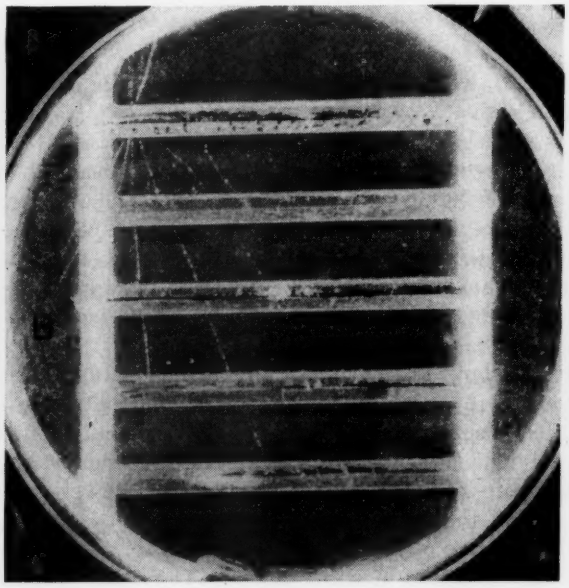

FIG. 12(B). A high energy nuclear interaction seen with an S trigger. The primary particle may be either charged or neutral and is estimated to have had an energy of at least 2500 Mev.

evidence that the interactions of neutral and charged particles involve energies of the same order of magnitude and hence that the initiating neutral and ionizing particles, most of which are secondaries from nuclear interactions occurring in the lead roof, have about the same average energies.

The multiplicity of lightly ionizing particles in all nuclear interactions occurring in the chamber, irrespective of whether their primaries are charged, neutral, or undetermined, is given in Fig. 11. The shaded portion of the histogram gives the frequency of nuclear interactions in which electrons or photons were generated with sufficient energy to make cascades of 5 or more particles at their maximum development. The frequency of cascade-accompanied nuclear interactions, compared with the total number of nuclear interactions, is only 17 percent of the frequency observed by Fretter.[6] Some of the disagreement may be accounted for by differences in the lower limit of cascade shower selected, and in the experimental arrangement. Fretter triggered on coincidences involving two counters below the chamber. Such coincidences are on the average more probable for showers including cascades than for penetrating showers with no cascade.

Since in the present experiment 72 percent of the nuclear interactions occurring in the lead plates in the chamber are made by secondaries from the interactions in the lead above, and there is little or no counter bias affecting the lower energy region of the size distribution of these secondary interactions, we are no doubt looking at phenomena of lower average energy than Fretter. Our selection of lightly ionizing particles from nuclear interactions is different from Fretter's selection of particles that penetrate at least one $\frac{1}{2}$-inch lead plate. That the majority of the lightly ionizing particles counted are not electrons is shown in Section 8.

The absence of cascade production at zero multiplicities is understandable since the primary energies involved in the production of the heavily ionizing particles by which these nuclear interactions were detected is relatively low. The absence of cascades amongst the high multiplicity events, though of questionable statistical significance, would indicate that the probability for the production of cascades in nuclear interactions does not increase with energy or multiplicity as rapidly as expected according to current theories.[8,9] This point requires further experimental test since penetrating particles in the cores of the cascades escape observation, and thus there is an observational bias against recording a high multiplicity event with an accompanying cascade. That this bias is not large is indicated by the fact that when high multiplicity nuclear interactions did occur, the angular spread of the penetrating particles was large (see for example Figs. 12 and 13) and hence in cascade-accompanied nuclear interactions (Figs. 4B and 5A) one would expect to see some of the penetrating particles.

There were many cases in which cascades occurred

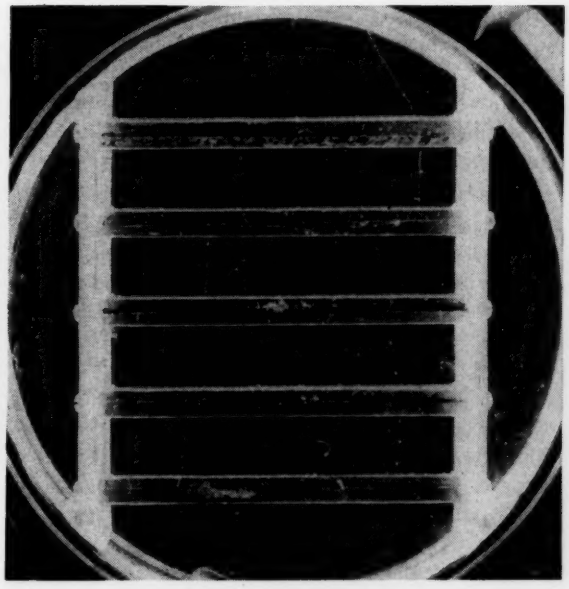

FIG. 13(A). A penetrating shower of at least nine particles, with no cascade radiation, seen with an *SP* trigger. There is very little scattering of most of the particles, and the minimum energy is estimated to be 20 Bev. The origin is at the bottom of the lead roof and we should be able to see cascade if it existed.

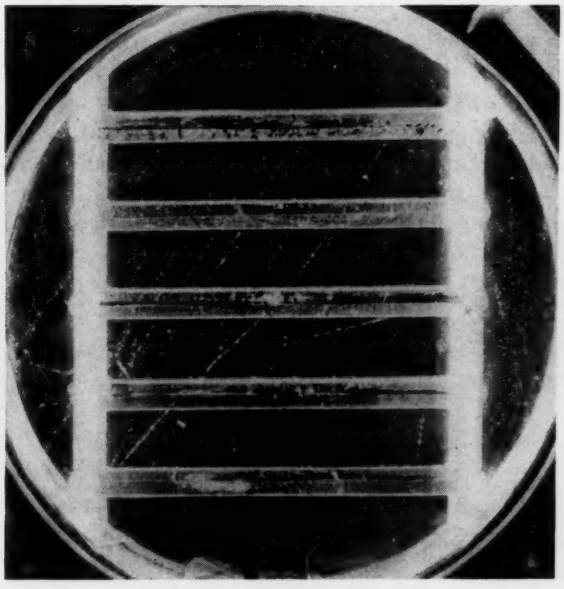

FIG. 13(B). A penetrating shower of at least eight particles seen with an *S* trigger, originating one inch above the bottom of the lead roof but exhibiting no cascade radiation. The particle showing the scattering and increased ionization is identified as a proton. The energy of this event is estimated to be greater than 8 Bev.

[8] L. I. Schiff, Phys. Rev. **76**, 89 (1949).
[9] Lewis, Oppenheimer, and Wouthuysen, Phys. Rev. **73**, 127 (1949).

TABLE III. The observed scattering angles suffered by 9 penetrating particles each of which traversed at least three ½-inch lead plates and had at least one scattering greater than 8°.

Penetrating particle number	Observed scattering angles in degrees 1	2	3	4
1	5.5	0.5	16.5	
2	1.0	19.0	9.0	
3	1.5	0.5	20.0	
4	4.5	10.0	1.0	
5	4.0	2.0	24.0	
6	0.5	13.0	0.0	
7	3.0	0.5	1.5	27.0
8	10.0	4.0	8.0	5.0
9	13.0	3.5	4.5	

unaccompanied by either penetrating particles discernable in the chamber of air showers outside the chamber (e.g., Fig. 5B). These are believed to be the products of other types of interaction, such as bremsstrahlung and knock-on processes of mesons and nucleons, or the decay of energetic unstable particles.

b. Nuclear Interactions above the Chamber

The distribution of the multiplicities of the visible penetrating particles from nuclear interactions originating above the chamber, i.e., either in the lead roof or in other material between the roof and the sensitive volume of the chamber, is given in Fig. 14 for two different methods of counter selection. The combined results are given in Fig. 15 where the shaded portion of the histogram represents the number of these nuclear interactions accompanied by cascades of 5 or more particles. No cascades were observed in the 8 nuclear interactions with multiplicity $\geqq 6$. Four of these occurred so high up in the lead roof that any existing cascade component could have been absorbed, while cascade radiation from the remaining four would have had a good chance of being detected if present. Interactions for which a multiplicity of one is recorded represent the few cases in which a nuclear interaction was detected by the presence of one penetrating particle together with a cascade, with a well-defined core, going in a different direction. The peak in the distribution curve is thus not to be considered as real, since no other interactions of multiplicity one were counted because they were indistinguishable from non-interacting single penetrating particles. The frequent triggering of the six counters at X (Fig. 1) by showers with low multiplities of penetrating particles is in many cases due to the simultaneous occurrence of a relatively high multiplicity of electrons emerging from the lead roof, and to the fact that the penetrating particles of such a shower do not necessarily all pass through the chamber.

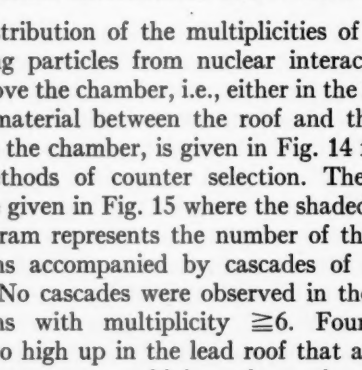

FIG. 14. The multiplicity distribution of the penetrating particles from nuclear interactions occurring above the chamber and selected by two different types of triggering coincidences.

6. SCATTERING OF THE PENETRATING PARTICLES IN THE LEAD PLATES

The projected angles through which each lightly ionizing penetrating particle from a nuclear interaction occurring in or above the chamber was scattered, on passing through a lead plate, were measured to the nearest 0.5 degree. In 9 out of 202 cases in which 3 or more scattering angles of a single penetrating particle from a nuclear interaction occurring above the chamber could be measured, the particle suffered a scattering $>8°$. The measured scattering angles for each of these 9 cases are given in Table III. In seven of these cases the largest scattering angle is four or more times the root mean square average of the other scattering angles recorded for the particular particle. These 7 scatterings are regarded as very probably different from the more usual Coulomb scatterings observed. The 202 penetrating particles traversed a total of 10,800 g/cm² of lead, which indicates a mean free path of $10{,}800/7 = 1550$ g/cm² for this type of interaction. It must be pointed out that the above criterion of selection, though necessary to distinguish this type of interaction from the Coulomb scattering, may limit us to the observation of less than

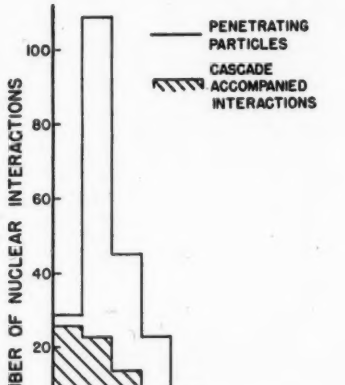

FIG. 15. The multiplicity distribution of the penetrating particles from all nuclear interactions observed to occur above the chamber. The shaded portion gives the number of these interactions in which electrons or photons were generated with enough energy to make cascades of 5 or more particles at their maximum development.

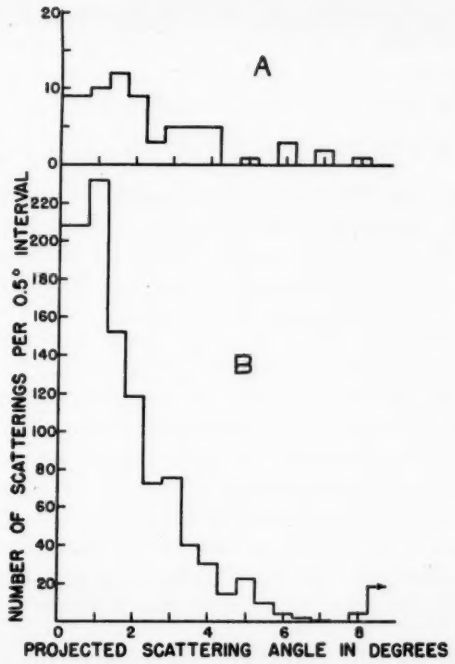

FIG. 16. The scattering angle distribution of the penetrating secondaries of nuclear interactions occurring (A) in the chamber and (B) above the chamber. Each scattering angle measured was that resulting upon passage of a particle through a ½-inch lead plate.

the actual number of such interactions taking place. However, nuclear scattering is expected to be, on the average, at rather large angles, so that it is not likely to miss a large fraction of them. It is more likely that a few of the large-angle scatterings observed are unusual cases of Coulomb scattering, so that the mean free path for nuclear scattering is longer than 1550 g/cm², which must be regarded as an approximate lower limit on the mean free path. The results thus indicate that the mean free path for nuclear interaction without the production of secondaries is at least 4 or 5 times that for nuclear interaction with the production of secondaries. This is in agreement with Fretter's measurements.‖

The distribution of the scattering angles is given in Figs. 16A and 16B for the penetrating particles from nuclear interactions occurring in and above the chamber respectively. The root mean square scattering angles are 3.0° and 2.3° respectively, neglecting angles $>8°$, a large fraction of which are likely non-Coulomb scatterings. According to the formula for the distribution of scattering angles of cosmic-ray particles given by Rossi and Greisen,[10] single particles with values of $p\beta=430$ Mev and 570 Mev respectively would have root mean square projected scattering angles in traversing ½-inch lead plates equal to the above averages. These can be considered as low estimates for the average values of $p\beta$ for these distributions for two reasons: (1) Averaging of the scattering angles essentially averages the reciprocal of $p\beta$, which gives undue weight to the particles of low momentum; (2) small scattering angles are most frequent and errors in measurement would tend to shift the distribution a little to larger angles.

The average multiplicity of the lightly ionizing secondaries of nuclear interactions occurring in the chamber has been given in Section 5 as 2.2. Using the above value of $p\beta=430$ Mev as representing the average energy of these secondaries, and assuming the relative numbers of ionizing and neutral secondaries to be 1.5 (the same as that estimated below in Section 7 for the penetrating secondaries of nuclear interactions occurring above the chamber), the average energy of the interacting particles is estimated to be $2.2\times0.43\times(1.5+1)/1.5=1.6$ Bev. If the lower energy neutral and ionizing heavy secondaries, as well as the cascade producing electron secondaries were also considered, it would be conservative to estimate the average energy as lying in the range 2 to 3 Bev. If the secondaries are emitted symmetrically in the center of mass system, in accordance with the symmetric pseudoscalar theory of meson production,[9] the median angle of emission with respect to the primary in the laboratory system, corresponding to this energy interval, ranges from 39° to 48° irrespective of whether the primary is a π-meson or a proton. The scalar theory[9] on the other hand would indicate a median angle $\mu/p\approx146/430=0.34$ radians or 19°, which may be considered as an upper limit since 430 Mev is a low estimate. Our measured value of the median angle, 36°, given in Section 4, is in rough agreement with the symmetric theory. This is in contradiction to Walker's results** which were obtained from counter data and favored the scalar theory.

7. RELATIVE NUMBER OF NEUTRAL AND CHARGED PENETRATING PARTICLES

It has already been mentioned that the average multiplicities of the nuclear interactions of ionizing and non-ionizing penetrating particles are nearly equal, and also that the lightly and heavily ionizing secondaries occur in the same relative numbers and with about the same angular distributions in showers generated by neutral and by ionizing particles. These similarities indicate

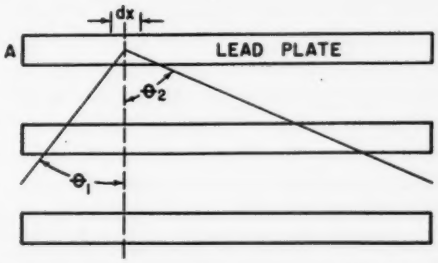

FIG. 17. Diagram showing the limiting values of the projected zenith angles, θ_1 and θ_2, between which a penetrating secondary from a nuclear interaction occurring in the interval dx of plate A must lie in order to show penetration.

‖ Given at Cosmic Ray Conference, Idaho Springs, Colorado (June, 1949).

[10] B. Rossi and K. I. Greisen, Rev. Mod. Phys. **13**, 240 (1941).

** W. D. Walker, Ph.D. thesis, Cornell University (1949).

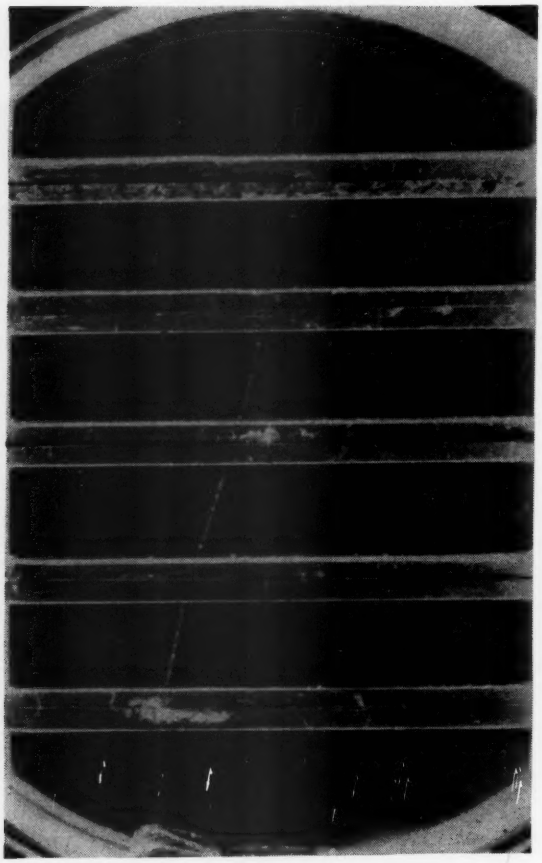

FIG. 18. A penetrating particle, which, by virtue of its scattering, ionization, and range is identified as a proton. From the theoretical relationships between these properties, the ionization relative to minimum ionization, in each of the compartments of the chamber starting from the top lies in the intervals 1.9–2.2; 2.2–2.5; 2.5–3; 3–4; and 4.5, respectively. This track was used for comparison in the estimation of the ionization of other tracks in the range 2–4 times minimum.

that the neutral and ionizing penetrating particles have about the same average energy, since all of the above properties are probably related to the energy of the primary. Of the three properties the multiplicities probably represent the best measure of the energies.

If the neutral and ionizing particles have the same mean free path for nuclear interaction, the relative numbers of the nuclear interactions of neutral and ionizing particles would be a fair measure of the relative numbers of the neutral and ionizing particles themselves. Since the six counters above the chamber respond to events of fairly large multiplicity of ionizing particles (both electrons and penetrating particles), the bias against the recording of nuclear interactions by neutral particles in the chamber is small. In the *S*-events there were 39 and 26 nuclear interactions in the chamber made by ionizing and neutral particles respectively, that had been generated in nuclear interactions which had occurred above the chamber. Hence the ratio of ionizing to neutral penetrating particles from nuclear interactions is 1.5 ± 0.4. Interacting particles unaccompanied by another penetrating particle were not counted as it was not clear in such cases whether the interacting particle (neutral or ionizing) was a member of a nuclear interaction occurring above the chamber.

8. THE NATURE OF THE SECONDARIES

From the 149 nuclear interactions of neutral and charged particles occurring in the lead plates of the chamber there was a total of 293 lightly ionizing secondaries (not including those which were obviously electrons) ejected in the forward direction. Of these, 119 (or a fraction 0.41) penetrated at least one lead plate. From the angular distribution of secondaries given in Fig. 7 and the assumption that they are all penetrating, the number expected to impinge on a lead plate and be visible in the following compartment can be calculated as follows: a minimum ionizing particle emerging from plate A in the region dx (Fig. 17) would be capable of exhibiting penetration in one or more succeeding plates if its direction lies in the projected zenith angular interval (as seen by the camera) determined by the limiting zenith angles θ_1 and θ_2. The fractional number of particles lying in this interval can be calculated from the projected zenith angular differential distribution $f(\theta)$ of Fig. 7 and is given by

$$\int_{\theta_1}^{\theta_2} f(\theta)d\theta \Big/ \int_{-\pi/2}^{\pi/2} f(\theta)d\theta.$$

To account also for those particles which escape by passing out of the field of view through the front or back of the chamber without penetrating a lead plate, a similar calculation must be made for the projection perpendicular to that seen by the camera and given by

$$\int_{\phi_1}^{\phi_2} f(\phi)d\phi \Big/ \int_{-\pi/2}^{\pi/2} f(\phi)d\phi,$$

where $f(\phi)$ is the same function as $f(\theta)$.

The fractional number of lightly ionizing particles capable of showing penetration is the product of these two integrals averaged over the length and width of the lead plate. Using the measured angular distribution of Fig. 7 and values of θ_1, θ_2, ϕ_1, ϕ_2 as functions of position, obtained from geometrical considerations, numerical integration yields 0.48 as the fraction. Since particles from plate 5 could show no penetration, only those coming from nuclear interactions in the first 4 plates can be counted. Since 0.93 of the nuclear interactions happened in the first four plates the fraction of particles which can show penetration is $0.93\times0.48=0.44$ This differs by only 0.03 from the observed fraction; thus probably less than 10 percent of the lightly ionizing tracks in the forward direction are electrons and this is assumed to be a negligible percentage.

A similar calculation may be carried out for the lightly ionizing particles traveling in the backward direction. A uniform angular distribution is used (see

Fig. 7), and a numerical integration, this time discounting the nuclear interactions occurring in the top plate, indicates that we should see 14 percent of the lightly ionizing particles penetrate one or more lead plates if they are all penetrating particles. We observed that 5 out of 63, or 8 percent, of the lightly ionizing particles crossed a lead plate. This indicates that at most 50 percent of the lightly ionizing particles in the backward direction could be electrons since there is little chance of an electron crossing a lead plate with small scattering. In making these estimates of the percentages of electrons we have neglected the small probability that a π-meson and the somewhat larger probability that a μ-meson may be a little less than twice minimum ionization and still not have enough energy to penetrate a plate. As a result these estimates are an upper limit for the fraction of electrons.

We now consider all tracks from nuclear interactions that are in the forward direction and have an ionization density between two and four times minimum as determined visually, by comparison with the proton track (see Fig. 18) that shows successive increases in ionization in crossing plates and finally stops. Calculations based on the range-momentum and ionization-momentum curves of Rossi and Greisen[10] show that π-mesons having 1.7 times minimum ionization and protons having 4.5 times minimum ionization are just able to penetrate a lead plate. Therefore, all tracks in the interval 2–4 times minimum ionization that then penetrate a plate must belong to particles of rest mass greater than that of a π-meson, while those that are unable to penetrate are very likely mesons; and, as has been shown by the experiment of Piccioni,[11] are π-mesons rather than μ-mesons.

We observe in all of the nuclear interactions occurring in the lead plates, 95 particles in the forward direction, in the range 2–4 times minimum ionization, of which 9 penetrate a plate, while 86 do not appear to penetrate. Using the zenith angular distributions of heavily ionizing particles as given in Fig. 6A and 6B we calculate, in a manner similar to that used for lightly ionizing particles, that 44 percent of these particles should be observed to penetrate if all were able to penetrate. There are thus $9/0.44=20$ heavily ionizing penetrating particles (protons) and $95-20=75$ nonpenetrating heavily ionizing particles. While the statistics are not good, the result indicates that secondaries in this ionization interval are more likely to be mesons than protons in spite of the fact that a fixed ionization interval represents a larger energy interval (by a factor $\sim 1840/320 \approx 6$) for protons than for π-mesons.

In one instance (Fig. 4A) a heavily ionizing secondary particle from a nuclear interaction (probably of a neutral particle) penetrates two lead plates after showing an ionization in the gas of more than four times the minimum. That there is little change in ionization and direction in crossing the fourth lead plate indicates that the particle is heavier than a proton. The apparent decrease in ionization just above and below the fifth plate could result from non-uniform illumination.

Out of all the penetrating tracks from nuclear interactions in the chamber which were <2 times minimum ionization, twelve could be identified as mesons because they had a greater increase in their ionization on crossing a plate than would be expected for a proton, while five tracks were identified as protons.

9. THE ABSORPTION OF THE SECONDARIES

The projected location of the point of origin of a nuclear interaction occurring in a lead plate in the chamber could, in most cases, be determined to the nearest 0.1 inch by backward extension of the visible portions of the paths of the secondaries. The distribution of the origins of nuclear interactions in the top, middle, and bottom thirds of the lead plates has already been given in Fig. 3. This absorption effect is due mainly to the fact that 85 percent of the nuclear interactions had their origins determined by the directions of emergence of heavily ionizing particles and that more of these particles are ejected downward than upward. In Table IV the interactions have been further subdivided into groups in accordance with their primaries being charged, neutral, or undetermined, and this time the number of particles is given instead of just the number of interactions. The total number of particles from each group and each $\frac{1}{3}$ of a lead plate thickness is divided into those moving upward and those moving

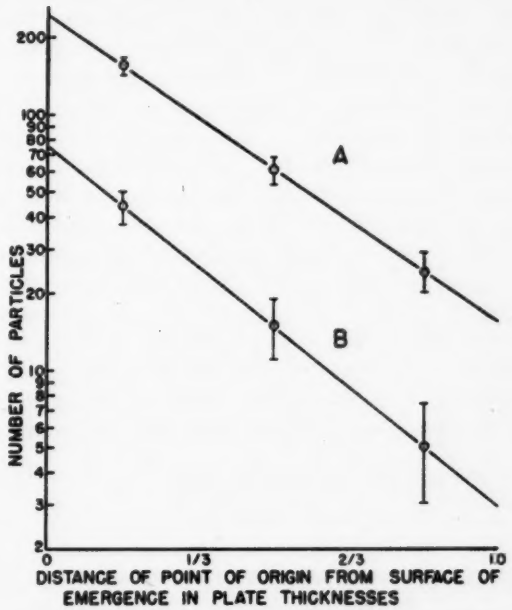

FIG. 19. Showing the absorption of the heavily ionizing particles, (A) in the forward direction and (B) in the backward direction, by the varying vertical thickness of lead between the points of origin of the particles in a plate and the sensitive part of the chamber. The ordinates are in numbers of particles per $\frac{1}{3}$ of a plate thickness.

[11] O. Piccioni, Phys. Rev. **75**, 1281 (1949).

TABLE IV. The frequency of occurrence of the lightly and heavily ionizing secondaries of nuclear interactions occurring in the lead plates of the chamber. The secondaries are grouped according to their point of origin in a lead plate, their direction of motion relative to that of the primary (forward or backward), and the nature of their primaries (charged, neutral, or undetermined).

Depth of point of origin in Pb plate in units of one-plate thickness (one plate =14.0 g/cm²)	Nuclear interactions of charged particles				Nuclear interactions of neutral particles				Nuclear interactions of particles of undetermined nature				Total			
	Heavily ionizing secondaries		Lightly ionizing secondaries		Heavily ionizing secondaries		Lightly ionizing secondaries		Heavily ionizing secondaries		Lightly ionizing secondaries		Heavily ionizing secondaries		Lightly ionizing secondaries	
	Forward	Backward	Forward	Backward	Forward	Backward	Forward	Backward	Forward	Backward	Forward	Backward	Forward	Backward	Forward	Backward
0 to 0.33	9	16	18	5	10	23	31	8	5	5	6	9	24	44	55	22
0.33 to 0.67	32	5	68	8	16	8	42	7	13	2	11	4	61	15	121	19
0.67 to 1.0	80	1	93	11	35	2	41	4	39	2	38	7	154	5	172	22

downward, and each of these classes into lightly ionizing and heavily ionizing particles.

The effective absorption of the heavily ionizing particles both in the forward and backward directions is shown by curves *A* and *B* respectively in Fig. 19. The two semilogarithmic curves are seen to be straight and almost parallel and indicate an effective exponential absorption with absorption coefficients of 2.8 ± 0.3 and 3.3 ± 0.6 per plate thickness (or 0.20 ± 0.02 and 0.24 ± 0.04 per g/cm² of lead) for the forward and backward particles, respectively. Most of these particles are more energetic at their origin than the heavily ionizing ones observed in stars in photographic emulsions.[12]

From the data of Table IV, it seems that the lightly ionizing secondaries in the forward direction also show as strong an absorption as the heavily ionizing secondaries. This however is only apparent and results from the fact that 85 percent of the nuclear interactions occurring in the chamber were detected by virtue of the presence of the heavily ionizing secondaries.

The ratio of heavily ionizing particles moving forward to those in the backward direction is seen from Table IV to be $237/64=3.7$. If we assume that at most 50 percent of the lightly ionizing tracks in the backward direction are electrons, as suggested by the estimate made in Section 8, and that all of the lightly ionizing tracks in the forward direction are heavier than electrons, we find $348/31=11$ for the maximum relative numbers of forward and backward traveling lightly ionizing mesons and protons. If on the other hand we assume that none of the particles (that do not generate cascades and are not visibly scattered in the gas) are electrons, we find $348/62=5.5$ for the minimum relative numbers of forward and backward traveling, lightly ionizing mesons and protons. Even this minimum ratio is higher than the ratio 3.7 for heavily ionizing particles.

[12] D. H. Perkins, Nature **160**, 299 (1947).

10. KNOCK-ON ELECTRONS OF PENETRATING PARTICLES

The projected angles θ were measured between knock-on electrons of energy greater than 1 Mev after emerging from a lead plate and the knock-on producing penetrating particles arising from nuclear interactions above or in the chamber. A $\cos^2\theta$ distribution provides satisfactory agreement with the observed numbers of these knock-ons in the forward direction—a less steep distribution than the $\cos^{2.5}\theta$ previously observed by the authors and E. D. Palmatier[13] when the penetrating particles were μ-mesons and were more nearly vertical.

In the present experiment there were 131 knock-ons in 1711 emergences of penetrating particles from a lead plate or 0.077 ± 0.007 knock-on per penetrating particle, a result not significantly different from that previously obtained for μ-meson produced knock-ons by Hazen[14] and by the authors.[13] The ratio of the number of the back-scattered knock-on electrons to the number of forward ones is 0.38 ± 0.06 whereas a value 0.25 ± 0.04 for this ratio was previously observed.[13]

The authors wish to thank Professors K. Greisen and G. Cocconi for suggesting this experiment and for their generous help both in solving experimental problems and in discussions of the results. They are grateful to the Research Corporation for a grant which covered the expense of performing this experiment. The cost of constructing the apparatus was provided through an ONR contract. The facilities of the Inter-University High Altitude Laboratories were of great help in performing the experiment.

[13] Brown, McKay, and Palmatier, Phys. Rev. **76**, 506 (1949).
[14] W. E. Hazen, Phys. Rev. **64**, 7 (1943).

Nuclear Dipole Vibrations and the Surface Symmetry Energy

R. D. PRESENT
University of Tennessee, Knoxville, Tennessee
(Received August 24, 1949)

The frequency of nuclear electric dipole vibrations of the type suggested by Goldhaber and Teller is derived on the basis of the semi-empirical nuclear model. The resulting formula, taken together with the (γ, n) and (γ, f) cross-section data of Baldwin and Klaiber, determines a lower bound for the term in the surface energy depending on $N-Z$ (surface symmetry energy). This is close to an upper bound estimated by Feenberg, and one may tentatively assume that the nuclear surface tension contains a factor $1-0.4(N-Z)^2A^{-2}$.

THE symmetry properties of the nuclear volume energy have been extensively treated but it has been customary to neglect the symmetry dependence of the surface energy. Recently, attention has been drawn to the possible dependence of the surface energy on isotopic spin, and an upper bound for the surface symmetry energy has been estimated from experimental data on isotopic abundances.[1] It is the purpose of this note to point out the connection between the nuclear electric dipole vibrations proposed by Goldhaber and Teller[2] and the semi-empirical nuclear model, and to show that this leads to a lower bound for the surface symmetry energy.

We consider first a slightly different derivation of the vibration frequency from that already given,[2] which eliminates part of the uncertainty in the nuclear constants and is also somewhat more general. The dipole vibration involves a relative displacement of the centroid of the protons from that of the neutrons. A varying gradient of the proton density is accompanied by a neutron density gradient in the opposite direction. The problem has been idealized in reference 2 to the relative motion of a homogeneous, incompressible ball of protons and a similar sphere of neutrons overlapping each other. Using this same approximation, we estimate the potential energy of the displacement from the change in the volume symmetry energy and the surface energy. The nuclear model used is based on the semi-empirical binding energy formula

$$-E_B=A\{-a_v+a_{\tau v}(N-Z)^2A^{-2}\}+A^{\frac{2}{3}}\{a_s-a_{\tau s}(N-Z)^2A^{-2}\}+a_cZ^2A^{-\frac{1}{3}}, \quad (1)$$

where the term in $a_{\tau s}$ is the surface symmetry energy and the other terms have their usual significance. The energy terms in a_v and a_c (Coulomb) do not change in the type of nuclear distortion considered.[3] The density of the volume symmetry energy is taken to be $a_{\tau v}\rho\{(\rho_N-\rho_Z)/(\rho_N+\rho_Z)\}^2$ where ρ_N, ρ_Z and ρ are the particle densities of neutrons, protons and nucleons, respectively. Consider a relative displacement ξ of the centers of the two spheres, where $|\xi|$ is small compared to the radius $R=r_0A^{\frac{1}{3}}$ but large compared to the effective thickness of surface layer ($\sim r_0$). The volume of extruded neutrons is $\pi R^2|\xi|$ and the change in the volume symmetry energy is readily found to be

$$\Delta E_{\tau v}=\pi R^2|\xi|\rho a_{\tau v}\cdot\{1-(N-Z)^2A^{-2}\}. \quad (2)$$

In the extruded regions $(\rho_N-\rho_Z)/(\rho_N+\rho_Z)\approx\pm1$, and it may seem questionable to use the binding energy formula for such an extreme departure from normal densities; in particular, higher powers of $(\rho_N-\rho_Z)/(\rho_N+\rho_Z)$ in the energy density and of $(N-Z)/A$ in the binding energy formula would seem to be required. This objection is not, however, serious, since (1) the idealized picture in which ρ_Z drops from a uniform value in the overlap region abruptly to zero in the extruded neutron layer is an approximation to an actually continuous change of density; and (2) the kinetic energy of the statistical model expanded in powers of $(N-Z)^2A^{-2}$ differs from the first two terms in the expansion by only two percent as $Z\to0$, and the potential energy in the "equal forces" approximation contains no higher power of $N-Z$ than $(N-Z)^2$.

The change in surface energy is readily seen to be

$$\Delta E_s=4\pi R^2(\mathrm{O}'-\mathrm{O})+2\pi R\mathrm{O}|\xi|, \quad (3)$$

where O and O′ are the surface tension of the undistorted nucleus and of the extruded region, respectively, and O′ is independent of ξ. The second term represents the energy of the extra area in the equatorial belt and leads to a small correction of the vibration frequency by a factor $(1+\beta A^{-\frac{1}{3}})^{\frac{1}{2}}$ where $\beta=2a_s/3a_{\tau v}\approx0.5$. This will be omitted in the following. Since the effective potential in a pure neutron fluid is very much less than (about one-fourth) that in normal nuclei, the surface tension O′ is evidently considerably smaller than O. We set $4\pi R^2(\mathrm{O}-\mathrm{O}')=A^{\frac{2}{3}}\delta$ and defer the analysis of δ in terms of the parameters of Eq. (1). The potential energy of deformation for $|\xi|\gg r_0$ is then given by $\Delta E_{\tau v}+\Delta E_s=\Delta E_{\tau v}-A^{\frac{1}{3}}\delta$. The potential energy for small displacements $|\xi|\lesssim r_0$ can evidently be written as $k\xi^2/2$, and the two expressions are to be joined continuously and with continuous derivative at a displacement $|\xi|=\epsilon$. The values of k and ϵ are obtained by solving these two equations simultaneously. The derivative

[1] E. Feenberg, Rev. Mod. Phys. **19**, 239 (1947).
[2] M. Goldhaber and E. Teller, Phys. Rev. **74**, 1046 (1948).
[3] To the extent that a proton density gradient is set up in the vibration, there will be an accompanying change in the electrostatic energy. This is neglected. Effects due to the finite compressibility of nuclear matter are also neglected.

equation yields (after substituting $A/(4\pi R^3/3)$ for ρ)

$$k=(3Aa_{\tau v}/4\epsilon R)\cdot\{1-(N-Z)^2A^{-2}\}. \quad (4)$$

Equating the energies and using Eq. (4), one obtains

$$\epsilon=(8r_0\delta/3a_{\tau v})\cdot\{1-(N-Z)^2A^{-2}\}^{-1}. \quad (5)$$

Thus ϵ is independent of A except for the small dependence through the curly bracket. The latter is nearly canceled by a similar variation of δ (see below); hence ϵ may be considered independent of A and Z.

The vibration frequency depends on the reduced mass of the two spheres:

$$\mu=4\pi R^3M\rho_Z\rho_N/3\rho=(MA/4)\cdot\{1-(N-Z)^2A^{-2}\}, \quad (6)$$

where M is the mass of a nucleon. Combining (4) and (6) gives

$$\hbar\omega=\hbar(k/\mu)^{\frac{1}{2}}=(3\hbar^2a_{\tau v}/\epsilon Mr_0)^{\frac{1}{2}}\cdot A^{-1/6}. \quad (7)$$

This is the same formula as that given by Goldhaber and Teller, although the interpretation of the constants is different. In comparing with the experimental results, we have included the small correction introduced by the second term of Eq. (3). The maxima in the (γ, n) and (γ, f) cross sections observed by Baldwin and Klaiber[4] come at values of $\hbar\omega=30$, 22, 18 and 16 Mev for C, Cu, Th and U, respectively. Averaging the last two results, the experimental ratios are: $(\hbar\omega)_C/(\hbar\omega)_{Cu}=1.36$ and $(\hbar\omega)_{Cu}/(\hbar\omega)_{Th-U}=1.29$. The theoretical ratios are 1.37 and 1.27; the agreement is better than the experimental and theoretical uncertainties would warrant. Recent measurements[5] on Ta show a maximum cross section at 15 Mev; this value is anomalously low when compared with the preceding data. It is worthy of note that the inclusion of an additional term[6] in the energy density containing $|\rho_N-\rho_Z|$ and corresponding to a volume symmetry term in $|N-Z|/A$ in Eq. (1), yields a dependence of $\hbar\omega$ on A at variance with the experiments. In this case the frequencies are multiplied by an additional factor which is approximately $[1+8(Z/A^2)]^{\frac{1}{2}}$ and the ratio $(\hbar\omega)_C/(\hbar\omega)_{Cu}$ is increased to 1.53.

In order to confirm the absolute magnitude of $\hbar\omega$ predicted by Eq. (7), it is necessary to know the value of ϵ the joining distance (the semi-empirical value of $a_{\tau v}=20$ Mev is well known[7]). Obviously ϵ is of the order of magnitude of $r_0\approx1.4\times10^{-13}$ cm, but a more precise estimate would seem dubious. Turning the problem around, we can determine ϵ from experiment and then use it to obtain further information about the nuclear surface energy. The data of Baldwin and Klaiber give $\epsilon=(3/4)r_0\approx1.1\times10^{-13}$ cm; this can be inserted in Eq. (5) to determine δ. The relation between δ and the constants of Eq. (1) will now be considered.

[4] G. C. Baldwin and G. S. Klaiber, Phys. Rev. **71**, 3 (1947); **73**, 1156 (1948).

[5] McElhinney, Hanson, Becker, Duffield, and Diven, Phys. Rev. **75**, 542 (1949).

[6] This term is discussed in R. D. Present, Phys. Rev. **72**, 7 (1947); footnote 7 of this paper is relevant to the application to C^{12}.

[7] H. A. Bethe and R. F. Bacher, Rev. Mod. Phys. **8**, 82 (1936).

The surface energy of the undeformed nucleus is (from Eq. (1))

$$\begin{aligned}E_s&=a_sA^{\frac{2}{3}}-a_{\tau s}A^{\frac{1}{3}}(N-Z)^2A^{-2}\\&=a_sA^{\frac{2}{3}}\{1-C_A(N-Z)^2A^{-2}\}\\&=a_sA^{\frac{2}{3}}\{1-C_\sigma(\sigma_N-\sigma_Z)^2(\sigma_N+\sigma_Z)^{-2}\}\end{aligned} \quad (8)$$

where σ_N and σ_Z denote the surface densities of neutrons and protons in the undeformed nucleus. Because of the electrostatic repulsion, the proton density must increase from the center to the surface of the nucleus, hence $(\sigma_N-\sigma_Z)/(\sigma_N+\sigma_Z)=\lambda(N-Z)/(N+Z)$ with $\lambda<1$. The departures from uniform density have been calculated by Feenberg;[8] his results lead to a value of λ (independent of Z and A) of 0.86. Hence $C_A=(0.86)^2C_\sigma$ for the undeformed nucleus. The surface energy of the deformed nucleus is then*

$$E_s'=a_sA^{\frac{2}{3}}\{1-C_\sigma(\sigma_N'-\sigma_Z')^2(\sigma_N'+\sigma_Z')^{-2}\}$$

neglecting possible higher powers of $\kappa=|\sigma_N'-\sigma_Z'|/(\sigma_N'+\sigma_Z')$. Hence

$$\begin{aligned}\delta&=a_sC_\sigma\{(\sigma_N'-\sigma_Z')^2(\sigma_N'+\sigma_Z')^{-2}-(\sigma_N-\sigma_Z)^2(\sigma_N+\sigma_Z)^{-2}\}\\&=a_{\tau s}(\kappa/\lambda)^2\{1-(\lambda/\kappa)^2(N-Z)^2A^{-2}\}.\end{aligned} \quad (9)$$

The idealized model of Goldhaber and Teller implies that $\lambda=\kappa=1$ since the proton density is uniform and the extruded layer of neutrons contains no impurity of protons. In this case ϵ is exactly independent of A and Z and we obtain from Eqs. (5) and (9) with $\epsilon=(3/4)r_0$ the result that $a_{\tau s}/a_{\tau v}=0.28$. Actually, one would expect a value of κ somewhat less than unity and in that case one obtains

$$\frac{a_{\tau s}}{a_{\tau v}}=\frac{3\epsilon}{8r_0}\cdot\frac{\lambda^2}{\kappa^2}\cdot\left\{\frac{1-(N-Z)^2A^{-2}}{1-(\lambda/\kappa)^2(N-Z)^2A^{-2}}\right\}. \quad (10)$$

The factor in brackets is nearly independent of κ and may be neglected. Hence for $\kappa<1$

$$a_{\tau s}/a_{\tau v}=0.28(0.86)^2\kappa^{-2}>0.21. \quad (11)$$

An upper bound for $a_{\tau s}/a_{\tau v}$ has been found by Feenberg.[9] The most stable value of A for each Z is estimated from nuclear abundance data and $a_{\tau v}$ calculated. The resulting values of $a_{\tau v}$ are not strictly constant but show a small monotonic variation with Z, which is attributed in part to the surface symmetry term. In this way Feenberg finds that $0<a_{\tau s}/a_{\tau v}<0.6$. On introducing certain specific assumptions about the semi-empirical constants, the upper bound can be reduced to 0.4. One may tentatively set $a_{\tau s}/a_{\tau v}=0.3$ so that $a_{\tau s}\approx6$ Mev. Since $a_s\approx15$ Mev, it follows that the nuclear surface tension undergoes a decrease of about two percent from one end of the periodic table ($N=Z$) to the other (U^{238}) because of symmetry effects. This justifies the previous neglect of the surface symmetry term in Eq. (1).

[8] E. Feenberg, Phys. Rev. **59**, 593 (1941).

* It is assumed that σ_N' and σ_Z' are constant over each hemisphere and that their values are exchanged at the equator.

[9] E. Feenberg, Rev. Mod. Phys. **19**, 239 (1947).

The Self-Stress of the Electron

F. ROHRLICH
Laboratory of Nuclear Studies, Cornell University, Ithaca, New York
(Received October 17, 1949)

The diagonal elements of the symmetrical energy-momentum tensor density of an electron at rest are calculated. The covariant formalism of Tomonaga, Schwinger, Feynman, and Dyson is used, and it is shown that it is necessary to use a relativistic cut-off in addition to the covariant separation of the infinite renormalizations. Therefore "formalistic regulators" are used in the form of additional neutral vector fields. The integrations are carried out with the Feynman method. The resultant vanishing value for the self-stress constitutes a proof of the consistency of the relativistic formalism.

It is also shown how the Feynman-Dyson method can be used for the calculation of expectation values of operators, of which the self-stress calculation constitutes an example.

THE SELF-STRESS PROBLEM

IN classical physics the finite charge distribution attributed to the electron could not be stable unless additional non-electromagnetic "cohesive" forces were postulated. The necessity of this requirement was also exhibited by the fact that a finite electron had a finite *non-vanishing* electromagnetic part of its experimental mass which spoiled the relation between kinetic energy and momentum. This is true even for the non-relativistic Abraham electron. For the relativistic Lorentz electron it can best be seen from the transformation properties of the energy-momentum tensor. Let $\Theta_{\mu\nu}$ be the energy-momentum tensor density of an electron moving with velocity v in the x direction; let the index zero indicate the rest system. Then energy and momentum transform as follows:[1]

$$E=-\int \Theta_{44}d\tau = -(1-v^2)^{-\frac{1}{2}}\left(\int \Theta_{44}^{(0)}d\tau_0 - v^2\int \Theta_{11}^{(0)}d\tau_0\right), \quad (1a)$$

$$p_x=-i\int \Theta_{41}d\tau = -v(1-v^2)^{-\frac{1}{2}}\left(\int \Theta_{44}^{(0)}d\tau_0 - \int \Theta_{11}^{(0)}d\tau_0\right). \quad (1b)$$

It follows from (1) and from the symmetry in the rest system that a consistent relativistic theory must yield

$$\Theta_{11}^{(0)}=\Theta_{22}^{(0)}=\Theta_{33}^{(0)}=0. \quad (2)$$

It is clear that the Eqs. (1) and (2) remain true in quantum theory. A direct verification of (2) for conventional quantum electrodynamics, however, so far led to difficulties because of the inherent infinities.

The recent developments in quantum field theory enable one to properly deal with these infinities. It is therefore the purpose of this paper to explicitly verify the vanishing of the self-stress and thus give a proof of the internal consistency of our present relativistic quantum electrodynamics.

[1] Here and throughout this paper we use natural units, $\hbar=c=1$.

In order to carry out this program it is important to realize that the formalism of Tomonaga,[2] Schwinger,[3] and Dyson[4] still suffers from divergent and undefined integrals. The covariant separation of these integrals from the infinite matrix element results in the finite expectation value of the observable in most cases. Exceptions are the calculation of self-energies, vacuum-polarization, scattering of light by light, and the self-stress. It is therefore necessary to introduce a relativistic cut-off, for example by the use of "regulators."[5] We shall consider the interaction of the electron field ψ with a set of neutral vector fields $A_\mu^{(i)}$ of mass M_i and coupling constant f_i ($i=0, 1, 2, \cdots$). At the end we shall pass to the limit[6] as $M_0\to 0$ and $M_i\to\infty$ ($i\neq 0$). The resulting integrals will be finite and well determined if the f_i and M_i satisfy certain conditions. In the course of the calculations the following condition will turn out to be necessary and sufficient:

$$\sum_i f_i^2=0. \quad (3)$$

We shall first give a simple argument which shows that the self-stress is identically zero to all orders and then carry out an explicit calculation to first order in $\alpha=e^2/(4\pi)$.[7]

A SIMPLE ARGUMENT[8]

The Lagrangian density for the system electron field —neutral vector meson fields is

[2] S. Tomonaga, Prog. Theor. Phys. **1**, 27 (1946); Koba, Tati, Tomonaga, Prog. Theor. Phys. **2**, 101, 198 (1947); S. Kanesawa and S. Tomonaga, Prog. Theor. Phys. **3**, 1, 101 (1948).

[3] J. S. Schwinger, Phys. Rev. **74**, 1439 (1948); **75**, 651 (1949); **76**, 790 (1949).

[4] F. J. Dyson, Phys. Rev. **75**, 486, 1736 (1949).

[5] W. Pauli and F. Villars, Rev. Mod. Phys. **21**, 434 (1949). References to earlier work on this subject are also found in this article.

[6] This "formalistic" use of the auxiliary fields is employed since any attempt at a consistent "realistic" theory leads to Bose-fields of negative energy and to other difficulties. See also reference 5.

[7] In the following we shall use Heaviside-Lorentz units and in general use the same notation as Schwinger and Dyson (references 3 and 4); note however that our $S_F(x)$ equals Dyson's $S_F(-x)$. We use ∂_μ for $\partial/\partial x_\mu$ and a bold letter like $\boldsymbol{A}$ for $\gamma_\mu A_\mu$.

[8] This type of argument was first used by A. Pais, Rev. Mod. Phys. **21**, 445 (1949) and led him to the wrong result $\Theta_{11}^{(0)}=(\alpha/2\pi)m\bar{\psi}\psi$. The reason for this finite non-vanishing result is

$$\mathfrak{L}(x)=-\sum_i[\bar{\psi}(x)(\partial-ief_iA^{(i)}+m)\psi(x)$$
$$+\tfrac{1}{4}F_{\mu\nu}'^{(i)}(x)-(M_i^2/2)A_\lambda^{(i)}A_\lambda^{(i)}] \quad (4)$$

from which one finds the symmetrized energy-momentum tensor density and the Hamiltonian density in the usual way. The latter is of the form

$$\mathfrak{IC}(x)=\mathfrak{IC}'(x)+m\bar{\psi}(x)\psi(x)$$
$$+\sum_i(M_i^2/2)A_\lambda^{(i)}(x)A_\lambda^{(i)}(x), \quad (5)$$

where $\mathfrak{IC}'(x)$ does not contain the masses explicitly. From Eqs. (5) and (4) we obtain

$$\Theta_{\mu\mu}^{(e)}=-m\bar{\psi}\psi=-m(\partial\mathfrak{IC}/\partial m),$$
$$\Theta_{\mu\mu}^{(i)}=-M_i^2A_\lambda^{(i)}A_\lambda^{(i)}=-M_i(\partial\mathfrak{IC}/\partial M_i), \quad (6)$$
$$\Theta_{44}=-\mathfrak{IC}.$$

For the rest system we have, omitting the index zero from now on

$$\Theta_{11}=\tfrac{1}{3}(\Theta_{\mu\mu}-\Theta_{44}). \quad (7)$$

The expectation value of Θ_{11} which we shall designate by $\langle\Theta_{11}\rangle$ in a state where there is one electron present and no other particle, is therefore

$$\langle\Theta_{11}\rangle=-\tfrac{1}{3}(m(\partial/\partial m)+\sum_i M_i(\partial/\partial M_i)-1)\langle\mathfrak{IC}\rangle$$

but since $\langle\mathfrak{IC}\rangle$ is simply the self-energy of the electron we have for dimensional reasons

$$\langle\mathfrak{IC}\rangle=\mathfrak{IC}_{\text{self}}^{(e)}=mf(m/M_i) \quad (8)$$

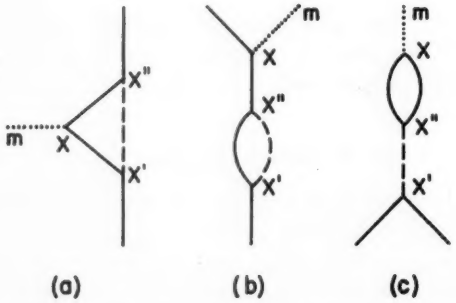

FIG. 1. Diagrams for the calculation of the interaction of an electron (full lines) with an external field (dotted lines) to second order in the coupling between the electron and its radiation field. For the calculation with regulators the photon lines (dashed lines) represent neutral vector mesons. (See Eq. (10).)

and

$$\langle\Theta_{11}\rangle=-\frac{m}{3}\left(m\frac{\partial}{\partial m}+\sum_i M_i\frac{\partial}{\partial M_i}\right)\left\langle\frac{\mathfrak{IC}}{m}\right\rangle$$
$$=-\frac{m}{3}\left(\frac{\partial}{\partial\log m}-\sum_i\frac{\partial}{\partial\log M_i}\right)f\left(\frac{m}{M_i}\right)$$
$$=0. \quad (9)$$

CALCULATION OF THE SELF-STRESS TO ORDER α

We shall use the Feynman[9]-Dyson[4] method to write down the matrix elements from the corresponding diagrams and evaluate the integrals with the Feynman method.

We first turn to the evaluation of $\Theta_{\mu\mu}^{(i)}=-m\bar{\psi}\psi$. As is shown in the Appendix, the expectation value of this operator is identical with the expectation value of the interaction energy of the ψ field with a constant external scalar field of strength m, i.e., we regard $-m\bar{\psi}\psi$ as the interaction energy of these two fields. The diagrams corresponding to that process for a state of one electron and no other particles present in first order of α are clearly these shown in Fig. 1. They are identical with those for the radiative corrections (Lamb-shift and correction to electron scattering), except that the external field is a scalar rather than a vector field. One finds[7]

$$\langle\Theta_{\mu\mu}^{(e)}(x)\rangle=-\tfrac{1}{2}\alpha m\pi\sum_i f_i^2\Big[\int\bar{\psi}(x')\gamma_\lambda S_F(x'-x)$$
$$\times S_F(x-x'')\gamma_\lambda\psi(x'')\Delta_F^{(i)}(x'-x'')dx'dx''$$
$$+\int\bar{\psi}(x')\gamma_\lambda S_F(x'-x'')\gamma_\lambda$$
$$\times S_F(x''-x)\psi(x)\Delta_F^{(i)}(x'-x'')dx'dx''$$
$$+\int\bar{\psi}(x')\gamma_\lambda\psi(x')\Delta_F^{(i)}(x'-x'')$$
$$\times Tr(\gamma_\lambda S_F(x''-x)S_F(x-x''))dx'dx''\Big], \quad (10)$$

and in momentum space

$$\langle\Theta_{\mu\mu}^{(e)}(p)\rangle=-(i\alpha m/4\pi^3)$$
$$\times\sum_i f_i^2\Big[\int\bar{\psi}(p)\gamma_\lambda\left(\frac{ip-ik-m}{(p-k)^2+m^2}\right)^2\gamma_\lambda\psi(p)\frac{d_4k}{k^2+M_i^2}$$
$$+\int\bar{\psi}(p)\gamma_\lambda\frac{ip-ik-m}{(p-k)^2+m^2}\gamma_\lambda\frac{ip-m}{p^2+m^2}\psi(p)\frac{d_4k}{k^2+M_i^2}$$
$$+\int\bar{\psi}(p)\gamma_\lambda\psi(p)\frac{1}{M_i^2}Tr\left(\gamma_\lambda\left(\frac{ik-m}{k^2+m^2}\right)^2\right)d_4k\Big]. \quad (11)$$

As explained in the appendix of the second paper of

found in that he did not take into account regulators. It is vital to the calculation of the self-stress that the theory be *finite*. Otherwise, it would be necessary to circumvent the direct integration which gives $(\alpha/2\pi)m\bar{\psi}\psi$ by the explicit use of the conservation laws $\partial_\mu\Theta_{\mu\nu}=0$. The situation is completely analogous to the calculations of the photon self-energy (G. Wentzel, Phys. Rev. **74**, 1070 (1948)) were the conservation of charge $\partial_\mu j_\mu=0$ has to be used explicitly in order to obtain the result zero.—I am grateful for a discussion on this point to Drs. S. Borowitz and W. Kohn who are calculating the self-stress along these lines.

[9] R. P. Feynman, Phys. Rev. **76**, 749, 769 (1949).

Feynman,[9] we have to introduce the auxiliary variables x into each integral, shift the origin such that the denominator depends only on k^2 and integrate with respect to d_4k. The following integrals occur in the first term of (11).

$$\sum_i f_i^2 \int \frac{k_\lambda^2 d_4k}{(k^2+a_i^2)^3} = -i\pi^2 \sum_i f_i^2 \ln a_i^2, \quad (12a)$$

$$\sum_i f_i^2 \int \frac{d_4k}{(k^2+a_i^2)^3} = \tfrac{1}{2} i\pi^2 \sum_i (f_i^2/a_i^2), \quad (12b)$$

where use was made of (3). The first term of (11) yields, therefore, after an easy calculation,

$$8i\pi^2 \bar{\psi}(p)\psi(p) \sum_i f_i^2 \int_0^1 x dx \{\ln[(M_i^2/m^2)(1-x)+x^2] + \tfrac{1}{2}(1-x+x^2)((M_i^2/m^2)(1-x)+m^2x^2)\}. \quad (13)$$

Whereas we could use the Dirac equation $(i\not{p}+m)\psi=0$ and $p^2+m^2=0$ without running into difficulties in the first term of (11), this is not so for the second term. One has of course to subtract the renormalization integral before the use of the Dirac equation is justified. Following Feynman[9] and Dyson[4] we have for the second term of (11)

$$\begin{aligned} &2i\pi^2 \int_0^1 dx \bar{\psi}(p)[i\not{p}(1-x)+2m][(i\not{p}-m)/(p^2+m^2)]\psi(p) \\ &\times \ln[(M_i^2/m^2)(1-x)+((p^2/m^2)+1)x-(p^2/m^2)x^2] \\ &-2i\pi^2 \int_0^1 dx \bar{\psi}(p) m(1+x)[(i\not{p}-m)/(p^2+m^2)] \\ &\times \psi(p) \ln[(M_i^2/m^2)(1-x)+x^2] \\ &= 2i\pi^2 \int_0^1 dx \bar{\psi}(p) \{(i\not{p}+m)(1-x)[(i\not{p}-m)/(p^2+m^2)] \\ &\times \psi(p) \ln[(M_i^2/m^2)(1-x)+((p^2/m^2)+1)x \\ &-(p^2/m^2)x^2] + m(1+x)[(i\not{p}-m)/(p^2+m^2)]\psi(p) \\ &\times \ln[1+(p^2+m^2)x(1-x)/(M_i^2(1-x)+m^2x^2)]\}. \end{aligned}$$

We expand the second logarithm and find after use of the Dirac equation

$$2i\pi^2 \int_0^1 dx \bar{\psi}(p)[(x-1)\ln[(M_i^2/m^2)(1-x)+x^2] + m(1+x)(-2m)x(1-x)/(M_i^2(1-x)+m^2x^2)]\psi(p). \quad (14)$$

The third term of (11) is easily seen to vanish;[9a] the "vacuum polarization" diagram (Fig. 1c) does not contribute. From (13) and (14) the expectation value (11) becomes

$$\langle \Theta_{\mu\mu}{}^{(a)}(p)\rangle = \frac{\alpha}{\pi} m\bar{\psi}(p)\psi(p) \sum_i f_i^2 \int_0^1 dx \{\tfrac{1}{2}(5x-1) \times \ln[(M_i^2/m^2)(1-x)+x^2] - (x^2-2x^3)/((M_i^2/m^2)(1-x)+x^2)\}.$$

An elementary integration leads in the limit $M_i \to \infty$ $(i \neq 0)$ $(M_0 \to 0)$, since $f_0=1$ by definition, with (3) to

$$\langle \Theta_{\mu\mu}{}^{(a)}(p)\rangle = (\alpha/2\pi) m\bar{\psi}(p)\psi(p)(3l_m+9/4), \quad (15)$$

where

$$l_m = \sum_{i\neq 0} f_i^2 \ln(M_i^2/m^2). \quad (16)$$

We now turn to the evaluation of

$$\Theta_{\mu\mu}{}^{(i)} = -M_i^2 A_\lambda{}^{(i)} A_\lambda{}^{(i)}.$$

This operator is again regarded as the interaction energy of the $A_\mu{}^{(i)}$ field with a constant scalar field of coupling M_i^2. The corresponding diagram is shown in Fig. 2: The vector meson emitted by the electron is scattered by the external field and then reabsorbed. This process is essentially different from the processes considered in Dyson's papers. It is, however, very similar to the "Lamb-shift" process, i.e., to Fig. 1a: Instead of the P brackets of 2 pairs $\bar{\psi}\psi$ and 1 pair $A_\mu A_\nu$ we now have 1 pair $\bar{\psi}\psi$ and 2 pairs $A_\mu A_\nu$. The missing pair of anticommuting operators introduces a minus sign in front of the matrix element,[10] the P bracket of the four A_μ's yields a factor[11] 2, and otherwise the integrals for Figs 1a and 2 differ only by the interchange of the S_F functions and the $\Delta_F{}^{(i)}$ functions. Thus we find

$$\langle \Theta_{\mu\mu}{}^{(i)}(x)\rangle = \frac{e^2}{4} \sum_i f_i^2 M_i^2 \int \bar{\psi}(x')\gamma_\lambda S_F(x'-x'') \times \gamma_\lambda \psi(x'') \Delta_F(x'-x) \Delta_F(x-x''), \quad (17a)$$

FIG. 2. Diagram for the calculation of the interaction of a virtual neutral vector meson (dashed lines) with an external field (dotted lines). (See Eq. (17a).)

[9a] Actually, the identically vanishing traces of one and three γ_μ's are multiplied by divergent integrals. Strictly speaking it would be necessary to use a cut-off; e.g., one can add electron fields of mass m_i and coupling constants g_i. As for the vacuum-polarization the conditions on them would be $\Sigma g_i{}^2=0$; $\Sigma g_i{}^2 m_i{}^2=0$.

[10] See Dyson's first paper (reference 4), Eq. (51).

[11] $P(\psi(x')\psi(x)\psi(x)\psi(x'')) = \tfrac{1}{2}\eta(x',x) S_F(x'-x) \tfrac{1}{2}\eta(x,x'') S_F(x-x'')$, $P(A_\mu(x')A_\lambda(x)A_\lambda(x)A_\nu(x'')) = 2\cdot\tfrac{1}{2}\delta_{\mu\lambda}\delta_{\nu\lambda}\Delta_F(x'-x)\Delta_F(x-x'')$. Note that the factor 2 would not occur if A_μ were a charged field and we had $P(A_\mu{}^*(x')A_\lambda(x)A_\lambda{}^*(x)A_\nu(x''))$.

$$\langle\Theta_{\mu\mu}{}^{(i)}(p)\rangle=\frac{i\alpha}{4\pi^3}\sum_i f_i{}^2M_i{}^2\int\bar{\psi}(p)\gamma_\lambda\frac{i\not{p}-i\not{k}-m}{(p-k)^2+m^2}$$

$$\times\gamma_\lambda\psi(p)\frac{d_4k}{(k^2+M_i{}^2)^2}. \quad (17b)$$

Again we introduce the variables x and find after a shift of origin and application of (12b)

$$\langle\sum_i\Theta_{\mu\mu}{}^{(i)}(p)\rangle=(\alpha/\pi)m\bar{\psi}(p)\psi(p)\sum_i f_i{}^2M_i{}^2$$

$$\times\int_0^1(1-x^2)dx/[M_i{}^2(1-x)+m^2x^2].$$

We see that for $i=0$ we find $\Theta_{\mu\mu}{}^{(0)}(p)=0$ indicating the vanishing value of the photon self-energy. The limit of the other fields gives, because of (3),

$$\langle\sum_i\Theta_{\mu\mu}{}^{(i)}(p)\rangle=-(3\alpha/2\pi)m\bar{\psi}(p)\psi(p). \quad (18)$$

The $\langle\Theta_{44}\rangle$ term is simply the self-energy of the vector mesons and the electron, taken in a state where there is only an electron present. Therefore

$$\langle\Theta_{44}\rangle=\langle\Theta_{44}{}^{(e)}\rangle=-\mathcal{H}_{\text{self}}^{(e)}$$

$$=(-\alpha/2\pi)\bar{\psi}\psi(-3l_m+\tfrac{3}{4}). \quad (19)$$

The last relation is easy to work out and agrees with Feynman's expression[12] if we use only *one* additional field[13] $M_1=\lambda$ and, because of (3), $f_1{}^2=-f_0{}^2=-1$.

The expectation value to order α of the self-stress, Eq. (6), becomes with (15), (18), and (19)

$$\langle\Theta_{11}(p)\rangle=\tfrac{1}{3}(\alpha/2\pi)m\bar{\psi}(p)\psi(p)$$

$$\times(3l_m+9/4-3-3l_m+\tfrac{3}{4})=0. \quad (20)$$

Since the l_m terms cancel, the result without regulators would also be finite but would not include the term (18) and thus yield Pais' result $(\alpha/2\pi)m\bar{\psi}\psi$. It should be pointed out here that in the use of regulators one usually adds the matrix elements corresponding to the auxiliary fields ($i=1, 2, \cdots$) to the matrix element which is to be regulated ($i=0$). This method does not work here. It would again mean omitting the term (18) and we would find the same result as without regulators.

In conclusion the author would like to thank Professor R. P. Feynman for very helpful discussions, and Professor J. R. Oppenheimer for his stimulating interest and the extremely profitable time which the author spent at the Institute for Advanced Study.

[12] Reference 9, second paper, Eq. (21).

[13] If one does not carry out the limiting process $M_1\to\infty$ this special case is identical with the proposals by F. Bopp, Ann. d. Physik **38**, 345 (1940); **42**, 575 (1943) and A. Landé and L. Thomas, Phys. Rev. **60**, 121, 514 (1940); **65**, 175 (1944). It is to be noted that this additional vector field has negative energy, since $f_1{}^2=-1$.

APPENDIX

Expectation Values in the Feynman-Dyson Formalism

Let ψ_H and $A_{\mu H}$ be the operators representing the electron and the electromagnetic fields in the Heisenberg representation; let ψ_H and/or $A_{\mu H}$ interact with an external field such that the interaction energy is $\mathcal{H}_H{}^{\text{int}}$. Let Φ and $\Psi(\sigma)$ denote the functionals in the Heisenberg representation and in the interacting representation. Then

$$\Psi(\sigma)=U(\sigma)\Phi \quad (A1)$$

and any operator $F_H(x)$ in the Heisenberg representation is related to the same operator in the interaction representation, $F(x)$, by[14]

$$F(x)=U(\sigma)F_H(x)U^{-1}(\sigma) \quad (A2)$$

such that the expectation value

$$\langle F_H(x)\rangle=(\Phi, F_H(x)\Phi)=(U^{-1}\Psi, F_HU^{-1}\Psi)=(\Psi, F\Psi).$$

Also

$$i(\delta\Psi(\sigma)/\delta\sigma)=(\mathcal{H}^{(i)}+\mathcal{H}^{\text{int}})\Psi(\sigma), \quad (A3)$$

where $\mathcal{H}^{(i)}=-j_\mu A_\mu$ and the missing subscript H indicates the interaction representation. A further transformation $S(\sigma)$ leads to the new functional $\Omega(\sigma)$ given by[3,4]

$$\Omega(\sigma)=S(\sigma)\Psi(\sigma) \quad (A4)$$

such that

$$i(\delta\Omega(\sigma)/\delta\sigma)=S^{-1}(\sigma)\mathcal{H}^{\text{int}}(x)S(\sigma)\Omega(\sigma), \quad (A5)$$

where

$$S(\sigma)=1+(-i)\int_{-\infty}^{\infty\sigma}dx_1\mathcal{H}^{(i)}(x_1)$$

$$+(-i)^2\int_{-\infty}^{\sigma}dx_1\int_{-\infty}^{\sigma_1}dx_2\mathcal{H}^{(i)}(x_1)\mathcal{H}^{(i)}(x_2)+\cdots.$$

The expectation value of $\mathcal{H}^{\text{int}}$ is

$$\langle\mathcal{H}^{\text{int}}\rangle=(\Omega(\sigma), S^{-1}(\sigma)\mathcal{H}^{\text{int}}(x)S(\sigma)\Omega(\sigma)). \quad (A6)$$

Consider now an operator O_H in the Heisenberg representation. It follows from (A2) that this operator in the Ω representation is $S^{-1}U^{-1}O_HUS=S^{-1}OS$. The expectation value is therefore

$$\langle O\rangle=(\Omega, S^{-1}OS\Omega). \quad (A7)$$

Apparently, diagrams can only be drawn for matrix elements of interaction energies, i.e., for expectation values of the type (A6), and at first sight it seems that the Feynman-Dyson method is incapable of calculating expectation values of operators in general, i.e., it seems not possible to immediately write down the integral (A7), because there is no corresponding diagram.

The fact that (A6) actually is only a special case of (A7) suggests the following simple method. Assume first that O is a scalar operator. Since O will always be bilinear in ψ and/or A_μ we can regard it as an interaction energy between the ψ and/or the A_μ field with some external field and solve this equivalent problem which can easily be put into diagrams. Thus the operator $O_H=\Theta_{\mu\mu H}{}^{(e)}=-m\bar{\psi}_H\psi_H$ is clearly the interaction energy of the ψ field with a constant scalar field. A similar reasoning holds for $\Theta_{\mu\mu}{}^{(i)}=-M_i{}^2A_\mu{}^{(i)}A_\mu{}^{(i)}$.

If the operator is not a scalar we can construct a scalar operator by multiplication with a corresponding operator. For example, the expectation value of $O_H=\bar{\psi}_H\sigma_{\mu\nu}\psi_H$ can be calculated by finding the expectation value of $\mathcal{H}_H{}^{\text{int}}=\bar{\psi}_H\sigma_{\mu\nu}F_{\mu\nu}{}^e\psi_H$, where $F_{\mu\nu}{}^e$ is a fictitious external field contragradient to $\sigma_{\mu\nu}$.

[14] Note that Eq. (A2) in general contains additional terms if $F_H(x)$ involves differential operators (see Schwinger, reference 3). This does not effect the arguments given below.

On the Effects of Internal Nuclear Motion on the Hyperfine Structure of Deuterium

FRANCIS LOW
Department of Physics, Columbia University, New York, New York
(Received October 3, 1949)

The effects of internal nuclear motion on the hyperfine structure of deuterium are investigated, using Dirac theory for the electron and non-relativistic theory for the nucleus. Although the final result is in fair agreement with experiment, theoretical and experimental uncertainties are at present too large to allow any conclusions to be drawn concerning the possible deviation of nucleon magnetic fields from those of simple dipoles.

I. INTRODUCTION

THE accurate measurement of the hyperfine structure of hydrogen and deuterium by Nafe and Nelson[1] is not in complete agreement with Fermi's formula:[2]

$$h\nu = 8\pi/3 \cdot (2I+1)/I \cdot \mu_0 \mu \psi^2(0), \tag{1}$$

where I is the nuclear spin in units of $\hbar$, μ_0 the Bohr magneton, μ the nuclear magnetic moment and $\psi(0)$ the Schrödinger wave function evaluated at the origin. Although there are slight corrections to ν_D and ν_H arising from the intrinsic electromagnetic moment of the electron[3] and from the use of the exact relativistic wave functions for D and H, their ratio

$$\nu_D/\nu_H = \tfrac{3}{4}(m_D/m_H)^3 \mu_D/\mu_P \tag{2}$$

should be independent of these effects, as well as of the natural constants entering into (1), except for the ratios μ_D/μ_P and m_D/m_H, the former of which is known from the experiments of Bloch, Levinthal, and Packard,[4] of Bitter, Alpert, Nagle, and Poss[5] and of Siegbahn and Lindstrom.[6] Here m_D and m_H are the reduced masses of the deuterium and hydrogen atoms.

Using the value of μ_D/μ_P given by Bloch, Levinthal, and Packard, and that of ν_D/ν_H given by Nafe and Nelson, one finds:

$$\nu_D/\nu_H = \tfrac{3}{4}(m_D/m_H)^3 \mu_D/\mu_P [1+(1.7\pm 0.1)\times 10^{-4}]. \tag{3}$$

A. Bohr[7] has shown that most of this discrepancy can be accounted for by taking into consideration the structure of the deuteron. He points out that when the electron is close to the nucleus it moves rapidly compared to the nuclear motion and will therefore be bound to the apparently stationary proton rather than to the deuteron center of mass. This will be a good approximation inside a distance, ρ, which is large compared with the nuclear radius, $d=(\hbar^2/MW_0)^{\frac{1}{2}}$, but much smaller than the atomic radius a_0. Here W_0 is the binding energy of the deuteron. The order of magnitude of ρ may be estimated from the critical electron momentum, p_c, at which the electron energy, E, is equal to some mean nuclear excitation energy, $\bar{W}_N$, and hence at which the frequencies of the electronic and nuclear motions are equal; since p_c turns out to be greater than mc we may write

$$E \sim c p_c \sim \bar{W}_N, \quad p_c \sim \bar{W}_N/c.$$

The distance, ρ, corresponding to p_c is then given by

$$\rho \sim \hbar/p_c \sim \hbar c/\bar{W}_N = (\hbar/mc)mc^2/\bar{W}_N. \tag{4}$$

It is obvious, from (4), that $d \ll \rho \ll a_0$. The contribution to the h.f.s. from inside ρ must be calculated using a wave function with the electron centered on the proton; the contribution from outside will be relatively insensitive to where the electron is centered.

In first approximation, then, the proton h.f.s. will be unaffected by the deuteron structure; the neutron moment, however, will appear to the electron as a moment density distributed around the proton, and therefore its effect will nearly cancel when the electron is in the nucleus. Since the h.f.s. interaction is $\sim 1/r^2$, equal spherical shells in the atom contribute about equally up to the atomic radius, and one would expect a relative correction

$$\epsilon \sim \epsilon_0 = -(\mu_N/\mu_D) d/a_0 = +1.82\times 10^{-4} \tag{5}$$

which is in very good agreement with the experimental result (3). Bohr finds just this number by neglecting the range of the neutron-proton force compared with the deuteron radius, that is by taking for the nuclear wave function $\phi \approx (e^{-R/d}/R)$, and hence $d/2$ for the average distance between nucleons. He points out that since $R\phi$ must actually go to zero at $R=0$ the average distance between nucleons will be increased and therefore ϵ will be larger, $\epsilon = \epsilon_0 + \epsilon'$, where $\epsilon' \sim b\epsilon_0/d$ and b is the range of the force. For a square well potential one finds exactly $\epsilon' = b\epsilon_0/d$. Since $b/d \sim \frac{1}{3}$, this is an appreciable correction.

Bohr then suggests that this discrepancy might be compensated by the deviation of the proton and neutron magnetic fields from simple dipole fields within distances comparable with the meson wave-length (or the range b) and shows that this might be expected to lead to a further correction $\epsilon'' \sim -b\epsilon_0/d$.

It appears, therefore, that the h.f.s. experiment might yield information on the structure of nucleons. In view

[1] J. E. Nafe and E. B. Nelson, Phys. Rev. **73**, 718 (1948).
[2] E. Fermi, Zeits. f. Physik **60**, 320 (1930).
[3] H. M. Foley and P. Kusch, Phys. Rev. **73**, 412 (1948).
[4] Bloch, Levinthal and Packard, Phys. Rev. **72**, 1125 (1947).
[5] Bitter, Alpert, Nagle, and Poss, Phys. Rev. **72**, 1273 (1947).
[6] K. Siegbahn and G. Lindstrom, Arkiv. f. Physik, Band 1 NR 6, 193 (1949).
[7] A. Bohr, Phys. Rev. **73**, 1109 (1948).

of this possibility it is of interest to evaluate all effects which do *not* depend on the nucleon structure as accurately as possible.

In the first place we would like to have a better estimate of the average distance between nucleons. In the second place, Bohr's model essentially ignores nuclear compared to electron excitation energies in the region where nuclear structure can influence h.f.s.; this is equivalent to the inequality $d \ll \rho$. Actually d is not very much smaller than ρ, and Bohr's assumption may not be sufficiently accurate for our purpose. It is necessary, then, to investigate in more detail the effect of the off-center Coulomb field on the deuterium wave function near the nucleus, and to compute the h.f.s. using this wave function. In order to carry out this program we will use ordinary first- and second-order perturbation theory. It will be convenient to start our calculation using an unperturbed electronic wave function which is centered on the proton; this wave function will give Bohr's result, and would be exact if ρ/d were sufficiently large. The relative correction to the neutron spin h.f.s. arising from the finiteness of ρ/d is found to be of the order of magnitude

$$\epsilon_N \sim -\epsilon_0(d/\rho)\log\rho/d. \tag{6}$$

That of the proton spin, in this order, is zero.

Furthermore, the effects of the deuteron D state on the h.f.s. correction must be considered. The spin moment correction will be smaller, since the neutron spin in the D state is more likely to be antiparallel than parallel to the spin in the S state. Also, since the electron will see no nuclear motion while it is inside ρ, that part of the normal orbital h.f.s. which comes from inside ρ will be missing, giving a relative correction to the h.f.s. of

$$\epsilon_L \sim -\rho/a_0 \sin^2\omega \sim -\epsilon_0(\rho/d)\sin^2\omega, \tag{7}$$

where $\sin^2\omega$ is the fraction of D state in the deuteron ground state. Although $\rho > d$, we shall see that ϵ_L is still small because the deuteron has so little orbital angular momentum.

II. THE HAMILTONIAN

We start from the Hamiltonian

$$H = H_e + H_c + H_D + H_N' + H_P' + H_L', \tag{1}$$

where H_e is the Dirac Hamiltonian of a free electron

$$H_e = c\mathbf{p}\cdot\boldsymbol{\alpha} + \beta mc^2. \tag{2}$$

H_c is the Coulomb proton-electron interaction

$$H_c = -e^2/|\mathbf{r}+\mathbf{R}/2|. \tag{3}$$

H_D is the deuteron Hamiltonian

$$H_D = P^2/M + V(\mathbf{R}, P_{ex}). \tag{4}$$

H_N', H_P' and H_L' are the neutron spin, proton spin and orbital h.f.s. interactions:

$$H_P' = e\boldsymbol{\alpha}\cdot\nabla_r \frac{1}{|\mathbf{r}+\mathbf{R}/2|} \times \boldsymbol{\mu}_P, \tag{5}$$

$$H_N' = e\boldsymbol{\alpha}\cdot\nabla_r \frac{1}{|\mathbf{r}-\mathbf{R}/2|} \times \boldsymbol{\mu}_N, \tag{6}$$

and

$$H_L' = -\frac{e^2}{c}\frac{\mathbf{v}\cdot\boldsymbol{\alpha}}{|\mathbf{r}+\mathbf{R}/2|} \tag{7}$$

and where $\mathbf{r}$ is the position vector of the electron relative to the deuteron center of mass, $\mathbf{p}$ is the momentum conjugate to $\mathbf{r}$, $\boldsymbol{\alpha}$, β are the Dirac sixteen component matrices

$$\boldsymbol{\alpha} = \begin{pmatrix} 0 & \boldsymbol{\sigma} \\ \boldsymbol{\sigma} & 0 \end{pmatrix} \quad \sigma_x = \begin{pmatrix} 0 & 1 \\ 1 & 0 \end{pmatrix} \quad \sigma_y = \begin{pmatrix} 0 & -i \\ i & 0 \end{pmatrix}$$

$$\beta = \begin{pmatrix} I & 0 \\ 0 & -I \end{pmatrix} \quad \sigma_z = \begin{pmatrix} 1 & 0 \\ 0 & -1 \end{pmatrix} \quad I = \begin{pmatrix} 1 & 0 \\ 0 & 1 \end{pmatrix},$$

$\mathbf{R}$ is the position vector of the neutron relative to the proton, $\mathbf{P}$ is the momentum conjugate to $\mathbf{R}$, M is the neutron-proton mass, or twice the reduced mass of the deuteron, P_{ex} is the coordinate exchange operator.

We will assume for convenience that the nuclear potential V may be written $V = [1 - t + tP_{ex}]V(\mathbf{R})$. Furthermore it can be shown that the use of the charge-exchange operator together with an identical particle formulation for the proton and neutron leads to the same results as our present simpler treatment.

We have left out the deuteron center-of-mass kinetic energy which has been shown by Breit and Meyerott[8] to necessitate the use of the reduced masses in $I(2)$ so long as internal nuclear motion is ignored. They have shown that the higher order corrections will be of order $m/M(e^2/\hbar c)^2 \log e^2/\hbar c$ which we may safely ignore. If, therefore, we imagine the problem solved in zero order without internal nuclear motion (as by Breit and Meyerott), it is evident that the wave function found may be split up into our wave function (with the true electron mass) plus a wave function which gives corrections of order m/M. The effect on our calculation of using both wave functions instead of the first will be of order $m/M(d/a_0)$ which is negligible. Finally, reduced mass corrections due specifically to the internal nuclear motion are included in the Hamiltonian (1) and can be shown to have very small effects.

The interaction of an electron with a vector potential $\mathbf{A}$ is

$$-c(-|e|/c)\boldsymbol{\alpha}\cdot\mathbf{A} = e\boldsymbol{\alpha}\cdot\mathbf{A}.$$

The vector potential of a fixed moment, $\boldsymbol{\mu}$, may be taken as

$$\mathbf{A}_\mu(\mathbf{r}) = \nabla_r(1/|\mathbf{r}-\mathbf{R}|)\times\boldsymbol{\mu}, \tag{8}$$

[8] G. Breit and E. R. Meyerott, Phys. Rev. **72**, 1023 (1947).

where $\mathbf{R}$ is the position of the moment, $\mathbf{r}$ that of the electron. At distances of the order h/Mc from the moment this potential must of course be modified because of the nucleon recoil. This modification would lead to a correction of order h/Mca_0 where a_0 is the atomic radius. Since a calculation of effects taking place at a distance h/Mc from the nucleon would involve a relativistic theory of the nucleon, we shall not attempt to compute this correction.

We therefore take for the spin part of the h.f.s. interaction:

$$H_P'=e\boldsymbol{\alpha}\cdot\nabla_r\frac{1}{|\mathbf{r}+\mathbf{R}/2|}\times\boldsymbol{\mu}_P, \tag{5}$$

$$H_N'=e\boldsymbol{\alpha}\cdot\nabla_r\frac{1}{|\mathbf{r}-\mathbf{R}/2|}\times\boldsymbol{\mu}_N. \tag{6}$$

The vector potential of the nuclear current is taken to be

$$\mathbf{A}_L(\mathbf{r})=-(e/c)\mathbf{v}/|\mathbf{r}-\mathbf{R}|, \tag{9}$$

where $\mathbf{R}$ is the position vector of the source and $-\mathbf{v}$ its velocity.[9–11] In our case, $\mathbf{A}_L=-(e/c)\mathbf{v}/|\mathbf{r}+\mathbf{R}/2|$ and

$$\mathbf{v}=(i/2\hbar)(H_D\mathbf{R}-\mathbf{R}H_D)=\dot{\mathbf{R}}/2. \tag{10}$$

Naturally, $\mathbf{v}\neq\mathbf{P}/M$ if exchange forces are present. However, if the vector and scalar potentials are to satisfy the Lorentz condition, and therefore the field strengths Maxwell's equations, it is necessary to take $\mathbf{v}$ instead of $\mathbf{P}/M$ as the source of $\mathbf{A}$. We are thus led to

$$H_L'=-(e^2/2c)\left[\frac{\boldsymbol{\alpha}\cdot\mathbf{v}}{|\mathbf{r}+\mathbf{R}/2|}+\frac{\boldsymbol{\alpha}\cdot(\mathbf{r}+\mathbf{R}/2)\mathbf{v}\cdot(\mathbf{r}+\mathbf{R}/2)}{|\mathbf{r}+\mathbf{R}/2|^3}\right], \tag{11}$$

where the second term arises since we are dealing, not with an electron or a proton in a fixed field but with an electron-proton interaction; however, since it can easily be shown to differ from the first by $\boldsymbol{\alpha}$ dot a gradient, we may for our purposes simply take

$$H_L'=-(e^2/c)\boldsymbol{\alpha}\cdot\mathbf{v}/|\mathbf{r}+\mathbf{R}/2|. \tag{7}$$

Finally, since $\mathbf{v}$ and $\mathbf{R}$ do not commute, (7) must be symmetrized.

III. TRANSFORMATION TO A COORDINATE SYSTEM CENTERED ON THE PROTON

It is convenient, as has already been mentioned, to start from an unperturbed wave function which centers the electron on the proton. This can most easily be done by applying the transformation U, where

$$Uf(\mathbf{r},\mathbf{R})=f(\mathbf{r}+\mathbf{R}/2,\mathbf{R})$$

or

$$U=e^{i\mathbf{p}\cdot\mathbf{R}/2\hbar}. \tag{1}$$

U is obviously unitary in the space of $\mathbf{R}$ and $\mathbf{r}$. H will be modified as follows:

$$U^{-1}H_eU=H_e, \tag{2}$$

$$U^{-1}H_cU=-e^2/r, \tag{3}$$

$$U^{-1}H_P'U=e\boldsymbol{\alpha}\cdot\nabla(1/r)\times\boldsymbol{\mu}_P, \tag{4}$$

$$U^{-1}H_N'U=e\boldsymbol{\alpha}\cdot\nabla_r(1/|\mathbf{r}-\mathbf{R}|)\times\boldsymbol{\mu}_N, \tag{5}$$

$$U^{-1}H_L'U=-e^2/c(\mathbf{v}'_x\cdot\boldsymbol{\alpha}/r), \tag{6}$$

where

$$\begin{aligned}\mathbf{v}'&=U^{-1}\mathbf{v}U=U^{-1}[\mathbf{P}/M+i/2\hbar(V\mathbf{R}-\mathbf{R}V)]U\\&=\mathbf{P}/M+\mathbf{p}/2M+i/\hbar V_{ex}\mathbf{R}e^{i\mathbf{p}\cdot\mathbf{R}/\hbar}\\&=\mathbf{v}+\mathbf{p}/2M-1/\hbar^2V_{ex}\mathbf{R}\mathbf{p}\cdot\mathbf{R}+\cdots.\end{aligned} \tag{7}$$

The second term of (7) involves no nuclear coordinates, and hence will not contribute to the h.f.s. The third term of (7) may also be omitted; in first-order it does not contribute to the h.f.s., in second-order it is zero, and in third-order it is negligibly small.

This leaves $\mathbf{v}'=\mathbf{v}$ and

$$U^{-1}H_L'U=-(e^2/c)\mathbf{v}\cdot\boldsymbol{\alpha}/r. \tag{8}$$

Finally,

$$\begin{aligned}U^{-1}H_DU&=U^{-1}P^2/MU+U^{-1}VU,\\U^{-1}P^2/MU&=P^2/M+\mathbf{p}\cdot\mathbf{P}/M+p^2/4M,\\U^{-1}VU&=(V-V_{ex})+V_{ex}e^{i\mathbf{p}\cdot\mathbf{R}/\hbar}\\&=V+i/\hbar V_{ex}\mathbf{p}\cdot\mathbf{R}-1/2\hbar^2V_{ex}(\mathbf{p}\cdot\mathbf{R})^2+\cdots,\end{aligned}$$

or

$$U^{-1}H_DU=H_D+H'+H'',$$

where

$$H'=\mathbf{p}\cdot\mathbf{v},\quad H''=p^2/4M-1/2\hbar^2V_{ex}(\mathbf{p}\cdot\mathbf{R})^2. \tag{9}$$

Collecting our results (2)–(9), we may rewrite the transformed Hamiltonian:

$$H=H_e+H_c+H_D+H'+H''+H_P'+H_N'+H_L',$$

where

$$\left.\begin{aligned}&H_e=c\mathbf{p}\cdot\boldsymbol{\alpha}+\beta mc^2,\quad H_c=-e^2/r,\quad H_D=P^2/M+V,\\&H'=\mathbf{p}\cdot\mathbf{v},\quad H''=p^2/4M-1/2\hbar^2V_{ex}(\mathbf{p}\cdot\mathbf{R})^2,\\&H_P'=e\boldsymbol{\alpha}\cdot\nabla(1/r)\times\boldsymbol{\mu}_P,\ H_N'=e\boldsymbol{\alpha}\cdot\nabla(1/|\mathbf{r}-\mathbf{R}|)\times\boldsymbol{\mu}_N,\\&H_L'=-(e^2/c)(\boldsymbol{\alpha}\cdot\mathbf{v}/r).\end{aligned}\right\} \tag{10}$$

The significance of most of these terms is obvious. H'' is a reduced mass correction due to the centering of the electron on the proton rather than on the deuteron. The term of principal interest is H' which expresses the tendency of the nuclear motion to center the electron on the deuteron.

We note that the expectation of the orbital h.f.s. interaction is zero, i.e., $\langle H_L'\rangle=0$; this is not surprising, since in a coordinate system in which the proton is at rest there is no nuclear current and hence no magnetic moment due to the motion of charges.

Before proceeding to our calculation we note that since the h.f.s. coupling for an electron S state is of the

[9] A. J. F. Siegert, Phys. Rev. **52**, 787 (1937).
[10] W. E. Lamb, Jr. and L. I. Schiff, Phys. Rev. **54**, 651 (1938).
[11] R. G. Sachs, Phys. Rev. **74**, 433 (1948).

form

$$W=a\boldsymbol{\sigma}\cdot\mathbf{I}$$

one must have

$$\Delta W=W(F=I+\tfrac{1}{2})-W(F=I-\tfrac{1}{2})$$
$$=2I+1/I\cdot W(F=I+\tfrac{1}{2})$$

and hence it is only necessary to calculate the expectation of W for an eigenstate of $F=I+\frac{1}{2}$. The simplest such eigenstate is the one for which $m_I=+I$ and $m_J=+\frac{1}{2}$. Since we shall put our results in the form of relative corrections we may leave out the factor $2I+1/I$.

IV. EVALUATION OF THE PROTON SPIN H.F.S. FOR THE UNPERTURBED WAVE FUNCTIONS

We have, from III (10):

$$\langle H_P'\rangle=\langle e\boldsymbol{\alpha}\cdot\nabla(1/r)\times\boldsymbol{\mu}_P\rangle$$
$$=\mathbf{A}\cdot\boldsymbol{\mu}_P \tag{1}$$

where

$$\mathbf{A}=(\psi_0,\ e\boldsymbol{\alpha}\times\nabla(1/r)\psi_0).$$

Making use of the approximation

$$\psi_0=(1+\boldsymbol{\alpha}\cdot\mathbf{p}/2mc)u(0)\psi_s(r)$$
$$=\left(1+i\frac{\boldsymbol{\alpha}\cdot\mathbf{r}}{2r}\frac{h/mc}{a_0}\right)u(0)\psi_s(r), \tag{2}$$

where

$$\psi_s(r)=\psi(0)e^{-r/a_0},$$

and $u(0)=\begin{bmatrix}1\\0\\0\\0\end{bmatrix}$ for spin up, $u(0)=\begin{bmatrix}0\\1\\0\\0\end{bmatrix}$ for spin down

we have

$$\mathbf{A}=e^3/\hbar c(u(0)\psi_s(r),\ (\boldsymbol{\sigma}\times\mathbf{r}/r)\times\nabla(1/r)u(0)\psi_s(r))$$
$$=8\pi/3\mu_0\psi^2(0)\boldsymbol{\sigma}, \tag{3}$$

and

$$\langle H_P'\rangle=8\pi/3\psi^2(0)\mu_0\langle\boldsymbol{\sigma}\cdot\boldsymbol{\mu}_P\rangle. \tag{4}$$

This is Fermi's formula for the h.f.s. of the proton moment in deuterium. $\langle\boldsymbol{\mu}_P\rangle$ includes the D state correction to the effective proton moment in the deuteron:

$$\langle\boldsymbol{\sigma}\cdot\boldsymbol{\mu}_P\rangle=\mu_P(1-\tfrac{3}{2}\sin^2\omega),$$

where $\sin^2\omega$ is the D state probability.

It is understood that there are corrections of order $(e^2/\hbar c)^2$ to (4) which arise from the approximation (2); however they will cancel in the deuterium-hydrogen ratio and be negligible in all higher order terms. The reduced mass corrections to (4) we have already discussed in II.

V. EVALUATION OF THE NEUTRON SPIN H.F.S. FOR THE UNPERTURBED WAVE FUNCTIONS

We have, again from III (10):

$$\langle H_N'\rangle=\langle e\boldsymbol{\alpha}\cdot\nabla_r(1/|\mathbf{r}-\mathbf{R}|)\times\boldsymbol{\mu}_N\rangle. \tag{1}$$

The nuclear wave function consists of an S and a D term:

$$\Phi_0=\Phi_S+\Phi_D.$$

$\langle H_N'\rangle$ may then be divided into three parts: an S term, a D term and a cross term. We will consider first the S term.

$$\Phi_S=\cos\omega/(4\pi)^{\frac{1}{2}}[\phi_S(R)/R]\chi,$$

where χ is a spin function and

$$\int_0^\infty\phi_s^2(R)dR=1.$$

If we call

$$\mathbf{B}=(\Phi_s,\ \nabla_r(1/|\mathbf{r}-\mathbf{R}|)\times\boldsymbol{\mu}_N\Phi_s)$$
$$=\cos^2\omega/4\pi\nabla_r\int dR\phi_s^2(R)\int d\Omega_R/|\mathbf{r}-\mathbf{R}|\times\boldsymbol{\mu}_N \tag{2}$$

and make use of the formulas

$$\left.\begin{aligned}1/|\mathbf{r}-\mathbf{R}|&=\sum_{l=0}^\infty R^l/r^{l+1}P_l(\cos\gamma)\quad R<r\\&=\sum_{l=0}^\infty r^l/R^{l+1}P_l(\cos\gamma)\quad R>r\end{aligned}\right\} \tag{3}$$

$$P_l(\cos\gamma)=4\pi/2l+1\sum_{m=-l}^{l}Y_{lm}^*(\theta,\phi)Y_{lm}(\Theta,\Phi), \tag{4}$$

where $\cos\gamma=\mathbf{r}\cdot\mathbf{R}/rR$, and the Y_{lm} are normalized spherical harmonics, then

$$\left.\begin{aligned}\int\frac{d\Omega_R}{|\mathbf{r}-\mathbf{R}|}=\int\frac{d\Theta\sin\Theta d\Phi}{|\mathbf{r}-\mathbf{R}|}&=4\pi/r\quad R<r\\&=4\pi/R\quad R>r\end{aligned}\right\} \tag{5}$$

and

$$\mathbf{B}=\cos^2\omega\nabla\left[\frac{1}{r}\int_0^r\phi_s^2dR+\int_r^\infty\phi_s^2/R^{dR}\right]\times\boldsymbol{\mu}_N$$
$$=\cos^2\omega\nabla\frac{1}{r}\int_0^r\phi_s^2(R)dR\times\boldsymbol{\mu}_N, \tag{6}$$

which is of the same form as $\mathbf{A}$ in IV except that $\nabla(1/r)$ is replaced by

$$\left(\nabla\frac{1}{r}\right)\int_0^r\phi_s^2(R)dR;$$

we may therefore write, using IV (3):

$$\langle H_N'\rangle_s=8\pi/3\cos^2\omega\mu_0\langle\boldsymbol{\sigma}\cdot\boldsymbol{\mu}_N\rangle_s\psi^2(0)2/a_0$$
$$\times\int_0^\infty e^{-2/a_0}dr\int_0^r\phi_s^2(R)dR \tag{7}$$

$$=8\pi/3\cos^2\omega\psi^2(0)\mu_0\langle\boldsymbol{\sigma}\cdot\boldsymbol{\mu}_N\rangle_s$$
$$\times\left[1-2/a_0\int_0^\infty R\phi_s^2(R)dR\right]. \tag{8}$$

The first term in the bracket evidently gives the Fermi formula for the neutron spin h.f.s. without the D state correction to the effective neutron moment. The second term, to which we shall return later, is Bohr's correction. All higher terms are negligible.

We consider next the D state expectation

$$\langle H_N'\rangle_D=\langle e\boldsymbol{\alpha}\cdot\nabla_r(\Phi_D,\ 1/|\mathbf{r}-\mathbf{R}|\times\boldsymbol{\mu}_N\Phi_D)\rangle, \tag{9}$$

$$\Phi_D=\sin\omega\phi_D(R)/RY_D(\Omega_R),\quad \int_0^\infty \phi_D{}^2(R)dR=1,$$

where

$$Y_D=\bar{S}_{12}\chi_1=[(2/20)^{\frac{1}{2}}\chi_1Y_{20}+(6/20)^{\frac{1}{2}}\chi_0Y_{21}+(12/20)^{\frac{1}{2}}\chi_{-1}Y_{22}],$$

$$\bar{S}_{12}=1/(32\pi)^{\frac{1}{2}}\left(\frac{3\boldsymbol{\sigma}_P\cdot\mathbf{R}\boldsymbol{\sigma}_N\cdot\mathbf{R}}{R^2}-1\right).$$

In the expansion (3) the only terms which do not integrate to zero over nuclear angles are the harmonics of order 0, 2 and 4. Those of order 4 need not be considered since their gradient will consist of harmonics of order 3 and 5 which will in turn integrate to zero over electron angles.

The zeroth-order term in (3) evidently gives an analogous result to the S state expectation:

$$\langle H_N'\rangle_D{}^{L=0}=8\pi/3\ \sin^2\omega\psi^2(0)\mu_0\langle\boldsymbol{\sigma}\cdot\boldsymbol{\mu}_N\rangle_D\times\left[1-2/a_0\int_0^\infty R\phi_D{}^2(R)dR\right], \tag{10}$$

$$\langle\boldsymbol{\sigma}\cdot\boldsymbol{\mu}_N\rangle_D=(Y_D,\ (\mu_N)_zY_D)=-\tfrac{1}{2}\mu_N.$$

The first term in (10) is the D state correction to the effective neutron moment that was missing from (8). The second term is a further correction of the Bohr type, which, as we have already mentioned, will decrease the entire correction because the D state spin is effectively pointing against the S state spin.

An elementary calculation based on the expansions (3) and (4) and on the approximation IV (2) shows that the terms of order two in (3) add

$$\langle H_N'\rangle_D{}^{L=2}=8\pi/3\ \sin^2\omega\mu_0\mu_N\psi^2(0)\times\int_0^\infty R/4a_0\phi_D{}^2(R)dR \tag{11}$$

and that the cross term

$$\langle H_N'\rangle_{DS}=2R\langle e\boldsymbol{\alpha}\cdot(\Phi_S\nabla_r(1/|\mathbf{r}-\mathbf{R}|)\times\boldsymbol{\mu}_N\Phi_D)\rangle \tag{12}$$

(where R indicates that only the real part is to be taken) adds

$$\langle H_N'\rangle_{DS}=(8\pi/3)\ \sin\omega\ \cos\omega\psi^2(0)\mu_0\mu_N\times\int_0^\infty (2)^{\frac{1}{2}}/4(R/a_0)\phi_D\phi_SdR \tag{13}$$

to (8) and (10).

From the second terms in (8) and (10) and from (11) and (13) we find a relative correction to the h.f.s. of

$$\epsilon=-\mu_N/\mu_D\Big[2/a_0\cos^2\omega\int_0^\infty R\phi_S{}^2dR-5/4a_0\sin^2\omega\int_0^\infty R\phi_D{}^2dR-(\sqrt{2}/4a_0\cos\omega\sin\omega\int_0^\infty R\phi_D\phi_SdR\Big] \tag{14}$$

or

$$\epsilon=-\mu_N/\mu_D\cdot d/a_0[\cos^2\omega\langle 2\alpha R\rangle_S-5/4\ \sin^2\omega\langle\alpha R\rangle_D-\sqrt{2}/4\ \cos\omega\ \sin\omega\langle\alpha R\rangle_{DS}], \tag{15}$$

where

$$\alpha=1/d=(MW_0/\hbar^2)^{\frac{1}{2}}$$

and W_0 is the binding energy of the deuteron.

VI. EVALUATION OF ϵ

We have available for the determination of the nuclear ground state wave functions the deuteron binding energy, which determines their asymptotic form through the constant $\alpha=1/d$, low energy scattering data which determines the "effective range," $r_0=1.59\times10^{-13}$ cm,[12] the deuteron magnetic moment which determines (non-relativistically) the D state probability and the deuteron quadrupole moment which essentially determines a cut-off for the D state radial wave function.

Our main task is to find a good number for $\langle 2\alpha R\rangle_S$ since the second and third terms of V (15) are quite small.

The asymptotic form of the S state wave function is:

$$\phi_s(R)\rightarrow Ce^{-\alpha R}. \tag{1}$$

Let us define two functions, u and v, such that $v=e^{-\alpha R}$ and

$$u=[\phi_s(R)]/C; \tag{2}$$

then

$$\frac{r_0}{2}=\int_0^\infty (v^2-u^2)dR. \tag{3}$$

The constant C is determined by (3):

$$C=(2\alpha/1-r_0\alpha)^{\frac{1}{2}}. \tag{4}$$

If, then, following (3), we put for convenience

$$\int_0^\infty R(v^2-u^2)dR=(r_0/2)^2\lambda, \tag{5}$$

where we expect $\lambda\sim1$, we have

$$\langle 2\alpha R\rangle_S=\int_0^\infty \phi^2{}_S\cdot 2\alpha RdR=1+\alpha r_0+(1-\lambda)(\alpha r_0)^2/(1-r_{0\alpha})=1+\alpha r_0+\delta. \tag{6}$$

[12] H. A. Bethe, Phys. Rev. **76**, 38 (1949).

The unknown λ should be fairly close to one, so that the correction term δ in (6) may be expected to be smaller than $(\alpha r_0)^2$. We shall find that this is in fact the case. Unfortunately, (6) is not as accurate as we might wish. As a check, we have calculated $\langle 2\alpha R\rangle_S$ for an exponential, square well and Hulthen potential, the latter having properties closely resembling those of the Yukawa potential.

One finds, for the square well:

$$\langle 2\alpha R\rangle_S = 1+\alpha r_0+0.07, \tag{7}$$

for the exponential well:

$$\langle 2\alpha R\rangle_S = 1+\alpha r_0-0.08, \tag{8}$$

and for the Hulthen well:

$$\langle 2\alpha R\rangle_S = 1+\alpha r_0+0.03. \tag{9}$$

In calculating (7)–(9) the two parameters available for each potential were of course chosen so that α and r_0 remained fixed.

We have in all, then,

$$\langle 2\alpha R\rangle_S = 1+\alpha r_0 \pm 0.07 = 1.37 \pm 0.07. \tag{10}$$

The remaining two terms in V (15) are so small that an accuracy of 25 percent in their calculation is sufficient. This may be obtained simply by using the asymptotic D state wave function

$$\left.\begin{aligned} &\phi_D = (A(2\alpha)^{\frac{1}{2}}/\alpha^2R^2)e^{-\alpha R}(1+\alpha R+\tfrac{1}{3}\alpha^2R^2) \text{ for } R>b \\ &\text{and} \\ &\phi_D = 0 \text{ for } R<b. \end{aligned}\right\} \tag{11}$$

A and b are to be found by simultaneously normalizing and matching the deuteron quadrupole moment. This procedure yields

$$A = 0.47, \quad \alpha b = \tfrac{1}{2}, \tag{12}$$

and an elementary integration shows that

$$\langle \alpha R\rangle_{DS} = 0.55 \pm 0.15, \quad \langle \alpha R\rangle_D = 0.66 \pm 0.15. \tag{13}$$

Choosing $\sin^2\omega$ so that it will give, in a non-relativistic calculation, the measured magnetic moment of the deuteron, we have:

$$\sin^2\omega = 0.04, \quad \cos^2\omega = 0.96. \tag{14}$$

Finally, inserting the results (10), (13) and (14) into V (15) gives

$$\epsilon = -\mu_N d/\mu_D a_0 (1.24 \pm 0.08). \tag{15}$$

VII. EFFECT OF H' ON THE NEUTRON SPIN H.F.S.

We note first that $H' = \mathbf{p}\cdot\mathbf{v}$ has transitions between nuclear states of opposite parity whereas $H_P' = e\boldsymbol{\alpha}\cdot\nabla(1/r)\times\boldsymbol{\mu}_P$ has transitions only between nuclear states of the same parity. Therefore, in this order, the effect of H' on the proton spin h.f.s. is zero.

The neutron term is:

$$E_N = -2\sum_m\left[\sum_{n+}\frac{(H_N')_{0n,\,0m}H_{n0,\,m0}'}{E_n-E_0+W_m-W_0} - \sum_{n-}\frac{(H_N')_{n0,\,0m}H_{0n,\,m0}'}{E_0-E_n+W_m-W_0}\right], \tag{1}$$

where $E_{n\pm}$ refer to electron energies and W_m to nuclear energies. Summation over the indices m and n will be understood, although frequently the indices will be left out for convenience of notation.

E_N arises from a distortion of the electronic wave function inside the distance ρ, which is smaller than the electron Compton wave-length. It is therefore reasonable to suppose that most of E_N comes from electron energies corresponding to momenta that are greater than mc, and that the continuum states of the Coulomb field may be replaced by plane waves.

Using the approximation

$$\phi(p) = \psi(0)(e^2/r)_{P0}(u(p),\, u(0))/E(p)-E_0, \tag{2}$$

where

$$\phi(p) = (u(p)e^{i\mathbf{p}\cdot\mathbf{r}/\hbar},\, \psi_0(r)),$$

$u(p)$ is a Dirac spinor amplitude and

$$(e^2/r)_{p0} = 4\pi\hbar^2/p^2,$$

we have:

$$H_N' = e\boldsymbol{\alpha}\cdot\nabla_r(1/|\mathbf{r}-\mathbf{R}|)\times\boldsymbol{\mu}_N,$$

$$(H_N')_{0n} = -i/\hbar e^{i\mathbf{p}\cdot\mathbf{R}/\hbar}\psi(0)(1/r)_{p0} \times(u(0),\, e\boldsymbol{\alpha}\times\mathbf{p}\cdot\boldsymbol{\mu}_N u(p))+O(e^2/\hbar c), \tag{3}$$

$$H_{n0,\,m0}' \cong \mathbf{v}_{m0}\cdot\mathbf{p}\phi(\mathbf{p}) = \mathbf{p}\cdot\mathbf{v}_{m0}\psi(0)(e^2/r)_{p0} \times(u(p),\, u(0))/E(p)-E_0, \tag{4}$$

$$E_N(+) = 2\psi^2(0)ie^2/h\sum_{P+}(1/r)_{p0}{}^2e^{i\mathbf{p}\cdot\mathbf{R}/\hbar}\frac{\mathbf{p}\cdot\mathbf{v}_{m0}}{E(p)-E_0} \times\frac{(u(0),\, e\boldsymbol{\alpha}\times\mathbf{p}\cdot\boldsymbol{\mu}_N u(p))(u(p),\, u(0))}{E(p)-E_0+W_m-W_0}$$

$$= 2\psi^2(0)ie^2/h\sum_{P}(1/r)_{p0}{}^2e^{i\mathbf{p}\cdot\mathbf{R}/\hbar}\frac{\mathbf{p}\cdot\mathbf{v}_{m0}}{E(p)-E_0} \times\frac{(u(0),\, e\boldsymbol{\alpha}\times\mathbf{p}\cdot\boldsymbol{\mu}_N\Lambda^+(\mathbf{p})u(0))}{E(p)-E_0+W_m-W_0}, \tag{5}$$

where

$$\Lambda^+(\mathbf{p}) = (c\mathbf{p}\cdot\boldsymbol{\alpha}+\beta mc^2+|E(p)|)/2|E(p)| = 1 \text{ for } E>0 = 0 \text{ for } E<0,$$

and where it is understood that the unlabeled nuclear operators in (5) go from the state 0 to m. Since the term we are calculating is only a small correction, we may for simplicity assume that the nuclear ground state is

spherically symmetric. In that case, on the average,

$$(u(0), \alpha\times\mathbf{p}\cdot\boldsymbol{\mu}_N\Lambda^+(\mathbf{p})u(0))=icp^2\boldsymbol{\sigma}\cdot\boldsymbol{\mu}_N/3E(p)$$

(where from now on $E(p)$ is always to mean a positive number) and (5) becomes:

$$E_N(+)=-(2/3)e^3c/h\psi^2(0)\boldsymbol{\sigma}\cdot\boldsymbol{\mu}_N\int\frac{d\mathbf{p}}{(2\pi\hbar)^3}(1/r)^2_{p0}\times\frac{p^2\mathbf{p}\cdot\mathbf{v}_{m0}e^{i\mathbf{p}\cdot\mathbf{R}/\hbar}}{E(p)[E(p)-E_0][E(p)-E_0+W_m-W_0]}.$$

Carrying through the same procedure for the negative energy sums one finds in all:

$$E_N=-4/3\pi\psi^2(0)e^3c\boldsymbol{\sigma}\cdot\boldsymbol{\mu}_N\int\frac{d\Omega_p dp\mathbf{p}\cdot\mathbf{v}_{m0}}{E(p)}\times\left[\frac{e^{i\mathbf{p}\cdot\mathbf{R}/\hbar}}{D+}-\frac{e^{-i\mathbf{p}\cdot\mathbf{R}/\hbar}}{D-}\right] \quad (6)$$

where

$$D\pm=(E(p)\mp E_0)(E(p)\mp E_0+W_m-W_0).$$

Integrating over angles,

$$E_N=\frac{16i}{3}\psi^2(0)e^3c\boldsymbol{\sigma}\cdot\boldsymbol{\mu}_N\mathbf{v}_{m0}\cdot\frac{\mathbf{R}}{R}\int_0^\infty\frac{pdp}{E(p)}\times\left[\frac{1}{D+}+\frac{1}{D-}\right]\frac{(pR/\hbar)\cos(pR/\hbar)-\sin(pR/\hbar)}{(pR/\hbar)^2}. \quad (7)$$

The integrand is seen to behave as a constant for small p, as $1/p$ for p greater than mc but less than h/R, and as $1/p^3$ for still greater momenta. Relativistic momenta, therefore, contribute most strongly, as was assumed. In fact, compared to the energies involved in (7), the rest energy of the electron is negligible, and we may set:

$$\frac{1}{D+}+\frac{1}{D-}\cong\frac{2E(p)}{c^2p^2}\cdot\frac{1}{cp+W_m-W_0}$$

so that

$$E_N=32i\psi^2(0)(e^3/3hc^2)\boldsymbol{\sigma}\cdot\boldsymbol{\mu}_N\mathbf{v}_{m0}\cdot\mathbf{R}J(a_m), \quad (8)$$

where

$$J(a)=\int_0^\infty\frac{dx}{x+a}\cdot\frac{x\cos x-\sin x}{x^3}$$

and

$$x=pR/h,\quad a_m=\frac{(W_m-W_0)}{hc}R\sim R/\rho\ll 1.$$

Since the parameter a is small, the integral may be expanded in powers of a; one finds:

$$J(a)=-\tfrac{1}{3}[\log(1/\gamma a)+4/3-(3\pi/16)a+\cdots], \quad (9)$$

$\gamma=1.78$ is Euler's constant.

The last term in (9) is negligible. Dropping it, we have, from (8):

$$E_N=-\frac{16i}{3}\psi^2(0)(e^3/\hbar c^2)\cdot\frac{2}{3}\sum_m\left\{\boldsymbol{\sigma}\cdot\boldsymbol{\mu}_N\left[\log\frac{1}{\gamma a_m}+\frac{4}{3}\right]\mathbf{R}\right\}_{0m}\cdot\mathbf{v}_{m0} \quad (10)$$

and dividing the logarithm into more manageable parts,

$$E_N=-\frac{16i}{3}\psi^2(0)(e^3/\hbar c^2)\mu_N\cdot\frac{2}{3}\left[\left(\log\frac{mc^2}{|W_0|}\frac{\hbar/mc}{\gamma\cdot d/2}+\frac{4}{3}\right)\langle\mathbf{R}\cdot\mathbf{v}\rangle-\langle\log(2\alpha R)\mathbf{R}\cdot\mathbf{v}\rangle-\sum_m\mathbf{R}_{0m}\cdot\mathbf{v}_{m0}\log\frac{W_m-W_0}{|W_0|}\right]. \quad (11)$$

The first two expectations are easily evaluated:

$$\langle\mathbf{R}\cdot\mathbf{v}\rangle=\langle\mathbf{R}\cdot[\mathbf{P}/M-i/2\hbar(\mathbf{R}V-V\mathbf{R})]\rangle=(3/2)i\hbar/M(1+\eta t), \quad (12)$$

where

$$\eta=-2M/3\hbar^2\langle R^2V(R)\rangle.$$

If the exchange potential is binding, then $\eta>0$. Although η depends on the well shape of V, it will be of the order of magnitude of force range divided by nuclear radius, and since t is probably smaller than one, their product will not vary sufficiently (corresponding to different assumptions as to well shape) to affect our results significantly. We recall that t was defined as the fraction of exchange force in the deuteron.

One finds for η, by direct calculation:

$\eta=\frac{1}{3}$ for a Hulthen well,
$\eta=\frac{2}{5}$ for a square well.

The second term in (11) contributes

$$\langle\log(2\alpha R)\mathbf{R}\cdot\mathbf{v}\rangle=3\hbar i/2M\left[\frac{1}{3}+\int_0^\infty\phi_s^2\log 2\alpha R dR-2t/3\int_0^\infty\phi_s^2\log 2\alpha R(MV/\hbar^2)R^2dR\right] \quad (13)$$

of which the last two terms are negligible.

Finally, the summation

$$K=\sum_m\mathbf{R}_{0m}\cdot\mathbf{v}_{m0}\log\frac{W_m-W_0}{|W_0|}$$

contributes about one-half of E_N. Therefore a 10 percent error in K will be cut to 5 percent in E_N. It turns out that to within 10 percent one can approximate K by

the simple formula

$$K\cong 3i\hbar/2M(1+\eta t)\left[\log\frac{3(1+\eta t)}{\langle\alpha^2R^2\rangle}+\frac{1}{3}\right]. \quad (14)$$

Note also that $\langle\alpha^2R^2\rangle$ is practically independent of assumptions about well shape:

$$\langle\alpha^2R^2\rangle=1/2(1-r_0\alpha). \quad (15)$$

From (11)–(14) we find a relative correction to the h.f.s. of

$$\epsilon_N=(4/\pi)(e^2/\hbar c)(m/M)\mu_N/\mu_D$$
$$\times\left\{(1+\eta t)\left[1+\log\frac{mc^2 2\alpha(\hbar/mc)\langle\alpha^2R^2\rangle}{|W_0|3\gamma(1+\eta t)}\right]-\frac{1}{3}\right\} \quad (16)$$

which, it is of interest to note, is of order of magnitude

$$\epsilon_N\sim-\epsilon_0 d/\rho[1+\log\rho/d], \quad (17)$$

where ρ is the critical distance defined in I (4).

Numerically,

$$\epsilon_N=(\mu_N/\mu_D)(d/a_0)[0.155(1+\xi t)\pm 10 \text{ percent}], \quad (18)$$

where $\xi=\frac{1}{4}$ for a Hulthen well, $\xi=\frac{3}{10}$ for a square well.

VIII. ORBITAL H.F.S.

We have seen in III that our unperturbed wave function gave zero orbital h.f.s. Therefore the effect of the perturbation H' on the wave function must give us both the normal orbital h.f.s. and the correction to it which was discussed in I.

The orbital h.f.s. is therefore given by

$$E_L=-2\sum_m\left[\sum_{n+}\frac{H_{0n,0m}'(H_L')_{n0,m0}}{E_n-E_0+W_m-W_0}\right.$$
$$\left.-\sum_{n-}\frac{H_{n0,0m}'(H_L')_{0n,m0}}{E_0-E_n+W_m-W_0}\right] \quad (1)$$

where

$$H'=\mathbf{p}\cdot\mathbf{v},\quad H_L'=-(e^2/c)\frac{\boldsymbol{\alpha}\cdot\mathbf{v}}{r}.$$

The neglect of electron energies in (1) leads simply to the expectation of the normal h.f.s. which until now has been missing. To see this, we add and subtract

$$E_F=-2\sum_m\sum_{n\pm}H_{0n,0m}'(H_L')_{n0,m0}/W_m-W_0 \quad (2)$$
$$=2ie^2/2c\hbar\langle\mathbf{p}\cdot\mathbf{v}\mathbf{R}\cdot\boldsymbol{\alpha}/r\rangle \quad (3)$$
$$=-2e^2/4\hbar Mc\langle(\mathbf{L}/2)\cdot\hbar\nabla\times\boldsymbol{\alpha}/r\rangle \quad \mathbf{L}=\mathbf{R}\times\mathbf{P}$$

plus terms which do not contribute to the h.f.s.

$$E_F=\tfrac{1}{2}\langle e\boldsymbol{\alpha}\cdot\nabla(1/r)\times e\mathbf{L}/2Mc\rangle, \quad (4)$$
$$E_F=\langle e\boldsymbol{\alpha}\cdot\nabla(1/r)\times\boldsymbol{\mu}_L\rangle, \quad (4')$$

since we are interested only in the real part of the expression. The factor $\frac{1}{2}$ in (4) appears because only one of the nuclear particles is charged. It is easily seen that, as stated, (4) is precisely the normal orbital h.f.s. interaction.

We are left with the difference of (1) and (4), which is a high energy term, and where we may again use the plane wave approximation. Notice that in deriving (4) no such approximation was made, or may be made, since the h.f.s. comes equally from all radii up to a_0.

Using the plane wave approximation for intermediate electron states, a straightforward calculation of the same type as the one in VII leads to

$$E_L'=E_L-E_F=4/3\cdot e^4/mc^3\cdot\psi^2(0)\sum_m\boldsymbol{\sigma}\cdot\mathbf{v}_{0m}\times\mathbf{R}_{m0}H(m), \quad (5)$$

$$H(m)=\int_0^\infty\frac{dx}{(1+x^2)^{\frac{1}{2}}}\left[\frac{1}{(1+x^2)^{\frac{1}{2}}+1+\delta_m}\right.$$
$$\left.+\frac{1}{(1+x^2)^{\frac{1}{2}}-1+\delta_m}\right],$$

where

$$\delta_m=(W_m-W_0)/mc^2\gg 1,\quad x=p/mc$$
$$H(m)=2/\delta_m[\log 2\delta_m+0(1/\delta_m^2)]$$

so that

$$E_L'=\frac{8}{3}\frac{e^4}{c}\psi^2(0)\sum_m\frac{\boldsymbol{\sigma}\cdot\mathbf{v}_{0m}\times\mathbf{R}_{m0}}{W_m-W_0}$$
$$\times\log\left[\frac{2|W_0|}{mc^2}\frac{(W_m-W_0)}{|W_0|}\right] \quad (6)$$

and since for a constant logarithm the sum would vanish

$$E_L'=\frac{8}{3}\frac{e^4}{c}\psi^2(0)\sum_m\boldsymbol{\sigma}\cdot\frac{\mathbf{v}_{0m}\times\mathbf{R}_{m0}}{W_m-W_0}\log\frac{W_m-W_0}{|W_0|} \quad (7)$$

which is a relative correction to the h.f.s. of

$$\epsilon_L=(4/\pi)(\mu_L/\mu_D)(e^2/\hbar c)mc^2/|W_0|\cdot L, \quad (8)$$

where

$$\mu_L=e\hbar/2Mc$$

and

$$L=\frac{1}{\hbar}\sum_m\boldsymbol{\sigma}\cdot M\mathbf{v}_{0m}\times\mathbf{R}_{m0}\frac{\log(W_m-W_0/|W_0|)}{(W_m-W_0)/|W_0|}. \quad (9)$$

ϵ_L is easily seen to be a correction of order

$$\epsilon_L\sim-\rho/a_0\sin^2\omega$$

since

$$(e^2/\hbar c)mc^2/|W_0|\sim\rho/a_0$$

and L is of order $\sin^2 w$.

Since L is small, we do not require high accuracy in its calculation, which would in any case be difficult to obtain, the effective uncertainty in the ground state being much greater here than in VII. We will therefore

calculate L using free intermediate nuclear states. Some justification for this procedure may be found from scattering experiments which appear to indicate very small phase shifts for odd states. Most of the error will thus come from inside the force range, and may be estimated by comparing the results for two different ground states, both of which are chosen to match the known deuteron magnetic moment and quadrupole moment, and both of which have the same asymptotic form.

We have seen in V that the D state wave function is

$$\Phi_D=\sin\omega(\phi_D(R)/R)[(2/20)^{\frac{1}{2}}\chi_1 Y_{20}+(6/20)^{\frac{1}{2}}\chi_0 Y_{21}+(12/20)^{\frac{1}{2}}\chi_{-1}Y_{22}]. \quad (10)$$

If we take

$$\left.\begin{aligned}\phi_D&=A(2\alpha)^{\frac{1}{2}}/\alpha^2R^2(1+\alpha R+\alpha^2R^2/3) && R>b\\ &=(2\alpha)^{\frac{1}{2}}(B\alpha^2R^2+C\alpha^3R^3) && R<b\end{aligned}\right\} \quad (11)$$

then a simple numerical integration leads to

$$L=-0.10\sin^2\omega. \quad (12)$$

If we take

$$\phi_D=(2\alpha)^{\frac{1}{2}}A\left[\frac{e^{-\alpha R}}{\alpha^2R^2}(1+\alpha R+\tfrac{1}{3}\alpha^2R^2)-\frac{e^{-\beta R}}{\alpha^2R^2}(1+\beta R+\tfrac{1}{3}\beta^2R^2)-\frac{1}{6}\frac{\beta^2-\alpha^2}{\alpha^2}e^{-\beta R}(1+\beta R)\right] \quad (13)$$

then we find

$$L=-0.08\sin^2\omega. \quad (14)$$

Choosing L to be the mean of (12) and (14), and allowing an extra 20 percent error for the intermediate states, we have:

$$L=-(0.09\pm0.03)\sin^2\omega \quad (15)$$

and

$$\epsilon_L=(4/\pi)(\mu_L/\mu_D)(e^2/\hbar c)(mc^2/|W_0|)L \quad (16)$$
$$=(\mu_N d/\mu_D a_0)(0.05\pm0.02).$$

IX. HIGHER ORDER TERMS

There remain terms of three types which must still be investigated:

(a) Second-order h.f.s. terms of the form

$$\delta_a\sim-\sum_n(H_p')_{0n}(H_p')_{n0}/E_n-E_0$$

which are of order $(e^2/\hbar c)^2m/M\log(e^2/\hbar c)m/M$ and hence negligible.

(b) Higher order corrections of H' on the h.f.s. of the form

$$\delta_b\sim\sum_{n,m}H_{0n}'H_{nm}'(H_p')_{m0}/(E_n-E_0)(E_m-E_0)$$

which are of order m/M, and

(c) Corrections of H'' on the h.f.s. of the form

$$\delta_c\sim-\sum H_{0m}''(H_P')_{m0}/E_p-E_0$$

which are also of order m/M. However, when the terms (b) and (c) are taken together they practically cancel, and the high energy difference which remains is of order $\hbar c/e^2(d/a_0)^2$ which is small enough to neglect.

X. RESULTS

We have found, in all, the following effects of the internal nuclear motion on the deuterium h.f.s.:

From the unperturbed wave function which Bohr chose as his starting point, the relative correction

$$\epsilon=-\mu_N d/\mu_D a_0(1.24\pm0.08) \quad (1)$$

and, due to a modification of this wave function, the relative correction

$$\epsilon_N=\mu_N d/\mu_D a_0[0.155(1+\xi t)\pm0.015],$$

where t is the fraction of exchange force and

$\xi=\frac{1}{4}$ for a Hulthen well,
$\xi=\frac{3}{10}$ for a square well.

One would expect t to be about $\frac{1}{2}$ (Serber) or $\frac{2}{3}$ (symmetric), and ξ to be about $\frac{1}{4}$ or $\frac{1}{3}$. We will choose ξt to be 0.16 for the purpose of assigning a number to our calculation; actually the difference between 0.16 and either of the two extremes that can be constructed using the above numbers is about 0.04 and negligible.

This gives

$$\epsilon_N=\mu_N d/\mu_D a_0(0.18\pm0.02). \quad (2)$$

From the absence of an orbital interaction inside the distance ρ the relative correction

$$\epsilon_L=\mu_N d/\mu_D a_0(0.05\pm0.02) \quad (3)$$

so that our final correction is

$$\epsilon+\epsilon_N+\epsilon_L=-\mu_N d/\mu_D a_0[1.01\pm0.12]$$
$$=+(1.83\pm0.22)\times10^{-4}. \quad (4)$$

It is worth remarking that over 60 percent of the final uncertainty comes from the calculation of $\langle 2\alpha R\rangle_S$ in VI, so that an improved knowledge of the S state wave function alone would make a much more accurate theoretical determination of the deuterium h.f.s. possible.

It must also be emphasized that we were forced to choose $\sin^2\omega=0.04$ in order for our non-relativistic calculation to be self-consistent, although this number is in considerable doubt, and of course adds to our uncertainty.

Although our result is in fair agreement with the experimental effect, $(1.7\pm0.1)\times10^{-4}$, the present accuracy of theory and experiment is not sufficient to exclude some deviation of the nucleons themselves from simple dipoles. An effect of order

$$[1.83+0.22-(1.7-0.1)]\times10^{-4}=0.45\times10^{-4}$$

is in fact large enough to allow corrections due to a nucleon structure extending over distances of the order of the range of the nuclear forces.

It should be added that the discrepancy was calculated using the value of μ_D/μ_P measured by Bloch, Levinthal, and Packard, who found

$$K=\mu_D/\mu_P=0.3070126\pm0.0000021. \quad (5)$$

However, Bitter and Siegbahn, measuring the same ratio, have found, respectively,

$$K=0.3070210\pm0.0000050 \quad (6)$$

and

$$K=0.3070183\pm0.0000015. \quad (7)$$

The result (7) is larger than (5) by about two parts in one hundred thousand, and would make the discrepancy (using Nafe and Nelson's determination of the h.f.s.) 1.5×10^{-4}, which would be hard to account for on the basis of this calculation alone.

In conclusion, then, we are not yet in a position to estimate structural effects. In order to do so, we need, on the one hand, a more accurate value for the deuteron-proton moment ratio, and on the other a better knowledge of the deuteron S state wave function.

ACKNOWLEDGMENT

The author wishes to thank Professor H. A. Bethe and Dr. A. Bohr, who gave generously of their time and interest, and whose help and criticism were indispensable.

PHYSICAL REVIEW VOLUME 77, NUMBER 3 FEBRUARY 1, 1950

Numerical Value of the Lamb Shift

H. A. BETHE AND L. M. BROWN
Laboratory of Nuclear Studies, Cornell University, Ithaca, New York

AND

J. R. STEHN
Knolls Atomic Power Laboratory, Schenectady, New York

(Received October 10, 1949)

The average excitation potential of the $2s$ state of hydrogen which occurs in the Lamb shift, is calculated numerically and found to be 16.646 ± 0.007 Ry. This gives a theoretical value of 1051.41 ± 0.15 megacycles for the Lamb shift, compared with the latest experimental value of 1062 ± 5. It is not known whether the discrepancy of 10 Mc can be explained by relativistic effects. Simple analytical approximations are discussed which make plausible the high value of the average excitation potential and give a good approximate value for it.

IN this paper, we are reporting two independent numerical calculations of the average excitation potential of the hydrogen atom which occurs in the formula for the Lamb shift.[1] The first calculation was done in 1947 by one of us (J.R.S.) with the help of Miss Steward, the second in 1949 by L.M.B.

I

The formula for the Lamb shift of a hydrogen level n_0, l has been derived by many authors[2] and is for s states

$$\Delta E(n_0,0)=\frac{8Z^4}{n_0^3}\frac{\alpha^3}{3\pi}\mathrm{Ry}\left(\ln\frac{\mu}{k_0(n_0,0)}-\ln 2+\frac{5}{6}-\frac{1}{5}\right) \quad (1)$$

and for states with $l\neq0$

$$\Delta E(n_0,l)=\frac{8Z^4}{n_0^3}\frac{\alpha^3}{3\pi}\mathrm{Ry}\left(\ln\frac{\mathrm{Ry}}{k_0(n_0,l)}+\frac{3}{8}\frac{c_{lj}}{2l+1}\right), \quad (2)$$

where

$$\begin{aligned} c_{lj}&=1/(l+1) \quad \text{for} \quad j=l+\tfrac{1}{2} \\ c_{lj}&=-1/l \quad \text{for} \quad j=l-\tfrac{1}{2}. \end{aligned} \quad (2a)$$

In these formulas, Z is the nuclear charge, n_0 the principal and l the orbital quantum number, $\alpha=e^2/hc$ the fine structure constant, Ry the Rydberg energy, $\mu=mc^2$ and k_0 the average excitation energy which we wish to calculate.

This average energy is defined by[3]

$$\ln\frac{k_0(n_0,l)}{\mathrm{Ry}}\sum_n|(n_0 0|p_x|n)|^2(E_n-E_0) =\sum_n|(n_0 l|p_x|n)|^2(E_n-E_0)\ln\frac{E_n-E_0}{\mathrm{Ry}}, \quad (3)$$

[1] W. E. Lamb and R. C. Retherford, Phys. Rev. **72**, 241 (1947); **75**, 1325 (1949).

[2] N. H. Kroll and W. E. Lamb, Phys. Rev. **75**, 388 (1949); J. B. French and V. F. Weisskopf, Phys. Rev. **75**, 1240 (1949); R. P. Feynman, Phys. Rev. **74**, 1430 (1948), and correction in Phys. Rev. **76**, 769 (1949), footnote 13; J. Schwinger, Phys. Rev. **76**, 790 (1949).

[3] H. A. Bethe, Phys. Rev. **72**, 339 (1947), quoted as A in the following. The definition is in Eq. (6).

TABLE I. Oscillator strengths for hydrogen.

Transitions from	$2s$	$2p$	
to	np	ns	nd
$n=1$	—	-0.138732	—
3	0.43486	0.01359	0.69576
4	0.10276	0.00305	0.12180
5	0.04193	0.00121	0.04437
large	$3.664n^{-3}$	$0.102n^{-3}$	$3.257n^{-3}$

where $(n_0l|p_z|n)$ denotes the matrix element of an arbitrary momentum component p_z corresponding to the transition from the "initial" state n_0, l, of energy E_0, to the final state n, of energy E_n. Note that on the left-hand side the matrix element from the initial state $l=0$ is involved, regardless of the value of l for which $k_0(n_0, l)$ is to be calculated: This definition is necessary because the sum on the left would vanish (see A) if we used $l\neq 0$ for the initial state. For s states, then, k_0 is actually the geometric average of the excitation energy E_n-E_0, with the weighting factor $p_{n0}^2(E_n-E_0)$; for other states, k_0 is defined in as close analogy to the s states as possible. The denominator Ry in the arguments of the logarithms could be omitted for s states; for $l\neq 0$, it serves to make the argument dimensionless and appears again in Eq. (2); any other constant energy would serve as well, but Ry is most convenient.

It is convenient to introduce the oscillator strength f by putting

$$|(n_0l|p_z|n)|^2=\tfrac{1}{2}m(E_n-E_0)f(n_0l, n) \tag{4}$$

and to use the energy change in Rydberg units,

$$\nu=(E_n-E_0)/\mathrm{Ry}. \tag{5}$$

Then (3) becomes

$$\ln(k_0(n_0, l)/\mathrm{Ry})\sum_n f(n_00, n)\nu^2=\sum_n f(n_0l, n)\nu^2\ln\nu. \tag{6}$$

The left-hand side may be evaluated by sum rules (reference 3, Eqs. (9) and (10)) and gives

$$\sum\nu^2 f(n_0, 0, n)=16/(3n_0^3). \tag{7}$$

For our case, $n_0=2$, therefore

$$\ln(k_0(2, l)/\mathrm{Ry})=\sum_n \tfrac{3}{2}f(2, l, n)\nu^2\ln\nu. \tag{8}$$

To evaluate this expression, we need the oscillator strengths for hydrogen. For transitions to the discrete spectrum, we have used the formula given by Bethe,[4] (Eq. (41.4)) and re-evaluated his Table 16 in which some numerical mistakes were found, some of which have been previously pointed out by other authors. The corrected values are given in Table I. For large $n(\geqq 6)$, we found it sufficient to use

$$g(2s, n)\equiv\tfrac{3}{2}f(2s, n)\nu^2=0.3436n^{-3}(1+\tfrac{1}{3}n^{-2}) \tag{8a}$$

$$g(2p, n)\equiv\tfrac{3}{2}f(2p, n)\nu^2=0.3149n^{-3}(1+4.24n^{-2}). \tag{8b}$$

[4] H. A. Bethe, *Handbuch der Physik* 24/1 (Verlag Julius Springer, Berlin, 1933), p. 273.

As is seen from Table II, the discrete final states n contribute only about 2 percent of the sum in (8) for the $2s$ state. For the $2p$ state, their absolute contribution is similar while in this case the continuum gives an almost negligible contribution. In either case, no great numerical accuracy is required for the discrete states.

For transitions to the continuum, we define the quasi-principal quantum number n by

$$E_n=+\mathrm{Ry}/n^2. \tag{9}$$

Then the oscillator strength for transitions from the $2s$ state into an interval $d\nu$ of the continuous spectrum is

$$df(2s, n)=4\nu^{-4}d\nu((4/3)+\nu^{-1})\times\exp(-4n\ \mathrm{arc\ cot}(n/2))/(1-e^{-2\pi n}). \tag{10}$$

The summation over n in (8) should be replaced by an integration over $d\nu$. For transitions from the $2p$ state to the continuous spectrum

$$df(2p, n)=(8/9)\nu^{-5}d\nu(\tfrac{3}{2}+\nu^{-1})\times\exp(-4n\ \mathrm{arc\ cot}(n/2))/(1-e^{-2\pi n}). \tag{11}$$

These formulas may be obtained from the expressions for the photoelectric absorption coefficient (reference 4, Eqs. (47.19), (47.20)), using the general relation between absorption coefficient and oscillator strength,

$$\tau=Nz2\pi^2e^2(h/mc)(df/dE), \tag{12}$$

where N is the number of atoms per cm^3, z the number of electrons in the given shell,[5] and df/dE the oscillator strength per unit energy interval, i.e. $(1/\mathrm{Ry})(df/d\nu)$. It should be noted that Eq. (47.20) of reference 4, like the original formula of Stobbe,[6] is too large[7] by a factor of 2; this mistake has been corrected in (11).

In Fig. 1 we have plotted the expression

$$g\equiv\tfrac{3}{2}\nu^3 df/d\nu \tag{13}$$

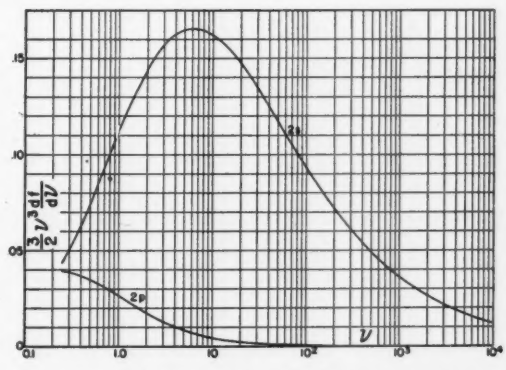

FIG. 1. The weight functions for the determination of the average excitation energy.

[5] Note that ν_2 in reference 4 is $\frac{1}{4}$Ry.

[6] M. Stobbe, Ann. d. Physik **7**, 661 (1930).

[7] This was pointed out to one of the authors (H.A.B.) many years ago. It is most easily verified by comparing the oscillator strength $df/d\nu$ just above and just below the energy $E_n=0$. It can also be verified by checking the sum rule analogous to (7), $\Sigma f(2p, n)\nu^2=0$, see Table II.

$vs.$ $\log\nu$, for $2s$ and $2p$. The integral under the $2s$ curve, after addition of the discrete spectrum, gives unity (Eq. (7)). The smallness of g for the $2p$ state is apparent.

For the numerical integration, we have used the integration variable n instead of ν, inserting

$$\nu=\tfrac{1}{4}+1/n^2. \tag{14}$$

It is easily seen that the integrand in (7) then behaves as dn for small n, and that in (8) as $dn\log n$. Because of the singularity of $\log n$ at $n=0$, numerical integration is not feasible. However, it is easy to expand the integrand (apart from the log) into a power series in n, which permits analytical integration. This procedure was used for n up to 0.05, while from there to 0.1 it was used as a check on the numerical work: The results agreed within 0.00005 which is beyond the accuracy attempted (0.0001).

TABLE II. Results of numerical integration.

	$2s$ State		$2p$ State
	Earlier Integration	Later Integration	Later Integration
Contribution to S:			
Discrete	0.02645	0.02645	−0.081366
Continuous	0.9736	0.97340	+0.081336
Total	1.00005	0.99985	−0.000030
Contribution to (8)			
Discrete	−0.0465	−0.04649	−0.030669
Continuous	2.8593	2.85840	+0.000685
Total	2.8128	2.81191	−0.02998
Total/S	2.8127	2.81233	
Adopted $\ln(k_0/\mathrm{Ry})$	2.8121±0.0004		−0.0300±0.0002
k_0/Ry	16.646 ±0.007		0.9704±0.0002

The numerical integration was done by Simpson's rule, using in the final calculation for the s state intervals[8] as follows:

from $n=0.05$ to 0.1, interval 0.0125
from $n=0.1$ to 0.2, interval 0.025
from $n=0.2$ to 1, interval 0.05.

From $n=1$ to ∞, we used $s=1/n$ as a variable, choosing intervals of 0.05 for s. The fourth differences of the integrand were of the order of 1 percent of the integrand itself (usually less) so that the error in the result may be expected to be about 1 part in 10,000. The earlier calculation was done with twice the intervals; the results of the two calculations agree within 0.0009 unit, after correction of a numerical mistake of 0.0031 unit in the earlier integration, and of 0.0007 unit in the discrete contribution, both of which were subsequently discovered. The error in Simpson's rule is roughly proportional to the fourth power of the interval used, so that the result of the second calculation should be high by 0.00006, an error considerably smaller than the rough estimate of 1 part in 10,000 from the fourth differences. As a check, the sum in (8) *without* the logarithmic factor was also calculated (denoted by S); according to (7), this should give unity for $2s$ and zero for $2p$. The deviation of 1.5 parts in 10,000 (Table II) for the s state indicates the accuracy attained; for the p state, the error is one-fifth of this. One can be doubtful whether it is more accurate to use the result (8) as it stands, or to divide it by the numerically calculated S; both results are given in Table II, and their mean is used as the final result. The probable error is taken as the whole difference between the two results; the main source of error is presumably in evaluation of the integrand (or of the discrete contribution) since the error from Simpson's rule should be less than 0.0001. The probable error for the $2p$ state was estimated from the difference of the earlier and the later calculation which was 0.0002.

II

These results can now be inserted into the Lamb effect formulas (1), (2). In the numerical factor in front, we should insert the Rydberg constant for hydrogen, rather than for infinite mass. This can be seen from the derivation;[3] the velocity matrix elements in A Eq. (6) are the same whether the reduced mass or the full mass is used for the electron whereas the energy differences E_n-E_m are proportional to the electron mass and thus to Ry_H. This can also be traced through A Eqs. (8) to (11). There is some doubt whether to use the reduced mass of the electron also in $\mu=\mathrm{mc}^2$ in (1); we shall do so which may cause an error of $1/1840=0.0005$ in the value of the parenthesis in (1). A larger uncertainty exists because of the neglect of relativistic corrections in (1) (see below).

For α we take the value deduced from hyperfine structure[9]

$$1/\alpha=137.041\pm0.005. \tag{15}$$

Then the constant factor in (1), the "Lamb constant," is, when expressed in frequency units:

$$(\alpha^3/3\pi)\mathrm{Ry}=135.549\pm0.015 \text{ megacycles}. \tag{16}$$

The uncertainty arises entirely from that of α. The first term in the parenthesis in (1) is

$$\ln(\mu/k_0(2s))=10.5336-2.8121=7.7215\pm0.0006. \tag{17}$$

The error includes 0.0004 from Table II, and 0.0005 from the questionable use of the reduced mass in μ. The value quoted by French and Weisskopf, 7.6906, referred to the *difference*

$$\ln(\mu/k_0(2s))-\ln(\mathrm{Ry}/k_0(2p))=7.7215-0.0295=7.6920,$$

according to our present calculation, the small difference between this and 7.6906 being due to numerical mis-

[8] The integrand was calculated at the intervals h stated. The integral from x to $x+2h$ is then $\frac{1}{3}h[f(x)+4f(x+h)+f(x+2h)]$.

[9] H. A. Bethe and C. Longmire, Phys. Rev. **75**, 306 (1949).

takes in our earlier calculation. The results are given in Table III. The error of the shift of $2s$ includes 0.11 Mc from the uncertainty of the Lamb constant (16), i.e. mostly of α, and 0.08 Mc from that of $\ln(\mu/k_0(2s))$, of which only 0.05_5 arises from the numerical calculation. For the p levels, the uncertainty is all due to the calculation of $k_0(2p)$.

The measured Lamb shift is the difference between the shifts of $2s$ and $2p_{\frac{1}{2}}$ state, *viz.*

$$L(2s)-L(2p_{\frac{1}{2}})=1051.41\pm0.15 \text{ megacycles} \quad (18)$$

in agreement with the calculated values previously given by French and Weisskopf, and Lamb and Kroll.[2] The latest published experimental value[10] is

$$L(\text{experimental})=1062\pm5 \text{ Mc}. \quad (19)$$

The discrepancy between (18) and (19) is twice the experimental error, which probably has been generously estimated. It is possible that this discrepancy is due to the neglect of relativistic corrections in the derivation of formula (1). These may not be negligible because the wave function of the hydrogen ground state has large Fourier components of high wave number. A rough estimate shows that these corrections are of relative order α, but without the logarithmic factor which gives the main contribution to (1). Thus the rough estimate would give a correction of order 1 Mc, too small to explain the discrepancy. Moreover, superficial reasoning would lead one to expect a decrease of the theoretical value. However, an explicit calculation of the relativistic corrections is now very urgent and may give a different result.

It has often been pointed out that a higher theoretical result would be obtained if the vacuum polarization effect were left out of (1), and that this effect can be separated from the main part of the Lamb effect in a relativistically invariant way. The vacuum polarization is represented by the term $-\frac{1}{5}$ in (1) and therefore contributes an amount

$$-27.110 \text{ Mc} \quad (20)$$

to the Lamb effect. If it were excluded, the result would be 16 Mc higher than the experimental value so that the agreement is not improved.

III

In this section, we shall try to give a qualitative understanding of the very large result, 16.646 Ry, which we found for the average excitation potential of the $2s$ state. As was pointed out, $\ln k_0$ is the average of $\ln(E_n-E_0)$ with the weight factor $\nu^2 f$. If we take the average of E_n-E_0 itself, rather than of its logarithm, with the same weight factor $\nu^2 f$, we get infinity. This

[10] R. C. Retherford and W. E. Lamb, Phys. Rev. **75**, 1325 (1949).

TABLE III. Lamb shifts.

	$2s$	$2p_{1/2}$	$2p_{3/2}$
First term in parenthesis	7.7215±0.0006	+0.0300±0.0002	+0.0300±0.0002
Total parenthesis	7.6707±0.0006	−0.0950±0.0002	+0.0925±0.0002
Level shift in megacycles	1038.53±0.14	−12.88±0.03	+12.54±0.03

is because we have (neglecting constant factors)

$$\sum(E_n-E_0)\nu^2 f\sim\sum(E_n-E_0)^2|p_{0n}{}^x|^2\sim\sum|(\partial V/\partial x)_{0n}|^2$$

$$=\langle(\partial V/\partial x)^2\rangle_{00}=\tfrac{1}{3}\langle(\nabla V)^2\rangle_{00}=\tfrac{1}{3}\int\frac{e^4}{r^4}\psi_0{}^2 4\pi r^2 dr. \quad (21)$$

This integral diverges at $r=0$ as dr/r^2 if ψ_0 refers to an s state. If the angular momentum of the state ψ_0 is not zero, the integral is finite. Now since the average of E_n-E_0 is infinite (for an s state), it is understandable that the average of $\ln(E_n-E_0)$ is large.

Further information can be obtained from the asymptotic behavior of the oscillator strength f, given by Eq. (10), for large frequencies; this is, considering (14):

$$\nu^2 df=(8/3\pi)\nu^{-\frac{1}{2}}d\nu=(16/3\pi)dn. \quad (22)$$

This shows that already the average of $\nu^{\frac{1}{2}}\sim(E_n-E_0)^{\frac{1}{2}}$, with the weight factor $\nu^2 df$, is infinite. The small contribution of the discrete transitions (Table II) is further evidence.

The most concrete picture is obtained from Fig. 1 in which $\frac{3}{2}\nu^3 df/d\nu$ is plotted against $\log\nu$. The maximum of the curve is seen to come at $\nu=7$ which is reasonably high, and the curve falls off much more slowly towards higher than towards lower ν. The required average $\log k_0$ is simply the center of gravity of the curve of Fig. 1, and a value of 16.6 for k_0 looks entirely reasonable.

It is easy to obtain simple analytic estimates of $\ln k_0$. This can be done by approximating the exact oscillator strength (10) by a simpler expression which can be easily integrated. Since we know already that the high frequencies are the most important, the simpler expression must be a close approximation to f at the high frequency end but need not be so for low frequencies. The simplest approximation is to set

$$dG\equiv\tfrac{3}{2}\nu^2 df=(8/\pi)dne^{-an}, \quad (23)$$

which agrees with (22) for small n, and to choose a in such a way that the integral of (23) over all n is unity as it must be according to (7). This gives

$$(8/\pi)\int_0^\infty dne^{-an}=(8/\pi a)=1. \quad (24)$$

Then the average of $\ln\nu$ becomes

$$\ln(k_0/\text{Ry})=\langle\ln\nu\rangle=-2\langle\ln n\rangle=-2a\int dne^{-an}\ln n$$

$$\equiv 2(\ln a+C)=2(\ln(8/\pi)+C), \quad (25)$$

where C is Euler's constant. Inserting numerical values, we get

$$\ln(k_0/\mathrm{Ry})=3.026, \quad k_0=20.6 \text{ Ry}, \tag{26}$$

which is slightly larger than the correct values

$$\ln(k_0/\mathrm{Ry})=2.812, \quad k_0=16.65 \text{ Ry}. \tag{27}$$

This simple calculation therefore gives the correct order of magnitude for k_0.

To get a closer approximation, we consider the asymptotic behavior of f in more detail. Expanding (10) in a power series in n, but keeping the power series in the denominator, one gets

$$dG\equiv\tfrac{3}{2}\nu^2 df=\frac{(8/\pi)dn}{1+\pi n+(\frac{2}{3}\pi^2-2\tfrac{1}{4})n^2+\cdots}$$

$$=\frac{(8/\pi)dn}{1+3.14n+4.33n^2+\cdots}. \tag{28}$$

The exponential in (23) gives instead

$$dG\equiv\tfrac{3}{2}\nu^2 df=\frac{(8/\pi)dn}{1+(8/\pi)n+32\pi^{-2}n^2+\cdots}$$

$$=\frac{(8/\pi)dn}{1+2.55n+3.24n^2+\cdots}. \tag{29}$$

Obviously, this expression falls off too slowly with increasing n. This error is compensated by a too-rapid decrease for very large n: Actually, g should behave as $d\nu\sim n^{-3}dn$ for $n\to\infty$, whereas (23) gives an exponential decrease. It is therefore understandable that (23) gives too high a value for the average $\ln k_0$.

To improve on the behavior for small n, we choose

$$dG=\frac{(8/\pi)dn}{(1+an)^{k+1}} \tag{30}$$

and determine the two constants a and k so that the linear term in n in the denominator of (28) is correctly given, as well as the integral. The latter condition requires

$$ka=8/\pi. \tag{31}$$

The former condition gives

$$(k+1)a=\pi. \tag{32}$$

The solution is

$$k=8/(\pi^2-8)=4.279, \quad a=(\pi^2-8)/\pi=0.5951. \tag{33}$$

The average of $-\ln n$ is then

$$-\langle\ln n\rangle=\ln a+\int\frac{kadn}{(1+an)^{k+1}}\ln an$$

$$=\ln a+\Psi(k-1)-\Psi(0) \tag{34}$$

where $\Psi(n)$ is the logarithmic derivative of the factorial function, i.e. of $\Gamma(n+1)$ (Jahnke-Emde's definition). With our numerical values

$$\ln(k_0/\mathrm{Ry})=\langle\ln\nu\rangle=-2\langle\ln n\rangle=2.7818$$
$$k_0=16.148. \tag{35}$$

This is very close to the correct values (27), and somewhat smaller. Expansion of (30) for small n gives

$$g=\frac{(8/\pi)dn}{1+(k+1)an+\frac{1}{2}(k+1)ka^2n^2+\cdots}$$

$$=\frac{(8/\pi)dn}{1+\pi n+4n^2+\cdots}, \tag{36}$$

which is rather close to the correct expression (28), even in the quadratic term. (36) is still above (28) for small n, so that we might still have expected a too large result for $\ln k_0$; it seems that the curve of (30) crosses the correct curve (10) three times.

These calculations make the large value of the average excitation potential appear plausible. Moreover, they make it likely that k_0 is nearly independent of the principal quantum number: The asymptotic expression for the oscillator strength for small n, including terms of relative order n, is independent of n_0, except for a factor n_0^{-3} which also occurs in the sum rule (7). Therefore, all the information we used in determining the constants a and k in (30) is independent of n_0, and the estimate (36) applies to all values of n_0.

On the Solar Origin of Cosmic Radiation. II.

H. ALFVÉN
The Royal Institute of Technology, Stockholm, Sweden
(Received October 10, 1949)

Teller-Richtmyer's theory of the origin of cosmic radiation is discussed. It is found that the magnetic field ("trapping field"), which they postulate in order to explain the isotropy of cosmic radiation, must be toroidal and have an extension of about 0.1 light year. A field of this type may be produced by the motion of the solar system relative to interstellar matter. The theory gives the energy spectrum and total intensity of cosmic radiation.

1. UPPER ENERGY LIMIT OF COSMIC RADIATION

THE idea of Teller-Richtmyer[1] that cosmic radiation may be a local solar phenomenon was developed in a recent paper.[2] Arguments were given for the existence of magnetic fields strong enough to confine cosmic radiation to the vicinity of the solar system. The acceleration of particles to cosmic-ray energies was supposed to take place in the solar magnetic field in the environment of the sun, but not on the sun itself. The supposed acceleration mechanism accounts at the same time for the magnetic storm effects on cosmic radiation.

In the present paper the theory shall be further discussed.

In the cited paper[2] the acceleration was assumed to be due to "solar activity" disturbances of the solar dipole field. In order to calculate the order of magnitude of particle energies it is reasonable to start from Störmer orbits in a dipole field. Assuming that the solar magnetic dipole has the moment a, the highest "momentum" $p_1(=H\rho)$ of a particle moving in a periodic orbit is given by

$$p_1=aR_\odot^{-2} \tag{1}$$

($R_\odot$=solar radius). This corresponds to a circular orbit close to the solar magnetic equator. This orbit is unstable, however, and consequently of little physical significance. The most important class of stable trajectories are trochoids in the equatorial plane. Usually the trochoids are superimposed by oscillations through the equatorial plane. The highest momentum trochoid in the equatorial plane is given by

$$p_2=a/(R_\odot^2)(3-2\sqrt{2})=0.172p_1. \tag{2}$$

As this orbit requires that the velocity component perpendicular to the equatorial plane is zero, it represents a special case, and in order to find orbits which can keep a great number of particles we must go still somewhat lower. On the other hand, special combinations of sunspot fields with the general magnetic field may give stable orbits even above p_2.

The energy V, in electron volts, of a particle with charge Ze is in the relativistic range

$$V_{\text{volt}}=300Zp. \tag{3}$$

Assuming the polar strength of the sun's dipole field to be 25 gauss (as an average between the high values and the low values reported) we have $a=4.2\times10^{33}$ gauss cm^3 and

$$p_2=1.5\times10^{11}\text{ gauss cm.} \tag{4}$$

This gives for protons

$$V=4.5\times10^{13}\text{ ev.} \tag{5}$$

Hence the highest proton energy which at present could be generated in the solar field is of the order 5×10^{13} ev. This does not necessarily mean that no protons with higher energies could be present in cosmic radiation, because the radiation which we now receive is the accumulated effect of generation processes during may be as much as 100 million years. If the solar field has been stronger than now during some part of this time, higher energies may be observed.

Higher energies could also be obtained under the present conditions by acceleration of multiply charged heavy atoms. A 30-fold ionized particle, such as has really been observed in cosmic radiation,[3] would be able to reach the energy 1.4×10^{15} ev. The very rare case of a completely stripped uranium atom would bring us up to 4×10^{15} ev.

2. MINIMUM ENERGY EMITTED FROM THE ACCELERATOR

Let us confine the discussion to orbits in the equatorial plane, which in any case gives the right order of magnitude. At a point at the solar distance R the maximum momentum of a trochoidal orbit is

$$p_3=aR^{-2}=p_1(R_\odot/R)^2. \tag{6}$$

A small increase in energy will change the orbit so that it goes to infinity. A small disturbance of the dipole field is able to produce the same effect. The main emission of particles from the accelerator will take place from orbits of this type. Particles with momenta smaller than p_3 will of course also be accelerated, and during large disturbances some of them will have a chance of being emitted, but the main emission is likely to occur from orbits close to p_3.

[1] E. Teller, Nuclear Physics Conference, Birmingham, 1948; Alfvén, Richtmyer, and Teller, Phys. Rev. 75, 892 (1949); R. D. Richtmyer and E. Teller, Phys. Rev. 75, 1729 (1949).
[2] H. Alfvén, Phys. Rev. 75, 1732 (1949).
[3] Freier, Lofgren, Ney, Oppenheimer, Bradt, and Peters, Phys. Rev. 74, 213 (1948); H. L. Bradt and B. Peters, Phys. Rev. 74, 1828 (1948).

Close to the sun the magnetic field is approximately a dipole field (although sometimes rather much disturbed), but at great distances the field H_T postulated by Teller and Richtmyer dominates. As the extension of the latter field should be much greater than the solar system dimensions, we may suppose it to be homogeneous within the solar system. At so large a solar distance that H_T dominates over the dipole field, particles do not drift around the sun in the way which is necessary for the acceleration process. Hence they are not accelerated or, in any case, the acceleration is not very effective. Still more important is that in the dipole field the particles oscillate through a stable equilibrium whereas outside it they are free to move away from the solar vicinity along the lines of force.

The limit R_T between H_T and the dipole field is given by

$$H_T \approx aR_T^{-3}. \tag{7}$$

Due to the finite extension of the dipole field there is an inferior limit p_4 to the particles emitted from the accelerator. This is of the order

$$p_4 = p_1(R_\odot/R_T)^2 = aR_T^{-2}. \tag{8}$$

Particles far below this limit will not be emitted if situated in the dipole field and if outside it, they will not

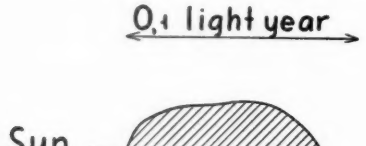

FIG. 1. Possible shape of the space in which cosmic radiation is trapped.

be accelerated very much. It seems reasonable to identify p_4 with the low energy cut-off in the cosmic-ray spectrum, which earlier has been attributed to the cut-off by the solar magnetic field.[4] This enables us to estimate H_T. Equations (7) and (8) give

$$H_T = a^{-\frac{1}{2}} p_4^{\frac{1}{2}}. \tag{9}$$

Putting the low energy cut-off equal to 5×10^9 ev ($p_4 = 1.7\times10^7$ gauss cm) we get

$$H_T \approx 10^{-6} \text{ gauss}. \tag{10}$$

A more detailed calculation shows that this result depends very much upon the assumption of the orientation of H_T in relation to the solar dipole and may easily be in error by a factor 10.

[4] L. Jánossy, Zeits. f. Physik **104**, 430 (1937); *Cosmic Rays* (Oxford University Press, London, 1948).

The limit R_T between the dipole field and H_T goes not very far from the earth's orbit.

3. MAXIMUM VOLUME OCCUPIED BY COSMIC RADIATION

According to our assumptions the whole cosmic radiation should be generated near the sun, so that, for example, a sphere with the radius R_δ equal to the earth's orbital radius encloses the whole region of generation. This must cause an anisotropy of the radiation observed on the earth. That this anisotropy is very small is explained by Teller and Richtmyer through the assumption of an extra-solar field H_T which traps the radiation and reflects it back again. Let us assume that the ratio of the radiation flux outward and inward through the sphere R_δ is $(1+\gamma)/(1-\gamma) \approx 1+2\gamma$, so that γ is a measure of the degree of anisotropy. Let us further assume that in average an emitted particle will pass through the sphere R_δ N times before being absorbed. As $(N+1)/N = 1+2\gamma$ we have

$$N = (2\gamma)^{-1}. \tag{11}$$

It is possible to find a relation between γ and the volume to which cosmic radiation is confined. The probability that a particle moving at random with velocity c within a volume U shall hit a surface πR_δ^2 during a small time Δt is $\pi R_\delta^2 c\Delta t/U$. If the average life of a particle is T, the sphere R_δ will be hit N times if $N = \pi R_\delta^2 cT/U$, which gives

$$U = 2\pi R_\delta^2 cT\gamma. \tag{12}$$

For the average life of a particle moving in interstellar space Fermi[5] gives $T = 6\times10^7$ years $= 2\times10^{15}$ sec. On the other hand Kane, Shanley, and Wheeler[6] find for a particle trapped in the solar magnetic field $T = 5000$ years. Our value should lie between these, but much closer to the upper value, because the particle spends most of its time in interstellar space. If we only want an upper limit to U we could put $T < 2\times10^{15}$ sec. The anisotropy γ is certainly less than 10^{-2}, probably even less than 10^{-3}. With $\gamma < 10^{-3}$ and $R_\delta = 1.5\times10^{13}$ cm we get

$$U < 0.8\times10^{50} \text{ cm}^3. \tag{13}$$

(The cube of a light year equals 10^{54} cm^3.)

It should be observed that the calculation of U is based on the assumption of a stationary state. If, for some reason, the output of the cosmic-ray generator has been much lower during the time we have observed cosmic radiation than the average output the last 100 million years, our calculations would be erroneous.

4. PROPERTIES OF THE TRAPPING FIELD

A sphere with the volume given by (13) would have a radius of about 3×10^{16} cm. In a field of the order

[5] E. Fermi, Phys. Rev. **75**, 1169 (1949).
[6] Kane, Shanley, and Wheeler, Rev. Mod. Phys. **21**, 51 (1949).

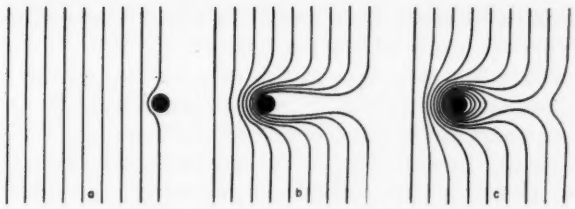

FIG. 2. Magnetic field disturbed by the motion of a body through a conducting medium.

10^{-5} gauss a particle with a momentum $p=10^{11}$ gauss cm has a radius of curvature which is not very much smaller. Hence it is obvious that scattering of the cosmic rays by an irregular magnetic field could not possibly prevent the radiation from spreading to a much larger volume.

If we assume the trapping field to be approximately homogeneous over a region of the order of 10^{16} or 10^{17} cm around the solar system, this field would no doubt prevent the radiation from escaping perpendicular to the field. In fact it would fill a circular cylinder with the radius of 2ρ. The maximum height of the cylinder must be

$$L=U/4\pi\rho^2=\tfrac{1}{2}R_\delta{}^2cT\gamma H_T{}^2/p^2. \qquad (14)$$

With $\gamma=10^{-3}$, $H_T=10^{-5}$ gauss and $p=10^{11}$ gauss cm we find $L=0.8\times10^{17}$ cm$\approx$0.1 light year. As we have chosen p in the upper part of the spectrum we cannot exclude the possibility of a higher anisotropy. Measurements on the high energy component alone are still somewhat uncertain and a value as high as $\gamma=0.1$ would perhaps not be in conflict with observations. This brings us up to $L=10$ light years as an upper limit. In a homogeneous field nothing would prevent the radiation from moving parallel to the field and spreading over a much larger distance. Hence the trapping field could not be approximately homogeneous over a distance of 10^{16}–10^{17} cm around the solar system.

If we drop the assumption of a homogeneous field, the radiation will be enclosed in a tube of flux of arbitrary shape. The magnetic field prevents the radiation from leaking out through the walls of the tube but it is free to move along the tube parallel to the field. As the part of the tube which it occupies must not surpass the length L there must be some "lock" at each end of the tube, which reflects back the radiation. This lock must be very effective because during its lifetime T a particle will reach the end of the tube a number of times n which is of the order

$$n=cT/2L=p^2/(R_\delta{}^2\gamma H_T{}^2). \qquad (15)$$

Even if we put γ as high as 0.1 and $H_T=10^{-5}$, n surpasses 10^6 for $p=10^{11}$ gauss cm. It seems quite impossible to find a mechanism which closes the ends of the tube so effectively that a particle has less than one chance in a million to pass. Certainly, if the field strength increases along the tube, particles moving toward increasing field will turn, but in order to make all but one in 10^6 turn, the field must increase by a factor of 10^6. This would bring us up to interstellar fields of the order 10 gauss which of course is impossible.

The problem could also be considered in the following way. In order to make a particle pass N times through the earth's orbital surface $\pi R_\delta{}^2$, the "hole" of the surface which locks in cosmic radiation must not be larger than $\pi R_\delta{}^2/N$, because a larger hole would mean that the radiation leaks out too rapidly.

It is easily seen that a series of locks, each with a smaller efficiency, does not change the order of magnitude.

The only possibility seems to be to assume that *the lines of force are closed lines* so that the flux tubes resemble toroids.

In this case L means the circumference of the toroid. The value of L which we have found, shows that the over-all dimension of the cosmic ray "doughnut" should be smaller than about one light year. An inferior limit is given by the diameter of the tube of force, which must at least equal 4ρ. With $H=10^{-5}$ and $p=10^{11}$ this gives 4×10^{16} cm. Thus the best guess of the size of the doughnut would be the order of 10^{17} cm (=0.1 light year).

5. PRODUCTION OF THE TRAPPING FIELD

In the earlier paper it was supposed that the trapping field postulated by Teller and Richtmyer was produced by the magneto-hydrodynamic mechanism which should convert part of the kinetic energy of local motions into magnetic energy. In a primary magnetic field, which may be extremely weak, the polarization due to local motions produces currents, which give rise to the trapping field. It is easily seen that these local currents through space should produce magnetic lines of force which are closed. This amplifies our conclusion that cosmic radiation is trapped by a closed field.

There is a close analogy between this production of the trapping field and the production of sunspots according to the magneto-hydrodynamic theory.[7] Due

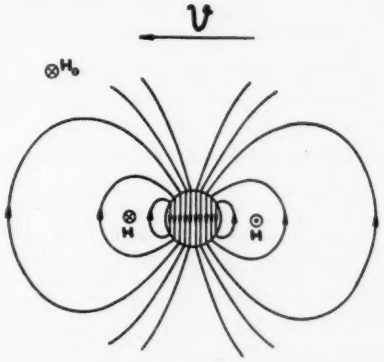

FIG. 3. Current system produced by the motion of a conducting sphere through a conducting medium in a magnetic field H_0. The current system produces a magnetic field H.

[7] H. Alfvén, M. N. R.A.S. **105**, 3, 382 (1945); Ark. f. mat., astr. o. fysik, **34** A, 23 (1948).

to the presence of a general magnetic field, local motions in the sun produce local magnetic fields (which later give rise to sunspots). The local fields are toroidal and their strength is more than 100 times larger than the general field.

The size of the trapping field as found in the preceding paragraph shows that the current system must be confined to the environment of the solar system. In any case its extension is small compared to interstellar distances. Hence it seems likely that the whole phenomenon should be associated with *the motion of the solar system relative to interstellar matter*. A mechanism which may produce the trapping field shall be proposed tentatively.

Suppose that a perfectly conducting body moves rectilinearly in a perfectly conducting medium in which a magnetic field is present. Let the field be homogeneous and perpendicular to the motion. Figure 2 shows qualitatively what occurs. The moving body drags the lines of force with it. The first result (Fig. 2b) is an amplification of the field in front of the body and a long tail of field behind it. Due to the elasticity of the lines of force the tail will break up as shown by Fig. 2c. When a stationary state is reached the moving body will be surrounded by a system of closed lines of force.

The problem can also be treated in the following way. Seen from the moving body the surrounding medium moves with a velocity which we call v. As there is a magnetic field H_0 in the medium, this is polarized seen from the body, so that there is an electric field $E=vH/c$. In the body this field produces a current, and when this current is closed through the surroundings, the current system of Fig. 3 is produced. It is easily seen that it produces a toroidal magnetic field.

In the ideal case we have discussed the motion in the surrounding medium produced by the body has been neglected. In the real case the moving body should probably not be identified with the sun itself but rather with the sun and the interstellar matter in its environment which it drags with it. Further the solar dipole field affects the phenomenon. The whole mechanism is no doubt very complicated and until a more detailed analysis has been made the results of this paragraph and the next are only tentative suggestions.

6. THE INTENSITY OF COSMIC RADIATION

As pointed out by Dungey and Hoyle[8] a magnetic field which traps cosmic radiation is subject to a pressure equal to the energy density of the radiation. This means that the magnetostatic pressure $p_H=H^2/8\pi$ outside the cosmic-ray doughnut must surpass the pressure inside it by the energy density of cosmic radiation, which amounts to $w=4\times10^{-13}$ erg cm^{-3}. The magnetostatic pressure of the trapping field may be of the same order of magnitude as w. In fact $H_T^2/8\pi=w=4\times10^{-13}$ gives $H_T=3\times10^{-6}$ gauss, which is an acceptable value for the trapping field.

When the solar system moves with the velocity v through an interstellar medium with density ϑ, the pressure p_f at the front should be of the order $p_f=\vartheta v^2$. Even this pressure may be of the same order as w and p_H. In fact, if $\vartheta=10^{-24}$ g cm^{-3}, an energy $w=4\cdot10^{-13}$ corresponds to $v=10^6$ cm/sec. which would be a possible value for the motion of the sun in relation to interstellar matter.

It is possible that the order of magnitude agreement between w, p_H, and p_f is not fortuitous. The value of H_T is not determined by the primary magnetic field, H_0, in interstellar space which was supposed to be its ultimate cause. Even an extremely weak primary field is enough to produce very large currents due to the good conductivity of interstellar matter. It is more reasonable that H_T is determined by the condition that the magnetic field in front of the advancing solar system should be strong enough to withstand the pressure due to the medium in which the motion takes place. This would give $p_H=p_f$.

The equality between p_H and w could be understood in the following way. Suppose that the sun generates so much cosmic rays that w surpasses p_H. Then the magnetic field cannot keep the radiation and the cosmic-ray doughnut will expand until w has diminished again to p_H. Thus the output of the solar generator does not determine the intensity but the volume filled by cosmic radiation. The intensity is ultimately determined by p_f, so if the resistance of interstellar matter to the solar motion changes, this would affect the cosmic-ray intensity.

7. THE ACCELERATION PROCESS

According to the earlier paper[2] the acceleration is due to electric fields produced at disturbances of the solar magnetic field, or in other words to the betatron action of magnetic field variations. It is important to observe that in average such variations produce a cumulative increase of the particle energy. This is in principle the same effect as discussed by Fermi.[5] The interaction between a variable magnetic field and a particle tends to increase the particle energy. In our case the details of the process could be understood in the following way.

In a dipole field charged particles move in Störmer orbits. In the orbits of most interest in this connection the motion consists of a trochoidal motion perpendicular to the magnetic field superimposed by oscillations parallel to the field. If the regular dipole field is disturbed in such a way that from time to time the magnetic field in some parts of it changes, the effect of this is twofold: 1. Particles passing a region with a static disturbance of the field are scattered from one Störmer orbit to another. 2. Particles moving in a region where the magnetic field in it changes, increase or decrease their energy.

[8] J. W. Dungey and F. Hoyle, Nature 162, 888 (1948).

Consider a number of particles moving in the dipole field. The first process tends to distribute them isotropically, so that in average their momenta p_0 are distributed in such a way that the motion parallel to the field accounts for $p_0/3$ and the motion perpendicular to the field for $2p_0/3$ (in the relativistic case). Suppose that in a region, where some of the particles move, the magnetic field increases by a factor α^2. This produces an increase by a factor α of the momentum perpendicular to the field, but it does not affect the motion parallel to the field. Hence the total momentum of a particle is

$$p'=p_0(\tfrac{1}{3}+2\alpha/3). \tag{16}$$

Let the particles then be subject to scattering so that their momenta becomes equally distributed on the three degrees of freedom. Hence the "parallel" momentum is $\frac{1}{3}p'$ and the "perpendicular" momentum $\frac{2}{3}p'$. If later the field in which they move decreases by a factor $1/\alpha^2$, their "parallel" momentum remains unchanged but their "perpendicular" momentum decreases by a factor $1/\alpha$. Hence the result of an increase of the field and a subsequent decrease back to the initial field strength is that the momentum has increased from p_0 to

$$p_0'=p_0\left(\frac{1}{3}+\frac{2}{3}\alpha\right)\left(\frac{1}{3}+\frac{2}{3\alpha}\right)=\frac{5+2(\alpha+\alpha^{-1})}{9}p_0. \tag{17}$$

This shows that if the magnetic field varies up and down an accumulated increase in particle momentum will occur.

Consider a moment when the solar field is undisturbed. Suppose that a certain disturbance occurs, after which the field goes back to its original conditions. The disturbance has increased the momenta of a group of particles by

$$\Delta p=Ap. \tag{18}$$

At the same time it has thrown a number of particles out of their normal orbits in such a way that they have been emitted into interstellar space. The number of particles lost by emission is Bn, where n is the total number of particles. Further during the time between two disturbances a number of Cn particles is lost by absorption (in interplanetary matter or by collisions with celestial bodies). Hence the total change Δn is

$$\Delta n=-(B+C)n. \tag{19}$$

A, B, and C are independent of n but may be functions of p. Supposing that a series of disturbances of the same type occurs we could find the spectrum of accelerated particles. Dividing (19) by (18) we obtain after integration

$$n=n_0\exp\left(-\int\frac{B+C}{A}\frac{dp}{p}\right),$$

where n_0 is an integration constant.

The spectrum emitted from the generator is

$$n_e=Bn_0\exp\left(-\int\frac{B+C}{A}\frac{dp}{p}\right).$$

According to Kane, Shanley, and Wheeler[6] cosmic-ray particles in certain trapped orbit move some thousand years before being absorbed. As this time probably is much larger than the time of the acceleration process, it is reasonable to neglect C except very close to the sun.

If there is an orbit with momentum p at a solar distance R, there is also a similar orbit at R' with the momentum $p'=p(R/R')^2$. If we suppose that the disturbance has the same character at R' as at R, particles with the momentum p' are affected in the same was as those with momentum p. Thus it is reasonable to assume that A and B are independent of p. This gives

$$n_e=n_0'p^{-B/A},$$

where $n_0'=n_0B$ is a constant. In a stationary state this emission should compensate the absorption in a tube of constant length but with a cross section proportional to p^2. This gives the energy spectrum of cosmic radiation as

$$N=N_0p^{-2-(B/A)},$$

where N_0 is a constant. Agreement with the observational exponent -2.8 is obtained if $B/A=0.8$. A theoretical calculation of B/A is probably rather complicated, but a qualitative discussion indicates that the quantity should be of the order unity. The formula should hold in a region extending to the neighborhood of the upper and lower limits given in Sections 1 and 2.

It should be observed that particles moving in the trapping field far away from the sun could also be accelerated by a similar process if the trapping field varies. The difference is that no loss of particles is produced by the disturbance itself. Instead the loss is only due to absorption in interstellar matter. Hence this process is of the same kind considered by Fermi and should also lead to a power spectrum. The "injection" which leads to some difficulty in Fermi's theory could be accomplished by the solar generator.

If observations of cosmic rays should give energies definitely in excess of the upper limits given in Section 1 this may be due to an earlier higher value of the solar dipole moment, but it may also be due to a subsequent Fermi acceleration in the trapping field. In both cases the considerations in Section 2 of the low energy cut-off would be erroneous.

On Some Low Ionizing Radiation Observed by Measurements of Cosmic Radiation at Great Depths

M. Miesowicz, L. Jurkiewicz, and J. M. Massalski
Physical Laboratory of the Mining Academy, Cracow, Poland
(Received September 22, 1949)

By measurements of twofold, threefold, and fourfold coincidences with a Geiger counter telescope, the underground rays at 660 and 540 m w.e. (water equivalent) have been divided into two components. One of the components is ionizing, discharging the counters with almost 100 percent efficiency, and has a strong maximum in the vertical direction. The other component discharges the counters with a very low efficiency, producing numerous twofold coincidences but practically no threefold or fourfold coincidences. It is isotropic in direction and rapidly absorbed in lead. This second component is thought to be composed of γ-rays of local radioactive origin. The telescope used in these experiments differed from that of Barnóthy and Forró in that it was protected from side showers by anticoincidence counters. The ratio of twofold to threefold coincidences was found to be about 1.4 instead of 20 as reported by Barnóthy and Forró at 1000 m w.e.

THE PROBLEM OF GREAT DEPTHS

As concerns the problem of cosmic radiation reaching great depths (some hundred m w.e.), it is assumed by most physicists that this radiation is a meson radiation (perhaps with some admixture of protons) accompanied by knock-on electrons, and cascade showers started by these.[1] Quite different views on this subject are given by Barnóthy and Forró[2] who assume that at depths greater than 500 m w.e. it is mainly non-ionizing radiation produced by the decay of μ-mesons which penetrates there. They consider that our instruments at those depths are operated by secondaries of that non-ionizing radiation.

These differences in views are derived from some anomalies observed by measurements of cosmic radiation at great depths. The best known anomaly is that giving the relation between the intensity of cosmic radiation and the depth. If we take the integral spectrum of mesons as given by the relation: $J=cE^{-\gamma}$, and we also take the losses of energy of mesons to be proportional to the depth H which they have traversed, we obtain the relation: $J=cH^{-\gamma}$. Now taking into account the experimental results, in the diagram log$J$ *versus* log$H$ we get a line which is broken at about 300 m w.e.[3] Up to 300 m w.e. we have the relation: $J=cH^{-1.8}$, and beyond that depth the exponent changes from the value 1.8 to 2.8.

Lyons[4] considers an additional loss of energy of very energetic mesons by radiation as a cause of this change of dependence of the intensity on the depth. That loss must be accentuated below 300 m w.e. A closer analysis of this process proves that the losses of energy suffered by mesons which have traversed such depths are too small to explain this phenomenon.

There are now in the literature of the subject two opinions[2,5] on this problem based on a similar assumption of meson decay. The introduction of meson decay influences the shape of the spectrum of the radiation at great depths. The mean range of decaying mesons is proportional to the energy. Then in the spectrum of decay products we shall have a lack of particles of the highest energies and this should be observed for energies for which the mean range of mesons is equal to or greater than the height at which mesons are produced in the atmosphere. In the spectrum of decay products of the form $E^{-1.8}$, we get the factor E^{-1} which explains the dependence observed, i.e., $J=cH^{-2.8}$, if we assume that all the radiation at great depths is produced by decay products of mesons. The main difference between Barnóthy and Forró and Greisen is that Barnóthy and Forró assume that at great depths we observe the neutral products of μ-meson decay, Greisen on the contrary introduces into this problem the process of the decay of π-meson into μ-meson. He evaluates in this way the energy by which the spectrum changes from the form $E^{-1.8}$ to $E^{-2.8}$. This energy ($E\approx10^{11}$ ev) is necessary for the meson to traverse some hundred m w.e. With this supposition it is not necessary to consider the cosmic radiation at great depths to be composed of neutral meson-decay products. The μ-mesons themselves are decay products.

But Barnóthy and Forró in the paper mentioned report among many interesting results also a phenomenon which they interpret as an argument for the opinion that at great depths we have to do especially with neutral meson-decay products. This phenomenon, mentioned in 1939,[6] was communicated at the Cracow Cosmic Rays Conference in October 1947. They observed at the depth of 1000 m w.e. that the radiation there measured was able to give many times more double than threefold coincidences in the same telescope. The ratio of threefold to double coincidences in their measurements was 0.05. Barnóthy and Forró express the opinion that this phenomenon proves the existence at great depths of a scarcely ionizing component of cosmic radiation. For this component the

[1] V. C. Wilson and D. J. Hughes, Phys. Rev. **63**, 161 (1943).
[2] J. Barnóthy and M. Forró, Phys. Rev. **74**, 1300 (1948).
[3] J. Clay and A. V. Gemert, Physics **VI**, 497 (1939).
[4] D. Lyons, Physik. Zeits. **42**, 166 (1941).
[5] K. Greisen, Phys. Rev. **73**, 521 (1948).
[6] J. Barnóthy and M. Forró, Phys. Rev. **55**, 870 (1939).

probability of threefold coincidences ought to be smaller than that of double ones.

The aim of this work, of which we are giving the provisional results in this paper, was to check this interesting phenomenon and to investigate more closely the properties of the radiation which produces it.

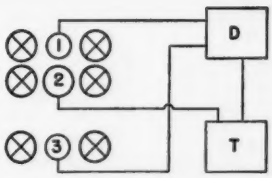

FIG. 1. Arrangement of counters.

DESCRIPTION OF THE APPARATUS

Our measurements were performed in the salt mine at Wieliczka near Cracow. The deepest level at our disposal was 282 m below ground. The layers above the telescope consisted of rocksalt, sandstone, gray slit, and silt with grains of rocksalt, gypsum, and anhydrite. The water equivalent was estimated from samples taken from different layers at different levels. The measurements were carried out in horizontal passages (about 2 m high) in the salt layers at two levels, 660 and 540 m w.e. The work in the salt mine requires the apparatus to be built very thoroughly. Salt powder and moisture are deposited during the work and therefore the whole apparatus must be tightly closed. These difficulties may be easier overcome if we use all-metal counters with earthed cathodes. Because of the very large fluctuations of voltage in the mine, the apparatus had to be supplied with a stabilizer stabilizing the voltage within wide limits. The magnetic stabilizer* which we used was very helpful in this matter. The special conditions of work also needed some additional arrangements to make work continuous and safe (such as an automatic switch for too low voltage, a delayed switch for switching on the high tension for register circuits, an electric clock starting by the above-mentioned delayed switch, etc.).

The measurements on the ratio of threefold to double coincidences were performed with an apparatus much improved in comparison with that of Barnóthy and Forró. The telescope consisted of three G-M counters 1, 2, and 3 (Fig. 1). The middle counter 2 was of larger dimensions than the two others. The telescope was protected against side showers by six anticoincidence counters. The double coincidences D of the counters 1 and 3, and the threefold coincidences T of the counters 1, 2, and 3 were registered simultaneously by two separate P.O. registers. In this way we have even for a not very great number of D coincidences a fairly small statistical error of the ratio T/D. This is very important here because of the very low intensity of cosmic radiation at the depths in which we have worked (the number of T coincidences at the lowest level is at the rate of about 1/hr.). In order to measure the double coincidences D, the resolving time of our apparatus had to be rather small. It was 2.6 μsec., which we obtained in such a way that the rectangular pulse coming from the counter amplifier was differentiated with a small time constant in the circuit of the grid of the Rossi valves.[7] The G-M counters we used were of the all-metal type filled with the usual argon-alcohol mixture.[7] The dimensions of the counters were:

counters 1 and 2	4.3×65 cm^2,
counter 3 and anticounters	5.2×70 cm^2.

The number of pulses per minute of these counters in the laboratory were about 650 for smaller and 900 for larger counters. The number of pulses per minute at the lowest level in the mine were about 70 and 100, respectively. After protecting the counters 1 and 2 by 5 cm Pb at the lowest level, the background rate dropped to 16/min. The low background rates of the counters were very convenient for our measurements.

THE MEASUREMENTS OF THE RATIO OF THREEFOLD TO DOUBLE, AND OF FOURFOLD TO THREEFOLD COINCIDENCES

In our preliminary measurements performed at two depths (660 m w.e. and 540 m w.e.) we found more double than threefold coincidences, proving in this way qualitatively even for those depths the existence of the effect found by Barnóthy and Forró at 1000 m w.e. We did not find, however, any difference between the number of threefold and fourfold coincidences. The results of the measurements are given in Tables I, II, and III. In all tables in the number of D coincidences there are subtracted the accidental coincidences.

INVESTIGATIONS OF THE PROPERTIES OF THE RADIATION CAUSING THE EXCESS OF DOUBLE OVER THREEFOLD COINCIDENCES

Let us write the number of double, threefold, and fourfold coincidences in the form:[8]

$$D=\lambda^2N+J, \quad T=\lambda^3N+J, \quad F=\lambda^4N+J,$$

where J is the intensity of the ionizing component of the radiation going through the telescope, for which we assume the efficiency of the G-M counter to be 1.0, N the intensity, and λ the efficiency of the G-M counter for the non-ionizing component. From our measurements of the ratio F/T, it follows that $\lambda^3N \ll J$; in other words, the number of threefold coincidences produced by non-ionizing component is negligible as compared with the number of threefold coincidences produced by the ionizing component. Then we may consider T as the intensity J of the ionizing component

* The authors are greatly indebted for the design and the construction of this to Mr. T. Czayka of the Cracow Mining Academy.

[7] M. Miesowicz and L. Jurkiewicz, Acta Phys. Polonica **IX**, 54 (1947).

[8] J. Clay and C. Levert, Physica **IX**, 158 (1942).

and write:

$$\frac{T}{D}=\frac{T}{\lambda^2 N+T}=\frac{T}{A+T},$$

where A gives the number of double coincidences due to the non-ionizing component. Table IV gives a comparison of the values of A and T for two depths.

If A is considered as a measure of the intensity of the non-ionizing component of cosmic radiation, we should have its strong dependence on the depth and its high relative intensity. The ionizing component, however, shows that the intensity decreases in accordance with the measurements of other authors. For the absorption coefficient we get from our figures the value 2.1 which, taking into account our rather poor evaluation of the water equivalent, is quite consistent within the limits of error with the values given by other authors.

The other characteristics of the component A correspond in general to those found by Barnóthy and Forró for radiation recorded by double coincidences. For the investigation of the angular dependence of the component A, the measurements of threefold and double coincidences in a horizontal position of the telescope have so far been carried out. The results are given in Table V.

From the figures given in Table V we can see that for the horizontal position of the telescope the number of threefold coincidences is negligible and the number of double coincidences is, within the limits of error, of the same value as A. This is an evidence for the isotropic character of the component A.

Then we investigated the influence of lead put between the counters on the ratio of T/D. The figures are given in Table VI.

From these figures we can see that the component A is absorbed with an absorption coefficient of about 0.5 cm^{-1} Pb.

TABLE I. Vertical telescope at a depth of 660 m w.e.

	Number of coincidences and time	Average rate per hr.
Threefold coinc. T	321	1.34±0.05
Double coinc. D	443	1.86±0.06
Time (in hr.)	239.46	
Ratio of threefold to double coinc.	$T/D=(72.5\pm2.7)$ percent.	

TABLE II. Vertical telescope at a depth of 540 m w.e.

	Number of coincidences and time	Average rate per hr.
Threefold coinc. T	454	2.08±0.07
Double coinc. D	660	3.01±0.08
Time (in hr.)	218.6	
Ratio of threefold to double coinc.	$T/D=(69.0\pm2.2)$ percent	

EFFICIENCY OF THE COUNTERS FOR THE COMPONENT A

Barnóthy and Forró, who evaluated the ratio T/D at 1000 m w.e. and found the value 0.05, interpret this figure as the efficiency of the counters for the radiation giving the coincidences. We think that this would be correct only in the case when the telescope has not also registered a number of ionizing particles for which the efficiency of the G-M counters is equal to 1.0, and for which the numbers of double and threefold coincidences are the same. For the efficiency λ of the counter for radiation causing the excess of double coincidences, we have $\lambda<T/D$. On the other hand, in these circumstances we cannot at all evaluate the specific ionization as Barnóthy and Forró do. They give the value of 0.04 ion/cm N.T.P. air for this radiation. It is not known beforehand whether this radiation reacts on the counter producing ions in the gas of the counter or whether it gives secondaries in the walls of the counter and those initiate the discharge in it. In the first case, however, the efficiency of the counter would depend on the specific ionization of the gas contained in it, but in the second case it would depend on the probability of emitting secondaries in the walls entering the counter.

For rough evaluation of the efficiency of the G-M counters for the radiation A, we compared the number of counts of a single counter caused by the radiation which is absorbed by 5 cm Pb with the number of double coincidences A. We have at 660 m w.e., for a counter of a length of $l=65$ cm and a diameter of $a=4.3$ cm, the number of counts without screening 80/min., with a screen of 5 cm Pb from all sides 16/min., the number of counts due to the radiation absorbed in 5 cm Pb 64/min. If we assume that this radiation is isotropic for all the sphere, we have a dependence between the number N of counts and the flux j of the radiation and an efficiency λ of the counters for this radiation of the form:

$$N=\pi^2 al[1+(a/2l)]\lambda j,$$

we get from it $\lambda j=0.022$/sterad. cm^2 min.

TABLE III. Vertical telescope at a depth of 540 m w.e.

	Number of coincidences and time	Average rate per hr.
Fourfold coinc. F	354	2.09±0.07
Threefold coinc. T	356	2.10±0.08
Time (in hr.)	169.3	
Ratio of fourfold to threefold coinc.	$F/T=0.995\pm0.04$	

TABLE IV. Comparison of the values of A and T for two depths.

Depth	Coincidences caused by non-ionizing comp. A	Coincidences caused by ionizing comp. T
540 m w.e.	0.93/hr.	2.08/hr.
660 m w.e.	0.52/hr.	1.34/hr.

TABLE V. The telescope in a horizontal position at 540 m w.e.

	Number of coincidences and time	Rate per hr.
Threefold coin. T	1	
Double coin. D	110	0.91
Time (in hr.)	129.6	

TABLE VI. The telescope in a vertical position at 540 m w.e.

Thickness of lead in mm	T/D	A	A/A(0 cm Pb)
0	0.690	0.93	1.00
5	0.795	0.49	0.53
10	0.906	0.19	0.20
15	0.930	0.13	0.14
50	0.989	0.02	0.02

Let us now assume the probability of double coincidences due to this radiation without any discussion of the particulars of the mechanism of this process. Let us take λ' as the efficiency of the telescope for the double coincidences for this radiation, i.e., λ' is the probability that the particle or photon which discharges the first counter enters the second one and discharges this also. If the radiation is isotropic and comes from the solid angle determined by the telescope, we get by simple integration for the number of double coincidences A:

$$A=\lambda\lambda' ja^2(l/h)\arctan(l/h),$$

where $h=18$ cm is the distance between the counters in the double coincidence telescope. We get from this equation, $\lambda'=0.005$, a value 10 times smaller than that given by Barnóthy and Forró.

CONCLUSIONS

The results of this work therefore show the following properties of the radiation giving the excess of double over threefold coincidences: (1) It is scarcely ionizing. (2) It is isotropic. (3) It is absorbed by about 50 percent in 0.5 cm Pb. All these properties seem to prove that this radiation is of photon character, and the absorption coefficient and the efficiency of the counter for this radiation also suggest that we may have here some γ-radiation with energy ($\sim$1 Mev) of perhaps natural radioactive substances.

It remains to explain the mechanism of the coincidences given by such radiation. Probably we may have to do here with an example of some interesting compound Compton effect. As a matter of fact it might be possible that a photon entering the first counter and discharging it might enter the second counter and give off another electron operating the counter.

It is possible to see from our evaluation of the efficiency of the counter for that radiation, assuming that the discharge in the counter is started by photons, that we get quite a reasonable figure for the efficiency for double coincidences. Of course, in this case, $\lambda'<\lambda$ because the loss of energy of photons in the first counter causes a drop in the efficiency, and the photons are dispersed causing in this way also an additional inefficiency.

The authors are very grateful to the Science Department of the Ministry of Education for financial aid which has made it possible to carry out this work. The authors are also obliged to the Polish Academy of Sciences and Letters for supplying our laboratory at Wieliczka in lead. The authors would also like to take this opportunity of thanking Managers of the Salt Mine at Wieliczka and all miners for their kind cooperation we have received in all our experiments at Wieliczka. Appreciation is also expressed to Mr. S. Wojtów and Mr. A. Mikucki for their valuable help.

Surface Impedance of Superconducting Tin, Mercury, and Lead at 9200 Mc/Sec.*

I. Šimon**
Research Laboratory of Electronics, Massachusetts Institute of Technology, Cambridge, Massachusetts
(Received October 10, 1949)

Surface resistance and the change of surface reactance of three superconducting metals (Sn, Hg, Pb) have been measured. The results were evaluated in terms of the penetration depth λ of Londons' theory (Figs. 6, 8) and the limiting values of λ for $T=0$ were obtained (Table I).

THE surface impedance of the normal (non-superconducting) metals at such low temperatures that the mean free path of the electrons is larger than the skin depth has been studied in great detail by Pippard,[1] Reuter and Sondheimer,[2] and others. The general validity of the theory seems to be well established (Maxwell,[3] Nowak[4]).

An analogous treatment for the superconducting metals has been given by Maxwell, Marcus, and Slater[5] and some use of the theory for the interpretation of experimental results has already been made.[3] Following the Londons' phenomenological theory of superconductivity,[6] two kinds of electrons, which react independently to the high frequency field, are assumed to exist below the transition temperature. Superconducting electrons appear in increasing number with decreasing temperature and do not exhibit any interaction with the metallic lattice. The finite (although very small) resistivity which is observed in a high-frequency field is due to the normal electrons which are still present at temperatures below the transition. The fraction of the persisting normal electrons is contained as a substantial parameter in the theory[5] and can be obtained from the measurements (under further assumptions which will be stated below).

It cannot be decided with certainty from the available experimental data whether or not the fraction of the normal electrons tends actually to zero with $T\rightarrow 0$ as is required by the theory. The presence of the superconducting electrons, however, manifests itself by a very definite and measurable change in the reactive part of the surface impedance (Fig. 1). The results may be interpreted in terms of the penetration depth λ for the static field; and this is actually done in this paper in order to facilitate the comparison with other investigations.

EXPERIMENTAL TECHNIQUES

The microwave-measurement techniques used for obtaining the Q's and the resonant frequencies were quite straightforward and are described in detail in another paper,[7] together with a description of the low temperature equipment.

The resonators used were of the coaxial, quarter-wave-length type, shown in Fig. 2. They were inserted in a wave guide (immersed in the liquid helium bath) and coupled to the field in a suitable manner. The simple form of the resonators made it possible to cast the tin and lead resonators in glass molds in vacuum so that the surface obtained was smooth and clean. The mercury resonators were frozen from liquid metal in a polished steel mold in a dry helium-gas atmosphere. Some difficulty was experienced with lead, as the metal adhered to the glass surface. To prevent this adhesion it was necessary to apply a small amount of silicone grease on the glass surface and during the removal of the silicone film from the metal (with degreasing agents, diluted HCl and distilled water) the surface was oxidized (and perhaps etched). Spectroscopically standardized, 99.995 percent pure tin and 99.998 percent pure lead (supplied by Johnson and Matthey Ltd., London) were used. The mercury was a chemically pure metal (Mallinckrodt), triple distilled in vacuum.

EVALUATION OF MEASUREMENTS

The surface impedance may be defined as a ratio of the tangential components of the electric and the mag-

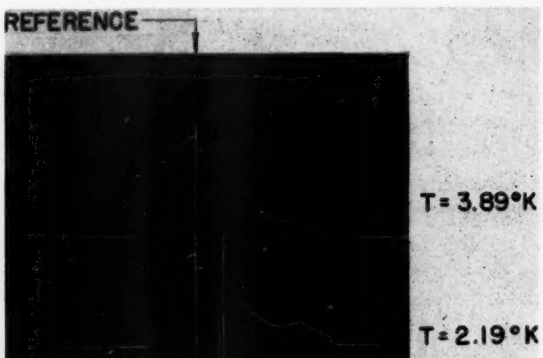

FIG. 1. Shift of the resonant frequency of a tin cavity in passing from the normal to the superconducting state.

* This work has been supported in part by the Signal Corps, the Air Materiel Command and the ONR.
** Now with Arthur D. Little, Inc., Cambridge, Massachusetts.
[1] A. B. Pippard, Proc. Roy. Soc. A191, 370, 385, 400 (1947).
[2] G. E. Reuter and E. H. Sondheimer, Proc. Roy. Soc. A195 (1948).
[3] E. Maxwell, thesis, M.I.T., Cambridge, Massachusetts (1948).
[4] W. B. Nowak, thesis, M.I.T., Cambridge, Massachusetts (1949); R.L.E. Technical Report No. 97, May 1949.
[5] Maxwell, Marcus, and Slater, R.L.E. Technical Report No. 109; also Phys. Rev. 74, 1234 (1948).
[6] F. London and H. London, Physica 2, 341 (1935).
[7] I. Šimon, R.L.E. Technical Report No. 126.

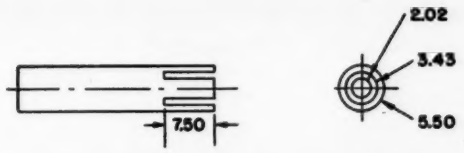

FIG. 2. Quarter-wave-length coaxial resonator (tin, No. Sn-5); dimensions are in mm.

netic fields at the surface of the metal: $Z=R+jX=E_t(0)/H_t(0)$. The aim of the measurements is to obtain R and X as functions of temperature. To this end the resonator made of a metal under investigation is cooled down and its Q and resonant frequency f_0 are measured. While R can be obtained directly from the measured Q, it is not practicable to obtain X from the measured resonant frequency due to the fact that f_0 is determined primarily by the geometrical shape and dimensions of the resonator whereas the intrinsic impedance of the metallic walls enters into the calculations only in a secondary way and to a very small extent. During the cooling, moreover, the geometrical dimensions change to a great extent in a nonlinear manner. This change prevents measuring the absolute value of X in the temperature region covering the non-superconducting state.

By passing the transition temperature and entering the superconducting state the change in surface impedance (especially in the real part) is very large and the thermal contraction has already "leveled off" and is negligible. This permits measuring the change Δf of the resonant frequency caused by the change of the surface reactance with fair accuracy. With the use of a result derived by Slater[8] it can be shown[3] that Δf and ΔX are related by an equation

$$\Delta X=-4\pi\mu_0 K\Delta f,$$

where K is a constant determined by the dimensions of the resonator. For a coaxial, quarter-wave-length resonator (Fig. 2)

$$K=c^{-1}(\epsilon_0\mu_0)^{-\frac{1}{2}}(\ln D/d)[2\Lambda_0/D+2\Lambda_0/d+8\ln D/d]^{-1}\Lambda_0,$$

where D, d are the diameters (Fig. 2), Λ_0 is the resonant wave-length and c is the velocity of light (the m.k.s. system of units is used throughout the paper). Furthermore,

$$R=2\pi\mu_0 K f_0 Q^{-1}.$$

The surface resistance R may be obtained on one hand from the measured value of Q. On the other hand R can be computed from the classical formula $R=(2\pi\omega_0\sigma 10^{-7})^{\frac{1}{2}}$ which is valid as long as the mean free path of the conduction electrons is small compared to the skin depth (σ denotes the d.c. conductivity). The computed values of R at 300°K agreed closely with the measured values in the case of tin and mercury (Table I). This agreement was considered as a proof that the effect of surface roughness was negligible. The discrepancy in the case of lead was attributed to a contamination of the surface.

In order to evaluate the measured values of R and ΔX in terms of the static penetration depth λ the theory of Marcus[5] has been applied. The basic assumption of the theory is that of the Londons' theory, i.e., of the coexistence of the "normal" and "superconducting" electrons below the transition point. The fraction $f_n=n_n/n$, (n_n is the number of the normal electrons and n is the total number of free electrons) of the electrons which remain in the normal state at a given temperature below transition is supposed to behave in accordance with the Reuter and Sondheimer theory[2] of the anomalous skin effect. Then the normalized surface resistance and reactance are given by the following expressions:

$$R/R_n=f_n^{-2/9}[I(\beta)/I(0)],$$
$$X/X_n=f_n^{-2/9}[I_1(\beta)/I_1(0)].$$

R_n and X_n are the values of R and X in the normal state just above the transition point. Functions $I(\beta)$ and $I_1(\beta)$ have been computed and tabulated by Marcus. The variable β reduces in the case of perfect reflection of the electrons on the metal boundary (case $p=1$ of the Reuter and Sondheimer theory) to

$$\beta=27/16(\delta_n/\lambda)^2 f_n^{-4/9},$$

where $\delta_n=R_n(2\pi\omega_0)^{-1}\times 10^7$ is the effective skin depth just above the transition.

Generally, f_n decreases with temperature rather rapidly, as may be inferred from the direct measurements of λ in static fields. We will use the assumption that the superconducting electrons are appearing in the same rate as the normal ones disappear, so that the total number remains constant, i.e., $n_s+n_n=n=$constant. It can be then shown from the Londons' theory that f_n is related to λ by means of a formula

$$f_n=1-(\lambda_0/\lambda)^2=1-(\lambda_0/\delta_n)^2(\delta_n/\lambda)^2,$$

where λ_0 denotes the zero-temperature limit of λ.

TABLE I. Experimental results for tin, mercury, and lead.[a]

	Sn	Hg	Pb	
σ_{300}	8.70×10^6	23.2×10^6	4.65×10^6	ohm^{-1} cm^{-1}
$1/R_{300}$, measured	15.3	9.55	9.50	ohm^{-1}
$1/R_{300}$, calculated	15.6	9.17	11.4	ohm^{-1}
$1/R_n$, measured	143	101	136	ohm^{-1}
Q_{300}, measured	299	205	205	
Q_n, measured	3200	2500	3070	
δ_n	19.6×10^{-3}	27.2×10^{-3}	20.5×10^{-3}	meter
f_0	9050	9200	9100	Mc/sec.
$(\Delta f/f_0)T=2°K$	1.85×10^{-4}	2.24×10^{-4}	1.95×10^{-4}	
$(\Delta f/f_0)T=0°K$ extrapolated	2.0×10^{-4}	2.4×10^{-4}	2.0×10^{-4}	
λ_0	4.65×10^{-3}	7.3×10^{-3}	5.4×10^{-3}	meter

[a] σ_{300} is the d.c. conductivity at room temperature (taken from International Critical Tables); R_{300} is the surface resistance at room temperature; Q_{300} and Q_n are the unloaded Q's of the resonators used at room temperature and at a temperature just above the transition point respectively; δ_n is the effective skin depth computed from the measured value of R_n; f_0 denotes the resonant frequency; $\Delta f/f_0$, the normalized frequency shift; and λ_0 is the limiting value of the static penetration depth for $T=0$.

[8] J. C. Slater, Rev. Mod. Phys. 18, 475 (1946).

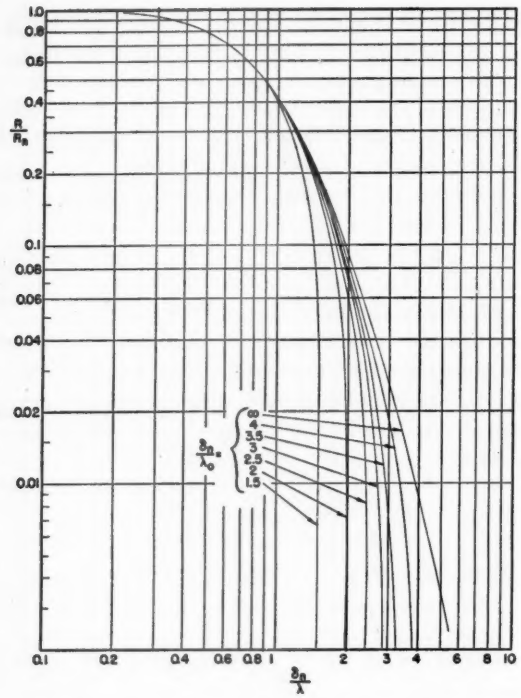

FIG. 3. Normalized surface resistance as a function of δ/λ for various values of the parameter δ_n/λ_0 computed from the theory in reference 5.

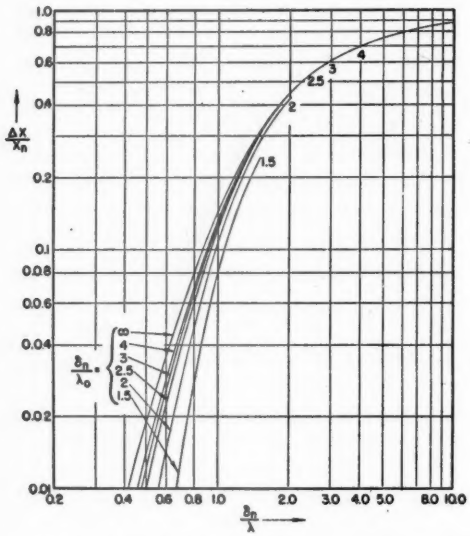

FIG. 4. Normalized surface reactance computed from the theory in reference 5.

Two sets of curves were prepared, plotting R/R_n and $\Delta X/X_n[=(X-X_n)/X_n=X/X_n-1]$ as functions of (δ_n/λ) for different values of the parameter (δ_n/λ_0) (Figs. 3 and 4). By comparing the measured values of R/R_n and $\Delta X/X_n$ (as functions of the temperature) with the theoretical values from the curves, we obtain the desired dependence of λ on the temperature. R_n and δ_n are known from the measurements in the normal state, λ_0 has to be known, or we can obtain it from the measurements of ΔX if we assume the validity of a formula of Reuter and Sondheimer, i.e., $X_n=\sqrt{3}R_n$ (in classical case, i.e., at sufficiently high temperatures is $X=R$). Then

$$\Delta X/X_n=-(2/\sqrt{3})Q_n\Delta f/f_0.$$

For very low temperatures, i.e., for β large, $I_1(\beta)$ can be shown to have a limit $\pi[2\sqrt{\beta}(4/3)^{\frac{1}{4}}\cos(1/3)]^{-1}$ and the theoretical value of $\Delta X/X_n$ has therefore a limit

$$\lim_{T\to 0}(\Delta X/X_n)=1.060(\delta_n/\lambda_0)^{-1}-1,$$

which is plotted in Fig. 5. Now, if we can extrapolate the measured curves of $(\Delta f/f_0)$ *versus* T towards $T=0$, we obtain the limiting value of $(\Delta X/X_n)$ and by using the curve in Fig. 5 we get (δ_n/λ_0) and eventually λ_0. We can then use the curves of Figs. 3 and 4 to obtain the dependence of λ *versus* T from both resistive and reactive measurements.

EXPERIMENTAL RESULTS

The results obtained for tin, mercury, and lead are summarized in Table I and the λ *versus* T curves are

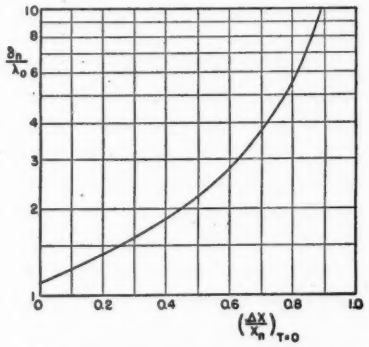

FIG. 5. Diagram for determination of the parameter δ_n/λ_0 from the extrapolated total change of the surface resistance.

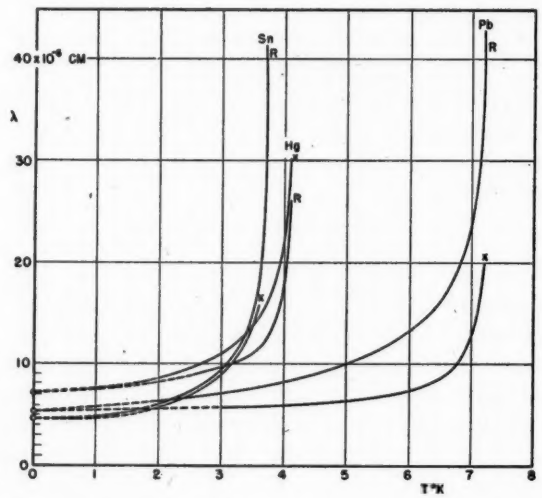

FIG. 6. Penetration depth λ as a function of temperature T. X and R denote the curves obtained from reactive and resistive data, respectively.

plotted in Fig. 6. The measured curves of R/R_n and $\Delta f/f_0$ *versus* T are shown in Fig. 7 for the case of tin, where the most complete data were obtained.

Our values of λ_0 are consistently lower than the values usually adopted ($\lambda_0 \approx 7.5\times10^{-8}$ m). This fact might be due to the approximative character of some of the assumptions which have been made in applying the theory. In particular no experimental verification of the validity of the relation $X_n=\sqrt{3}R_n$ could be obtained with our measurements. If the value of X_n were closer to the classical value, i.e., if $R_n<X_n<\sqrt{3}R_n$ we might obtain higher values of λ_0. As a matter of fact, if we use a value, e.g., $\lambda_0=7.5\times10^{-8}$ m for tin, and enter the curves in Figs. 3 and 4 with the measured values of Fig. 7 for the respective value of the parameter $\delta_n/\lambda_0=2.6$, we obtain a good agreement with the curves of Pippard and Maxwell (Fig. 8). The value of λ_0 in the case of mercury lies closer to the usually adopted value, but this result might be due to the fact that the d.c. conductivity is not constant below the transition-point and thus δ_n tends to decrease with lower temperatures.

The two curves shown in Fig. 6 for each metal and marked by R and X (for resistive and reactive data, respectively) ought actually to coincide. The deviation of the X-curve in the case of mercury was probably caused by an accidental break-in of the helium vapor into the resonator during the low temperature run, whereas the large discrepancy of the R-curve in the case of lead was attributed to the surface imperfection which manifested itself by an anomalous behavior also in the non-superconducting state.

Another quantity which can be compared with the theory was obtained in the case of tin, i.e., the initial slope of the resistance-curve just below the transition point. From a plot of Fig. 7 in expanded scale, a slope of 14 ± 2 per degree K was obtained. This is in fair agreement with the observation of Pippard at 1200 Mc/sec.[1] from which we can derive a slope of 48 per degree K. Ratio of these slopes is 3.4, whereas from the theory one should expect a change amounting to the $\frac{2}{3}$-power of the ratio of the frequencies, which is in this case equal to 3.84. If we compare our slope with that of Maxwell,[3] which is 8.0 at 24,000 Mc/sec. we obtain a ratio 1.75, whereas the ratio of frequencies raised to the $\frac{2}{3}$-power is 1.92.

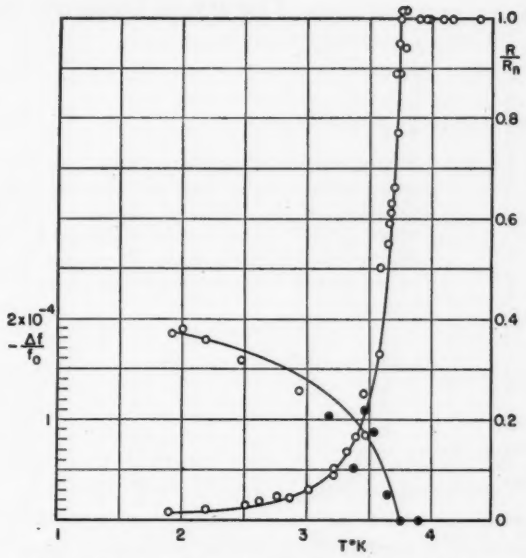

FIG. 7. Normalized surface resistance (circles) and the change in resonant frequency (dots) as functions of temperature for tin.

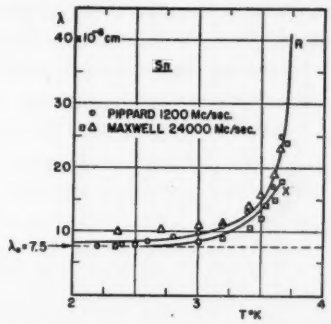

FIG. 8. Penetration depth λ as a function of temperature (for tin) compared with the results of Pippard (see reference 1) and Maxwell (see reference 3), when a value of $\lambda_0=7.5\times10^{-6}$ cm is used for the evaluation of the data.

ACKNOWLEDGMENTS

I am indebted to Professor J. C. Slater for the kind hospitality with which he introduced me to the Cryogenics Group and for many stimulating suggestions during this investigation. My best thanks belong further to all the members of the Cryogenics Group for their friendship and valuable help. Finally, I wish to express my gratitude to Professors J. A. Stratton, A. G. Hill, H. L. Hazen, and J. B. Wiesner for support on the part of the Research Laboratory of Electronics.

Theory of Impurity Scattering in Semiconductors

E. CONWELL* AND V. F. WEISSKOPF†
University of Rochester, Rochester, New York
(Received October 5, 1949)

Experiments by Lark-Horovitz and collaborators on the Hall effect and resistivity of germanium semiconductors have shown that the simple theory of lattice scattering alone cannot explain the temperature dependence of the resistivity. Another probable source of resistance is scattering by ionized impurity centers. This resistance can be calculated by using the Rutherford scattering formula. Evaluation of the collision terms in the Lorentz-Boltzmann equation of state is made by assuming that scattering of an electron by one ion is approximately independent of all other ions. This results in a resistivity given by (in ohm cm):

$$\rho = 2.11\times 10^{13}\kappa^{-2}T^{-\frac{1}{2}}\ln\{1+36\kappa^2 d^2(kT)^2e^{-4}\},$$

where d is half the average distance between impurity ions and κ the dielectric constant of the semiconductor.

EXPERIMENTS on the electrical properties of germanium semiconductors yield curves for resistivity as a function of temperature which cannot be explained by the theory of lattice scattering alone. The temperature behavior of the mobility indicates the existence of another scattering mechanism, especially at low temperatures.[1] It was pointed out by Lark-Horovitz‡ that another obvious source of resistance is scattering by the ionized impurity centers. This contribution to the resistivity is calculated here. Due to their relatively small density, the conduction electrons in a semiconductor obey Maxwell-Boltzmann statistics. Since the electrons have thermal energies and correspondingly large wave-lengths, their motion can be considered free and their scattering by the impurity ions is given by the Rutherford formula. The problem is then one of calculating the resistivity arising from Rutherford scattering of electrons (or holes) by a random distribution of impurity ions.

The system of free electrons in a semiconductor acted upon by a constant external field is in a state of dynamic equilibrium when a steady current is flowing. This implies that the number of particles per unit volume of phase space remains constant in time. From this condition it is possible to derive the form of the distribution function when there is an applied field by following the classical development of Lorentz.[2]

Consider a small volume of phase space $d\tau$ around x, y, z, v_x, v_y, v_z. Then $f(x, y, z, v_x, v_y, v_z)d\tau$ is the number of particles in $d\tau$ at time t. There are two ways in which this number may change: by acceleration by the electric field and by collisions. In a homogeneous isotropic medium, with uniform field E_z applied in the z direction, the rate of change due to the field is given by:[3]

$$\left(\frac{\partial f}{\partial t}\right)_{\text{drift}} = \frac{E_z e}{m}\frac{\partial f}{\partial v_z}, \tag{1}$$

where $\partial f/\partial v_z$ is to be evaluated in the particular volume of phase space under consideration. The rate of change due to collision is given by:

$$(\partial f/\partial t)_{\text{collision}} = b - a, \tag{2}$$

where b represents the number of particles entering a unit volume of $d\tau$ in unit time as a result of collisions and a represents the corresponding number leaving in a similar manner. In the steady state:

$$\frac{df}{dt} = \left(\frac{\partial f}{\partial t}\right)_{\text{drift}} + \left(\frac{\partial f}{\partial t}\right)_{\text{collision}} = 0 \tag{3}$$

or, using (1) and (2):

$$-\frac{E_z e}{m}\frac{\partial f}{\partial v_z} = b - a. \tag{4}$$

The calculation of the collision term is simplified by assuming (1) infinite mass for the scattering center, (2) perfectly elastic collisions, and (3) that scattering of an electron by one ion can be treated to a first approximation as independent of all other ions. As a result of the second assumption, only the direction of the electron velocity changes in a collision. It is convenient to introduce the spherical coordinates v, θ, φ instead of v_x, v_y, v_z. According to the third assumption, the electron is scattered by one ion at a time, i.e., by the one to which it is closest. If $2d$ is the average distance between nearest neighbor impurity ions, then, to this approximation, an electron is scattered by a particular ion only when it comes within distance d of that ion. As a result, one can express the number of electrons scattered out of unit volume of $d\tau$ in unit time into the solid

* Now at Brooklyn College, Brooklyn, New York.
† Now at Massachusetts Institute of Technology, Cambridge, Massachusetts. This paper was completed in 1943 and its publication was delayed by a number of circumstances.
[1] Lark-Horovitz, Middleton, Miller, and Walerstein, Phys. Rev. 69, 258 (1946). K. Lark-Horovitz, Contractor's Final Report NDRC 14-585 (November, 1945), pp. 27-33.
‡ Personal communications.
[2] A. A. Lorentz, *Theory of Electrons* (G. E. Stechert and Company, New York, 1923), pp. 266.
[3] Reference 2, p. 268.

angle $d\Omega'$ at θ', φ' as:

$$f(v, \theta, \varphi)N\sigma(\theta, \theta')vd\Omega',$$

where N is the number of impurity ions per cm^3, $\sigma(\theta, \theta')$ the Rutherford scattering cross section, v the relative velocity of the electron and the scattering center (which, by the first assumption, is just the electron velocity). The term a is the integral of the above expression over θ', φ'. From the previous considerations, however, it is apparent that the integration is not to be carried out over all θ'. The limitation on impact parameter is equivalent to a limitation on θ' which can be expressed by the relationship:

$$\tan[(\theta'-\theta)/2]=Ze^2/(\kappa mv^2\beta), \tag{5}$$

where κ is the dielectric constant of the medium and β the impact parameter. For the largest possible impact parameter, d:

$$\theta'-\theta=(\theta'-\theta)_{\min}=2 \text{ arc } \tan Ze^2/(\kappa mv^2d). \tag{6}$$

This gives the lower limit for integration over θ'. Since this formula and the Rutherford scattering cross section depend only on the change of direction or $\theta'-\theta$, it is possible to choose axes to set θ equal to 0°. The expression for a is then:

$$a=Nv\int_{\theta'=\theta'_{\min}}^{\pi}\int_{\varphi'=0}^{2\pi} f(v, \theta, \varphi)\sigma(\theta')d\Omega'. \tag{7}$$

The term b is evaluated in much the same manner as a. The final result for $b-a$ is:

$$b-a=Nv\int_{\theta'=\theta'_{\min}}^{\pi}\int_{\varphi'=0}^{2\pi}[f(v, \theta', \varphi') - f(v, 0, \varphi)]\sigma d\Omega'. \tag{8}$$

When substituted in (4) this gives the integral equation:

$$-\frac{E_z e}{m}\left(\frac{\partial f}{\partial v_z}\right) = Nv\int_{\theta'=\theta'_{\min}}^{\pi}\int_{\varphi'=0}^{2\pi}[f(v, \theta', \varphi')-f(v, 0, \varphi)]\sigma d\Omega'. \tag{9}$$

The form for the solution of this equation used by Lorentz and others in conductivity problems is suggested by physical considerations. The effect of applying the field is to superimpose on the random thermal motion a small net drift of electrons in the direction opposite to the field (in the field direction for conduction by holes). This suggests for the new distribution function the expression:

$$f=f_0-v_z\chi(v)=f_0-v\cos\theta\chi(v), \tag{10}$$

where

$$f_0=A\exp(-mv^2/2kT); \quad A=n(m/2\pi kT)^{\frac{3}{2}}, \tag{11}$$

n being the number of conduction electrons per cm^3 and $\chi(v)$ a function to be determined.

Since the additive term is much smaller than f_0, it can be neglected in evaluating $(\partial f/\partial v_z)$ at v, 0, φ. Integration of $b-a$ is completely straightforward. From Eq. (9) one obtains the following expression for χ:

$$\chi(v)=\frac{\kappa^2m^2v^3AE_z\exp(-mv^2/2kT)}{\pi Ne^3kT\ln G}, \tag{12}$$

where

$$G=1+\kappa^2m^2v^4d^2e^{-4}. \tag{13}$$

From $\chi(v)$ either the mean free path for this type of scattering or the resistivity can be obtained simply. To obtain the former, one uses:[2]

$$\chi(v)=(l/v)eE_z[(\partial f_0)/(\partial\epsilon)] \tag{14}$$

which gives

$$l(v)=\kappa^2m^2v^4/\pi Ne^4\ln G. \tag{15}$$

To obtain the resistivity, we use:[4]

$$j=\sigma E_z=-e\int_{v=0}^{\infty}\int_{\theta'=0}^{\pi}\int_{\varphi'=0}^{2\pi} v^4\chi\cos^2\theta'\sin\theta' dv d\theta' d\varphi'. \tag{16}$$

From (16), after integration over θ', φ', one gets

$$\sigma=\frac{2\kappa^2m^2A}{3Ne^2kT}\int_{v=0}^{\infty}\frac{v^7\exp(-mv^2/2kT)dv}{\ln(1+\kappa^2m^2v^4d^2e^{-4})}. \tag{17}$$

This integral converges. Since the logarithm is a slowly varying function, a good approximation to the value of the integral can be obtained by substituting for the logarithm its value at the maximum of the function in the numerator. This maximum occurs at

$$v^2=6kT/m. \tag{18}$$

The simplified integral is readily evaluated. This yields a resistivity (in ohm çm) (all constants in c.g.s. units):

$$\rho=9\times10^{11}\pi^{\frac{3}{2}}e^2m^{\frac{1}{2}}2^{-7/2}\kappa^{-2}(kT)^{-\frac{3}{2}} \times\ln\{1+36\kappa^2d^2(kT)^2e^{-4}\}. \tag{19}$$

When there is no intrinsic* conductivity, n is equal to N, the number of ionized impurity centers and hence N and n do not explicitly appear in Eq. (19). So the dependence on the density of impurity centers occurs only in the logarithmic term, through the factor d^2.

Generally the temperature behavior of the resistivity due to impurity scattering is more strongly influenced by the $T^{-\frac{3}{2}}$ in Eq. (19) than by the T^2 term in the logarithm, and hence this resistivity rises as the temperature decreases. This increase is due to the decrease of mean electron velocity with drop in T and the consequent increase in the scattering effect of the impurity

[4] Reference 2, p. 272.

* Observed at higher temperature, due to electrons in the conduction band equal in number to the holes in the full band.

ions. On the other hand, for an impurity semiconductor, the resistivity due to lattice scattering generally decreases with decreasing temperature because of the T^{-1} dependence of the mean free path.[5] Hence, the importance of the impurity ion scattering resistivity in determining total resistivity increases as temperature decreases.[6]

[5] A. Sommerfeld and H. Bethe, *Handbuch der Physik XXIV* (1933), Vol. 12, p. 560.

[6] K. Lark-Horovitz and V. A. Johnson, Phys. Rev. **69**, 258 (1946). K. Lark-Horovitz, Contractor's Final Report, NDRC 14–585 (November, 1945), pp. 36–41.

PHYSICAL REVIEW VOLUME 77, NUMBER 3 FEBRUARY 1, 1950

Evaluation of the Stiffness Coefficients for Beryllium from Ultrasonic Measurements in Polycrystalline and Single Crystal Specimens*

LOUIS GOLD
Air Force Cambridge Research Laboratories, Cambridge, Massachusetts

(Received August 15, 1949)

The pulsed ultrasonic method has been applied to the determination of the stiffness coefficients for beryllium. The constants $c_{11}=30.8\times10^{11}$ dynes/cm^2, $c_{33}=35.7$ were evaluated from compressional wave velocities in single crystals by extrapolating a plot of the effective stiffness coefficient *versus* $\sin^2\theta$ (θ being the angle between the hexagonal axis and the direction of wave propagation) to the points $\theta=\pi/2$ and 0. The values $c_{12}=-5.8$, $c_{44}=11.0$ were derived from an analysis relating the average effective stiffness stiffness coefficients for compressional and shear waves with the shear modulus and Lame's constant. The latter data were calculated from measurements of longitudinal and transverse body wave velocities in polycrystalline metal. To find the coefficient $c_{13}=0.87$, the established values for the other constants were employed in the general relation for the effective stiffness coefficient of the form $C_l=f(c_{jk}{}'s, \theta)$.

Several criteria have been used to assess the validity of the c_{jk} data: (1) The ratio of c_{11}/c_{33} is in accord with the c/a ratio for the hexagonal close-packed structure of beryllium; (2) the compressional and shear wave anisotropy factors of $c_{33}/c_{11}=1.16$ and $c_{44}/\frac{1}{2}(c_{11}-c_{12})=1.68$, respectively are in harmony with the observed transmission properties of polycrystalline beryllium; and (3) the experimental and theoretical curves for the directional variation of the effective compressional stiffness coefficient agree quite well.

1. INTRODUCTION

THE literature contains the stiffness coefficients of only three hexagonal metals, these being magnesium, zinc, and cadmium.[1] Some recent work on the preparation of large beryllium crystals has made available several adequate-sized single crystals of beryllium for ultrasonic velocity measurements from which the c_{jk} constants were determined.[2]

It was found that essentially all of the crystal specimens were so oriented that measurements along ideal directions were virtually precluded. This condition eliminated any hope of obtaining the best possible accuracy, and, therefore, redetermination would be warranted when better crystals could be had. Nevertheless, the values for the $c_{jk}{}'s$ of beryllium are determinable to the order of accuracy common to the other hexagonal metals.

The method employed for evaluating the stiffness coefficients of beryllium is unique and has not been reported previously. It is based upon the following experimental data:

(1) Compressional and shear wave velocities in polycrystalline metal.

(2) Compressional wave velocities in single crystal specimens having their crystallographic axes differently oriented with respect to the direction of propagation. Deriving the coefficients from this information requires the conditions, (1) the crystal belongs to classes 21–27 of Voigt's designation, thus having five independent constants, (2) the crystal is not too anisotropic.

The first of these conditions permits one to considerably simplify the expressions for the various wave velocities;[3] the functions $v=f(\alpha, \beta, \gamma, c_{jk}{}'s, \rho)$ can be reduced to $v=F(\theta, c_{jk}{}'s, \rho)$ where θ, the angle between the hexagonal axis and the direction of wave propagation, takes the place of the three direction cosines α, β, and γ. The second condition makes possible certain extrapolation and approximations which will be described in detail. If the crystal is too anisotropic it becomes very difficult to obtain velocity data for polycrystalline specimens because of the poor multiple echo patterns.[4] Beryllium exhibited excellent patterns, so it appeared reasonable at the outset to infer that it was not a highly anisotropic crystal. The significance of this feature will be accounted for later.

2. EXPERIMENTAL ASPECTS

Apparatus for the pulsed-ultrasonic measurements was of the nature already described in a number of

* This paper is based on work performed at the Metallurgical Project, Massachusetts Institute of Technology, under Contract No. W-7405-eng-175 for the AEC.

[1] R. F. S. Hearmon, Rev. Mod. Phys. **18**, 409 (1946).

[2] L. Gold, Rev. Sci. Inst. **20**, 115 (1949).

[3] H. E. Mueller (private communication).

[4] W. P. Mason and H. J. McSkimin, J. Acous. Soc. Am. **19**, 464 (1947). W. Roth, J. App. Phys. **19**, 901 (1947).

publications.[5] The data were taken at room temperature with microsecond pulses at 10 mc. It was found that the optimum procedure for obtaining good velocity data required, (1) the use of salol films both for the longitudinal and transverse modes, (2) recording range readings on the scope pattern at the first discontinuity in the linear sweep produced by an echo. The oil film coupling between transducer and specimen gave rise to relatively large fluctuations in the echo intervals, principally because of its tendency to distort the pulses and make readings difficult. Apparently, better reproducibility of the echo intervals is achieved by reading to the very front edge of the pulse rather than a fixed db down from the bottom of the pulse.

Two possible ways of arriving at an average value for the range intervals were employed. For the polycrystalline specimens, where a number of good echoes could be obtained, it was convenient to plot the range readings *versus* the echo number and then to compute the average echo interval from the slope. This procedure is not practical where a large number of echoes are observed, whence for the single crystals differences in range for the various echoes were averaged numerically.

Velocity measurements for the single crystals were limited to compressional waves because of uncertainty in interpreting the multiple echo patterns for the shear waves; since two shear modes are excited simultaneously, it is difficult to resolve the pattern into the shear components, particularly when the velocities of propagation are not widely divergent.*

The orientation of the beryllium crystals was determined by the well-known back-reflection Laue technique, followed by stereographic projection. The angle between the hexagonal axis and the axis of the specimen is accurate to about 1–2°, a value which is sufficient for the over-all accuracy of the final data.

3. RESULTS FOR POLYCRYSTALLINE BERYLLIUM

Data was taken on a wide variety of samples of extruded flake, vacuum-cast lump, etc. There did not appear to be any significant divergence of results, in spite of the fact that preferred orientation was undoubtedly present in some of the specimens. This is substantial evidence for the relative isotropy of beryllium. In general, better patterns were manifest for longitudinal vibration than for transverse vibration; pulse distortion was more pronounced for the shear waves, a condition which makes the shear velocity measurement of lower accuracy.

Some rough estimates of the attenuation for compressional and shear oscillations, indicated that the latter was somewhat larger. If one interprets this as "scattering" losses at the crystal boundaries, then it can be inferred that beryllium has a higher degree of shear anisotropy than compressional anisotropy.[6] This conclusion is a useful one for checking the c_{jk} values as will be demonstrated.

Table I summarizes all the data one can obtain from ultrasonic propagation measurements in an isotropic substance. The compressional velocity is seen to be in excellent accord with the Sawyer-Kjellgren reported value;[7] the manner in which S-K obtained this value is not clear, but presumably it was based upon the composite oscillator technique. Quite recently Squire *et al.* have reported ultrasonic velocity measurements in beryllium;[8] their values agree very well with the table values.

The elastic constants were computed by means of the standard relations of elasticity theory.[9] Young's modulus for the static stress-strain method agrees very well with the dynamic value. The compressibility value is in fair agreement with those obtained by the high pressure technique.[10] Considering the differences in experimental approach, the agreement is much better than anticipated; very likely, the result obtained by the ultrasonic method is more reliable.

The values for Poisson's ratio is surprisingly low. By combining the literature values for the compressional velocity and the compressibility, the comparative figures listed were derived from the relation

$$\nu=(3-v_l^2\beta\rho)/(3+v_l^2\beta\rho), \tag{3}$$

where v_l is the compressional velocity, β the compressibility and ρ the density of beryllium. Thus, it is reasonably certain that the Poisson ratio for beryllium is the lowest for any of the known metals and alloys.

As an item of general interest, it was thought worthwhile to calculate the theoretical value for the characteristic temperature of beryllium for comparison with the value derived from specific heat measurements. The relation used is the classical Einstein-Debye equation

$$\nu_{\max}=\left\{\frac{9}{4\pi}\frac{N}{V}\frac{1}{(1/v_l^3)+(2/v_t^3)}\right\}^{\frac{1}{3}} \tag{3.1}$$

where $\nu_{\max}$, the characteristic frequency of the crystal lattice, is related to the characteristic temperature Θ by the relation $\Theta=(h/k)\nu_{\max}$. The various symbols defined and evaluated are

N—atoms per cell = 2
V—volume of unit cell = 16.0×10^{-24} cm³
v_l—longitudinal wave velocity = 1.26×10^{6} cm/sec.
v_t—transverse wave velocity = 0.888×10^{6} cm/sec.
h—Planck's constant = 6.64×10^{-27} erg-sec.
k—Boltzmann's constant = 1.37×10^{-16} erg/°k.

[5] J. R. Pellam and J. K. Galt, J. Chem. Phys. **14**, 608 (1946). H. B. Huntington, Phys. Rev. **72**, 321 (1947).

* Mode separation is facilitated when the crystal constants have been established previously.

[6] W. P. Mason and H. J. McSkimin, J. App. Phys. **19**, 940 (1947).

[7] C. B. Sawyer and B. J. Kjellgren, Ind. Eng. Chem. **30**, 501 (1938).

[8] Rice Institute Progress Report N6onr-224 Task Order No. 3, October 1, 1948.

[9] A. E. H. Love, *Mathematical Theory of Elasticity* (Dover Publications, New York, 1944).

[10] P. W. Bridgman, Proc. Am. Acad. **68**, 27 (1933). Richards, Hall, and Mair, J. Am. Chem. Soc. **50**, 3304 (1928).

TABLE I. Data for polycrystalline beryllium.

For extruded flake metal	
Compressional velocity	1.265×10^{6} cm/sec.
S and K value (method not reported)	1.26×10^{6} cm/sec.
Shear velocity	0.888×10^{6} cm/sec.
Young's modulus	2.965×10^{12} dynes/cm^2 (4.300×10^{7} lb./in.^{2})
Lit. value (stress-strain method)	4.26×10^{7} lb./in.^{2})
Shear or rigidity modulus	1.465×10^{12} dynes/cm^2
Bulk modulus	1.014×10^{12} dynes/cm^2
Compressibility	0.985×10^{-12} cm^2/dyne
Bridgman value (high pressure tech.)	0.874×10^{-12}
Richard *et al.* (high pressure tech.)	0.95×10^{-12}
Poisson's ratio	0.0122
Based on Bridgman value	0.0754
Based on Richards value	0.035
Lamé's constant	0.038×10^{12} dynes/cm^2
Characteristic temperature	
From Debye-Einstein rel'n	1430°K
From specific heat data	1000°K

Calculation gives $\nu_{max}=2.96\times10^{13}$/sec. and $\Theta=1430°$.K The specific heat value is 1000°K.

4. RESULTS FOR SINGLE CRYSTALS

Four single crystals with dimensions of the order of 1 in. diameter and 1–2 in. in length were employed for the compressional velocity measurements. Data for three of the specimens are included in Table II.

It is evident that the velocity is comparatively insensitive to crystal orientation; the values listed were computed from the relation

$$v=1.670\times10^{9}(l/2\Delta y) \tag{4}$$

which converts the radar scope range readings to velocity values, l being the specimen length and Δy the range interval. The results for the fourth specimen are omitted since they were found subsequently to be questionable when the data were used in arriving at the c_{jk}'s.

5. BASIC STIFFNESS COEFFICIENT RELATIONS AND THE DETERMINATION OF c_{11} AND c_{33}

The body wave velocities in a hexagonal crystal of classification D^{4}_{6h} can be expressed as follows:

$$v_l=\left(\frac{c_l}{\rho}\right)^{\frac{1}{2}},\quad v_{t_1}=\left(\frac{c_{t_1}}{\rho}\right)^{\frac{1}{2}},\quad v_{t_2}=\left(\frac{c_{t_2}}{\rho}\right)^{\frac{1}{2}}, \tag{5.1}$$

where

$$\begin{aligned} c_{t_1}&=\tfrac{1}{2}(c_{11}-c_{12})\sin^2\theta+c_{44}\cos^2\theta\\ c_{t_2}&=\tfrac{1}{2}[(c_{11}+c_{44})\sin^2\theta+(c_{33}+c_{44})\cos^2\theta-\varphi(c_{jk},\theta)]\\ c_l&=\tfrac{1}{2}[(c_{11}+c_{44})\sin^2\theta+(c_{33}+c_{44})\cos^2\theta+\varphi(c_{jk},\theta)]. \end{aligned} \tag{5.2}$$

The angle between the direction of wave propagation and the hexagonal axis is θ. For the function $\varphi(c_{jk},\theta)$ one has

$$\begin{aligned} \varphi(c_{jk},\theta)=\{&(c_{11}-c_{44})^2\sin^4\theta+(c_{33}-c_{44})^2\cos^4\theta\\ &+2\sin^2\theta\cos^2\theta[(c_{11}-c_{44})(c_{44}-c_{33})\\ &+2(c_{13}+c_{44})^2]\}^{\frac{1}{2}}. \end{aligned} \tag{5.3}$$

It is evident that a plot of c_l *versus* θ should permit extrapolation to $\theta=\pi/2$ and 0 where $c_l=c_{11}$ and c_{33}, respectively. Since only three reliable points were available, some misgiving as to the reliability of such a solution for c_{11} and c_{33} was at first manifest; however, several considerations established a modicum of confidence in this approach.

A review of the results for the metals cadmium, zinc, and magnesium indicated that extrapolation is apt to be more accurate if one plots c_l *versus* $\sin^2\theta$. Moreover, since beryllium is comparatively isotropic c_{11} should not be too different from c_{33} and also the extrapolation at the end points should be gradual. Figure 1 shows the c_l *versus* $\sin^2\theta$ plot with the extrapolation values for c_{11} and c_{33} identified.

If one interprets the significance of the c_{jk} constants along the c and a axes of a hexagonal crystal, additional confirmation of the derived values for beryllium is possible. Effectively, c_{11} and c_{33} are measures of the bonding strength along the a and c axes, respectively. Hence, in hexagonal crystals of similar electronic configuration, it is apparent that the ratio c_{11}/c_{33} should have some correlation with regard to the axial ratio c/a. Figure 2 is what may be conveniently termed an anisotropy plot for hexagonal metals. It is surprising how closely the four points lie on a straight line. For the ratio $c/a=1.63$, corresponding to the axial ratio for the ideal hexagonal close-packed structure, $c_{11}/c_{33}=1$. This is in accord with the idea that the cohesive forces along the [001] and [210] directions should be the same when the H.C.P. structure is truly attained; where the c/a ratio is loss than 1.63, c_{11} should be less than c_{33} which is the state of affairs for beryllium.

Thus, the inference can be made that the greater the deviation from the ideal c/a ratio for close-packing the more anisotropic will the metal be with regard to body wave propagation. The predicted position for cadmium not being in very good agreement with the experimental value might indicate errors in the determination of c_{11} and c_{33}; it would be of interest to redetermine these values.

6. DETERMINATION OF c_{12}, c_{13}, AND c_{44}

In principle, the cross constants should be determinable from Eqs. (5.2) and (5.3). By selecting points from the curve of c_l *versus* $\sin^2\theta$ in Fig. 1, one might attempt to evaluate the cross constants c_{12}, c_{13}, and c_{44}. This approach, however, is not practicable because of the transcendental nature of the equations involved.

TABLE II. Data for single crystals of beryllium.

Specimen	Length (inches)	Range interval (yards)	$v_l\times10^{6}$ cm/sec.	$c_n\times10^{12}$ dynes/cm^2	θ
(1)	1.714	1100	1.30	3.14	52°
(2)	1.283	800	1.34	3.33	33°
(3)	1.533	990	1.29	3.09	67°

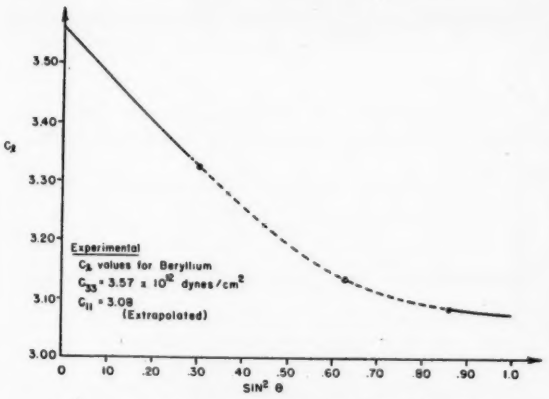

FIG. 1. Variation of the values of c_l for beryllium with $\sin^2\theta$ (experimental).

Now for the polycrystalline data there are the relations

$$\bar{c}_l=2\mu+\lambda, \quad \bar{c}_t=\mu, \tag{6}$$

where μ is the shear modulus and λ Lamé's constant. These average values are related to the c_{jk} constants as clearly

$$\bar{c}_l=\frac{1}{2}\cdot\frac{2}{\pi}\int_0^{\pi/2}(c_{11}+c_{44})\sin^2\theta+(c_{33}+c_{44})\cos^2\theta d\theta + \frac{1}{2}\cdot\frac{2}{\pi}\int_0^{\pi/2}\varphi(c_{jk},\theta)d\theta \tag{6.1}$$

$$\bar{c}_{t1}=\frac{2}{\pi}\int_0^{\pi/2}[\tfrac{1}{2}(c_{11}-c_{12})\sin^2\theta+c_{44}\cos^2\theta]d\theta, \tag{6.2}$$

$\bar{c}_{t2}$ is essentially (6.1), but with a minus sign in front of the second integral.

Making use of the fact that beryllium is at least moderately isotropic, we assume that $\bar{v}_{t1}=\bar{v}_{t2}$ so that we can write

$$\bar{c}_{t1}=\bar{c}_{t2}=\bar{c}_t. \tag{6.3}$$

This assumption is vital in the procedure for finding expressions for $\bar{c}_l$ and $\bar{c}_t$ in terms of the stiffness coefficients. Several criteria form the basis of latter checking the soundness of (5.6), as well as the entire line of attack. These are:

(1) The theoretical curve for c_l based upon the c_{jk} values should agree with the experimental curve of Fig. 1.

(2) The cross constants c_{12}, c_{44}, c_{13} must be small compared to c_{11} and c_{33} because Poisson's ratio is low.

(3) The transverse velocities must be comparable when evaluated from the c_{jk} data.

Proceeding then with the analysis

$$\bar{c}_{t1}=\tfrac{1}{2}[\tfrac{1}{2}(c_{11}-c_{12})+c_{44}] \tag{6.4}$$

and

$$\tfrac{1}{2}[\tfrac{1}{2}(c_{11}-c_{12})+c_{44}]=\frac{1}{\pi}\int_0^{\pi/2}[(c_{11}+c_{44})\sin^2\theta + (c_{33}+c_{44})\cos^2\theta d\theta-\frac{1}{\pi}\int_0^{\pi/2}\varphi(c_{jk},\theta)d\theta, \tag{6-5}$$

from which one obtains

$$\frac{1}{\pi}\int_0^{\pi/2}\varphi(c_{jk},\theta)d\theta=\tfrac{1}{4}(c_{11}+c_{13}+2c_{44})-\tfrac{1}{2}[\tfrac{1}{2}(c_{11}-c_{12})+c_{44}] =\tfrac{1}{4}(c_{33}+c_{12}). \tag{6.6}$$

The integral in (6.6) would be quite impossible to evaluate by direct integration. Clearly, relation (6.3) circumvents this barrier and permits ready solution of $\bar{c}_l$. The relation for $\bar{c}_l$ is accordingly

$$\bar{c}_l=\tfrac{1}{4}[c_{11}+c_{12}+2(c_{33}+c_{44})]. \tag{6.7}$$

From relations (6), (6.4), and (6.7) one can write down the simultaneous equations

$$\begin{cases} c_{11}+c_{12}+2(c_{33}+c_{44})=4(2\mu+\lambda) \\ \tfrac{1}{2}(c_{11}-c_{12})+c_{44}=2\mu. \end{cases} \tag{6.8}$$

Putting in the values for c_{11}, c_{33}, μ and λ these become

$$\begin{cases} 2c_{44}+c_{12}=1.62 \\ 2c_{44}-c_{12}=2.78 \end{cases} \tag{6.9}$$

which give the solutions

$$c_{44}=1.10, \quad c_{12}=-0.58. \tag{6.10}$$

The remaining constant c_{13} can next be calculated from (5.2) and (5.3), using the values for the identified $c_{jk's}$ and selecting some value for c_l and θ. The result is

$$c_{13}=0.87.$$

7. DISCUSSION OF DERIVED c_{jk} VALUES FOR BERYLLIUM

Table III is a comparison of the stiffness coefficients for beryllium with those of magnesium, zinc, and cadmium. The data of Wright, Bridgman, and Gruen-eisen-Goens were the result of the static measurements

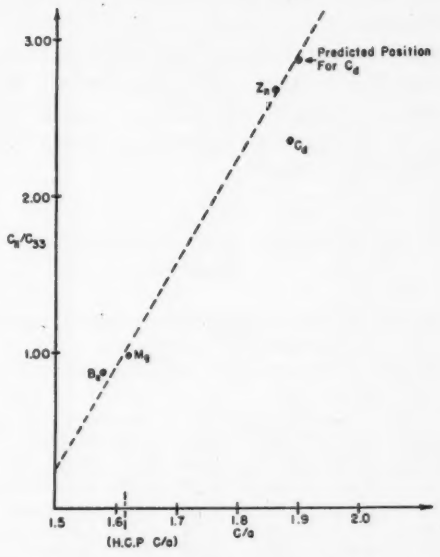

FIG. 2. Anisotropy plot for hexagonal metals showing bonding strength variation.

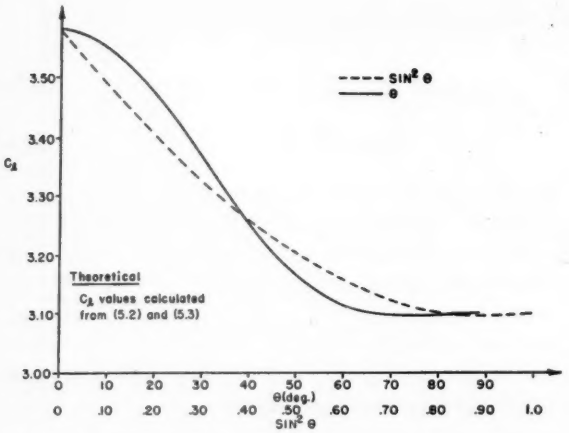

FIG. 3. Variation of c_l for beryllium with $\sin^2\theta$ (theoretical).

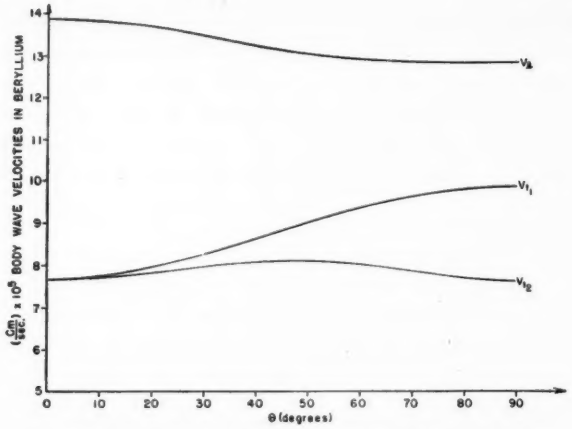

FIG. 4. Variation of body wave velocity with orientation.

on many crystals; it is evident that the differences between the various sets is generally much greater for the cross constants. This would seem to indicate greater likelihood of error in c_{44}, c_{12}, and c_{13}, and is apt to be the case for the beryllium values. As a rough assessment of the over-all accuracy of the beryllium constants, it would be reasonable to believe that they are of the same order of accuracy as the other data in Table III.

Confirmation of the general correctness of the stiffness coefficients is revealed in Fig. 3 which gives the theoretical c_l plot calculated from the listed values. The $\sin^2\theta$ plot if compared with Fig. 1 will be seen to fit the experimental curve quite gratifyingly; the end points would, of course, have to match, but the fact that the entire curve is in accord indicates the validity of the calculations. The c_l *versus* θ curve demonstrates why a better extrapolation for the c_{11} and c_{33} constants is possible with $\sin^2\theta$ as the abscissa. If the former had been used, the c_{33} value would have been found to be somewhat higher.

Recalling that beryllium is relatively more isotropic for compressional waves than shear waves, we now compare the ratios c_{33}/c_{11} and $1/2(c_{11}-c_{12})c_{44}$ which are a measure of the degree of anisotropy—being unity for complete isotropy. Thus

$$c_{33}/c_{11}=1.16, \quad \frac{c_{44}}{\frac{1}{2}(c_{11}-c_{12})}=1.68 \qquad (7)$$

TABLE III. Stiffness coefficients for hexagonal metals (c_{ik} values$\times 10^{11}$ dynes/cm^2).

Metal	c_{11}	c_{33}	c_{44}	c_{13}	c_{12}	Source
Mg	5.65	5.87	1.68	2.32	1.81	Wright
	5.94	5.94	1.14	2.03	2.03	Bridgman
Zn	16.1	5.42	4.00	4.32	4.37	Grueneisen-Goens
	15.9	6.21	4.00	3.23	4.82	Bridgman
Cd	12.1	5.13	1.85	4.81	4.42	Grueneisen-Goens
	10.9	4.60	1.56	3.98	3.75	Bridgman
Be	30.8	35.7	11.0	−5.8	8.7	

which corroborates the observed transmission properties of polycrystalline beryllium.

Finally, Fig. 4 shows how the body wave velocities vary with orientation. The compressional velocity curve is quite flat as compared to the two shear velocity curves. Although the shear waves have velocities which differ as much as approximately 20 percent for propagation along the a axis, the average velocities agree to within roughly 10 percent.

8. CONCLUSION AND ACKNOWLEDGMENT

The stiffness coefficients for beryllium have been evaluated in a manner which necessitated cross checking of all sorts. It has been shown that the results are in conformity with a number of experimental facts and basic principles. The need for accurate measurement of the coefficients for beryllium is certainly unquestionable, but the same may be said for the other hexagonal metals.

The author is indebted to a number of individuals for helpful discussions and services rendered. The single crystals of beryllium were the result of a crystal growing research project sponsored by Professors Cohen and Kaufmann of the Massachusetts Institute of Technology Metallurgy Department. The equipment used for the ultrasonic velocity measurements was furnished by the Massachusetts Institute of Technology Research Laboratory of Electronics, thanks to Dr. J. K. Galt. The advice of Mr. D. L. Arenberg in regard to the technique of ultrasonic measurements was invaluable.

Professor H. E. Mueller was kind enough to outline the simplification of the hexagonal relations for the body wave velocities. The essential details are given in the Appendix.

APPENDIX

The relation for the body wave velocities in crystals has been derived by Christoffel.[11] Solutions of the cubic equation

$$C^3-I_1C^2+I_2C-I_3=0 \qquad (8)$$

[11] K. B. Christoffel, Ann. di Matematica (2) 8, 193 (1877).

define the compressional and two shear velocities. I_1, I_2 and I_3 are the invariants

$$\begin{aligned} I_1&=k_{11}+k_{22}+k_{33}\\ I_2&=k_{11}k_{22}+k_{22}k_{33}+k_{11}k_{33}-(k_{12}^2+k_{23}^2+k_{13}^2)\\ I_3&=k_{11}k_{22}k_{33}+2k_{12}k_{13}k_{23}-(k_{12}^2k_{33}+k_{13}^2k_{22}+k_{23}^2k_{11}). \end{aligned} \tag{9}$$

For the Voigt classes 21–27, the c_{jk}'s are

$$\begin{aligned} c_{11}&=c_{22},\quad c_{23}=c_{13},\quad c_{44}=c_{55}\\ c_{66}&=\tfrac{1}{2}(c_{11}-c_{12}) \end{aligned} \tag{10}$$

with all other stiffness coefficients but c_{33} zero. The k's are then

$$\begin{aligned} k_{11}&=c_{11}(\alpha^2+\beta^2/2)-c_{12}(\beta^2/2)+c_{44}\gamma^2\\ k_{22}&=c_{11}(\alpha^2/2+\beta^2)-c_{12}(\alpha^2/2)+c_{44}\gamma^2\\ k_{33}&=c_{44}(\alpha^2+\beta^2)+c_{33}\gamma^2\\ k_{12}&=\tfrac{1}{2}(c_{11}+c_{12})\alpha\beta\\ k_{13}&=(c_{13}+c_{44})\alpha\gamma\\ k_{23}&=(c_{13}+c_{44})\beta\gamma, \end{aligned} \tag{11}$$

where α, β, and γ are the direction cosines for the angles between the direction of wave propagation and the orthogonal axes corresponding to the direction [001], [120], and [100] in the hexagonal system.

Solution of Eq. (1) at this point looks hopeless. If we transform (11) to Eulerian angles, it can be shown that the invariants will not contain the azimuthal angle, and that, therefore, the roots of (8) will only contain the angle between the hexagonal axis and the direction of wave propagation. Making the substitutions

$$\begin{aligned} \alpha&=\cos\varphi\sin\theta\\ \beta&=\sin\varphi\sin\theta\\ \gamma&=\cos\theta \end{aligned} \tag{12}$$

the k's can be written as

$$\begin{aligned} k_{11}&=[A+B\cos^2\varphi]\sin^2\theta+c_{44}\cos^2\theta\\ k_{22}&=[A+B\sin^2\varphi]\sin^2\theta+c_{44}\cos^2\theta\\ k_{33}&=c_{44}\sin^2\theta+c_{33}\cos^2\theta\\ k_{12}&=B\cos\varphi\sin\varphi\sin^2\theta\\ k_{13}&=(c_{13}+c_{44})\cos\varphi\cos\theta\sin\theta\\ k_{23}&=(c_{13}+c_{44})\sin\varphi\cos\theta\sin\theta, \end{aligned} \tag{13}$$

where

$$A=\tfrac{1}{2}(c_{11}-c_{12}),\quad B=\tfrac{1}{2}(c_{11}+c_{12}).$$

Using relations (13) in (9) one has

$$\begin{aligned} I_1&=2A\sin^2\theta+B\langle\cos^2\varphi+\sin^2\varphi\rangle+2c_{44}\cos^2\theta+c_{44}\sin^2\theta+c_{33}\cos^2\theta;\\ I_2&=\langle\sin^4\theta\rangle[A^2+AB+\langle B^2\sin^2\varphi\cos^2\varphi\rangle]+c_{44}\cos^4\theta\\ &\quad+(2A+B)c_{44}\cos^2\theta\sin^2\theta+(c_{44}\sin^2\theta+c_{33}\cos^2\theta)\\ &\quad\times[2c_{44}\cos^2\theta+(2A+B)\sin^2\theta]-\langle B^2\sin^4\theta\cos^2\varphi\sin^2\varphi\rangle\\ &\quad+(c_{13}+c_{44})^2\cos^2\theta\sin^2\theta; \end{aligned} \tag{14}$$

$$\begin{aligned} I_3&=\langle(c_{44}\sin^2\theta+c_{33}\cos^2\theta)[B^2\sin^4\theta\sin^2\varphi\cos^2\varphi+\cdots]\rangle+\cdots\\ &\quad+\langle 2(c_{13}+c_{44})^2B\cos^2\theta\sin^4\theta\cos^2\varphi\sin^2\rangle\\ &\quad-\langle(c_{44}\sin^2\theta+c_{33}\cos^2\theta)B^2\sin^4\theta\cos^2\varphi\sin^2\varphi\rangle\\ &\quad-\langle(c_{13}+c_{44})^2\cos^2\theta\sin^2\theta[2B\sin^2\theta\sin^2\varphi\cos^2\varphi+\cdots]\rangle, \end{aligned} \tag{15}$$

where the terms in $\langle\ \rangle$ cancel, eliminating the φ terms. Relations (5.2) and (5.3) follow directly as the solutions of Eq. (8).

A Note on the Quantization of Dissipative Systems

WESLEY E. BRITTIN
University of Colorado, Boulder, Colorado
(Received September 16, 1949)

The work of E. Kanai shows that the quantization of dissipative systems by use of a Hamiltonian formalism involving the time explicitly leads to results in disagreement with experience. We discuss the quantization of dissipative systems in a manner such that the time does not enter explicitly. It is shown that in the Heisenberg representation the only kind of dissipative forces consistent with the formalism are those which are functions of the coordinates alone. There exists no Schrödinger representation unless the forces are non-dissipative.

E. KANAI[1] has shown that it may be possible to put the equations of motion for a dissipative system into Hamiltonian form and then quantize them in the usual way. For example, the Hamiltonian of the damped oscillator may be taken to be

$$H=(1/2m)e^{-\alpha t}P^2+(1/2)m\omega^2e^{\alpha t}x^2, \tag{1}$$

where $P=me^{\alpha t}\dot{x}$, with the corresponding canonical commutation relation

$$[x, P]=i\hbar \tag{2}$$

or

$$[x, \dot{x}]=i\hbar e^{-\alpha t}/m. \tag{3}$$

The quantized system has no stationary states, and the expectation values of various dynamical variables behave in a manner agreeing with the correspondence principle. However, Eq. (3) which is equivalent to

$$\Delta x\Delta\dot{x}\geqslant\hbar e^{-\alpha t}/m \tag{4}$$

violates the uncertainty principle for an oscillator,

$$\Delta x\Delta\dot{x}\geqslant\hbar/m. \tag{5}$$

Equation (5) is valid for the oscillator even when damping is taken into account, but to get the correct result one must treat the coupled system—oscillator plus radiation field.[2] Kanai conjectures that it is probably impossible to express adequately the interaction between the electron and its own field by means of simple dissipative forces.

The reason for the violation of the usual principle of uncertainty would appear to stem from the explicit dependence of H and P on the time. The purpose of the present note is to show that the quantization of dissipative systems not involving the time explicitly can be carried out consistently in the Heisenberg representation only if the generalized forces are functions of position, and not at all in the Schrödinger representation. We thus support Kanai's conjecture, and it seems probable that although the classical description of a dissipative system is complete, a complete quantum mechanical description can only be had by considering the dissipative system as a sub-system of a non-dissipative system. The observables of the sub-system can then be inferred from the quantum mechanical behavior of the larger non-dissipative system.

Assume that the motion of the dissipative system can be described classically by the general Lagrange equations

$$\frac{d}{dt}\frac{\partial L}{\partial\dot{q}^i}-\frac{\partial L}{\partial q^i}=F_i, \quad i=1, \cdots, f, \tag{6}$$

where

$$L=L(q, \dot{q}) \quad \text{and} \quad F_i=F_i(q, \dot{q}).$$

Define the momentum P_i conjugate to q^i by

$$P_i=(\partial L)/(\partial\dot{q}^i), \quad i=1, \cdots, f, \tag{7}$$

where we assume

$$J=det\left\|\frac{\partial^2L}{\partial\dot{q}^i\partial\dot{q}^j}\right\|\neq 0. \tag{8}$$

Define the Hamiltonian $H(q, P)$ by

$$H(q, P)=P_i\dot{q}^i-L, \tag{9}$$

where repeated indices indicate summation from 1 to f. Then Eqs. (6) may be expressed in "Hamiltonian form,"[3]

$$\dot{q}^i=(\partial H)/(\partial P_i), \quad \dot{P}_i=-(\partial H)/(\partial q^i)+Q_i, \quad i=1, \cdots, f, \tag{10}$$

where $Q_i=Q_i(q, P)=F_i\{q, \dot{q}(q, P)\}$. The equation of motion of any dynamical variable $A(q, P)$ which does not depend explicitly upon time may be written

$$dA/dt=[A, H]+(\partial A/\partial P_i)Q_i, \tag{11}$$

where the Poisson bracket $[A, H]$ of A and H is defined by

$$[A, H]=\frac{\partial A}{\partial q^i}\frac{\partial H}{\partial P_i}-\frac{\partial A}{\partial P_i}\frac{\partial H}{\partial q^i}. \tag{12}$$

The passage to quantum theory is brought about in the Heisenberg representation by replacing the dynam-

[1] E. Kanai, Prog. Theor. Phys. **3**, 440 (1948).
[2] See for example H. Bauer and J. H. D. Jensen, Zeits. f. Physik **124**, 580 (1948).
[3] The reason for introducing the Hamiltonian is so that the theory will have the form of usual quantum theory if the F_i are zero

ical variables by time dependent operators. The Heisenberg operators must satisfy the classical equations of motion and the commutation relations. The commutation relations follow from the requirement that the operator corresponding to $[A, B]_{\text{class}}$ is

$$\frac{AB-BA}{i\hbar}\equiv\frac{[A,B]}{i\hbar}.$$

Thus denoting the Heisenberg operators by $A(t)$

$$[q^i(t), P_j(t)]=i\hbar\delta_j^i, \quad i,j=1,\cdots,f, \tag{13}$$

and

$$i\hbar\frac{dA(t)}{dt}=[A(t),H(t)]+i\hbar\frac{\partial A(t)}{\partial P_i(t)}Q_i(t). \tag{14}$$

The commutation relations (13) must be consistent with the equations of motion (14), thus

$$[dq^i(t)/dt, P_j(t)]+[q^i(t), dP_j(t)/dt]=0, \tag{15}$$

or

$$[[q^i(t),H(t)],P_j(t)]+[q^i(t),[P_j(t),H(t)]+i\hbar Q_j(t)]=0. \tag{16}$$

Therefore

$$[q^i(t),Q_j(t)]=0, \quad i,j=1,\cdots,f. \tag{17}$$

Since the generalized force $Q_j(t)$ commutes with each of a complete set of commuting operators, it must be a function of them,[4]

$$Q_j(t)=Q_j(q(t)). \tag{18}$$

The only dissipative systems which may be treated by the above formalism, therefore, are those for which the generalized forces are functions of the coordinates.

The Heisenberg representation is characterized by time-dependent operators $A(t)$ and a time-independent state vector ψ_0. The Schrödinger representation is characterized by time-independent operators A_0 and a time-dependent state vector $\psi(t)$. The two representations are related by a time-dependent unitary transformation $T(t)$,

$$\psi(t)=T\psi_0, \quad T^+=T^{-1}. \tag{19}$$

The expectation value of a dynamical variable A for a given state is given by

$$\langle A\rangle=(\psi_0, A(t)\psi_0)=(\psi(t), A_0\psi(t)), \tag{20}$$

where (ψ,φ) represents the scalar product of the two vectors ψ,φ. From

$$A(t)=T^+A_0T, \tag{21}$$

and the definition

$$\mathfrak{K}=i\hbar\ln T, \tag{22}$$

we obtain

$$i\hbar(dA(t)/dt)=T^+[A_0,(d\mathfrak{K}/dt)]T. \tag{23}$$

Therefore, using the Heisenberg equations of motion,

$$[A_0,H_0]+i\hbar(\partial A_0/\partial P_i^0)Q_i^0=[A_0,(d\mathfrak{K}/dt)]. \tag{24}$$

Put

$$G=d\mathfrak{K}/dt-H_0; \tag{25}$$

then

$$[A_0,G]=i\hbar(\partial A_0/\partial P_i^0)Q_i^0. \tag{26}$$

Let $A_0=q_0^i$, then according to (26),

$$[q_0^i,G]=0, \tag{27}$$

and

$$G=G(q_0). \tag{28}$$

Let $A_0=P_j^0$, then

$$[P_j^0,G]=-i\hbar[(\partial G/\partial q_0^j)]=i\hbar Q_j,$$

or

$$Q_j=-[(\partial G/\partial q_0^j)], \quad j=1,\cdots,f. \tag{29}$$

Therefore there exists no Schrödinger representation for dissipative systems according to the present formalism, since (29) shows that the only forces consistent with the formalism are those derivable from a scalar potential $G(q)$.

[4] P. Dirac, *Quantum Mechanics* (Oxford University Press, New York, 1947), third edition, p. 78.

Letters to the Editor

PUBLICATION of brief reports of important discoveries in physics may be secured by addressing them to this department. The closing date for this department is five weeks prior to the date of issue. No proof will be sent to the authors. The Board of Editors does not hold itself responsible for the opinions expressed by the correspondents. Communications should not exceed 600 words in length.

Mass Spectrographic Identification of Radioactive Lanthanum Isotopes*

R. A. NAUMANN,** F. L. REYNOLDS, AND I. PERLMAN
Radiation Laboratory and Department of Chemistry, University of California, Berkeley, California
December 12, 1949

TWO neutron deficient isotopes of lanthanum, one new and the other previously tentatively assigned, have been given mass assignments by the technique of dispersing the isotopes on a photographic plate with a mass spectrograph. These and other light isotopes of lanthanum were prepared and some of their radioactive characteristics determined by absorption methods and with a low resolution beta-ray spectrometer.

In some experiments, pure $CsNO_3$ was irradiated with 30-Mev alpha-particles and this was followed by the isolation of the lanthanum fraction. The mass spectrograph showed a single radioactivity at mass number 135; and by following the decay of this line on the photographic plate through a slit arrangement, a 19-hour half-life was obtained. This confirms the mass assignment previously made by other methods.[1] Since this irradiation should have produced La^{136} and La^{134} as well as La^{135}, it was inferred that La^{136} and La^{134} have half-lives less than about 20 minutes since it required several hours to make the exposure on the mass spectrograph. The isotope La^{136} had previously been reported as a 2-hour positron emitter,[1] but the observed activity has since been shown to be F^{18} which partially went through the particular chemical separation employed. A search was made for La^{136}, and it proved to be the 10-minute period reported by Maurer[2] from the irradiation of barium with deuterons. The assignment was made to La^{136} since the ratio of the 10-minute period to the 19-hour period increased with decreasing alpha-particle energy on cesium in the range below 30 Mev, as would be expected for the (α,n) reaction in relation to the $(\alpha,2n)$ reaction. Furthermore, the preparation of this activity in good yield by Maurer[2] using 5.8-Mev deuterons on barium would now point to La^{136} in view of the present knowledge of La^{138}, La^{137}, and La^{135}, unless one assumes the 10-minute activity to be a metastable state of one of these isotopes. Very recently Robertson, Carss, and Pool,[3] using separated stable barium isotopes as targets, have definitely proved this period to be associated with La^{136}. The characteristics of La^{136} which we determined are a half-life of 9.5 minutes, positron of 2.1 Mev determined with the spectrometer, and x-rays in high abundance from which it is estimated that about $\frac{1}{3}$ of the decay is by positron emission and $\frac{2}{3}$ by electron-capture.

The irradiation of cesium with 50-Mev alpha-particles resulted in a new lanthanum activity of 4.0-hour half-life. This activity has positrons of about 1.2 Mev, a conversion electron line of 0.26 Mev determined with the spectrometer, a harder gamma-ray of 0.8 Mev measured by lead absorbers, and K x-rays in high yield. This activity apparently decays predominantly by electron-capture since the positrons were only a few percent as abundant as the x-rays.

The 4-hour period was assigned to La^{133} by the mass spectrograph method. Figure 1 shows the original photographic plate

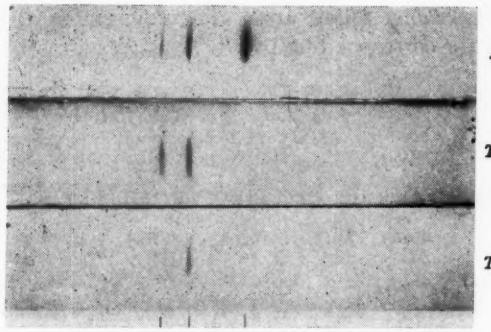

FIG. 1. Mass spectrographic analysis of radioactive lanthanum isotopes by transfer technique. (Exposures for transfer plates T_1 and T_2 given in the text.)

(A) and two transfer plates (T_1 and T_2) made by exposing successively blank photographic plates with the receiver plate. The upper picture, A, shows the receiver plate with the line for stable lanthanum at mass number 139 (actually measured as the singly ionized oxide), and two other lines at 135 and 133. The middle plate, T_1, is the first transfer plate exposed for 24 hours after analysis showing that the lines at 133 and 135 are caused by radioactivities. The bottom plate, T_2, made by a 72-hour exposure following the first one, shows only the 19-hour La^{135} since the 4-hour La^{133} had decayed.

Our thanks are due Mr. B. Rossi, Mr. J. Vale, and the members of the groups operating the 60-inch and 184-inch cyclotrons, and Mr. J. G. Conway for showing the $CsNO_3$ used to be spectrographically pure.

* The work described in this paper was performed under the auspices of the AEC.
** Now at Princeton University, Princeton, New Jersey.
[1] J. B. Chubbuck and I. Perlman, Phys. Rev. **74**, 982 (1948).
[2] W. Maurer, Zeits. f. Naturforschung **2a**, 586 (1947).
[3] Robertson, Carss, and Pool, Bull. Am. Phys. Soc. **24**, No. 7, 14 (1949).

Measurement of the Earth's Magnetic Field at High Altitudes at White Sands, New Mexico*

S. F. SINGER
Applied Physics Laboratory, Johns Hopkins University, Silver Spring, Maryland
AND
E. MAPLE AND W. A. BOWEN, JR.
Naval Ordnance Laboratory, White Oak, Maryland
December 19, 1949

AN Aerobee[1] rocket containing a total field magnetometer was fired at the White Sands Proving Ground, New Mexico (geomagnetic latitude 41° North) on April 13, 1948, at 1441 MST. The rocket reached a height of 372,000 feet (114 km) above sea level. Telemetered data gave the value of the earth's magnetic field during flight. The magnetometer measured the sum of the squares of three perpendicular components of the field so as to give an output independent of its orientation and thus obviate the need for stabilization of the instrument inside the rolling and precessing rocket. The magnetic effects of the rocket and instrumentation were quite small and were canceled by means of a system of compensating coils placed around the magnetometer. The residual error was mainly due to the inherent orientational error of the magnetometer itself and produced a roll-modulation of amplitude less than one milligauss. In analysis of the data, this error was averaged graphically over each roll period (about 1 second). A

system of magnetic calibrations applied periodically during the flight checked the magnetometer for possible drift or change in sensitivity. The over-all accuracy of the corrected data is estimated to be 1.0 mG or better.

The principal results of this first flight are:

(i) *The field strength decreases with altitude in accordance with calculations based on potential theory.* The experimental data (Fig. 1) show a decrease in the magnetic field with altitude which

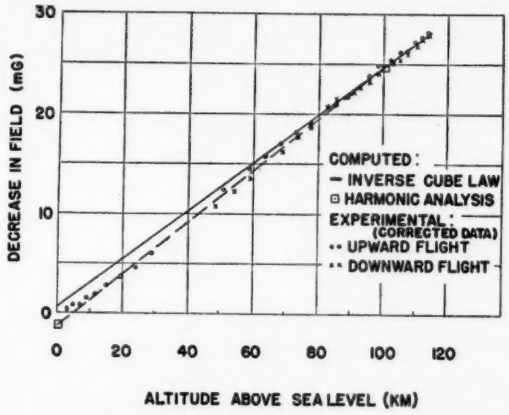

FIG. 1. Decrease of earth's magnetic field (from actual field near the surface) *vs.* altitude above sea level. Aerobee A-6 Flight, White Sands, New Mexico, April 13, 1948. Calculated curves adjusted to fit experimental points at 100 km.

agrees within 2 milligauss with the inverse cube fall-off based on the simple approximation that the earth's field can be described by that of a dipole. The accuracy of the determination of the missile altitude is ±1 km. The experimental decrease from sea level to 114 km is 28 mG, the calculated decrease 26.9 mG. It can be seen from Fig. 1 that the experimental data are in somewhat better agreement with a calculation of the altitude variation near White Sands based on harmonics up to the sixth degree[2] as used in achieving an empirical description of the magnetic field at the earth's surface.

(ii) *No evidence could be obtained, either for or against the existence of circulating current sheets in the upper layers of the atmosphere in view of the smallness of the expected effect at the latitude of the experiment.* This experiment was the first step in an attempt to obtain direct evidence concerning the existence and nature of circulating current sheets in the upper atmosphere. These current systems have been proposed in order to explain the regular diurnal variation of the magnetic field at sea level and are by some theories assumed to be located primarily in the *E* layer of the ionosphere.[3] This first flight at geomagnetic latitude 41°N was intended chiefly as a test of the method and instrumentation. The discontinuity expected in passing through the postulated current-layer is only 10 to 20 gamma (0.1 to 0.2 mG)[4] compared to a decrease in the main field of 28 mG over the total flight. This effect is too small to be detectable by the present equipment. However, a flight is forthcoming at a more favorable location. At the geomagnetic equator the expected discontinuity is 2 to 3 mG compared to a decrease in the main field of only 13 mG.

A fuller account of this work is being submitted to the *Journal of Geophysical Research.*

We wish to thank the Navy Bureau of Ordnance and the ONR for their support of this project and the U. S. Naval Unit at the White Sands Proving Ground for its capable performance of the field operations involved in firing the Aerobee. We would like to express our appreciation to Drs. J. A. Van Allen and L. R. Maxwell for their active encouragement, to our associates at the Naval Ordnance Laboratory, in particular Dr. E. A. Schuchard for advice on magnetometer problems and Mr. C. J. Aronson, and at the Applied Physics Laboratory to Dr. F. L. Verwiebe and to Messrs. J. F. R. Floyd, L. W. Fraser, J. E. Sugrue, and B. J. Chaffee.

We are particularly indebted to Dr. E. H. Vestine of the Department of Terrestrial Magnetism, Carnegie Institution of Washington for helpful advice on problems of the geomagnetic field.

* Supported by the Navy Bureau of Ordnance and the ONR under Contracts NOrd 7386 and NRO81-017.

[1] For a general description of the Aerobee Sounding Rocket as a vehicle for research in the upper atmosphere, see: J. A. Van Allen, L. W. Fraser, and J. F. R. Floyd, Science **108**, 746 (1948).

[2] E. H. Vestine, I. Lange, L. Laporte, and W. E. Scott, "The geomagnetic field, its description and analysis," Department of Terrestrial Magnetism, Carnegie Institution of Washington, Publication 580 (1947).

[3] *Terrestrial Magnetism and Electricity*, edited by J. A. Fleming (McGraw-Hill Book Company, Inc., New York, 1939).

[4] E. H. Vestine, APL/JHU CM-480 (1948).

The Beta-Rays of K^{40} *

P. R. BELL,** BOYD WEAVER,*** AND J. M. CASSIDY
Oak Ridge, Tennessee
December 8, 1949

THE beta-spectrum of K^{40} has been measured from an enriched sample by use of the scintillation spectrometer. Enriched material was prepared by electromagnetic separation at Y-12. The sample used consisted of 12.2 mg of KCl mounted on 0.5 mg/cm² polyethylene. The surface density of the sample was estimated to be 2.5 mg/cm². The K^{40} content of the potassium in this sample was 1.31±0.05 percent as measured at Y-12 by mass spectrometer.

An anthracene crystal used as the scintillation phosphor was cemented to an RCA C-7132 photo-multiplier. The crystal was covered with an aluminum foil light reflector 0.1–0.2 mg/cm² thickness. The factor relating pulse height to energy was obtained by calibration with the conversion line of Cs^{137}.

The pulse distribution obtained with and without an absorber between the crystal and the sample is shown in Fig. 1. The difference between the background curve and that with sample and absorber is too small to measure accurately.

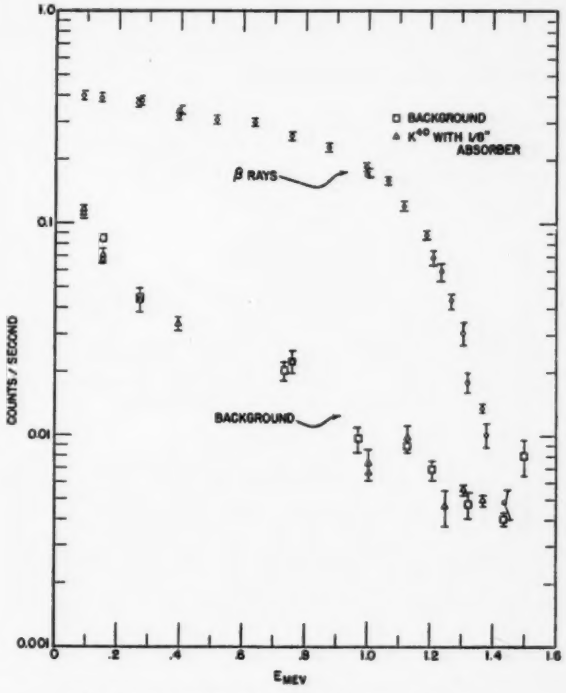

FIG. 1. Pulse distribution with and without absorber. (K^{40} 12.2 mg 1.31 percent.)

The data were corrected for the resolution of the instrument by the method of Owen and Primakoff[1] and a Fermi-Kurie plot made. Figure 2 shows the result as the upper curve. The line is quite

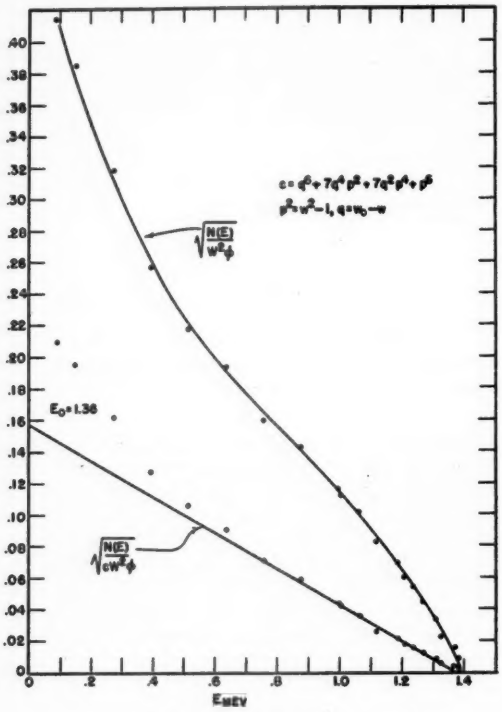

FIG. 2. K^{40} Kurie plot.

concave to the energy axis above 700 kev and the end point is 1.36±0.05 Mev.

The correction term for the third forbidden axial vector or tensor interaction produces the lower curve in Fig. 2 when applied to the data. This curve is about as good a fit to a straight line in the higher energy half of the spectrum as was obtained from P^{32} measured under the same conditions.

* This document is based on work performed under Contract No. W-7405, eng. 26 for the Atomic Energy Project at Oak Ridge.
** Oak Ridge National Laboratory, Oak Ridge, Tennessee.
*** Y-12 Research Laboratory, Oak Ridge, Tennessee.
[1] G. E. Owen and H. Primakoff, Phys. Rev. **74**, 1406 (1948).

Phase Relations in He^3–He^4 Solutions

B. WEINSTOCK, D. W. OSBORNE, AND B. M. ABRAHAM
Argonne National Laboratory, Chicago, Illinois
December 12, 1949

IN a previous letter the depression of the lambda-temperature of He^4 by the addition of He^3 was reported,[1] but the question of whether the lambda-transition remains second order, as proposed by Stout,[2] or becomes first order with the consequent existence of two liquid phases below the lambda-temperature, as proposed by de Boer,[3] remained unanswered. It is possible to decide between these two possibilities by means of vapor pressure measurements. To this end, the vapor pressures of 20.3 mole percent and 25.5 mole percent solutions of He^3 in He^4 have been measured.

Before examining the experimental results, consider the phase diagram for He^3-He^4 solutions according to the calculations of de Boer,[3] as shown in Fig. 1. In the regions labeled I and II a single liquid phase exists in equilibrium with the vapor; in the

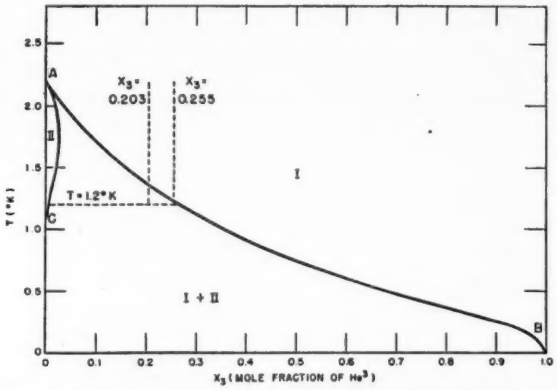

FIG. 1. Phase diagram of He^3-He^4 solutions according to J. de Boer.

region labeled I+II two liquid phases are present in equilibrium with each other and with the vapor. If this diagram is correct, it can be seen that when a 20.3 percent He^3 solution is cooled to 1.2°K, a temperature below the lambda-temperature given by curve *AB*, two liquid phases are in equilibrium, and the compositions of the liquids are given by the intersection of the dashed horizontal line with the curves *AB* and *AC*. When a 25.5 percent He^3 solution is cooled to 1.2°K the same two liquid phases appear;

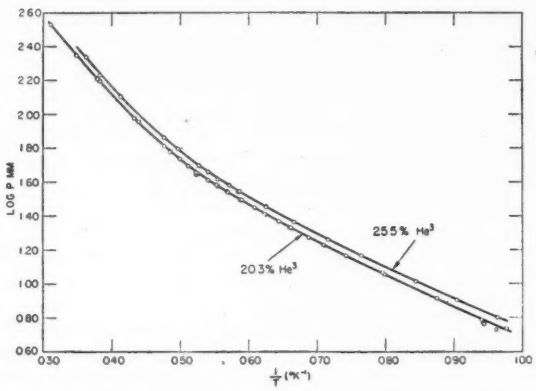

FIG. 2. Vapor pressures of 20.3 percent and 25.5 percent solutions of He^3 in He^4.

their concentrations are the same as for the 20.3 percent solution, but their relative amounts are different. It follows that the vapor pressures of the 20.3 percent and of the 25.5 percent He^3 solutions must be equal at 1.2°K and indeed at any other temperature in the region I+II. The same conclusion can be reached directly by application of the phase rule, for if two liquid phases and a vapor phase are present in equilibrium in a two component system there is only one degree of freedom, and hence the vapor pressure must be a function of the temperature alone and independent of concentration.

The vapor pressure data are plotted in Fig. 2. It can be seen that the vapor pressures of the two solutions are not equal at any temperature down to the lowest temperature studied, 1.04°K, which is well below the lambda-temperatures previously measured, namely 1.65° and 1.56°K,[1] and also below the lambda-temperatures given by the curve *AB* in Fig. 1. These data eliminate the possibility that two liquid phases coexist in equilibrium with the vapor below the lambda-temperature, at least down to 1.04°K and in the concentration range 0 percent to 20 percent He^3.*

Since there is only one liquid phase present above and below the lambda-temperature, the concentration of He^3 in liquid I, which is stable above the lambda-temperature, must be equal to that in liquid II, which is stable below the lambda-temperature. Further, it can be deduced thermodynamically that the transition must remain second order. It can easily be shown that for any arbitrary variation dx in the He^3 concentration the condition for equilibrium between the two liquid phases is

$$\Delta S dT - \Delta V dP = 0, \tag{1}$$

where ΔS and ΔV are the differences in molal entropy and volume, respectively.[4] Hence,

$$\Delta V (dP/dx)_T = 0. \tag{2}$$

Since the experimental data show that $(dP/dx)_T$ is not zero,

$$\Delta V = 0, \tag{3}$$

and similarly from (1)

$$\Delta S = 0. \tag{4}$$

Equations (3) and (4) are the conditions for a second-order transition.

The vapor pressure measurements show these solutions deviate from ideality above their lambda-temperatures, in the sense that the vapor pressures are higher than given by Raoult's law. Below their lambda-temperatures the non-ideal behavior becomes more marked, increasing rapidly as the temperature is lowered. The latter observation is in qualitative agreement with the model suggested by Taconis, Beenakker, Nier, and Aldrich,[6] although the quantitative behavior appears to be different. These measurements will be extended and reported in greater detail in a subsequent paper.

The authors are indebted to Professors J. W. Stout and Lester Guttman for many stimulating discussions on this problem.

* It should be remarked that a narrow temperature region with two liquid phases, on the order of a few hundredths of a degree wide, is not ruled out by the data, but this possibility is considered to be unlikely. In any case, such a situation would be practically indistinguishable from a second-order transition.

[1] Abraham, Weinstock, and Osborne, Phys. Rev. **76**, 864 (1949).
[2] J. W. Stout, Phys. Rev. **76**, 864 (1949).
[3] J. de Boer, Phys. Rev. **76**, 852 (1949).
[4] See for example J. W. Stout, Phys. Rev. **74**, 605 (1948), Eq. (8), or E. A. Guggenheim, *Thermodynamics* (North-Holland Publishing Company, Amsterdam, 1949), pp. 188–9.
[6] Taconis, Beenakker, Nier, and Aldrich, Phys. Rev. **75**, 1966 (1949).

Effects of Electrical Forming on the Rectifying Barriers of *n*- and *p*-Germanium Transistors

J. BARDEEN AND W. G. PFANN
Bell Telephone Laboratories, Murray Hill, New Jersey
December 12, 1949

THE amplifying properties of transistors made with *n*- or *p*-germanium can be improved by an electrical forming or power treatment of one of the point electrodes. W. H. Brattain[1] discovered that transistor action in *n*-type germanium having a resistivity of the order of one to ten ohm-centimeters can generally be improved by passing large reverse currents through the collector. Later, it was discovered that transistor action in *p*-type germanium could be greatly enhanced by passing a large forward current through the emitter.[2] Since this initial work, other members of the Bell Telephone Laboratories' staff have contributed to our knowledge of the effects of various forming treatments. The purpose of the present note is to present some qualitative data on forming and to give a tentative interpretation of the results in terms of modifications of the rectifying barrier layer at the contact.

The forming treatments which we shall describe involve applications of direct current in either the forward or reverse direction for times of the order of seconds or less. The extent of the changes caused by forming depends in part on the surface treatment of the germanium and in part on the material used for the point contact. We have used phosphor bronze points on surfaces which were ground and etched.

Transistor action depends on the presence of an inversion layer or change of conductivity type in the barrier layer of the emitter contact. In the case of *n*-germanium, there is evidence that such a barrier layer exists at the free surface, independent of the contact, and hence effective emitter action is obtained without electrical forming. Such a barrier layer is shown schematically in the energy level diagram of Fig. 1a. The position of the Fermi level at the surface, closer to the filled band than to the conduction band, is determined by the energy levels of electrons in surface states.

Since the same surface treatment has been used for both *n*- and *p*-germanium, the surface states and position of the Fermi level at the free surface of *p*-germanium are expected to be similar to those for *n*-germanium, as shown in Fig. 1b. Unless a barrier layer is formed by the metal contact, little or no rectification to *p*-germanium is to be expected. It is, indeed, found that a metal point contact to *p*-germanium makes a poor rectifier unless there is some electrical forming or power treatment.

Forming may affect the surface layers, and thus the height of the barrier layer, ϕ_s, as well as the distribution of donor and acceptor ions in depth in the vicinity of the contact. While it is believed that both effects occur, we shall be concerned with forming methods in which the principal results can be interpreted in terms of changes in ϕ_s. Changes in ion concentrations may predominate with heavy forming such as may be produced by large current pulses. That the germanium and its surface layers are affected is indicated by the fact that a formed point may be replaced by another point, with little change of characteristics.[3]

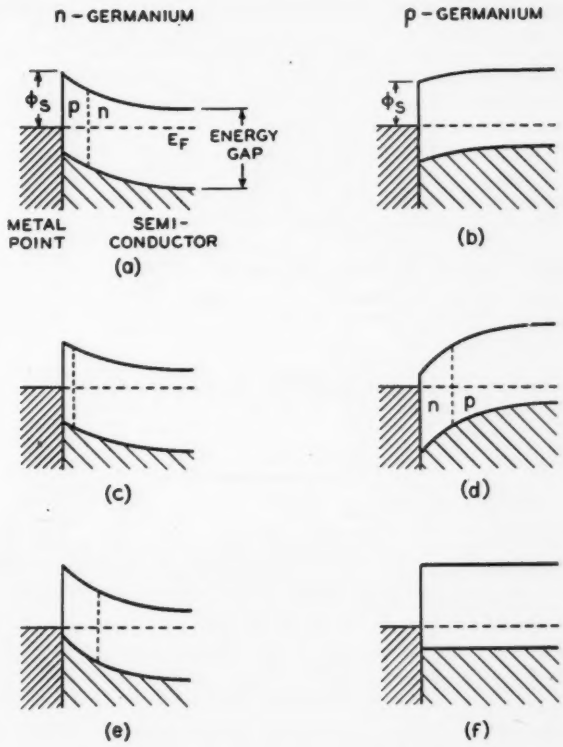

FIG. 1. Energy level diagrams showing effects of electrical forming on the rectifying barriers at contacts with *n*- and *p*-germanium: (a, b)—unformed; (c, d)—formed by negative current; (e, f)—formed by positive current.

The observed changes in characteristics produced by forming are given in Table I for both n- and p-germanium. The conventional direction of current is positive for flow of positive charge from point to germanium. This is the forward rectifying direction for n-type semiconductors and the reverse for p-type. These qualitative changes can be interpreted in terms of changes in ϕ_s if we assume that a *positive* forming current *increases* ϕ_s and that a *negative* forming current *decreases* ϕ_s. These changes are in the directions which would result from the movement of donor or acceptor ions from the interior of the germanium to the surface under the influence of the field of the forming current.

TABLE I. Changes in characteristics of rectifying junctions produced by forming.

	n-Germanium		p-Germanium	
Forming current	Forward current	Reverse current	Forward current	Reverse current
Unformed	Large; mostly holes; good emitter of holes	Small; good rectifier	Small; mostly holes; poor emitter of electrons	Large; poor rectifier
Negative	Hole current smaller	Greater; collector formed	Electron current increased, emitter formed	Little change
Positive	Little change	Smaller	Little change	Greater

As illustrated in Figs. 1a and 1b, which respresent unformed points, there is a good rectifying junction with n-germanium and a poor one with p-germanium. Because of the inversion layer, the forward current in the former case consists largely of holes, although conduction electrons are normally in excess in the interior. A decrease in ϕ_s, caused by a negative forming current, as shown in Fig. 1c, enhances the electron current in the reverse direction in n-germanium and improves the point as a collector. This is accompanied by a decrease in hole current in the forward direction. For p-germanium, as shown in Fig. 1d, a negative forming current may produce an inversion layer of n-type conductivity, and thus increase the emission of electrons. The reverse characteristic, while altered in shape, is not changed greatly in magnitude. A positive forming current decreases ϕ_s, as shown in Figs. 1e and 1f, making the reverse current in n-germanium smaller and impairing the rectification in p-germanium.

Actually, there are probably large variations in ϕ_s over the contact area, and the changes of ϕ_s indicated in Fig. 1 should be interpreted merely as giving the trends in a qualitative way. For example, it is necessary to have only a few "low spots" in the barrier to give a relatively large reverse current through a point contact to n-germanium, and a few spots with an inversion layer may be sufficient to make a reasonably good emitter function in p-germanium.

[1] J. H. Bardeen and W. H. Brattain, Phys. Rev. **75**, 1208 (1949).
[2] W. G. Pfann and J. H. Scaff, Phys. Rev. **76**, 459 (1949).
[3] Experimental results of W. H. Brattain and G. R. Price.

Composite of Experimental Measurements of the Energy-Distribution among Beta-Particles from Tritium

E. P. COOPER* AND F. T. ROGERS, JR.
U. S. Naval Ordnance Test Station, Inyokern, California
December 5, 1949

THE beta-decay of tritium (radiohydrogen, $_1H^3$), though of very long life, is evidently "allowed," and is characterized by an extraordinarily low energy. Since there has occasionally been some doubt as to the validity of the Fermi theory of allowed transitions in the low energy region, as for instance for Cu^{64}, it is of considerable interest to see how well the theory agrees with the observed beta-spectrum of tritium. For Cu^{64} it was necessary[1] to consider relativistic and screening effects on the electron wave function in order to obtain essential agreement with the Fermi theory in the low energy part of the spectrum, and energies of the order of 0.1 Mev were "low." For H^3, the whole spectrum lies at such extremely low energies (<20 kev) that relativistic effects must be negligible. Further, since the effect of screening is not important if $(2\pi/137)(Z/\beta)$, the ratio of the wave-length of the outgoing electron to the radius of the K-shell, is small in comparison with unity, screening should not appreciably affect the H^3 decay. (For a 10-kev electron from H^3 $2\pi Z/137\beta \sim 0.23$, whereas for a 0.1-Mev electron from Cu^{64} $2\pi Z/137\beta \sim 2.4$.) Obviously the beta-decay of tritium represents a simple and relatively critical test of the theory in the low energy limit.

Several direct determinations have recently been made of the energy-distribution function for the H^3 beta-particles. Curran, Angus, and Cockcroft[2,3] have published four sets of data, and Byatt, Rogers, and Waltner[4] one. Hanna and Pontecorvo have published data for the upper-energy region,[5] and so have Graves and Mayer.[6] All these investigators report essential agreement with the Fermi theory in the particular energy regions used. To show the basic consistency of these measurements and, taken together, their ultimate degree of accord with the Fermi theory, we have constructed a composite of the various published spectra. From Fermi plots (using the non-relativistic Coulomb field factor) of each set of data, scale-factors were obtained which would adjust and normalize that set to a common pair of variables; after the adjustment of each set, averages were taken at convenient intervals, a very few points being discarded on the basis of applicable statistical criteria. The composite so obtained is shown by the points in Figs. 1 and 2, together with the spectrum as predicted by the Fermi theory. Even though the published data are not in all cases corrected for "resolution," this method of striking

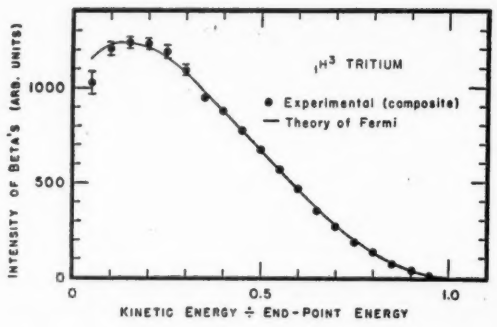

FIG. 1. The continuous beta-spectrum from tritium. The points are averages of the several sets of extant data. The average deviations are equal to or less than the radii of the points as plotted, except where otherwise indicated.

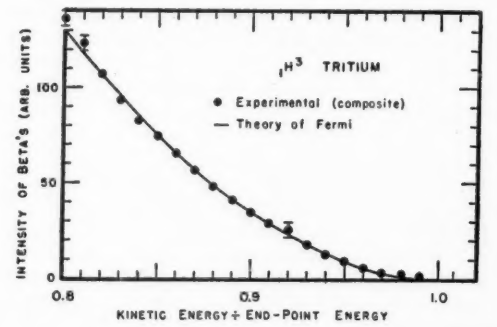

FIG. 2. High energy portion of the continuous beta-spectrum from tritium.

an average would seem to be largely valid for distributions if not for end-point energies.

In view of the great difficulty of measuring the beta-spectrum of H^3, the concordance of adjusted data is remarkable. In terms of average deviations from the mean, it appears that the shape of the distribution function is now known to a precision of about 3 percent from 0.5 to 5.5 kev, about 1 percent from 6 to 11 kev, about 5 percent from 11.5 to 17.5 kev, and about 25 percent on up to within 2 percent of the end-point energy. Equally remarkable is the fact that the deviations of the composite from the theoretical spectrum are generally comparable with (in most cases less than) the corresponding average deviations of the measurements, except at the very lowest and highest energies where the measurements are very uncertain. A Fermi plot of the points in Figs. 1 and 2 is extremely satisfying from 2.5 to 18 kev; although the point at 0.9 kev is somewhat low, the points at 1.8 kev and above 18 kev are high (this last one about 100 percent).

* Foothill Laboratory, Pasadena, California.
[1] C. S. Cook and L. M. Langer, Phys. Rev. **73**, 601 (1948).
[2] Curran, Angus, and Cockcroft, Phil. Mag. **40**, 53 (1949).
[3] Curran, Angus, and Cockcroft, Phys. Rev. **76**, 853 (1949).
[4] Byatt, Rogers, and Waltner, Phys. Rev. **75**, 909 (1949).
[5] G. C. Hanna and B. Pontecorvo, Phys. Rev. **75**, 983 (1949).
[6] E. R. Graves and D. I. Mayer, Phys. Rev. **76**, 183 (1949), and private communication.

Natural Ferromagnetic Resonance

A. J. E. Welch and P. F. Nicks
Imperial College of Science and Technology, London, England
and
Alan Fairweather and F. F. Roberts
Post Office Research Station, Dollis Hill, London, England
October 28, 1948

WHILE studying the magnetic properties of a number of magnesium ferrites, and related spinels, evidence was obtained in a few cases of a resonance with sufficiently small damping to produce a peak in the curve of permeability *versus* frequency for unmagnetized samples. Figure 1 shows the results

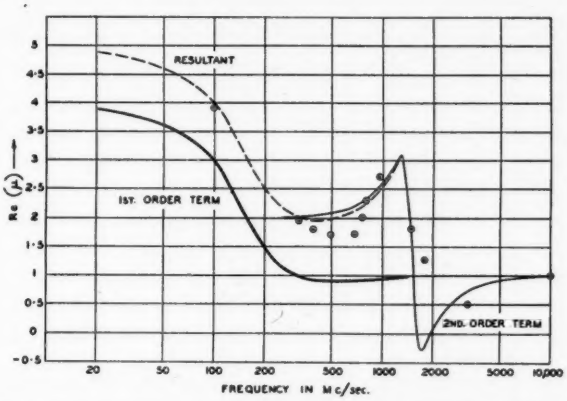

FIG. 1. Natural ferromagnetic resonance. ⊙ ⊙ ⊙ are points measured on Mg ferrite sample.

found for a particular magnesium ferrite. In the region where the resonance occurred, the measurements were carried out in terms of standing-wave observations in a coaxial line containing the sample adjacent to the short-circuited end. Care was taken that higher modes, which might propagate within the sample, were not excited. The results may be interpreted in terms of an extension of the Landau-Lifshitz theory[1] as amended by Kittel.[2] It may be deduced from Kittel's formula,

$$\frac{\chi}{\chi_0}=\frac{\omega_0^2+\lambda^2\mu_0+j\omega\lambda}{\omega_0^2+\lambda^2\mu_0-\omega^2+j\omega\lambda(1+\mu_0)}$$

that the real part of χ, $Re(\chi)$, can only be become negative if $\lambda<\omega_0$ but that it can exceed its static value χ_0 only if $\lambda<\omega_0/\mu_0$. Now, in fact, it has been found that all ferrites which are appreciably ferromagnetic show negative values of $Re(\chi)$ over some part of the range 1000 Mc/sec. to 10,000 Mc/sec., but hitherto none has been found with the positive peak in $Re(\chi)$. Where the positive peak has occurred in our results it has been superimposed upon a basic curve of falling χ, as seen from Fig. 1. The complete susceptibility can thus be regarded to a second approximation as the sum of two parts, each part represented by an equation of the above form. In the example given, the basic part contributes about three-fourths of the total low frequency susceptibility, has a resonance frequency, $\omega_0/2\pi$, of about 140 Mc/sec., and a damping ratio λ/ω_0 of about 0.5; the remaining one-fourth of the *LF* susceptibility has a resonance frequency of about 1500 Mc/sec. and a damping ratio of about 0.1. The observed shape of this resonance, however, appears to be much less sharp than that required by the formula; the addition of a third component enables a better fit to be obtained.

If Frenkel's form[3] of the absorption is used in place of Kittel's, the general frequency behavior is similar, but $Re(\chi)$ is then negative for $\omega>\omega_0$ for all values of the relaxation time τ, while $Re(\chi)/\chi_0$ exceeds unity at some frequency only if $\tau>\pi/\omega_0$. A slightly better fit to the observed points is obtainable with two components of Frenkel's form than of Kittel's, and the relaxation time for both components is near 10^{-9} sec.

At low frequencies the formula gives a loss component which varies with frequency in the same way as an eddy current loss, and it has been found that the measured apparent eddy current loss of several ferrites is of the order of magnitude predicted by the formula from high frequency measurements.

It has also been observed that the application of a sufficiently strong transverse static magnetic field restores the 10,000 Mc/sec. susceptibility to about one-fourth the *LF* value. This suggests that the first term (which is dominant at low frequencies) is insensitive to external fields, whereas the second term behaves as implied in Kittel's analysis, i.e., ω_0 increases with increase of the static field.

The interpretation of the two resonance frequencies in terms of internal fields would seem to imply rather smaller fields than have hitherto been suggested but the precise magnitudes involved would seem to depend considerably on the geometry assumed for them.

Acknowledgment is made to the Chief Scientist of the Ministry of Supply and to the Engineer-in-Chief of the General Post Office for permission to make use of the information contained in this letter.

[1] Landau and Lifshitz, Physik Zeits. Sowjetunion **8**, 153 (1935).
[2] C. Kittel, Phys. Rev. **73**, 155 (1948) and other papers.
[3] J. Frenkel, J. Phys. U.S.S.R. **9**, No. 4, 299 (1945).

Beta-Spectrum and Decay Scheme of $_{65}Tb^{160}$

S. B. Burson, K. W. Blair, and D. Saxon
Argonne National Laboratory, Chicago, Illinois
December 22, 1949

THE β-spectrum of Tb^{160} has been investigated in the Argonne 180° spectrometer. The purified sample of Tb_4O_7 from Oak Ridge was bombarded in the Argonne heavy water pile for about 90 days and allowed to cool for about one month. The activity of a portion of the sample was then followed for ~3 months indicating a half-life of 71±1 day.

The source of ~0.1 mg/cm² was prepared on a Nylon backing

TABLE I. Internal conversion electrons in Tb^{160}.

E	Line assignment	γ-energy
31.0±0.35 kev	$K(\gamma_1)$	84.9 kev
76.0±0.7	$L(\gamma_1)$	85.1
83.8±0.7	$M(\gamma_1)$	85.3
144.5±1.5	$K(\gamma_2)$	198.4
192.3±1.6	$L(\gamma_2)$	201.4
246.1±1.8	$K(\gamma_3)$	300.0
832 ±4.5	$K(\gamma_4)$	886
877 ±4.5	$L(\gamma_4)$	886
920 ±4.7	$K(\gamma_5)$	964
962 ±5.0	$L(\gamma_5)$	971

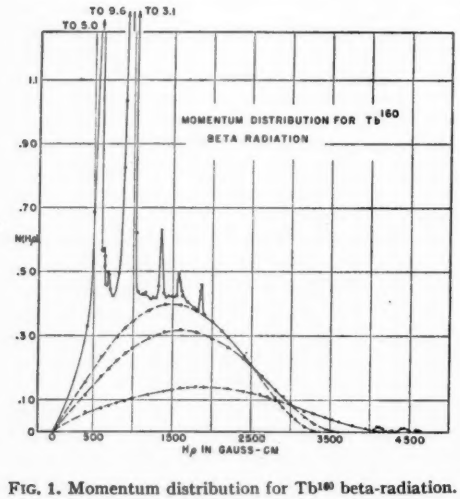

FIG. 1. Momentum distribution for Tb^{160} beta-radiation.

of ~0.1 mg/cm². The counter window was of several layers of Nylon totaling 0.08 mg/cm². A spectrometer resolution of 2 percent in $H\rho$ was used.

The momentum plot of the spectrum is shown in Fig. 1. The lines in this plot may be assigned to conversion electrons from several gamma-rays of Dy as given in Table I.

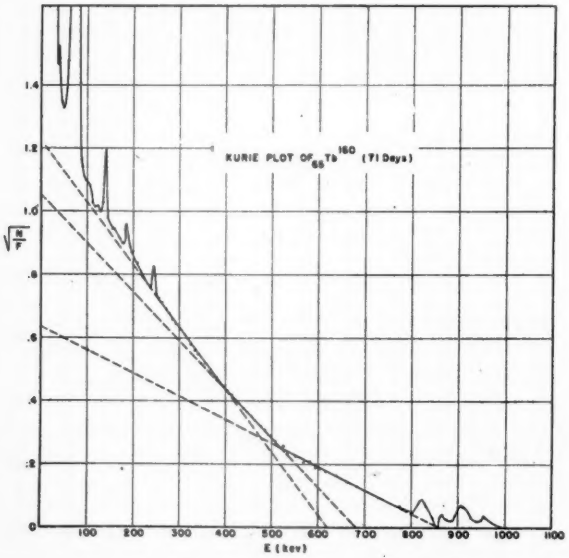

FIG. 2. Kurie plot of $_{65}Tb^{160}$ (71 days).

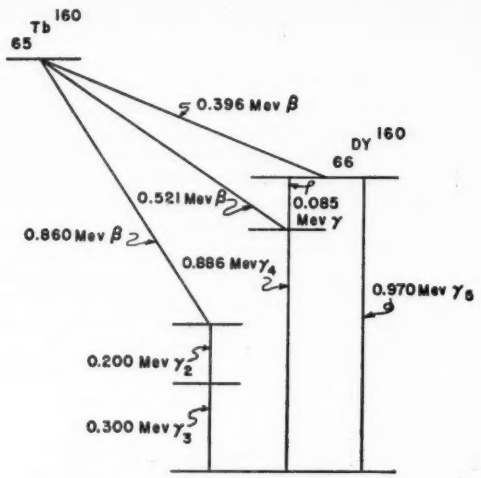

FIG. 3. Proposed decay scheme for $_{65}Tb^{160}$.

The gamma-ray energies of 85, 200, and 300 kev agree well with those previously reported by Cork, Shreffler, and Fowler.[1] The gamma-ray of 212 kev reported by these authors was not observed.

The peaks on the momentum plot at approximately 640 and 690 gauss-cm corresponding to energies of 34.8±0.8 and 39.8±1.0 have been assigned to Auger electrons.

The Kurie plot of the Fermi theory is shown in Fig. 2. The plot appears to consist of three linear portions down to an energy of ~230 kev below which there is an upward trend. Extrapolations of the linear portions of the plot give β-end points of 860±10, 521±10, and 396±10 kev.

A search for positive radiation yielded no evidence for a positron decay. In view of this and the above energy values of the β's and γ's the decay scheme of Fig. 3 is proposed.

Values from the extrapolated linear portions of the Kurie plot were replotted on the momentum diagram (the dashed lines) with corrections being made at the extreme low energy end for the window absorption. Comparison of the areas under the curves corresponding to the three betas indicated the relative intensities of the three to be $\beta_{860}:\beta_{521}:\beta_{396}::1.00:0.96:0.39$.

[1] J. M. Cork, R. G. Shreffler and C. M. Fowler, Phys. Rev. **74**, 240 (1948).

The Beta-Spectrum of He^6 *

V. PEREZ-MENDEZ AND H. BROWN
Pupin Physics Laboratories, Columbia University, New York, New York
December 19, 1949

THE beta-ray spectrum of He^6 has been investigated in a beta-spectrometer for gaseous emitters.[1]

This spectrum was first investigated by Bjerge,[2,3] using a cloud chamber. Subsequent absorption measurements by Sommers and Sherr[4] gave an energy end point of (3.5±0.6) Mev. Rustad[5] found an end point of (3.2±0.2) Mev, and a half-life of (0.84±0.02) sec. Holmes[6] gives a half-life of (0.823±0.013) sec. The spectrum is of considerable theoretical interest because of the low ft value and the high maximum energy.

The He^6 is produced by a (n,α) reaction by bombarding finely divided beryllium powder with fast neutrons from the cyclotron. In order to obtain high specific activity of He^6, it was necessary in this experiment to employ a modification of the internal probe technique used previously with gaseous targets. By placing the

beryllium inside the cyclotron chamber, the volume of powder usable is limited, but the solid angle subtended by it at the neutron source is considerably increased (to about 8 percent of 4π).

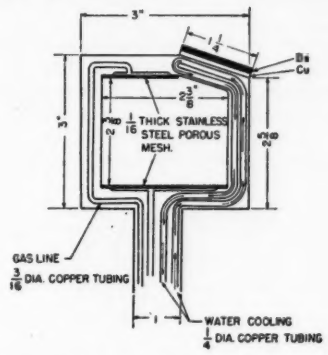

FIG. 1. Schematic diagram of probe for production of He^6.

To this end, a hollow chamber (Fig. 1) was designed, of approximate dimensions 3 in.×3 in.×1½ in. It was constructed from a copper block and soldered onto a 1-in. brass pipe so as to fit through the lock into the cyclotron chamber. The beryllium metal powder was of extremely fine grain size (of the order of 1 micron); it is held in place by two porous stainless steel screens, which are soldered to frames inside the chamber.

To produce neutrons from the deuteron beam of the cyclotron, a press-fitted Be-Cu plate was soldered onto the probe at an angle, with the Be face out. Helium gas was used as a carrier, and was circulated continuously through the probe.

Because of the short lifetime of He^6, the counting circuits were operated automatically by a series of relays in connection with a motor driven cam-shaft. This apparatus turned the cyclotron on for about 2.5 sec.; ¼ sec. after the cyclotron was turned off, the monitor and spectrometer counters were turned on for a period of 2 sec.; after another ¼-sec. time interval the entire cycle was repeated.

The active gas was pumped into a source chamber which was separated from the spectrometer chamber of a semicircular focusing magnetic spectrometer by a Saran window. The monitor determined the amount of activity in the chamber; by subtracting backgrounds and taking the ratio of the spectrometer counter reading to monitor counter reading the He^6 spectrum was obtained. The window thickness was about 1.8 mg/cm² and the thickness of the gaseous source about 0.1 mg/cm².

Because of the comparatively low intensity obtained, wide slits were used and the resolution of the spectrometer was about 6 percent. One of the spectra so obtained, plotted in a Fermi plot, and without correcting for resolution or window absorption, is shown in Fig. 2. The tailing off at the high energy end is due to the poor resolution. The end point, obtained from an average of such plots following subtraction of the energy loss (~5 kev) in the source window near the end point, is $E_0=7.30$ mc², corresponding to a maximum energy of (3.215±0.015) Mev. Furthermore, the spectrum seems to be allowed at least down to 200 kev, which corresponds to a range of 95 percent of the spectrum. Using Holmes' value of the half-life, one obtains a value of ft for He^6 of 570±3 percent, which is the smallest value known. Both the low ft value and the allowed shape of the spectrum tend to confirm the Gamow-Teller selection rules, assuming that He^6 has a spin of zero.

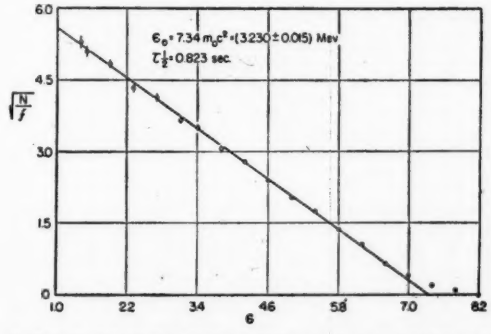

FIG. 2. Fermi plot of the He^6 beta-spectrum, uncorrected for resolution and window absorption. E is the total energy in units of mc². f is the Fermi function $\eta^2F(Z, E)$, N the number of electrons per unit momentum range. $(N/f)^{\frac{1}{2}}$ is plotted in arbitrary units. The value given for $\tau_{\frac{1}{2}}$ is that of Holmes.

We wish to thank the U. S. AEC, which aided materially in the performance of this research.

* Assisted by the AEC.

[1] H. Brown and V. Perez-Mendez, Phys. Rev. 75, 1276 (1949). A forthcoming paper will describe this instrument in detail.
[2] T. Bjerge and K. J. Brostrom, Kgl. Danske Vid. Sels. Math.-Fys. Medd. 16, No. 8 (1938).
[3] T. Bjerge and K. J. Brostrom, Nature 138, 400 (1936).
[4] H. S. Sommers, Jr. and R. Sherr, Phys. Rev. 69, 21 (1946).
[5] B. M. Rustad (private communication).
[6] Holmes, Proc. Phys. Soc. London 62, 293 (1949).

An Anomalous Dielectric Effect of Vacuum-Sputtered CaF_2 Layers

ERKKI A. LAURILA
Technical Physics Laboratory, Finland Institute of Technology, Helsinki, Finland
December 22, 1949

ASSUMING that crystal defects have an influence on dielectric properties of ionic crystals, I have investigated the properties of vacuum-sputtered layers of CaF_2. It is well known that just after sputtering, the layers are composed of small separate crystals which slowly change into a compact crystalline layer. In my experiments I observed an anomalous effect which is perhaps to be interpreted as a result of the crystal defects, but which is greater than expected. The experiments indicate that just after sputtering, the effective dielectric constant ϵ of the fluorspar was of the order 150–6000. In a few hours or days the dielectric constant diminished to a value of the normal magnitude of 7–10. Simultaneously the resistance of the layer, which at first was relatively small, increased to a value corresponding to the conductivity of the normal crystalline CaF_2.

The layers were formed on a glass plate as a plate condenser as indicated in Fig. 1. The thickness of the CaF_2 layer was measured optically, and the capacitance of the plate condenser by a common a.c. bridge and from the discharge curve of the condenser. The a.c. resistance was estimated by loss-angle measurements. The d.c. resistance was measured with a Wheatstone bridge or estimated from the discharge curve. Some typical results are shown in Table I.

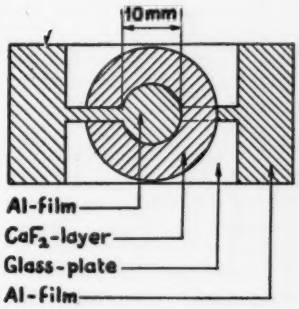

FIG. 1. Glass plate condenser.

TABLE I. Characteristics of CaF_2 layers.

Thickness A.u. (10^{-7} cm)	Time after sputtering	Capacitance μF	A.c. resistance $k\Omega$	D.c. resistance $k\Omega$	Dielectric constant
1000	0	5.0	1.25		550
	30 sec.	1.5	8.5		165
	5 min.	1.2	14.5		130
	24 hr.	1.1	18.0	>1000	120
	48 hr.	0.22			24
3000	0	3.0	1.75		990
	10 min.	2.7	2.45		895
	2 hr.	1.7	3.10	100	560
	18 hr.	0.03	175	>1000	9.9
	14 day	0.03	200		9.9
10000	0	4.0	1.35		4400
	1 min.	2.4	2.20		2600
	5 min.	2.0	2.90	70	2200
	15 hr.	0.017	310	700	19
	7 day	0.005	>1000	>1000	5.5

In ten such condensers examined the thickness of the CaF_2 layer varied between 1000 and 20000 angstrom units. The precision of the measurements is too small to draw any definite conclusions. It seems, however, that the evaluated dielectric constant increases with increasing thickness of the CaF_2 layer and probably approaches asymptotically a certain limiting value. It is also clearly seen that the a.c. resistance is considerably smaller than the d.c. resistance. This fact may be interpreted by a hesteresis phenomenon. Also the slope of the discharge curve makes this interpretation probable.

Finally it should be pointed out that a CaF_2 condenser several days or weeks old resumes the anomalous high capacitance when moistened by water.

The experimental work was carried out by Mr. E. Vesa. The investigation continues.

The Response of the Anthracene Scintillation Counter to Monoenergetic Electrons*

JOHN I. HOPKINS**
Oak Ridge National Laboratory, Oak Ridge, Tennessee
December 12, 1949

IT has been determined previously that the light pulse produced by an electron striking a phosphor substance such as anthracene is approximately proportional to the energy of the impinging electron over limited ranges of energies.[1,2] One desires to know how the pulse height for monoenergetic electrons varies with energy from an energy of a few kev up to an energy of several Mev.

A 180 cm single-lens β-ray spectrometer with an aperture of approximately 0.3 cm was used to supply the monoenergetic electrons. It was equipped with a sliding baffle so that the γ-ray and external background could be determined and the correction of counts made at each pulse height setting. Approximately 50 microcuries of Cs^{137} evaporated on to a thin Formvar film served as a source of electrons. The energy of the conversion electrons (630 kev) was used to determine the spectrometer constant. The end plate of the spectrometer at the counter end was made of soft iron and had at its center a mica window having $\frac{3}{8}$ inch diameter and 1 mg/cm² thickness. An anthracene crystal 1.3 cm in thickness was attached with Canada balsam to the photosensitive area of an RCA-5819 photo-multiplier tube. The crystal was then covered with a 0.2-mil light-reflecting aluminum foil and mounted directly in front of the window. A soft iron shield surrounding the scintillation counter, in conjunction with the end plate of the spectrometer, served to prevent variations in magnetic field in the region of the photo-multiplier tube.

The output from the photo-multiplier was fed into a preamplifier and linear amplifier[3] combination and counts recorded on a scaler. The output from a pulse generator was used to check the amplifier for linearity and to determine the zero of the pulse height dial.

Counts per second *versus* pulse height data were recorded for each chosen energy and the differential curves plotted to determine the pulse height giving the maximum number of counts per second. Some typical curves are shown in Fig. 1 where the counts per

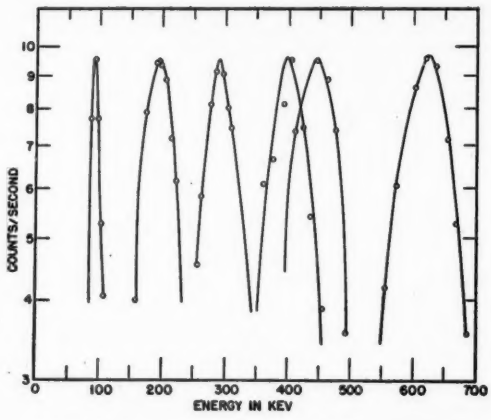

FIG. 1. Counting rate as a function of electron energy.

second have been normalized and plotted against the energy of the electrons in kev. These curves are within the expected statistical variation of the counts per second. It is estimated that the energy corresponding to a maximum number of counts per second for these curves is determined to an accuracy of ± 1.0 kev near 100 kev and to ± 4.0 kev from 400 to 665 kev.

In Fig. 2 is shown the pulse height variation with energy. It is noted that there is a slight deviation from linearity below 125 kev. Absorption data for electrons given by Glendenin[4] were used to

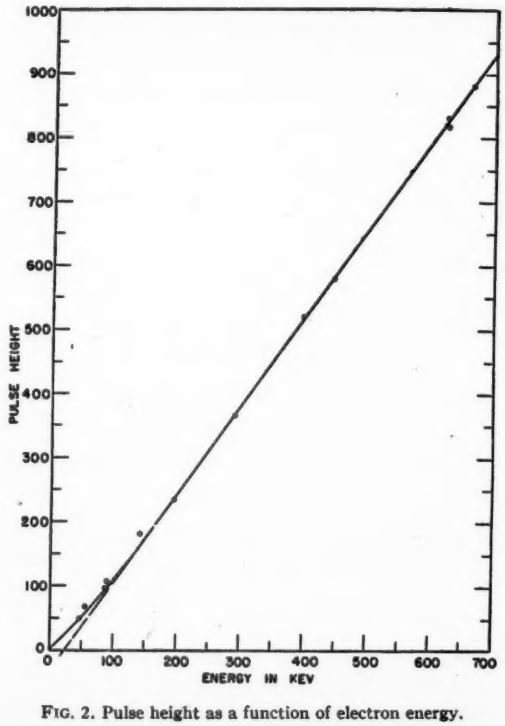

FIG. 2. Pulse height as a function of electron energy.

account for energy losses due to the absorption by the mica window, air space, and aluminum foil. Possible unaccountable errors in this experiment may be due to (1) background variations, since the spectrometer was located in the pile building, (2) magnetic variations near the photo-multiplier tube and (3) generator hash in the magnet current at times.

Work is being continued to further investigate the pulse height-energy variation in the low energy range and in the energy range above 650 kev.

Many thanks are due P. R. Bell for his constant advice and the Oak Ridge National Laboratory for the experimental facilities afforded.

* This document is based on work performed under Contract No. W-7405, eng. 26 for the Atomic Energy Project at Oak Ridge National Laboratory.
** On leave from Vanderbilt University, Nashville, Tennessee, 1949–1950.
[1] H. Kallmann, Natur und Technik (July, 1947).
[2] M. Deutsch, M.I.T. Technical Report No. 3 (December, 1947).
[3] W. H. Jordan and P. R. Bell, Rev. Sci. Inst. 18, 703 (1947).
[4] L. E. Glendenin, Nucleonics 2, 12 (1948).

Energy Bands and Mobilities in Monatomic Semiconductors

W. SHOCKLEY AND J. BARDEEN
Bell Telephone Laboratories, Murray Hill, New Jersey
December 12, 1949

FOR a cubic crystal subject to a homogeneous strain, ϵ_{ij}, the linear shift in energy band with strain may be expressed in the form

$$E=E_0+\Sigma\beta_{ij}\epsilon_{ij}=E_0+E_1\Delta, \tag{1}$$

where $\Delta=\epsilon_{11}+\epsilon_{22}+\epsilon_{33}$ is the dilation since all terms containing ϵ_{ij} with $i\neq j$ must vanish by symmetry. The shifts in the energy levels corresponding to the top of the filled band, E_f, and the bottom of the conduction band, E_c, produced by a periodic dilation of a lattice wave are shown schematically in Fig. 1(a). As illustrated, the bands may shift in opposite directions. In crystals with the diamond structure, such as Ge and Si, the energy gap, E_G, decreases with a positive dilation; in others, such as Te, the shift is in the opposite direction. The difference between the shifts in E_c and E_f is equal to the shift in E_G:

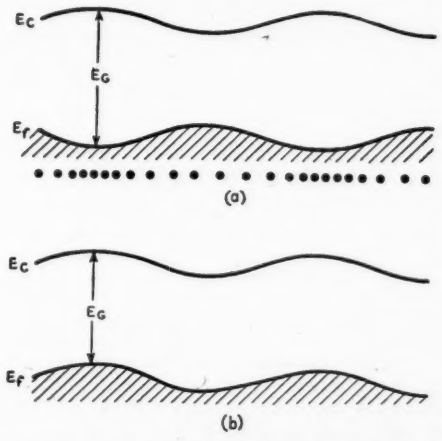

FIG. 1. (a) Shift of energy bands with varying dilation. (b) Shift of energy bands with varying electrostatic potential.

$$E_{1G}=E_{1c}-E_{1f}. \tag{2}$$

On the other hand, a varying electrostatic potential makes the bands move up and down together, as in Fig. 1(b).

The theories of Peckar[1] and of James[2] may be extended to show that the effective mass concept may be applied to gradual shifts in energy bands produced by distortions as well as by a varying electrostatic potential.[3] In both cases, the position of the energy band may be used as an effective potential for the electron provided that the variation is sufficiently gradual. This is the case for shifts caused by lattice vibrations of long wave-length which interact with electrons of thermal velocities in semiconductors.

It is thus possible to calculate scattering by lattice waves by taking as the interaction potential, $U(\mathbf{r})$, the shift in energy band resulting from dilation, $E_1\Delta(\mathbf{r})$:

$$U(r)=E_1\Delta(\mathbf{r}). \tag{3}$$

The matrix element involved in scattering,

$$M_{kk'}=\int\psi_{k'}^*U(\mathbf{r})\psi_k d\tau=\int\exp[i(\mathbf{k}-\mathbf{k}')\cdot r]E_1\Delta(\mathbf{r})d\tau \tag{4}$$

vanishes unless $\mathbf{k}'=\mathbf{k}\pm\mathbf{q}$, in which case

$$|M_{kk'}|^2=E_1^2|\mathbf{q}\cdot\mathbf{A}_q|^2, \tag{5}$$

where $\mathbf{A}_q$ is the complex amplitude of the lattice wave of wave vector $\mathbf{q}$. The interaction constant C used by Sommerfeld and Bethe and by Seitz[4] is equal to $(3/2)E_1$; that used by Wilson is equal to E_1.

The expression for mobility, μ, derived in the usual way, may be expressed in the form:

$$\begin{aligned}\mu&=2(2\pi)^{1/2}e\hbar^4\rho c_l^2/3m_e^{5/2}(k_0T)^{3/2}E_1^2\\&=(3.2\times10^{-6})\rho c_l^2/T^{3/2}E_1^2\ \text{cm}^2/\text{volt sec}.\end{aligned} \tag{6}$$

In deriving the numerical factor we have set the effective mass ratio equal to unity and expressed E_1 in ev. The product of the density, ρ, and the square of longitudinal wave velocity, c_l^2, can be expressed in terms of the elastic constants.

Equation (6) may be used to derive $|E_{1c}|$ and $|E_{1f}|$ from mobilities of conduction electrons and holes, respectively. The calculations for diamond, Si, Ge, and Te, together with relevant data, are given in Table I. The anisotropy of Te has been neglected.

TABLE I. Derivation of shift of energy bands with dilation from mobility data and comparison with shift of energy gap with dilation.

	Diamond	Silicon	Germanium	Tellurium
$\rho c_l^2\times10^{-12}$ (c.g.s.)	10.8[a]	2.0[c]	1.55[b]	0.5[c]
μ_n (electrons) (cm²/volt sec., 295°K)	900[d]	300[e]	3500[f]	530[g]
μ_p (holes) (cm²/volt sec., 295°K)	>200[h]	100[e]	1700[f]	530[g]
$\mu_n T^{\frac{3}{2}}$	45×10^5	15×10^5	180×10^5	27×10^5
$\mu_p T^{\frac{3}{2}}$	$>10\times10^5$	5×10^5	86×10^5	27×10^5
$\lvert E_{1c}\rvert$ (ev)	8.8	6.5	1.7	2.4
$\lvert E_{1f}\rvert$ (ev)	<30	11.3	2.4	2.4
$\lvert E_{1c}\rvert+\lvert E_{1f}\rvert$	<39	17.8	4.1	4.8
$\lvert E_{1G}\rvert$ (ev)	?	~30[i]	~5[i]	5.0[i]

[a] Longitudinal velocity in [110] direction calculated from elastic constants. See R. F. S. Hearmon, Rev. Mod. Phys. 18, 409 (1946).
[b] Calculated from elastic constants measured by McSkimin, Mason, and Bond on single crystal sample prepared by K. M. Olson.
[c] Estimated from compressibility.
[d] C. C. Klick and R. J. Maurer, Phys. Rev. 76, 179 (1949).
[e] Reference 5.
[f] Unpublished data of J. R. Haynes.
[g] Vivian A. Johnson, Phys. Rev. 74, 1255 (1948).
[h] K. G. McKay (private communication).
[i] See text.

If E_{1c} and E_{1f} have opposite signs, as in Fig. 1(a), we should have

$$|E_{1G}|=|E_{1c}|+|E_{1f}|. \tag{7}$$

Various independent estimates of $|E_{1G}|$, given in the last row of the table, are in reasonable agreement with (7). These estimates were obtained as follows:

Silicon. The variation of E_G with temperature, derived from intrinsic concentration,[5] combined with the thermal expansion coefficient.

Germanium. (a) As for Si, (b) change of intrinsic conductivity with pressure,[6] (c) change of resistance of $n-p$ junction with pressure.[7]

Tellurium. From analysis of Bridgman's data on variation of intrinsic conductivity with pressure.[8] The high mobility of electrons and holes in germanium is thus correlated with a small shift in energy gap with dilation.

[1] S. Peckar, J. Phys. USSR, 10, 431 (1946).
[2] Hubert M. James, Phys. Rev. 76, 1602 (1949).
[3] A proof, together with a direct calculation of the pertinent matrix element without making use of the effective mass concept, will be given in a forthcoming paper by the authors.
[4] See A. Sommerfeld and H. Bethe, *Handbuch der Physik*, Vol. XXIV, 1; A. H. Wilson, *The Theory of Metals* (Cambridge University Press, London, 1936); Frederick Seitz, Phys. Rev. 73, 549 (1948).
[5] G. L. Pearson and J. Bardeen, Phys. Rev. 75, 865 (1949).
[6] P. H. Miller and Julius Taylor, Phys. Rev. 76, 179 (1949) and personal communication from Professor Miller.
[7] Unpublished measurements of G. L. Pearson.
[8] John Bardeen, Phys. Rev. 75, 1777 (1949).

Color Centers in Calcium Fluoride and Barium Fluoride Crystals

ALEXANDER SMAKULA
Engineer Research and Development Laboratories, The Engineer Center and Fort Belvoir, Fort Belvoir, Virginia
November 25, 1949

THE color centers produced photochemically (x-rays, ultraviolet light) or additively (metal vapor, electrons) have been investigated by Pohl[1] and his school mainly in monovalent ionic crystals, such as, alkali halides. The first results on color centers produced by x-rays in calcium fluoride (CaF_2) and barium fluoride crystals (BaF_2) are presented in this note.

Natural and synthetic crystals of calcium fluoride and synthetic crystals of barium fluoride were used. The thickness of the crystals was between 0.5 and 1.0 cm. Hard x-rays (200 kv, 10 ma) were used to produce a uniform coloration throughout the entire crystals. The exposure time varied from 0.5 to 5.0 hours. Immediately after exposure to x-rays, the transmission of the colored crystals was measured with a Beckman spectrophotometer in the spectral region from 2200A to 10,000A. No change in coloration occurred during measurements.

The absorption spectrum of color centers in calcium fluoride

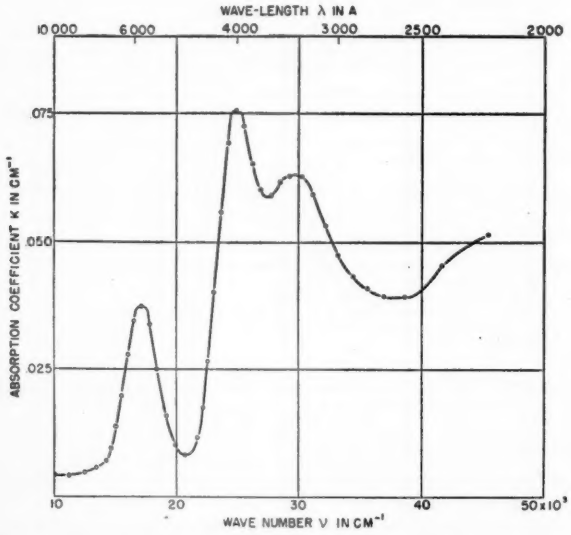

FIG. 1. Absorption spectrum of color centers in calcium fluoride (CaF_2) crystal [$k=(1/d)\log_{10}(I_0/I)$; 200 kv, 10 ma, exposure 5 hours].

crystals is reproduced in Fig. 1. The three absorption bands fall at 5800A, 4000A, and 3350A. A strong increase of absorption toward shorter wave-length indicates a fourth band with a maximum below 2200A.

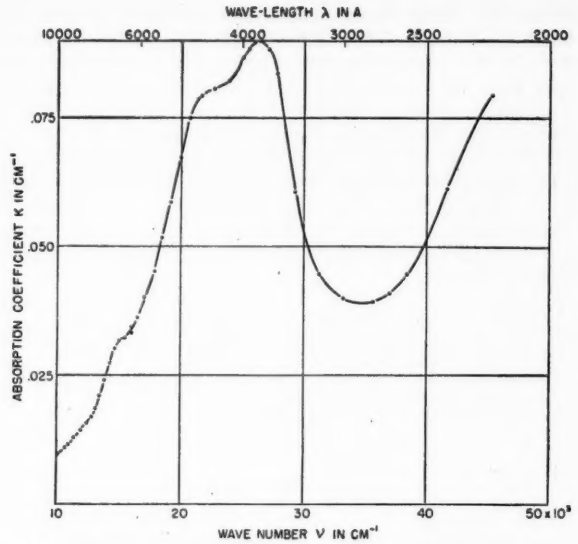

FIG. 2. Absorption spectrum of color centers in barium fluoride (BaF_2) crystal [$k=(1/d)\log_{10}(I_0/I)$; 200 kv, 10 ma, exposure 0.5 hour].

In Fig. 2 is given the absorption spectrum of color centers in barium fluoride crystal. As for calcium fluoride, three absorption bands are seen at 6700A, 4800A, and 3800A. A fourth band below 2200A is also apparent. As compared with calcium fluoride the bands are shifted to longer wave-lengths and they overlap to a greater extent.

The formation of absorption bands with increase of exposure time is shown in Fig. 3. All three bands show saturation with

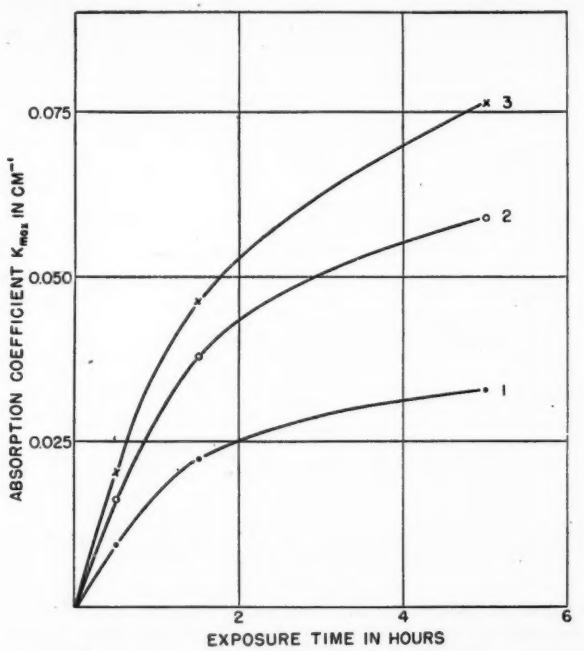

FIG. 3. Change of the absorption band intensity of calcium fluoride with increase of exposure time to x-rays (200 kv, 10 ma). 1. Absorption band at 5800A, 2. Absorption band at 3350A. 3. Absorption band at 4000A.

increase in exposure similar to the saturation of the coloration of alkali halides.[2]

In additively colored natural calcium fluoride crystals Mollwo[3]

found two bands, one at 5250A and the other at 3700A. The additive color centers can be produced at high temperatures only. The absorption bands were obtained only if the crystals are cooled down to room temperature very rapidly. When they were cooled slowly no absorption bands were found. By proper cooling the shape and position of the band in the visible could be changed (probably resulted in the formation of colloids).

As compared with alkali halides, the absorption spectra of colored calcium and barium fluorides show some similar and some different properties. These similar properties can be noted: saturation of coloration with exposure time; half-widths of absorption bands; and bleaching by heat or light.

The differences are as follows: Only two bands appear in alkali halides after a small exposure to x-rays, as was the case here; one is the strong band, called the F-band after Pohl;[1] and the other a weak band, called the M-band after Seitz[4] (the M-bands were discovered by Ottmer[5] and later investigated by Molnar[6]). In calcium fluoride and in barium fluoride, at least four bands can be seen. In alkali halides the F-band can be transformed into the M-band by exposure to the light absorbed by the former. In calcium fluoride and barium fluoride, the transformation of one band to another one seems to be impossible, at least at room temperature. The relationship, vd^2=constant (v=frequency of the F-band, d=lattice constant) which has been found by Mollwo[7] for F-bands of alkali halides is not valid for any of the bands of calcium fluoride and barium fluoride.

From preliminary experiments on bleaching by heat and light one can assume that the absorption bands of the color centers in calcium fluoride and barium fluoride are independent. Although the nature of color centers may be generally the same as in alkali halides, electrons trapped in lattice defects, further investigations are necessary for their quantitative explanation.

Grateful acknowledgment is given Mrs. R. K. Wilkinson for transmission measurements.

[1] R. W. Pohl, Physik. Zeits. **39**, 36 (1938).
[2] A. Smakula, Göttengen Nachrichten 110 (1929).
[3] E. Mollwo, Göttengen Nachrichten 1, 79 (1934).
[4] F. Seitz, Rev. Mod. Phys. **18**, 348 (1946).
[5] R. Ottmer, Zeits. f. Physik **46**, 798 (1928).
[6] J. P. Molnar, "The absorption spectra of trapped electrons in alkali halide crystals," M.I.T. thesis (1940).
[7] E. Mollwo, Göttengen Nachrichten 97 (1931).

Gamma-Rays of K^{40}

P. R. Bell and J. M. Cassidy
Oak Ridge National Laboratory, Oak Ridge, Tennessee*
December 8, 1949

THE gamma-ray emitted by K^{40} has been reported as 1.55 Mev by absorption in lead, and no evidence for softer gamma-rays was found.[1,2] The scintillation spectrometer has been used to investigate the K^{40} gamma-radiation and to search for annihilation radiation associated with possible positron emission.

The gamma-rays produce Compton electrons in an anthracene crystal and the spectrum of these Compton electrons is measured by determining the pulse distribution from an RCA C-7132 photomultiplier to which the anthracene crystal is cemented.

Figure 1 shows the arrangement of the sample (which was 1300 g of normal KCl) and the anthracene crystal and photo-multiplier. The beta-rays were absorbed by the $\frac{1}{8}$-inch aluminum wall surrounding the crystal. The entire assembly was shielded by 2 inches of lead.

The gamma-ray was compared with the low energy gamma-ray from Na^{24}(1.38 Mev),[3] the gamma-ray of Zn^{65}(1.12 Mev)[4] and the conversion line of Cs^{137}(0.632 Mev).[5] The Na^{24} sample was placed on top of the KCl container leaving the KCl in place. The distribution of pulses from the K^{40} and part of the distribution

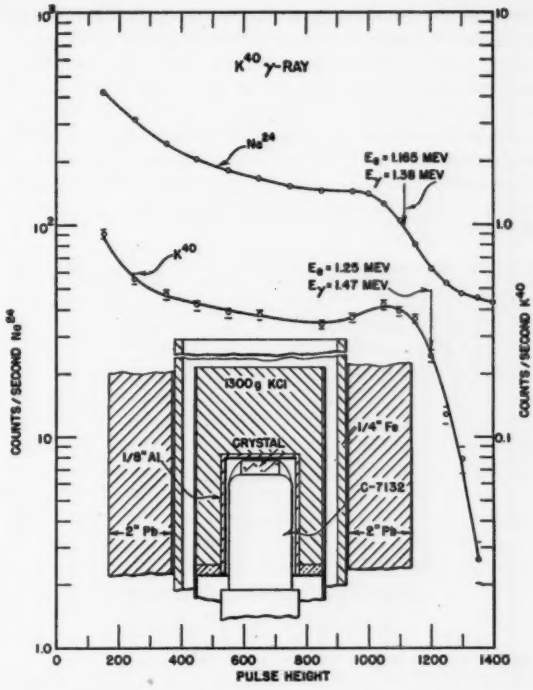

FIG. 1. Arrangement of apparatus and distribution of pulses.

produced by Na^{24} are also shown in Fig. 1. The background counting rate was quite negligible.

The maximum energy of the Compton electrons was determined in two ways: (1) the maximum slope of the break and (2) the half-counting rate point (in the case of Na^{24} the counts due to the upper gamma-ray were subtracted).

The results of several determinations are given in Table I. A search was then made for annihilation radiation. Figure 2 shows

TABLE I. Energy of Compton electrons.

Comparison radiation	Energy from Maximum slope	Energy from Half-counting rate
Na^{24}	1.47 Mev	1.49 Mev
Na^{24}	1.39 Mev	1.42 Mev
Cs^{137}	1.47 Mev	1.48 Mev
Zn^{65}	1.47 Mev	1.46 Mev
average	1.45 ±0.04 Mev	1.46 ±0.04 Mev

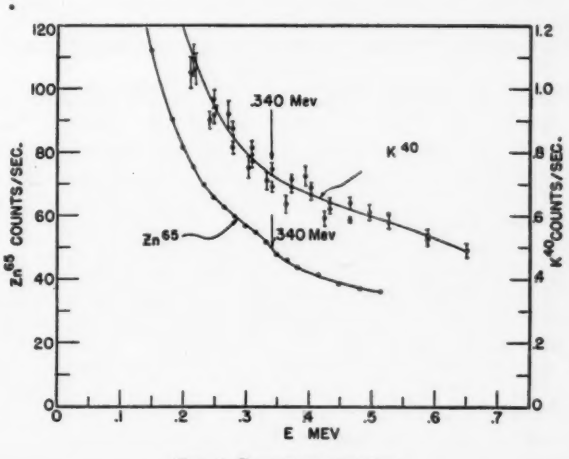

FIG. 2. Gamma-ray spectra.

the part of the gamma-ray spectrum in which a step should be found if annihilation radiation were present. Also shown is the curve obtained for the Zn^{65} spectrum in this region. Zn^{65} has about 5 annihilation quanta per 100 gamma-rays.[6] The number of annihilation quanta per gamma-ray in K^{40} must be less than half the number from Zn^{65}. Therefore the number of positrons emitted must be less than 1 percent of the K capture transitions to the excited state of A^{40}. This lack of positron emission makes it improbable that there is any large number of K captures to the ground state of A^{40}.

* This document is based on work performed under Contract No. W-7405, eng. 26 for the Atomic Energy Project at Oak Ridge National Laboratory.

[1] O. Hirzel and H. Waffler, Helv. Phys. Acta 19, 216 (1946).
[2] E. Gleditsch and T. Graf, Phys. Rev. 72, 640 (1947).
[3] K. Siegbahn, Phys. Rev. 70, 127 (1946).
[4] Jansen, Laslett, and Pratt, Phys. Rev. 76, 430 (1949).
[5] Peacock and Mitchell, Phys. Rev. 75, 1272 (1949).
[6] Good and Peacock, Phys. Rev. 69, 680 (1946).

Zenith Angle Dependence of Extensive Air Showers

H. L. KRAYBILL
Sloane Physics Laboratory, Yale University, New Haven, Connecticut*
December 12, 1949

FROM the altitude dependence of extensive air showers one can calculate the zenith angle dependence of the showers at a given depth, under the following assumptions: (1) The shower primaries are isotropic at the top of the atmosphere, (2) the multiplication and disappearance of the shower particles in the atmosphere is a function solely of the mass of matter traversed and not of the path length or density, (3) the lateral spread of shower particles at a given depth is inversely proportional to air density in accordance with cascade theory, (4) the particles in the showers have the same direction as the primary particle which produced the shower, and (5) the value of γ, defined as $d\log C/d\log A$, where C is the counting rate and A is the counter area, is known for showers incident from the vertical.

By use of an altitude curve[1] obtained by the author, the zenith angle dependence was calculated for an atmospheric pressure of 50 cm of Hg. The shower detector consisted of three Geiger counters uniformly spaced in a straight line. Spacing between adjacent counters was 1.4 meters. The effect of counter geometry was taken into account, although the calculated zenith angle dependence is only weakly sensitive to the counter geometry. The value of γ was assumed to be constant and equal to 1.5 between sea level and 50 cm of mercury.[2] By the use of a generalized Gross transformation[3] the zenith angle distribution was then obtained as:

$$M(t,\theta)=\frac{2.2C(t/\cos\theta)-(t/\cos\theta)C'(t/\cos\theta)}{2\pi}\cos^{0.7}\theta.$$

$C(t)$ is the observed counting rate as a function of altitude. $M(t,\theta)$ is the rate of showers per steradian which would be counted at thickness t and zenith angle θ, by an isotropic detector having the same vertical sensitivity as the counter arrangement.

Numerical application of this formula to the altitude curve gives a zenith angle dependence for the axes of the air showers which can be approximately represented by $\cos^5\theta$ between 0° and 40°, but which decreases somewhat more rapidly than $\cos^5\theta$ at larger zenith angles.

An experimental test of the above zenith angle distribution was attempted at Climax, Colorado, at a pressure of 49.5 cm of mercury, by using the directional sensitivity of long cylindrical counters. When the axes of such counters are vertical, their counting rate is strongly sensitive to the breadth of the zenith angle distribution of the showers. The counting rate of these counters with their axes horizontal is less sensitive to the zenith angle distribution. Table I lists the horizontal-to-vertical counting ratio for counters of lateral cross section 2.44 cm by 33 cm, having the same disposition in a horizontal plane, calculated for various assumed zenith angle distributions of the showers.

TABLE I. Values of the horizontal/vertical counting ratio (R), calculated for various assumed zenith angle distributions. The values were computed for cylindrical counters with a sensitive area of 2.44 cm×33 cm.

Assumed angular distribution	Calculated value of R
$\cos^2\theta$	1.86
$\cos^5\theta$	2.33
$\cos^9\theta$	3.16
$\cos^{15}\theta$	4.21
angular distribution at 50 cm of Hg, calculated from altitude curve of reference 1	2.56

The counting rates of the counters shown in Fig. 1 were determined at Climax. The horizontal-to-vertical ratios (R) are shown in Table II. These ratios are not sensitive to the counter arrangement. The best experimental value of R is 2.12±0.07. This is the value of R to be expected for a zenith angle distribution of about $\cos^4\theta$. This value is lower than the value of 2.56 which was calculated from the altitude dependence.

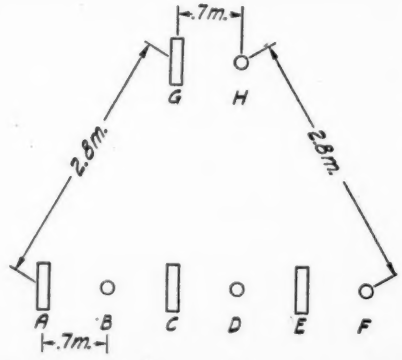

FIG. 1. Vertical view of arrangement of horizontal and vertical counters, used to test zenith angle distribution of extensive air showers at Climax, Colorado. The coincidences *ACE, AEG, ACEG, BDF, BFH, BDFH*, were recorded. Sensitive area of each counter is 2.44 cm by 33 cm.

TABLE II. Counting rates of the counter arrangement shown in Fig. 1.

Time	Coincidence type	Counts	Rate
220	*ACE*	1621	7.37±0.18*
220	*AEG*	1563	7.11±0.18
220	*BDF*	765	3.47±0.12
220	*BFH*	738	3.35±0.12
220	*ACEG*	1018	4.63±0.15
220	BDFH	474	2.15±0.10
Coincidence ratios			R
ACE/BDF			2.12±0.08*
AEG/BFH			2.12±0.09
ACEG/BDFH			2.15±0.12

* This is the standard deviation due to statistical fluctuations.

The cause of the above difference is not clear. Some of it is due to scattering of the shower particles in the air and to multiplication in material surrounding the counters. The counters were enclosed in boxes of 0.8-mm sheet iron, under a canvas tent in the open air. The tent was 10 feet from a metal shack about 15 feet square by 10 feet high. However, the fact that R did not vary with the counter geometry indicates that the shack did not appreciably affect its value.

Narrow showers[4] incident at large zenith angles would tend to

favor the vertical counters and produce the discrepancy observed. However, the narrow showers have appreciable effect only at counter spreads less than 90 cm. Thus the arrangements *AEG* and *BFH* of Fig. 1 are not affected by narrow showers from any direction.

I am indebted to the Climax Molybdenum Company for the use of their facilities while carrying out this experiment, and to the University of Chicago for lending some of the equipment which was used. I also wish to thank Professor C. G. Montgomery for helpful discussions.

* Assisted by the Joint Program of the ONR and the AEC.
[1] H. Kraybill, Phys. Rev. **76**, 1092 (1949).
[2] G. Cocconi and V. Cocconi Tongiorgi, Phys. Rev. **75**, 1058 (1949).
[3] L. Janossy, Zeits. f. Physik **101**, 129 (1936).
[4] J. Wei and C. G. Montgomery, Phys. Rev. **76**, 1488 (1949).

The "1947 Values" of the Atomic Constants and the Revision of the Faraday Constant*

JESSE W. M. DUMOND
California Institute of Technology, Pasadena, California
December 5, 1949

IT is well known that the two precision determinations of the Faraday by electrochemical methods (1) by the silver voltameter,[1] (2) by the iodine voltameter[2] fail to agree by considerably more than their estimated probable errors warrant.

$$F_{Ag}=9650.5 \text{ e.m.u./g} \quad \text{(physical scale)},^{3}$$
$$F_{I}=9652.2 \text{ e.m.u./g} \quad \text{(physical scale)}.^{3}$$

Nevertheless, F_{Ag} has long been the value accepted, perhaps in part because it has been regarded *as correct by definition.*

It seems to the writer that such an empirical definition is unfortunate and this universal constant should preferably be defined in a *fundamentally significant* way, i.e., as the quantity of electricity, N_0e, (N_0=Avogadro's number and e=the electronic charge) or the charge *associated with* one gram-atomic weight of singly ionized atoms. Fortunately, in this more fundamental sense of the Faraday it can now be, and recently has been precisely measured. J. A. Hipple, H. Sommer, and H. A. Thomas at the National Bureau of Standards[3] determine by means of their newly developed "omegatron" the charge-to-mass ratio e/M_{H^+} for gaseous H^+ ions. After multiplication by the isotopic weight of H^+ (1.007580 ± 0.000003) they obtain the Faraday (in the sense here proposed). A preliminary result is

$$F=9652.8\pm0.8 \text{ e.m.u./g (physical scale)}$$

indicating that the iodine Faraday (rather than the silver) was nearer the truth.

The Faraday can be computed from certain spectroscopic data without appeal to electrochemistry and R. T. Birge was the first to point out[4] that when this is done one obtains a value somewhat higher than F_{Ag} (though less accurately). Now both F_{Ag} and F_I were determined before the discovery of isotopes and it occurred to the writer of this letter as early as 1940 that the facts (1) that iodine is isotopically pure and (2) that silver consists of two isotopes in nearly equal abundance might explain the F_I-F_{Ag} discrepancy.

In 1948, E. R. Cohen and the writer published[5] a least-squares analysis (here designated D and C '48) of the existing data on the atomic constants. Some eleven different precision measured values each representing a different function of the four unknowns, F, N_0, m, and h, formed the basic input data from which an overdetermined set of observational equations was adjusted by least-squares to obtain compromise output values of the above four unknowns. The adoption of four unknowns F, N_0, m and h (instead of three, $e(=F/N_0)$, m and h) for the least-squares adjustment (designated in the paper as the "new viewpoint") was a new departure in such analyses (expressly introduced because of the uncertainties in F) which led to a complete reclassification of several of the eleven input data. Other important influences beside the direct electrochemical data were thus free to operate in the least-squares adjustment leading to the output value of F. For the direct electrochemical data on F the average of F_{Ag} and F_I was used in D and C '48. The final least-squares-adjusted output value for F obtained from this analysis came out

$$F=9652.2\pm0.7 \text{ e.m.u./g (physical scale)}$$

in close agreement with F_I rather than F_{Ag}.

Largely because of this higher output value of F there has been a perhaps natural reluctance among some physicists to accept the revised values obtained in D and C '48 (some 33 values of different important constants and conversion factors were there computed). A chief purpose of this letter is to point out that the new corroboration from the work of Hipple and his associates now largely removes the cause of this reluctance. Also, since D and C '48 appeared, further evidence[6] in favor of the higher Faraday has been obtained as a by-product of a measurement[7] of the wavelength of the annihilation radiation.

Undoubtedly, the entire least-squares analysis should be repeated using the final Hipple value of F (when it is available) and perhaps ignoring F_{Ag} and F_I completely unless improvements can be made in these electrochemical determinations as regards at present unknown systematic errors. Although the results in D and C '48 were very insensitive to the directly measured x-ray value of h/e, it might also be wise to postpone such a final least-squares analysis until the h/e discrepancy (now under investigation at this Institute) can also be cleared up. In the meanwhile, the writer believes the values given in D and C '48 can now be provisionally used with considerably more confidence than heretofore.

* Assisted by the Joint Program of the ONR and AEC.
[1] M. G. W. Vinal, Comptes Rendus, **3**, 95 (1932).
[2] M. G. W. Vinal and S. J. Bates, Bull. Bur. Stand. **10**, 425 (1914). Since this paper, some revisions in F_{Ag} and in atomic weights have failed to eliminate the $F_{Ag}-F_I$ discrepancy.
[3] Hipple, Sommer, and Thomas, Phys. Rev. **76**, 1877 (1949).
[4] R. T. Birge, Reports on Progress in Physics (British) **VIII**, 121–122 (1942).
[5] J. W. M. DuMond and E. R. Cohen, Rev. Mod. Phys. **20**, 82 (1948). Attention is called to the fact that slight revisions to the original published values in this paper have been made since the discovery of a small numerical error. These revisions appear in Rev. Mod. Phys. **21**, 651 (1949).
[6] J. W. M. DuMond, Phys. Rev. **75**, 1267 (1949).
[7] DuMond, Lind, and Watson, Phys. Rev. **75**, 1226 (1949).

A Note on the $Li^7(p,n)Be^7$ Reaction and an Excited State of Be^7

T. A. HALL
Institute for Nuclear Studies, University of Chicago, Chicago, Illinois
December 21, 1949

BECAUSE of interest in the homogeneity of the neutrons produced in the $Li^7(p,n)$ reaction, we have re-examined data obtained two years ago with a Van de Graaff generator, using this reaction as a monoenergetic neutron source to study the resonance scattering of neutrons on helium.[1] In this experiment the neutrons crossed a proportional counter containing helium, and the energy distribution of the helium recoils was recorded. Since the neutron energies studied (0.8 to 1.6 Mev) were too low for significant D-wave scattering, the distribution curves should have been parabolas, corresponding to superposition of S and P waves. Instead, for all neutron energies used above 1.2 Mev (and for no lower energies), well-defined distortions in the curves were observed. From the largest recoil energy where distortion appears, one can calculate an excitation energy of Be^7, assuming that such a state has made the neutron beam di-energetic. The results are shown in Table I for all five curves where the effect was noted.

TABLE I. Implied excitation energy of Be^7.

Run	E_p	E_n	R	E_n'	E
1	3.02	1.25	0.63	0.78$_5$	0.45
2	3.02	1.25	0.63	0.78$_5$	0.45
3	3.12	1.35	0.57	0.76	0.54
4	3.12	1.35	0.64	0.87	0.45
5	3.38	1.6	0.70	1.13	0.44

(Three of these curves are shown in reference 1.) E_p is the energy in Mev of the Van de Graaff protons, E_n the energy of the main neutron group, R the ratio of recoil energy at the anomalous peak to maximum recoil energy, E_n' the energy of the postulated slower neutron group, and E the excitation energy of Be^7 which would cause such a group.

Table I shows that only one run was inconsistent with the excited state hypothesis, the location of the distorted peak was in fact exceptionally vague in this one case. While the anomalous peak cannot be localized sufficiently to give a precise measure of the excitation energy, the other four runs put it between 420 and 480 kev.

Recent precision measurements indicate that such a Be^7 state exists.[2,3] However, the excitation of this state by 3 Mev protons striking lithium has escaped previous observation.[4] The reason perhaps is that the Li(p,n) yield curve, which was studied by Freier, Lampi, and Williams, does not offer as sensitive a test as the helium recoil data, in which the slower neutrons at optimum energies produce resonant forward-scattered recoils which are superposed, in the distribution curves, upon non-resonant faster neutron recoils of unfavorable scattering angle. If the implications drawn from this helium data are correct, the traces of the slower neutron group should be observable in many neutron resonance studies, especially by comparing resonance data taken with both Li(p,n) and D(d,n) neutron sources.

As to helium scattering itself, in reference 1 the smallness of the ratio of maximum to minimum differential scattering cross sections in all of the curves was taken to indicate a split resonance level, but this apparently small ratio may also be due really to a slower neutron group.

[1] T. A. Hall and P. G. Koontz, Phys. Rev. **72**, 196 (1947).
[2] J. C. Grosskreutz and K. B. Mather, Bull. Am. Phys. Soc. **24**, No. 7, H5(A) (Chicago, 1949) report a state at 0.470±0.070 Mev.
[3] Brown, Chao, Fowler, and Lauritsen, Bull. Am. Phys. Soc. **24**, No. 8, D11(A) (Stanford, 1949) report a state at 0.435±0.008 Mev.
[4] Freier, Lampi, and Williams, Phys. Rev. **75**, 901 (1949).

Fast Protons from the Absorption of π^--Mesons by Nuclei*

STEPHEN TAMOR**
University of Rochester, Rochester, New York
December 12, 1949

BY use of a very simple model for the production of stars resulting from the absorption of π^--mesons by nuclei it is possible to estimate (a) the number of "fast" protons (energy >30 Mev) in the stars, and (b) the average excitation energy. We assume that the meson is absorbed by a single proton in the nucleus producing a neutron which moves at high speed through a "gas" of nucleons, while momentum is conserved by the recoil of one or more neighboring nucleons. The fast nucleons may escape from the nucleus without collision or may undergo one or more collisions, thereby heating up the nucleus. Thus star fragments from π^--absorptions fall into two categories: high energy nucleons arising directly from the absorption process, and evaporation fragments whose energies are low and determined by the energy loss of the initial nucleon in traversing the nucleus. If the mean free path of the fast nucleons is of the order of or larger than the nuclear diameter, we would expect large numbers of fast nucleons as well as total excitation energies of the evaporation stars low compared to the meson rest mass of 146 Mev.

If, in addition to the collision cross section, the average energy loss per collision is known, one can estimate the probability that a nucleon makes a specified number of collisions before leaving the nucleus and the excitation energy of the residual nucleus. The energies involved are sufficiently high that, to a first approximation, the binding of the nucleons can be ignored. The total $n-p$ scattering $n-p$ scattering cross section is taken as $6.8/E$ barns where E is measured in Mev,[1] and we assume $\sigma_{nn}=\sigma_{p-p}=\frac{1}{2}\sigma_{n-p}$.[2] Since the nucleus is treated as a Fermi gas, the exclusion principle discriminates against collisions with small momentum transfer, thereby increasing the effective cross section by a factor of about 1.45.[3] The energy loss per collision has been estimated by Serber[4] as 25 Mev for energies of the order of 100 Mev. The calculation is greatly simplified by assuming forward scattering. The error involved is difficult to estimate, but is surely not very large and probably leads to a slight overestimate for the number of fast protons.

Two different models were used for the calculations.[5] I. The recoil momentum is taken up by a single nucleon so that the absorption results in two nucleons moving in opposite directions, each with half the meson rest energy. The recoil particle can be a neutron or a proton, and on the basis of an α-particle model the ratio of neutrons to protons is 2:1. Use of the ratio obtained by counting all neutrons and protons in the nucleus gives almost identical results. II. The recoil is a triton, the residual part of the α-particle of which the absorbing proton is taken to be a member. Using a triton binding energy of 8 Mev,[6] we find that the neutron carries away 95 Mev while the recoil triton has 31 Mev. The entire energy of the trition goes into heating up the nucleus.

With model I one calculates the probabilities that both nucleons make zero collisions, one makes one and the other zero, etc. After more than one collision the nucleon energy is degenerated below 30 Mev and is considered to be "lost" in the evaporation star. With model II the single nucleon is "lost" after more than two collisions. In this way one obtains an estimate of the number of absorptions which produce no stars (by star we mean evaporation star) and the number which yield fast protons. In all these calculations it is assumed that a charge exchange occurs in half the neutron-proton collisions.

The calculations were carried out for π^--absorptions in nitrogen and in silver so as to make possible a comparison with the observations in nuclear emulsions. The important results are given separately in Table I for nitrogen (taken as typical of the C, N, O group) and for silver (representing Ag, Br) since it should be possible experimentally to distinguish between the π^--stars produced in the light and heavy elements of the emulsion.

Evaporation stars of energy less than 40 Mev are classified separately since an excitation of that magnitude will produce stars consisting almost entirely of neutrons in nuclei as heavy as silver[7] and are therefore not observed. It is worth noting that model II

TABLE I.

	Model	Nitrogen	Silver
Number of fast protons (E>30 Mev) per 100 π^--mesons absorbed	I	48	24
	II	12	13
Average excitation energy of evaporation star	I	31 Mev	78 Mev
	II	55 Mev	70 Mev
Number of π^--absorptions giving no evaporation star (per 100)	I	28	8
	II	0	0
Number of evaporation stars with excitation <40 Mev per 100 π^--absorptions	I	31	12
	II	64†	43†

† The escaping fast nucleon is always a neutron.

predicts a large number of π^--absorptions in silver which produce no observable prongs (except possibly recoil nuclei) while model I predicts very few. Both models lead to a substantial number of fast protons too energetic to be accounted for by an evaporation process.

Meson absorptions giving rise to fast protons have been observed in photographic plates by Perkins[8] and by Cheston and Goldfarb[9] at Rochester. The data appear to fit reasonably well with our model II but the results are still inconclusive.

The author wishes to express his gratitude to Professor R. E. Marshak for his guidance throughout the work and to Messrs. W. Cheston and L. Goldfarb for many valuable discussions.

* Preliminary results were reported by Professor R. E. Marshak at the Idaho Springs Cosmic Ray Conference in June 1949.
** AEC Predoctoral Fellow.
[1] Hadley, Kelly, Lieth, Segrè, Wiegand, and York, Phys. Rev. **75**, 351 (1949).
[2] The calculation was also done using $\sigma_{n-n}=\sigma_{p-p}=\sigma_{n-p}$. This gives about 20 percent fewer fast protons and slightly higher excitation energies but no significant changes in the principle features of the result.
[3] M. L. Goldberger, Phys. Rev. **74**, 1269 (1948).
[4] R. Serber, Phys. Rev. **72**, 1114 (1947).
[5] Similar models were suggested independently by Heidmann and Leprince-Ringuet, Comptes Rendus **226**, 1716 (1948).
[6] L. Rosenfeld, *Nuclear Forces* (Interscience Publishing Company, New York, 1948), p. 301.
[7] V. F. Weisskopf, Los Alamos Report 24, Lecture XXXVI.
[8] Perkins, Phil. Mag. **40**, 601 (1949).
[9] W. Cheston and L. Goldfarb, paper to be presented at New York meeting, February 1950.

Upper and Lower Bounds of Eigenvalues

TOSIO KATO
Physics Department, Faculty of Science, Tokyo University, Tokyo, Japan
November 30, 1949

THE Ritz variational method gives only upper bounds of eigenvalues of Hermitian operators. Many authors[1] attempted to generalize the method and derived various formulas to estimate lower bounds of eigenvalues. But it seems that as yet the mutual relations and relative merits of these formulas have not been fully discussed from a systematic point of view.

We carefully examined these formulas and reached the conclusion that the formula of Temple[1] is the most precise one among them notwithstanding that it is the oldest as well as the simplest one.

Moreover, we could generalize the Temple formula to the case of higher eigenvalues of operators which are not necessarily bounded below. Let λ be a non-degenerate eigenvalue of a Hermitian operator H and let $\alpha<\beta$ be two numbers such that the interval (α, β) contains λ but no other points of the spectrum of H. Let w be an approximate eigenfunction and calculate

$$\eta=(w, Hw)/\|w\|^2, \quad \epsilon=\|(H-\eta)\|/\|w\|.$$

Then we can show that

$$\eta-\frac{\epsilon^2}{\beta-\eta}\leqq\lambda\leqq\eta+\frac{\epsilon^2}{\eta-\alpha}, \tag{1}$$

provided $\epsilon^2<(\eta-\alpha)(\beta-\eta)$.

This formula is symmetric with respect to upper and lower bounds, as it should be. If in particular λ is the lowest eigenvalue, we can put $\alpha=-\infty$ and (1) reduces to the Ritz-Temple formula. It should be noted that (1) gives λ within the error of the order ϵ^2, which is very small if ϵ is small, i.e. w is a good approximate eigenfunction. Also we can show that (1) is in precision not behind any of the formulas cited above,[1] so long as the latter is not incorrect. In fact, it can even be shown that (1) is the best possible estimate if η, ϵ, α and β are the only available data.

Another advantage of (1) is that it can be applied to higher eigenvalues without the preliminary procedure of orthogonalization which is necessary in the Ritz method.

We can also estimate the error of the approximate eigenfunction w. Further (1) can be generalized to the case of degenerate eigenvalues.

These formulas proved to be very useful in approximate solution of eigenvalue problems of various kinds. For instance, they give much more narrow range of errors than hitherto supposed in the calculation of eigenvalues by the relaxation method.[2] Also we hope that they can successfully be applied to problems of quantum mechanics. Their application to the eigenvalue problem of the deuteron with the meson potential is now in progress.

Detailed account will appear shortly in Journal of the Physical Society of Japan.

[1] G. Temple, Proc. Lond. Math. Soc. **29**, 257 (1928); Proc. Roy. Soc. **119**, 276 (1928); D. H. Weinstein, Phys. Rev. **40**, 797 (1932); **41**, 839 (1932); Proc. Nat. Acad. Sci. **20**, 529 (1934); F. Trefftz, Math. Ann. **108**, 595 (1933); J. K. L. MacDonald, Phys. Rev. **46**, 828 (1934); W. Romberg, Physik Zeits. Sowjetunion **8**, 516 (1935); **9**, 546 (1936); R. A. Newing, Phil. Mag. **24**, 114 (1937); A. F. Stevenson, Phys. Rev. **53**, 199 (1938); G. Horvay, Phys. Rev. **56**, 214 (1939); L. Collatz, Zeits. f. angew. Math. Mech. **19**, 224, 297 (1939); E. Kamke, Math. Zeits. **45**, 788 (1939); G. Temple and W. G. Bickley, *Rayleigh's Principle and Its Applications to Engineering* (London, 1933).
[2] R. V. Southwell, *Relaxation Methods in Engineering Science* (Oxford University Press, London, 1940).

Neutrons from $Li^7(p,n)Be^7$ *

V. R. JOHNSON, M. J. WILSON LAUBENSTEIN, AND H. T. RICHARDS
University of Wisconsin, Madison, Wisconsin
December 23, 1949

IF nuclear forces are charge independent, one expects Be^7 to have a low lying level equivalent to the well-known 478-kev level in its mirror nucleus, Li^7. Earlier work by one of us[1] on the neutrons from $Li^7(p,n)Be^7$ failed to detect such a level. However, with the old Ilford halftone emulsions then available, the observed neutron group was very asymmetric and was approximately 700 kev in half-width; hence neutrons of energy corresponding to Be^7 excited could easily have been missed if of low intensity.

Recently, Grosskreutz and Mather[2] reported from this same reaction neutron groups corresponding to levels in Be^7 at 205 kev, 470 kev, and 745 kev, and comparable in intensity to the main group. Because of the importance of this result on the charge independence hypothesis of nuclear forces, we have re-examined this spectrum with the improved post-war nuclear emulsions. Thin (30–60 kev thick) targets of metallic lithium evaporated upon a tantalum backing were bombarded by 3.34-Mev and 3.96-Mev homogeneous protons from the Wisconsin electrostatic generator. 100 micron thick Eastman NTA emulsions (glass-backed) were mounted 15 cm from the target and at 0° and 60° to the proton beam.

After processing, the tracks were measured in a microscope with an oil immersion objective to achieve minimum depth of focus. The observed recoil proton energy, E_p, is equal to $E_n\cos^2\theta$, where E_n is the neutron energy and θ is the angle of recoil with respect to the incident neutron. If the incident neutron is along the x axis and y is in the plane of the emulsion, then

$$\tan\theta=(R_z^2+R_{xy}^2\sin^2\chi)^{\frac{1}{2}}/R_{xy}\cos\chi,$$

where R_z is the z projection of the track, R_{xy} is the projection on the xy plane, and χ is the angle R_{xy} makes with the x axis. R_z is the only one of these quantities difficult to measure accurately. Experimentally we observed the uncertainty in R_z to be about 0.5 micron, which uncertainty must be multiplied by a factor 2.5 because of the shrinkage of these concentrated emulsions upon processing. To minimize this resultant uncertainty in θ, we therefore accepted only tracks with a dip angle in the processed emulsion of $\leq 3°$. Recoils out to $\chi=15°$ were, however, accepted since

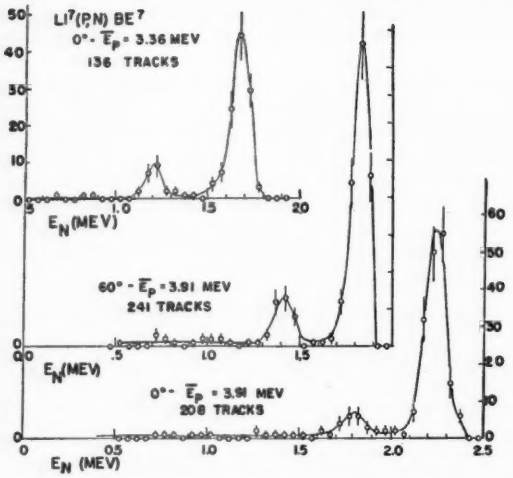

FIG. 1. Energy of neutrons from $Li^7(p,n)Be^7$.

this angle could be measured by our goniometer eyepiece to better than a degree.

Our observed mean ranges (appropriately corrected for recoil angle) were used in conjunction with the accurately known neutron energies to obtain three points on a range energy curve for the NTA emulsions. These data agreed within a few percent with the data for Ilford "Nuclear Research" emulsions,[3] so the shape of the latter curve was used to extrapolate our data to lower energies.

Our data plotted in energy intervals is shown in Fig. 1. Two groups of neutrons are clearly resolved on all the data and correspond to a level in Be^7 at 435±15 kev. This value is in agreement with that recently reported[4] for this same level as produced in the $B^{10}(p,\alpha)Be^7$.

The observed relative intensity of the low energy group (when corrected for $n-p$ scattering cross section) is 0.09±0.02 for the 0°, E_p=3.91-Mev data; 0.16±0.03 for the 60° data; and 0.17±0.05 for the 0°, E_p=3.31-Mev data. The indicated statistical uncertainty in the above ratio is, we feel, less by probably a factor of two than the true uncertainty. The cause of this additional uncertainty is the difficulty of applying uniformly for short and long tracks the criteria that the dip angle $\lesssim 3°$.

* This work was supported in part by the AEC and in part by the Wisconsin Alumni Research Foundation.

[1] See Fig. 1 of LADC-32 or MDDC-39(Perlman, Richards, and Speck).
[3] J. C. Grosskreutz and K. B. Mather, Bull. Am. Phys. Soc. 24, No. 7, 15 (1949).
[3] Lattes, Fowler, and Cuer, Proc. Phys. Soc. London 59, 883 (1947).
[4] Brown, Chao, Fowler, and Lauritsen, Bull. Am. Phys. Soc. 24, No. 8, 11 (1949); also T. Lauritsen and Thomas, *ibid.*

The Electromagnetic Concentration of Be^{10}

C. P. KEIM, H. W. SAVAGE, AND BOYD WEAVER
Y-12 Research Laboratory, Carbide and Carbon Chemicals Corporation, Oak Ridge, Tennessee
December 23, 1949

Be^{10} present as a small fraction in Be^9 irradiated in the pile has been successfully enriched by the electromagnetic process. The weak specific activities in the beryllium charge material used in the electromagnetic separation indicated that the Be^{10} was present to the extent of about one part in 500,000. After the Be^{10} was enriched in the calutron, the specific activity of the enriched Be^{10} showed that it had been given an enrichment factor* of 870 and 1200 in the two samples processed. This enriched material has made it possible to determine the interesting beta-spectrum of Be^{10}. (These spectral results are being reported by D. J. Hughes, Argonne National Laboratory, and P. R. Bell, Oak Ridge National Laboratory, in separate letters.)

A few milligrams of beryllium enriched in Be^{10} were obtained from the calutron separations. Although calutron data indicated enrichment factors in excess of 3000, some cross contamination took place to dilute the product. Among the factors which contributed to the success of this enrichment were: a careful preparation of anhydrous beryllium chloride; the use of specially prepared spectroscopically pure isotope collectors; accurate process control to obtain high ion beam resolution; quantitative refinement of the enriched isotopic beryllium; and strict adherence to safety precautions to protect personnel from beryllium compounds.

Although this achievement was the result of the combined efforts of a large part of the personnel in the Isotope Research and Production Division, Y-12 Research Laboratory, particular credit is due W. C. Davis, who prepared some of the beryllium chloride and who did the chemistry on some of the enriched beryllium, L. O. Love, who with his associates, conducted the calutron operations, and S. F. Fairbourne, who with Mr. Love, directed certain chemical and calutron services. Especial appreciation is due D. J. Hughes and C. Eggler, Argonne National Laboratory, and P. R. Bell, Oak Ridge National Laboratory, who supplied the irradiated beryllium and some of the beryllium chloride to be used as charge material in the calutron and who provided the enrichment factors based on the specific activities they obtained.

This report is based on research carried out under contract for the AEC by the Isotope Research and Production Division at the Carbide and Carbon Chemicals Corporation, Y-12 Research Laboratory, Oak Ridge, Tennessee.

* Enrichment factor is the ratio Be^{10}/Be^9 in the product beryllium to the ratio Be^{10}/Be^9 in the starting beryllium.

General Relation between Genuine and Chance Coincidences and Its Application to Measurement of High Activity Sources

Z. BAY*
George Washington University, Washington, D. C.
AND
M. M. SLAWSKY
National Bureau of Standards, Washington, D. C.
December 19, 1949

IN an attempt to set up a useful standard radioactive source it was decided to use the coincidence method for the measurement of about one millicurie of Co^{60}. The problem of measuring a large source by this method presents several experimental difficulties. In the process of resolving these difficulties a very general relationship between the genuine coincidences N_g, and chance coincidences N_c, was derived by one of us.[1] At the same time the necessity of measuring the number of events registered in the individual channels of the coincidence device was eliminated.

In general, the difficulties of this type of measurement can be attributed to the fact that the equipment is required to have the highest possible resolution and efficiency. For this reason we used two electron multipliers feeding directly into a high resolution coincidence circuit.[2] It was felt that any addition to the coincidence circuit, in order to measure the number of counts in each channel, would have the undesirable effect of (1) distorting the pulse shape, thus increasing the response time and (2) discriminating against some coincidences which otherwise would have been recorded,

thus in effect reducing the efficiency of the circuit. Therefore, a procedure was devised for measuring N_0, the disintegration rate of the source, without the determination of the counting rates N_1 and N_2 in the individual channels.

The total number of coincidences N is given, under conditions discussed elsewhere,[3] by the well-known equation,[4]

$$N=N_g+N_c=(N_1N_2/N_0)+2N_1N_2\tau, \tag{1}$$

where τ is the resolving time. It is apparent from this equation that it is not necessary to measure N_1 and N_2 if a measurement of N_c and τ is made. For strong sources the measurement of N_c is necessary in any case and therefore involves no additional effort. The difference in the procedure is simply the substitution of a determination of τ for the determination of N_1 and N_2. The disintegration rate is then given by:

$$N_0=N_c/2\tau N_g. \tag{2}$$

It was in the determination of τ that it became evident that the resolving time had to be redefined. The meaning of τ and N_g becomes ambiguous when there are (1) pulses of unequal size with varying probability of being recorded as coincidences and (2) randomly distributed delays in the counters and the coincidence circuit.

Fortunately, the whole difficulty of the definition of τ and N_g can be avoided as shown in reference 1 by the equation:

$$N_c=N_0\int_{-\infty}^{+\infty}N_g(T)dT, \tag{3}$$

where T is the time delay deliberately put in either channel, $N_g(T)=N(T)-N_c$ as a function of T. Equation (3) gives N_0 to any desired accuracy[3] in terms of directly measurable quantities.

The integral in Eq. (3) is proportional to N_0 and independent of any time delays in the source or in the equipment. Therefore, it gives (1) a definition of the resolving time to be used in determining the presence of genuine coincidences and in the measurement of decay constants, and (2) the value of N_0 regardless of any kind of time delays, whether they are in the source or in the equipment. That is, N_0 can be determined for a source when there is a delay between the related particles emitted, such as by the parent and the daughter in a radioactive decay series.

* This author's work supported by the ONR.

[1] Z. Bay (to be published).
[2] Z. Bay and G. Papp, Rev. Sci. Inst. 19, 565 (1948).
[3] M. M. Slawsky (to be published).
[4] J. V. Dunworth, Rev. Sci. Inst. 11, 167 (1940).

On the Motion of Particles in a Traveling Wave Linear Accelerator*

JOHN R. TERRALL
Massachusetts Institute of Technology, Cambridge, Massachusetts
September 19, 1949

IN the linear motion of a point charge, unless the energy of the charge changes by mc^2 or greater in a distance of the order of e^2/mc^2,[1] the particle's own field, which gives rise to radiative effects, may be neglected in the Lorentz equations of motion

$$dp^\mu/ds=(e/mc^2)F^{\mu\nu}p_\nu$$
$$(p^\mu=dx^\mu/ds=\text{energy}-\text{momentum vector}/mc^2). \tag{1}$$

Thus, in a linear accelerator we may safely regard $F^{\mu\nu}$ as the external field alone.

Now, a traveling wave field moving with phase velocity β_w along the $x'(\equiv x)$ direction is written as a function of the Lorentz invariant phase $\phi=k_\mu x^\mu=\omega t-kx$. Only the component $F^{14}=-F^{41}=\epsilon f(\phi)$ of the field is effective in changing the energy of particles in motion along the x direction. Here ϵ is the magnitude of the electric field in the x direction. Integration of Eq. (1) with β_w constant will give the energy of a particular particle from the equation

$$E-\beta_w(E^2-1)^{\frac{1}{2}}+U(\phi)=H, \tag{2}$$

where

$$E\equiv(1-\beta^2)^{-\frac{1}{2}}=(\text{kinetic plus rest energy})/mc^2$$

and

$$U(\phi)=\frac{e\epsilon/k}{mc^2}\int f(\phi)d\phi=\epsilon\int f(\phi)d\phi. \tag{3}$$

$p=mc^2(E^2-1)^{\frac{1}{2}}$ is the algebraic momentum of the particle and changes sign if the direction of motion reverses. The term $\beta_w(E^2-1)^{\frac{1}{2}}$ appears in Eq. (2) when we use a fixed system of coordinates with respect to which the wave field is moving. It can be transformed away by using a Lorentz system moving with respect to the fixed system with velocity β_w in the x direction. The term mc^2H is a constant of the motion (with respect to ϕ), the Hamiltonian of the particle, and from Eq. (2) we find that p and $-\phi/k$ are conjugate momentum and coordinate.

Equation (2), when solved for the energy E, gives the following results:

$$E(\phi)=\begin{cases}(1-\beta_w^2)^{-1}\{\chi(\phi)\pm\beta_w[\chi^2(\phi)-(1-\beta_w^2)]^{\frac{1}{2}}\}\cdots\beta_w\neq1,\\ \frac{1}{2}\{\chi(\phi)+[1/\chi(\phi)]\}\cdots\beta_w=1,\end{cases} \tag{4}$$

where

$$\chi(\phi)=H-U(\phi). \tag{5}$$

Plots of $(E(\phi)-1)^{\frac{1}{2}}=p/mc$ are given by Slater[2] for two cases of a sinusoidal field $\epsilon\sin\phi$: $\beta_w=0.5$ and $\beta_w=1$. Equations (4) represent the kinematical trajectory in energy-wave phase space of a particle under the influence of the field. An important consequence of these equations is that a particle has no chance of attaining unlimited kinetic energy unless the accelerating wave is traveling with the speed of light ($\beta_w=1$), for $|\chi(\phi)|$ must be bounded in the physical problem (if $k\neq0$). Even for $\beta_w=1$, the initial conditions (which determine H) must be such that a certain real relative phase ϕ exists for which $U(\phi)\rightarrow H$, in order that unlimited energy be kinematically possible.

In Eq. (4), if $\beta_w\neq1$, we see that only when $\chi^2(\phi)-(1-\beta_w^2)$ is positive will there be real (and hence physical) solutions for the energy $E(\phi)$. If $\beta_w>1$, any particle can kinematically assume all values of relative phase. This is nothing more than the physical fact that a particle can never travel as fast as the field in this case —it will continually slip back in relation to a point moving with the wave. If $\beta_w<1$, there can be (depending on H) certain relative phases for a given particle for which the radical is imaginary. Particles in this category can never advance, or fall behind the wave, beyond a phase for which the radical vanishes. Physically this means that certain particles may be, so to speak, "locked" to the wave in closed orbits. For $\beta_w=1$, those particles will be locked for which ϕ is real in the equation $U(\phi)=H$.

The dynamical solution of Eq. (1), that is, energy as a function of distance traveled in the field, is obtained by integrating

$$dE/dx=(e/mc^2)F^{14}=kdU/d\phi,$$

which gives

$$\int\frac{dE}{(dU/d\phi)(E)}=kx.$$

For a sinusoidal field, the shape function $f(\phi)$ is a circular function so that

$$\left(\frac{dU/\epsilon}{d\phi}\right)^2+(U/\epsilon)^2=1$$

and we have

$$(\pm)\int_{E_0}^{E(x)}\frac{dE}{[\epsilon^2-\{E-\beta_w(E^2-1)^{\frac{1}{2}}-H\}^2]^{\frac{1}{2}}}=k(x-x_0). \tag{6}$$

We must bear in mind that if the momentum $(E^2-1)^{\frac{1}{2}}$ changes sign, the integral will lead to a negative contribution to x. The integral in Eq. (6) is, in general, elliptic.

For a $\beta_w=1$ accelerator we have observed that very high energies are theoretically attainable by some of the particles. The energy

of those particles for which ϕ is real in $U(\phi)=H$ will, for a sinusoidal field at least, approach asymptotically a linear function of distance, as may be seen in the following:

$$E^2\gg 1: \quad E-(E^2-1)^{\frac{1}{2}}\rightarrow 1/2E.$$

Thus, for high energy,

$$\left.\begin{matrix}\beta_w=1\\ E^2\gg 1\end{matrix}\right): \quad \frac{dE}{dx}\rightarrow k[e^2-\{(1/2E)-H\}^2]^{\frac{1}{2}},$$

$$\left.\begin{matrix}\beta_w=1\\ E^2\gg 1\\ E\gg 1/2H\end{matrix}\right]: \quad \frac{dE}{dx}\rightarrow k[e^2-H^2]^{\frac{1}{2}}=\text{constant}.$$

A more general solution of the dynamical motion, which is equivalent to Eq. (6) for a sinusoidal field, is that obtained by finding $\phi(x)$. This solution is:

$$\left.\begin{aligned}&\beta_w\neq 1: \quad (1-\beta_w^2)^{-1}\int_{\phi_0}^{\phi(x)}d\phi\left\{\frac{\pm\beta_w\chi(\phi)}{[\chi^2(\phi)-(1-\beta_w^2)]^{\frac{1}{2}}}-1\right\}=kx,\\ &\beta_w=1: \quad \int_{\phi_0}^{\phi(x)}\frac{d\phi}{\chi^2(\phi)}-[\phi(x)-\phi_0]=2kx,\end{aligned}\right\} \quad (7)$$

where the $\pm$ sign depends on which branch of the $E(\phi)$ curve in Eq. (4) the particle is orbiting. Here there are no restrictions on the shape function $f(\phi)$ of the field, from which $\chi(\phi)$ is obtained. When Eq. (7) is solved for $\phi(x)$, we can then use Eq. (3) to find $U[\phi(x)]$ and finally Eq. (2) to get $E(x)$. The expressions in Eq. (7) might be called the equations of bunching.

It is a general result of the foregoing solutions that the energy spectrum of a beam of particles from a traveling wave linear accelerator is a strong function of the initial phase spread of the beam so that pre-bunching is a necessity for any appreciable final energy homogeneity of the beam.

Detailed considerations of all the above questions will be taken up in a forthcoming paper.

* This work has been supported in part by the Air Materiel Command, the Army Signal Corps, and the ONR.

[1] See J. Schwinger, Phys. Rev. 75, 1912 (1949).
[2] J. C. Slater, Rev. Mod. Phys. 20, 505, 508 (1948).

Note on Nuclear Models

HOFF LU
University of Chekiang, Hangchow, China
November 21, 1949

NUCLEAR models in which the protons are concentrated on or near, or uniformly distributed over, the surface of a sphere have been recently proposed by several investigators.[1-3] For the same value of Coulomb repulsion energy, a given nucleus represented by such a neutron-core model will be smaller than that by the usually assumed model in which the protons are uniformly distributed over the volume of a sphere. In other words, the new model will yield a smaller value of r_0 in the formula $r=r_0A^{\frac{1}{3}}$ for nuclear radii than the customary model, when it is computed either from the semi-empirical binding-energy equation[4] or from a comparison of the binding energies of contiguous isobars.[5]

Assume the protonic charge be uniformly distributed over the surface. Then, the constant coefficient of the Coulomb energy term in the semi-empirical equation[4] is $a_3=\frac{1}{2}(e^2/r_0)$ instead of $a_3\approx(3/5)(e^2/r_0)$ so that with the value of a_3 given in Lapp and Andrews' book, we find, for this neutron-core model,

$$r_0=1.23_{+}\times 10^{-13}\text{ cm},$$

and, for the customary model, $r_0=1.48\times 10^{-13}$ cm. Also, the difference in Coulomb energy of two contiguous isobars due to the additional repulsion of the extra proton in the Coulomb field of the isobar with the lower Z is now $C=(Z+\frac{1}{2})e^2/r$ instead of $C=(6/5)Ze^2/r$ so that, with Bethe's value of C for ${}_7N^{13}-{}_6C^{13}$, we have, for this neutron-core model,

$$r_0=1.34_{-}\times 10^{-13}\text{ cm},$$

instead of 1.47×10^{-13} cm obtained by Bethe for the customary model. The two results from the new model do not appear to agree as well as those from the customary model. This, however, is not entirely unexpected, since for a nucleus as light as C^{13} our new model with charge spread over a surface layer cannot be anything but a very crude model, and we should expect that, for the isobar N^{13} having the extra proton, a model with a proton on the surface of the C^{13} model should be closer to the true situation. Thus, by considering the charge of the extra proton to remain unspread, we have $C=Ze^2/r$, giving $r_0=1.23_{-}\times 10^{-13}$ cm, which brings the two results in agreement again.

Comparing the above results with the value $r_0\approx 1.5\times 10^{-13}$ cm for most α-emitters as given by Gamow's theory of α-decay, one may, at first sight, stick to the customary model. However, on our proton-shell model, one should expect that the radius, R, of a nucleus of mass number A as defined in Gamow's theory should be equal to our model radius, r, for a nucleus of mass number $(A-4)$ plus an effective radius, r_α, of α-particle. Since r_α cannot be well defined, and since our formula

$$r=1.23\times 10^{-13}A^{\frac{1}{3}}\text{ cm} \quad (1)$$

is not expected to hold for very light nuclei, we may calculate r_α from the values of R and r. A more accurate calculation of the nuclear radii of α-emitters have been recently made by Preston.[6] His values of R give r_0 that range from 1.28 (ThC–ThC″) to 1.62×10^{-13} cm (Th−MsTh$_1$) with a great majority of cases having r_0 around 1.5×10^{-13} cm. Using these values of R, we find r_α to range from 0.28 to 2.4×10^{-13} cm with a great majority of cases within 1.7 to 1.8×10^{-13} cm. These latter values are somewhat less than 1.96×10^{-13}, the value given by (1). This is reasonable since ${}_2He^4$ is very tightly bound as is well known (it is the only element hitherto unaffected by neutron bombardment).

Recently, Fernbach *et al.*,[7] using data of scattering of fast neutrons by nuclei from Li to U, have shown that $r_0=1.37\times 10^{-13}$ cm. Weisskopf and Ewing[8] have also obtained the best fit of data on the anomalous scattering of protons by medium weight nuclei by assuming $r_0=1.3\times 10^{-13}$ cm. These values are in better agreement with ours than what the customary model gives.

Therefore, it appears likely that the proton-shell neutron-core model is closer to the true nuclear structure than the customary model.

[1] J. G. Winans, Phys. Rev. 71, 379 (1947); 72, 435 (1947).
[2] B. Davison and W. H. Watson, Phys. Rev. 71, 742 (1947).
[3] I. N. Sneddon and B. F. Tonschek, Proc. Camb. Phil. Soc. 44, 402 (1948).
[4] R. E. Lapp and H. L. Andrews, *Nuclear Radiation Physics* (Prentice-Hall, Inc., 1948) p. 146, Eqs. (7) and (8).
[5] H. A. Bethe, Phys. Rev. 54, 436 (1938).
[6] M. A. Preston, Phys. Rev. 69, 535 (1946).
[7] Fernbach, Serber, and Taylor, Phys. Rev. 75, 1354 (1949).
[8] V. F. Weisskopf and D. H. Ewing, Phys. Rev. 57, 472 (1940).

Measurement of Some Weak γ-Ray Intensities

G. R. BISHOP, RICHARD WILSON, AND H. HALBAN
Clarendon Laboratory, Oxford, England
December 19, 1949

WE have measured the intensities of some weak high energy γ-rays by counting the photo-protons produced by the disintegration of deuterium in an ionization chamber counter.[1] The 2.62 Mev γ-ray from Rd Th was used for energy calibration. The intensities have been measured relative to other γ-ray lines

TABLE I. Intensities of some weak γ-rays.

Source	Rd Th* (Th C″)			Radium* (RaC′)	Radium* (RaC″)	Ga_{72}		La_{140}		Mn_{56}		Na_{24}
Half-life	1.9 yr. (3 min.)			$(3\times10^{-7}$ sec.)	(1½ min.)	14.08±0.02 hr.		40.0±0.1 hr.		2.586±0.005 hr.		1490±0.02
Expected energy	3.2	3.13	2.89	3.0	4.0	3.05	3.35	2.5	—	2.66	2.96	4.14
Observed energy	—	—	—	—	—	3.05±0.1	3.35±0.1	2.55±0.05	2.9±0.1	2.7±0.2	3.0±0.1	—
Observed intensity (photons/disintegration)	<0.001	<0.0015	<0.003	<0.0001	<0.05	~0.0013	~0.0003	~0.04	~0.001	~0.001	~0.002	$<5\times10^{-5}$
Theoretical intensity	0.001	0	0	—	1	~0.0004	~0.0004	—	—	0.0003	0.0003	5×10^{-5} or 10^{-3}

* With these sources, the intensities have been expressed in terms of the disintegration of the decay products shown in the brackets.

producing photo-disintegration for those isotopes (Th C″, Ga_{72}, Na_{24}) where this was possible, or otherwise from pile activation data.

The half-lives of some of the sources have been redetermined by a method previously described.[2] In some cases the high energy γ-rays coincided with expected crossover transitions; in other cases the crossover transition was not found.

The results obtained are given in Table I.

Th C″. The theoretical intensity of the high energy lines has been calculated from the decay scheme of Oppenheimer,[3] using the formula for the half-life of an excited state quoted by Segrè and Helmholtz.[4] The results agree with those of Bell and Elliott[5] who also failed to find the lines. The limit of the measurement is set by the neutron background of the source. It is suspected that such a background was the cause of the small (1–3 percent) effect found by Ellis.[6]

Radium C′. This line is suggested by long range α-particle data.[7] The neutron background gives a limit to the accuracy.

Radium C″. We fail to find this line. Observations have been reported by absorption[8] and by Compton recoil in a cloud chamber.[9] Moreover, the energy balance

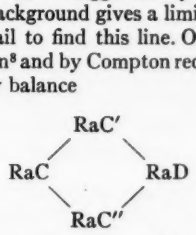

leaves an energy of 5.8 Mev for the RaC″—RaD transition. The β-ray has an energy 1.8 Mev[8,10] in agreement with the assignment on the Sargent diagram.[11] The branching ratio RaC″ to RaC′ is 0.04 percent. Our measurements indicate that the energy balance of 4 Mev is not carried away by γ-rays having an energy which is bigger than 2.8 Mev.

Ga_{72}. These "crossover" lines agree with the expected energies of "crossover" transitions from the decay scheme of Haynes.[12] The 2.21 and 2.51 Mev γ-rays are themselves crossover transitions so that they are probably quadrupoles, and the other γ-rays dipole transitions. The theoretical intensities for the 3.05 and 3.35 Mev crossover γ-rays have been calculated from the formula of Segrè and Helmholtz[4] assuming octupole radiation.

La_{140}. The 2.55 Mev line agrees with the measurements of Wattenberg[13] and Hanson[14] but the 2.9 Mev line has not been reported before. It does not correspond to any crossover energy so it may be due to an impurity. The energy is not, however, consistent with an impurity of Na^{24}.

Mn_{56}. The lines agree with crossover transitions with the established decay scheme (Siegbahn[15]). The 2.7 Mev γ-ray is difficult to locate in the presence of the higher energy γ-ray, but the intensities are in contradiction to the results of Russell.[16] The theoretical intensities are calculated on the assumption of competition of octupole with quadrupole radiation.

Na^{24}. The theoretical intensity of the crossover transition has been calculated by using the spin values assigned by Brady and Deutsch.[17] The 4.14 Mev γ-ray would be a 16-pole in competition with either a quadrupole 2.76 Mev γ-ray or a quadrupole 1.38 Mev γ-ray, giving two possibilities. Our results suggest that the 2.76 Mev γ-ray is emitted first in agreement with the results of inelastic scattering of protons and neutrons;[18] this leads to an intensity for the crossover transition of 5×10^{-5}. The suggestion that the 2.76 Mev γ-ray is a dipole[19] would lead to an intensity of 10^{-3}.

We gratefully acknowledge the cooperation of the Isotope Division, AERE Harwell who supplied the artificial radioactive sources used, and are indebted to Mr. C. H. Collie for interesting discussions.

[1] Wilson, Collie, and Halban, Nature **163**, 245 (1949).
[2] R. Wilson and G. R. Bishop, Proc. Phys. Soc. London **62**, 457 (1949).
[3] J. R. Oppenheimer, Proc. Camb. Phil. Soc. **32**, 328 (1936).
[4] E. Segrè and A. C. Helmholtz, Rev. Mod. Phys. **21**, 271 (1949).
[5] R. E. Bell and L. G. Elliott, Can. J. Research, **A26**, 379 (1948).
[6] C. D. Ellis, Proc. Phys. Soc. London **50**, 213 (1938).
[7] Rutherford, Ward, and Lewis, Proc. Roy. Soc. **A131**, 684 (1931).
[8] Devon and Neary, Proc. Camb. Phil. Soc. **33**, 154 (1937).
[9] S. Nishida, Proc. Phys. Math. Soc. Japan **19**, 809 (1937).
[10] Lecoin and Goldstein, Comptes Rendus **13**, 119 (1936).
[11] N. Feather and H. O. W. Richardson, Proc. Phys. Soc. London, **41**, 452 (1948).
[12] S. K. Haynes, Phys. Rev. **74**, 423 (1948).
[13] Wattenberg, Fields, Russell, and Sachs, Phys. Rev. **71**, 497 (1947).
[14] A. O. Hanson, Phys. Rev. **75**, 1794 (1949).
[15] K. Siegbahn, Arkiv. f. Mat. Astro. Fys. **33A**, No. 10 (1946).
[16] Russell, Sachs, Wattenberg, and Fields, Phys. Rev. **73**, 545 (1948).
[17] E. L. Brady and M. Deutsch, Phys. Rev. **74**, 151 (1948).
[18] E. H. Rhoderick, Nature **163**, 898 (1949); Beghian, Grace, Preston, and Halban, Phys. Rev. **77**, 286 (1950).
[19] E. R. Rae, Phil. Mag. **40**, 1155 (1949).

On the Classification of the Spectrum of Singly Ionized Uranium*

J. RAND MCNALLY, JR.
Carbide and Carbon Chemicals Corporation, Oak Ridge, Tennessee
December 12, 1949

NEW results on the analysis of the spectrum of singly ionized uranium (U II) have been reported recently.[1–3] Numerous earlier reports on this complex spectrum are available.[4–8] It has been found that two, as yet unconnected, systems of energy states exist analogous to the situation in Th II (see Table I).[9,10] The Amsterdam investigators have predicted Group B as being more tightly bound than Group A while the others[8] conclude oppositely.

Van den Bosch[1,3] has searched for energy differences of the order of 20,000 cm^{-1} between these two systems, finds no significant differences, and concludes that the energy separation may be less than this figure. Search for possible levels belonging to the configurations f^3dp and f^2sp and combining with the odd levels of Group B (presumably f^4p) led him to accept as real 17 even levels above 50,000 cm^{-1}, thus placing the low level of Group A roughly 20,000 cm^{-1} above the lowest level of Group B.

However, the inclusion by van den Bosch of approximately eleven arc lines and two lines classified elsewhere as transitions involving these seventeen new high even levels, and his use of a wave-number spread amounting to as much as 0.21 cm^{-1} in one case, as well as the lack of additional supporting data, suggest that most if not all of these seventeen levels are probably fortuitous. Also, the use of Amsterdam wave-length data supple-

TABLE I. Comparison of lowest levels from configurations in U II and Th II.

	U II Configuration	U II Lowest level	Th II Configuration	Th II Lowest level
Group A	$5f^37s^2$	0 cm^{-1}	$6d7s^2$	0 cm^{-1}
	$5f^36d7s$	289	$6d^27s$	1860
	$5f^36d^2$	4585	$6d^3$	7001
Group B	$5f^47s$	(0)	$5f7s^2$	4490
	$5f^46d$	(7850)	$5f6d7s$	6168
			$5f6d^2$	12,486

menting the data of the *M.I.T. Wavelength Tables*[11] increases the opportunity for chance coincidences.

The wave-length data would seem to support the idea that Group A is below Group B by about 2000 to 6000 cm^{-1}. For example, of a total of 45 persistent lines, of which only eleven weak ones remain unclassified, only three have been definitely assigned to the system having four $5f$ electrons.

Search for new levels at Oak Ridge using IBM punched card equipment and about 3000 selected lines from the *M.I.T. Wavelength Tables* has been undertaken in an attempt to discover these important connecting levels. A spotting interval of 0.10 cm^{-1} for recurrences among allowed combinations of listed wave numbers and known levels has turned up numerous fortuitious levels as well as several real ones. Our experience with fortuitous occurrences indicates that the distribution of wave numbers is sufficiently non-random that predictions of the expected number of recurrences are underestimates by about 30 percent.

* This document is based on work performed for the AEC by Carbide and Carbon Chemicals Corporation, at Oak Ridge, Tennessee.

[1] J. C. van den Bosch, thesis, Amsterdam (June, 1948).
[2] J. C. van den Bosch and G. J. van den Berg, Physica **15**, 329 (1949).
[3] J. C. van den Bosch, Physica **15**, 503 (1949).
[4] G. R. Harrison and J. R. McNally, Jr. (private communication), Manhattan Project (January, 1945); Manhattan Project Technical Series (June, 1946).
[5] Ph. Schuurmans, Physica **11**, 419 (1946).
[6] Ph. Schuurmans, thesis, Amsterdam (December, 1946).
[7] Schuurmans, van den Bosch, and Dijkwel, Physica **13**, 117 (1947).
[8] J. R. McNally, Jr. and G. R. Harrison, J. Opt. Soc. Am. **39**, 636A (1949).
[9] McNally, Harrison, and Park, J. Opt. Soc. Am. **32**, 334 (1942); J. R. McNally, Jr., J. Opt. Soc. Am. **35**, 390 (1945).
[10] deBruin, Klinkenberg, and Schuurmans, Zeits. f. Physik **121**, 667 (1943); **122**, 23 (1944).
[11] *MIT Wavelength Tables* (John Wiley & Sons, Inc., New York, 1939).

On the Relativistic Electromagneto-Ionic Theory of Wave Propagation

V. A. BAILEY
School of Physics, University of Sydney, Sydney, Australia
November 21, 1949

DR. L. R. WALKER has very courteously sent me a copy of his letter to the editor in which he discusses a recent paper by J. A. Roberts[1] and makes some critical remarks on my theory of plane waves in an ionized medium which is subjected to static electric and magnetic fields.[2-4] These remarks call for some comment and a brief statement on some recent developments of the theory.

Dr. Walker states first that "Roberts' Eq. (1), a special case of one derived by Bailey, is said to be non-relativistic, . . ." and later states that "It would appear that an inconsistent neglect of relativistic terms affects the nature of the plane wave solutions quite radically."

In the first statement the phrase "is said" implies doubt. Since the only alternative to the adjective "relativistic" is "non-relativistic" and the first adjective is certainly not applicable to my equation this doubt is not justified. There can be only one relativistic dispersion equation and all other proposed equations which are not exactly equivalent to it must be non-relativistic. These others may differ among themselves as to the number of terms in U^2/c^2 which they neglect, where U is the electron drift velocity, and there is no *a priori* reason to suppose that the equation which neglects all such terms provides the best insurance against erroneous conclusions. Dr. Walker's second quoted statement seems to imply that there is such an *a priori* reason.

The dispersion equation in question was originally developed on substantially the same lines as the dispersion theory of H. A. Lorentz and the magneto-ionic theory of Appleton, Nichols and Schelling and others. These authors unhesitatingly combined Maxwell's field equations, which they knew to be relativistic, with the non-relativistic equation of motion of the electrons. As yet nobody has charged them with "an inconsistent neglect of relativistic terms." Perhaps the term "inconsistent" is used by Dr. Walker to mean "incomplete."

One of the principal applications of the theory is to the sun's atmosphere near active sunspots. As Giovanelli[5] has suggested that in such regions the electrons may attain velocities comparable with that of light it early became clear that the relativistic theory would require to be developed. This was done in July last but was temporarily left dormant on account of the pressure of other work. Then early in September I learned from Dr. Walker that he had developed the relativistic theory for the medium without a magnetic field and so arrived at the conclusions referred to above. It now seems desirable to set out briefly the results of my own work.

Relative to a system of reference K' in which the electrons have no drift motion the dispersion equation is derived for a plane wave of the form

$$A' \exp(i(\omega' t' - L'l'x' - L'm'y')), \tag{1}$$

where l', m' are direction cosines and both ω' and L' may be complex numbers. (This yields a generalization of the well-known magneto-ionic equation.) On transforming this equation and (1), by means of the Lorentz transformation, to a parallel system of reference K moving relatively to K' along $O'x'$ with the velocity $-U$, the following equation is obtained for the dispersion of a wave of the form

$$A \exp(i(\omega t - Llx - Lmy)), \tag{2}$$

where ω is now always taken as real:

$$XY^2 - (\beta^2\Omega_x^2 + \Omega_T^2)\beta RZY + (\beta^2 S\Omega_x + Lm\Omega_y)^2 Z(c^2p_0^2 + \tau Z) = 0, \tag{3}$$

where

$$X = \beta^2R^2 - \tau c^{-2}(Z + \beta^2R^2) - p_0^2 - i\beta^2\nu R,$$
$$Y = BR(Z + p_0^2) - i\beta\nu Z, \quad \beta = (1 - U^2/c^2)^{-\frac{1}{2}},$$
$$Z = c^2L^2 - \omega^2, \quad R = \omega - Ull, \quad S = Ll - \omega U/c^2,$$
$$p_0^2 = 4\pi N_0 e^2/m_0, \quad \boldsymbol{\Omega} = (-e/\beta m_0 c)\mathbf{H}, \quad \Omega_T^2 = \Omega_y^2 + \Omega_z^2,$$

N_0 is the rest density of the electrons, each of charge e and rest-mass m_0, $\mathbf{H}$ is the static magnetic field, ν is the collision-frequency, τ is one-third of the mean square velocity of electron agitation, and (l, m, o) are the direction-cosines of the direction of propagation.

When $U^2 \ll c^2$, $\tau \ll c^2$ and the frame of reference is changed by rotation about Oz until Ox is parallel to the direction of propagation (3) is transformed to the following approximate equation of dispersion of a wave of the form $A \exp(i(\omega t - Lx))$:

$$XY^2 - \Omega^2RZY + (L\Omega_x - c^{-2}\omega\mathbf{U}\cdot\boldsymbol{\Omega})^2 Z(c^2p_0^2 + \tau Z) = 0. \tag{4}$$

This differs from the original non-relativistic equation (reference 4, Eq. (2)) only by quantities which are of the second and higher orders of smallness in U and τ. We therefore conclude that when $U^2 \ll c^2$, $\tau \ll c^2$ the original equation with the terms in U_T^2 omitted is a good approximation to the relativistic one. The omission of the terms in U_T^2 is in general unimportant since these are always small compared with certain others in the same equation. But in Roberts' special case of oblique propagation with $H = 0$, $\tau = 0$ and $\nu = 0$ they lead to what is now seen to be an erroneous conclusion.

Nevertheless Roberts was fully justified in obtaining this as a logical deduction from the only developed theory then available for his purpose.

The derivation in detail of the relativistic equation given above will be published later.

[1] J. A. Roberts, Phys. Rev. **76**, 340 (1949).
[2] V. A. Bailey, J. Roy. Soc. N.S.W. **82**, 107 (1948).
[3] V. A. Bailey, Austral. J. Sci. Research **1**, 351 (1948).
[4] V. A. Bailey, Phys. Rev. **75**, 1104 (1949).
[5] R. G. Giovanelli, Nature **161**, 133 (1948).

Calculation of Decay Times from Coincidence Experiments

Z. Bay*
George Washington University, Washington, D. C.
December 12, 1949

USING delayed coincidence circuits for the measurement of short radioactive half-lives one has to measure the genuine coincidence rate N_ϑ as a function of an artificial delay time T deliberately put in either channel. The mean life Θ has to be calculated from the delay curve $N_\vartheta(T)$ of the experiment.

Such calculations[1,2] are generally based on some assumptions or knowledge concerning the time delays in the equipment and concerning the resolving time τ. The result of the calculations is a theoretical delay curve, which can be compared with the measured delay curve.

It is easy to show that Θ can be calculated in a simple way without knowing the time delays within the equipment, without knowing τ, and without using any theoretical delay curves.

Our method is based on the calculation of the moments of delay curves. It will be proved in another paper[3] that all the moments of the delay curve $N_\vartheta(T)$ can be calculated from the moments of two curves:

1. A delay curve $\nu_\vartheta(T)$ which is measured under the condition that the corresponding event (which give counts in the individual channels) have no time delay between them (e.g., γ–γ-coincidences with negligible time delay or a single particle which traverses both counters). $\nu_\vartheta(T)$ is thus the characteristic delay curve of the equipment.

2. The curve giving the probability $p(t)dt$ of the time delay between t and $t+dt$ of the two events in the actual decay-experiment (e.g., in a decay experiment, where the parent gives counts in one channel and the daughter with the mean life Θ gives counts in the other channel, $p(t)=(1/\Theta)\exp(-t/\Theta)$.

Measuring $N_\vartheta(T)$ and $\nu_\vartheta(T)$ we normalize both to the same area, i.e.,

$$\int_{-\infty}^{+\infty} N_\vartheta(T)dT=\int_{-\infty}^{+\infty}\nu_\vartheta(T)dT=I. \tag{1}$$

Then,

$$M^{(n)}[N_\vartheta(T)]=M^{(n)}[\nu_\vartheta(T)]M^{(0)}[p(t)]+\binom{n}{1}M^{(n-1)}[\nu_\vartheta(T)]M^{(1)}[p(t)]+\cdots+\binom{n}{n-1}M^{(1)}[\nu_\vartheta(T)]M^{(n-1)}[p(t)]+M^{(0)}[\nu_\vartheta(T)]M^{(n)}[p(t)], \tag{2}$$

where we use the well-known definition:

$$M^{(n)}[f(x)]=\int_{-\infty}^{+\infty}x^n f(x)dx. \tag{3}$$

Equations (2) are valid under the most general circumstances,[3] e.g., when equal or unequal time delays, due to different decay times, occur in both counting channels. In such cases $p(t)$ is composed of the different decay functions.

The use of (2) permits the determination of all the moments of $p(t)$ and hence $p(t)$ is completely determined.

To show the use of (2) in the simple case given above (parent gives counts in one channel, daughter with a mean life Θ in the other), we take the first moment:

$$M^{(1)}[N_\vartheta(T)]=M^{(1)}[\nu_\vartheta(T)]+I\Theta.$$

Thus:

$$\Theta=\frac{M^{(1)}[N_\vartheta(T)]}{I}-\frac{M^{(1)}[\nu_\vartheta(T)]}{I}, \tag{4}$$

which states that the "center of gravity" of the delay curve in a decay experiment will be displaced by the mean life of the daughter substance. If the delay curve of the equipment in symmetric around $T=0$, then Θ is simply the "center of gravity" of the delay curve of the decay experiment. It is obvious that Θ can be determined accurately in this way from measurable quantities, even if the $N_\vartheta(T)$ and $\nu_\vartheta(T)$ curves overlap appreciably, in which case one usually says that Θ is smaller than the resolving time τ of the equipment.

When the counts from the same daughter substance appear in both channels (e.g., γ–γ-experiments), we get symmetric delay curves and use the second moment of the delay curves for the determination of Θ. In experiments, where two or more decay processes occur, we take more moments for the calculation of the decay constants.

* The author's work is supported by the ONR.
[1] F. W. Van Name, Phys. Rev. **75**, 100 (1949).
[2] D. Binder, Phys. Rev. **76**, 856 (1949).
[3] Z. Bay (to be published).

On the Energy Spectrum of Heavy Nuclei in Primary Cosmic Radiation

M. S. Vallarta
Instituto de Física, Universidad de México, México, D. F.
November 14, 1949

BRADT and Peters[1] have obtained recently the intensity of heavy nuclei in primary cosmic radiation reaching the earth at 55° and 30° north geomagnetic latitudes. According to their figures, the ratio I/I' of the intensities at these two latitudes is 4 for helium, 3.4 for carbon, nitrogen, and oxygen, and 3.5 for nuclei of atomic number greater than 10. The difference between these ratios is not significant and lies within the experimental error.

If one assumes that most of the heavy nuclei in the experiment of Bradt and Peters reach the point of observation at an angle not greater than 30° from the zenith, one can attempt to make an estimate of the energy spectrum of the heavy nuclei, assumed to be of the form K/E^γ, using for this purpose the geomagnetic latitude effect for particles arriving essentially in the vertical direction.

The principle of this analysis has already been outlined.[2] To begin with, the geomagnetic effects depend only on the value of the energy of the particle measured in Störmers. Therefore, the energy in Störmers is first converted into energy in more usual units, say in Bev, for different values of Z from $Z=2$ to $Z=30$. Knowing these, one can plot curves giving the geomagnetic cut-off at the two latitudes as a function of the atomic number Z. The results of our calculation are contained in Table I.

TABLE I. Cut-off energy.

Z	2	6	8	10	15	20
Cut-off at 55° (Bev)	1.4	4.2	5.6	7.0	10.5	14.0
Cut-off at 30° (Bev)	14	42	56	70	105	140
γ	1.60	1.53	1.53	1.53	1.56	1.56

The difference of γ between $Z=2$ and $Z=20$ does not seem to be significant. The average value of γ is 1.64. Thus their spectrum is not significantly different from that of the primary protons which seem to constitute the majority of the primary cosmic radiation.

It is obvious that the result reported here is only a first approximation and is subject to revision. For clearly, the photographic plate is a very poor directional instrument and, in addition, there are at present only two measured points on the curve of the latitude effect of the heavy nuclei.

It is a pleasure to thank Professor J. R. Oppenheimer for his kind hospitality at the Institute for Advanced Study.

[1] H. E. Bradt and B. Peters (private communication). I am indebted to the authors for informing me of their results before publication. These figures seem to agree with the results of the University of Minnesota's group reported at the Chicago meeting of the American Physical Society, November, 1949.
[2] Vallarta, Perusquía, and de Oyarzábal, Phys. Rev. **71**, 393 (1947).

Longitudinal Photons in Quantum Electrodynamics

F. J. Dyson
University of Birmingham, England
December 12, 1949

IN the covariant electrodynamics of Tomonaga and Schwinger[1] considerable complications are introduced whenever the effects of longitudinal and transverse photons are considered separately. Schwinger has pointed out that such a separation is in practice unnecessary, but he has been obliged to start from a treatment with separation in order to demonstrate that a treatment without separation is permissible.[2] Another discussion of the question was given by Hu,[3] but again an elimination of the longitudinal field had to be performed in order finally to show that such an elimination was unnecessary. In the radiation theory of Feynman[4] the longitudinal and transverse photons are never separated; but the argument justifying this procedure[4a] is not immediately applicable to the Schwinger formalism. The present author's formal proof[5] of equivalence of the Schwinger and Feynman theories takes for granted the validity of the unseparated treatment of the radiation field. A simple proof of the correctness of the unseparated treatment of the field, within the framework of the Schwinger theory, is therefore still lacking. The purpose of this letter is to sketch such a proof.

Let a_λ, a_λ^* be absorption and emission operators for photons, so that

$$A_\mu(x)=\sum_{k,\lambda}(a_\lambda e^{ik\cdot x}+a_\lambda^* e^{-ik\cdot x})e_{\lambda\mu}g(k), \tag{1}$$

where e_λ is the polarization vector of the photon λ, and $g(k)$ is a certain function of k. Corresponding to a single momentum k, we may choose the e_λ, $\lambda=1, 2, 3, 4$, so that

$$e_\lambda\cdot e_\mu=\delta_{\lambda\mu}, \quad (e_3+ie_4)_\mu=f(k)k_\mu. \tag{2}$$

Then $\lambda=1, 2$ are transverse photons, $\lambda=3, 4$ longitudinal and scalar. This choice of e_λ, together with the reality condition for the A_μ, implies that a_λ^* is the Hermitian conjugate of a_λ for $\lambda=1, 2, 3$, and of $(-a_\lambda)$ for $\lambda=4$. The vacuum state Ψ_0 satisfies the conditions

$$a_1\Psi_0=a_2\Psi_0=0 \quad \text{(definition of vacuum)}, \tag{3}$$
$$(a_3+ia_4)\Psi_0=0 \quad \text{(supplementary condition)}. \tag{4}$$

Also the a_λ satisfy commutation relations

$$[a_\lambda, a_\mu]=[a_\lambda^*, a_\mu^*]=0, \quad [a_\lambda, a_\mu^*]=\delta_{\lambda\mu}. \tag{5}$$

From (2)–(5) one deduces the vacuum expectation values of products of two a_λ as follows. Let a function $\phi(k)$ be defined by

$$\langle a_3^* \; a_3\rangle_0=(e_3\cdot k)^2\phi(k).$$

Then by (2) and (4)

$$\langle a_3^* \; a_4\rangle_0=(e_3\cdot k)(e_4\cdot k)\phi(k)$$

and similarly

$$\begin{aligned}&\langle a_\lambda^* \quad a_\mu\rangle_0=\phi(k)(e_\lambda\cdot k)(e_\mu\cdot k), \quad \lambda,\mu=1,2,3,4,\\ &\langle a_\lambda \quad a_\mu^*\rangle_0=\delta_{\lambda\mu}+\phi(k)(e_\lambda\cdot k)(e_\mu\cdot k).\end{aligned} \tag{6}$$

These relations yield

$$\begin{aligned}&\langle A_\mu(x)A_\nu(x')+A_\nu(x')A_\mu(x)\rangle_0\\ &\qquad=\hbar c\delta_{\mu\nu}D^{(1)}(x-x')+(\partial^2/\partial x_\mu\partial x_\nu)\Phi(x-x'),\end{aligned} \tag{7}$$

where Φ is a function left undetermined by the conditions (2)–(5). Schwinger[6] gives as his prescription that we are to take $\Phi=0$ in (7). Within the Schwinger theory, this prescription is the only point at which the correctness of the treatment of longitudinal photons comes in question.

In consequence of the gauge-invariance of electrodynamics, and in accordance with the argument of Feynman cited above, (7) will always be used in the evaluation of matrix elements of operators of the form

$$\int K_{\mu\nu}(x, x')A_\mu(x)A_\nu(x')dxdx', \tag{8}$$

where $K_{\mu\nu}$ is a tensor satisfying the conservation laws

$$\partial K_{\mu\nu}/\partial x_\mu=0, \quad \partial K_{\mu\nu}/\partial x_\nu'=0. \tag{9}$$

The second term on the right of (7) contributes zero to all matrix elements of (8). Therefore all results of the theory are independent of Φ, and will be given correctly by taking $\Phi=0$ in (7). This fact justifies the unseparated treatment of the transverse and longitudinal fields.

[1] S. Tomonaga *et al.*, J. Phys. Soc. Japan **2**, 172, 199 (1947); Prog. Theor. Phys. **2**, 198 (1947). J. Schwinger, Phys. Rev. **74**, 1439 (1948); **75**, 651 (1949); **76**, 790 (1949).
[2] See the discussion leading to Eq. (3.40), J. Schwinger, Phys. Rev. **75**, 668 (1949).
[3] Ning Hu, Phys. Rev. **76**, 391 (1949).
[4] R. P. Feynman, Phys. Rev. **74**, 1430 (1948); **76**, 769 (1949).
[4a] R. P. Feynman, Phys. Rev. **76**, 780 (1949), Section 8.
[5] F. J. Dyson, Phys. Rev. **75**, 486 (1949).
[6] J. Schwinger, Phys. Rev. **75**, 668 (1949), Eqs. (3.40) and (3.41).

The Microwave Spectrum of Bromine Monofluoride*

D. F. Smith, M. Tidwell, and D. V. P. Williams
K-25 Research Laboratories, Carbide and Carbon Chemicals Corporation, Oak Ridge, Tennessee
December 21, 1949

SIX lines have been observed in the region 20.9 to 21.5 thousand megacycles per second when BrF_3 or BrF_5 was admitted to the absorption cell. These six lines become considerably more intense when F_2 and Br_2 are admitted to the cell at approximately equal pressures, and six additional weak lines become observable. The line frequencies and the Stark shifts can be readily interpreted as the $J=0\leftrightarrow1$ transition for BrF. The existence of this spectrum constitutes the first direct evidence for the chemically stable existence of this particular diatomic halide.[1] The earlier observations of the emission spectrum[2] in addition to verifying the physical stability of BrF, suggest that this compound should be chemically stable.

The line frequencies, with their assignments, are given in Table I. In Table II, the constants derived from the spectrum assuming a BrF model are presented. The large values of the nuclear quadrupole coupling constant and of the dipole moment to be expected

TABLE I. Observed transitions and frequencies $J=0\leftrightarrow 1$.

$v=0$	$Br^{79}F$	$Br^{81}F$
F 3/2–1/2	20,985.5 mc/sec.	20,928.4 mc/sec.
3/2–5/2	21,202.6	21,110.4
3/2–3/2	21,475.4	21,337.5
$v=1$		
F 3/2–1/2	20,828.9 mc/sec.	20,772.3 mc/sec.
3/2–5/2	21,045.6	20,954.6
3/2–3/2	21,319.4	21,181.7

TABLE II. Molecular constants of BrF.

	$Br^{79}F$	$Br^{81}F$
B_e	10,706.9$_8$ mc/sec.	10,655.7
I_e	$78.355(10)^{-40}$ g cm^2	$78.658(10)^{-40}$
α	156.3 mc/sec.	155.8 mc/sec.
r_e	$1.759(10)^{-8}$ cm	
μ	1.29 debye units	
eqQ	+1089.0 mc/sec.	+909.2

in this dihalide are to be noted. The most convincing evidence that this spectrum is due to BrF is obtained when the ratio of B_e values derived from the spectrum 0.995213, is compared with that computed from the mass measurements of the bromine isotopes[3] 0.995207.

While the fit of the triplets to the conventional quadrupole coupling expression, including second-order corrections, was not entirely satisfactory, the precision of the frequency measurements did not appear to justify the evaluation of the magnetic coupling factor, as was done for the dihalide FCl by Gilbert, Roberts, and Griswold.[4]

* This document is based on work performed under contract for the AEC by Carbide and Carbon Chemicals Corporation, at Oak Ridge, Tennessee.

[1] H. S. Booth and J. T. Pinkston, Chem. Rev. **41**, 421 (1947).
[2] VanPeter Heinz Broderson and Hans Joachim Schumacher, Zeits. f. Naturforschg. 2a, 358 (1947).
[3] K. Ogata, Phys. Rev. **75**, 200 (1949).
[4] Gilbert, Roberts, and Griswold, Phys. Rev. **76**, 1723 (1949).

Intensity Distribution of the Second Positive ($C^3\Pi\rightarrow B^3\Pi$) Band System of Molecular Nitrogen

R. W. NICHOLLS
Department of Physics, University of Western Ontario, London, Ontario, Canada
December 12, 1949

RECENT interest shown in the intensity distributions of the vibrational band-systems of molecular nitrogen radiated from auroral displays, and from the night sky[1] prompts this brief account of some calculations of the intensity distributions of the second positive band system, made in connection with an experimental investigation being undertaken here of the kinetics of excitation of the energy levels of molecular nitrogen in gaseous electrical discharge.

The integrated intensity of a molecular band may be written:

$$I(v',v'')=CN(v')E^4(v',v'')p(v',v''), \qquad (1)$$

where $N(v')$ is the population of molecules in the v' vibrational level of the upper electronic state concerned in the transition, $E(v',v'')$ is the energy radiated in the transition between v' and v'', v'' is the vibrational level in the lower electronic state upon which the transition ends, and

$$p(v',v'')=\left|\int_{-\infty}^{\infty}\psi(v')M\psi(v'')dx\right|^2,$$

where $\psi(v')$ and $\psi(v'')$ are the respective wave functions of the levels v' and v'', x is the internuclear separation, and M is the dipole moment of the molecule. p is a fractional transition probability as $\Sigma_{v''}p(v',v'')=1$ for each v'. C is a constant of proportionality.

Following a method suggested and used first by Pearse and Gaydon,[2] and later used by Miss Pillow,[3] we have calculated the values of $p(v',v'')$ by numerical integration of the wave-function product, for all the observed bands of the second positive system of nitrogen under the same conditions of simplifying approximation as are used in references 2 and 3. Briefly, these are (a) treating M as constant, and (b) linearly distorting the Hermite polynomial forms of $\psi(v')$ and $\psi(v'')$ expected for a harmonic oscillator, to fit the empirical, yet experimentally justified Morse curves for the $C^3\Pi$ and $B^3\Pi$ states of nitrogen.

These values of $p(v',v'')$ are shown in Table I. Table II shows

TABLE I. $p(v',v'')$.

v' \ v''	0	1	2	3	4	5	6	7	8	9	10
0	0.53	0.27	0.12	0.05	0.02	0.01					
1	0.43	0.04	0.21	0.12	0.08	0.07	0.05	0.00			
2	0.21	0.39	0.01	0.10	0.08	0.07	0.08	0.05	0.00$_3$		
3	0.01	0.37	0.26	0.02	0.03	0.06	0.07	0.10	0.08	0.00	
4	—	0.04	0.45	0.16	0.08	0.01	0.04	0.04	0.08	0.09	0.01

TABLE II. $p(v',v'')E^4(v',v'')$.

v' \ v''	0	1	2	3	4	5	6	7	8	9	10
0	100	40	14	4.8	1.3	0.39					
1	110	8.9	32	14	7.7	5.3	2.7	0.01			
2	67	99	1.6	17	11	7.2	6.2	2.9	0.15		
3	3.1	120	67	4.5	5.9	7.4	7.6	8.4	5.1	0.00$_3$	
4	—	15	150	43	17	1.0	5.6	4.6	6.8	6.0	0.64

the values of $E^4(v',v'')p(v',v'')$ adjusted to a value of 100 at the (0, 0) band. It will be evident from Eq. (1) that the values of Table II, when compared with measured intensities will yield information relating to the population $N(v')$ of the upper level concerned in the transition, and therefore to the probable major mechanism responsible for the excitation of the level.

Similar calculations are being made for the other molecular nitrogen band systems and for the NOβ- and γ-systems in connection with the experimental work referred to above. The possible geometry of a three-dimensional representation of the Tables I and II is also being worked upon.

While these calculations were being made an interesting paper by Bates[1] appeared, in which some similar work was reported. However, as data for far fewer bands of the second positive system were reported there, it is thought worth while to present the above calculations.

[1] *The Emission Spectra of The Night Sky and Aurorae* (The Physical Society, London, 1948); D. R. Bates, Proc. Roy. Soc. **A196**, 217 (1949).
[2] R. W. B. Pearse and A. G. Gaydon, Proc. Roy. Soc. **A173**, 37 (1939).
[3] M. E. Pillow, Proc. Phys. Soc. London **62**, 237 (1949).

New Types of Microwave Transitions Involving *l*-Type Doubling in OCS and HCN*

R. G. SHULMAN** AND C. H. TOWNES
Columbia Radiation Laboratory, Columbia University, New York, New York
December 12, 1949

MICROWAVE measurements of the vibration-rotation interaction called *l*-type doubling are available for a number of linear *XYZ* molecules.[1] Two new types of transitions involving this interaction have been observed which confirm the expected

TABLE I. Observed lines in HCN and values of l-type doubling constant q.

J	Frequency in mc	q=frequency/$J(J+1)$ mc
6	9,460±30	225.2±0.8
8	16,147.67±0.1	224.273±0.002
10	24,689.96±0.1	224.454±0.001
11	29,650±30	224.6±0.3
12	35,043.24±0.1	224.635±0.001

functional dependence of l-type doubling on the vibrational and rotational quantum numbers.

For the $J=1\rightarrow2$ transition of OCS, l-type doubling in the vibrational state $v_2=1$ produces a splitting of 25.34 mc. The corresponding doublets for the vibrational state $v_2=3$ have been found at 24,411±2 mc and 24,459±2 mc. Within experimental error, these show a separation just twice that of the $v_2=1$ state in accordance with the theory of Nielsen and Schaffer.[2]

A search of the HCN spectrum was made between 21,500 and 25,000 mc in an attempt to find the rotational spectrum of the dimer, $(HCN)_2$. Lines due to this dimer were expected under the conditions of search to have absorption coefficients several times greater than the minimum detectable value 5×10^{-9} cm^{-1}, but no lines due to $(HCN)_2$ were found. However, a line of intensity 3×10^{-8} cm^{-1} was found at 24,689.96 mc. The Stark components split from the above frequency according to the formula $\Delta\nu=AE^2M^2$, where E is the field strength and M the magnetic quantum number. This behavior and the number and relative intensities of Stark components showed clearly that the line corresponded to a $J=10$, $\Delta J=0$ transition. In order for the dimer $(HCN)_2$ to produce a line of the observed intensity it would have to be approximately 1 percent abundant at 10^{-2} mm Hg pressure. This appears impossible from previous measurements.[3] After checking carefully that the lines were not due to impurities, and after finding other similar lines with different values of J, the series of lines was identified as due to transitions directly between two l-type doublet states of the same J for HCN molecules in the first excited bending mode. The separation of such states should be $\nu=qJ(J+1)$, where q is the l-type doubling constant. Table I shows that frequencies of the five lines measured (some measured roughly with a wave meter, others accurately with a frequency standard) fit this formula very well. The values of q obtained from the accurately measured $J=8$, 10 and 12 lines of Table I show a systematic deviation proportional to J and of the order $q(B/\omega_2)$, which is to be expected in higher approximation. Extrapolating the values of q to $J=0$, one obtains $q=223.549$ mc.

TABLE II. Dipole moment of HCN in state $J=10$, $v_2=1$ from Stark displacement of $|M|=10$ component.

Displacement $\Delta\nu$ in mc	Square of field strength E^2(e.s.u./cm)^2	Dipole moment μ-debye units
54.48	411.93	2.943
60.4	455.31	2.949
61.65	454.07	2.980
		Average $\mu=2.957$

Stark effects for each of these lines show definitely the values of J listed in Table I and that $\Delta J=0$. The apparent lack of Stark displacement of the $M=0$ component is in agreement with expectations for the assigned transitions. A measurement of the molecular dipole moment was obtained for the state $v_2=1$, $J=10$, by measuring the Stark splitting $\Delta\nu$ of the $|M|=10$ component of the line at 24,689.96 mc. The results displayed in Table II give a dipole moment of 2.957±0.025 debye units. This is in good agreement with determinations by other methods[4] of the average dipole moment for gaseous HCN.

A further check on the identification of these HCN lines was obtained by comparison of intensities at 300°K and 195°K. Relative intensities agreed with the assumption that the lines were due to an excited molecule of energy $\omega_2=712$ cm^{-1} above the ground state.

The value $q=223.549$ mc is very different from the value 42 mc obtained from infra-red measurements.[5] However, it is supported by theoretical expectations. According to Nielsen,[6]

$$q=\frac{2B^2}{\omega_2}[1+4\sum_{S'}\xi_{SS'}{}^2\lambda_S/(\lambda_{S'}-\lambda_S)].$$

The term represented by a summation is somewhat difficult to evaluate. However, in the half-dozen other molecules for which l-type doubling has been measured, the first term $2B^2/\omega_2$ is less than the observed value of q by about 30 percent. For HCN, $2B^2/\omega_2=184.1$ mc, which is less than the measured value by a similar amount.

* Work sponsored jointly by the Signal Corps and ONR.
** Present address: Chemistry Department, California Institute of Technology.
[1] Townes, Holden, and Merritt, Phys. Rev. 74, 1113 (1948).
[2] H. H. Nielsen and W. H. Shaffer, J. Chem. Phys. 11, 140 (1943).
[3] R. A. Ruehrwein and W. F. Giauque, J. Am. Chem. Soc. 61, 2940 (1939).
[4] L. G. Wesson, "Tables of electric dipole moments," MIT Laboratory for Insulation Research.
[5] G. Herzberg, Rev. Mod. Phys. 14, 219 (1942).
[6] H. H. Nielsen, Phys. Rev. 75, 1961 (1949).

PHYSICAL REVIEW VOLUME 77, NUMBER 3 FEBRUARY 1, 1950

Proceedings of the American Physical Society

MINUTES OF THE MEETING OF THE NEW ENGLAND SECTION AT WILLIAMS COLLEGE, WILLIAMSTOWN, MASSACHUSETTS, OCTOBER 22, 1949

THE thirty-third meeting of the New England Section of the American Physical Society was held at the Thompson Physical Laboratory, Williams College, Williamstown, Massachusetts on Saturday, October 22, 1949. Approximately one hundred members of this section were in attendance. The program included three invited papers, which formed a symposium on magnetism, and nine con-

tributed papers relating to research. The abstract of the paper relating to the teaching of physics will appear in the American Journal of Physics.

At the business meeting the following officers were elected for 1950:

Chairman: R. D. EVANS, M.I.T.
Vice Chairman: T. SOLLER, Amherst College.
Secretary-Treasurer: A. G. HILL, M.I.T.
Members of the Executive Committee: N. C. LITTLE, Bowdoin College and J. C. STREET, Harvard College.

A. G. HILL, *Secretary-Treasurer*
M. I. T.
Cambridge, Massachusetts

Symposium on Magnetism

Recent Advances in Ferromagnetism. R. M. BOZORTH, *Bell Telephone Laboratories.*
The Literature of Ferromagnetism. L. W. MCKEEHAN, *Yale University.*
Magnetic Susceptibility of Metals and Alloys. A. R. KAUFMANN, *M.I.T.*

Contributed Papers

A Neoclassical Approach to Blackbody Radiation. B. LIEBOWITZ, *New York City.*—We ascribe to the linear electronic oscillators of a blackbody the classical properties: (a) The continuum of all energy levels from 0 to ∞ is accessible to each oscillator; (b) the populations of the levels are determined by the Boltzmann factor; (c) when an oscillator radiates it does so according to the classical formula $d\epsilon/dt = 8\pi^2\gamma^2e^2\epsilon/3mc^3$. We depart from classical theory by assuming that no oscillator radiates unless its energy ϵ exceeds a threshold value ϵ_0. These assumptions with Wien's displacement law lead to the radiation formula: $\psi_\lambda = [32\pi^2e^2h^2\gamma/3m\lambda^5][(1+\lambda KT/hc)\exp(-hc/\lambda KT)]$. γ is an adjustable constant. h may be at least approximately equated to Planck's h. The energy-frequency relation $\epsilon_0 = h\nu$ refers to the *threshold* energy. Adjusting γ to fit Planck's formula near the peak, we get $\gamma hc = (10r_0)^{-1}$, where r_0 = electronic radius. The experimental data do not seem sufficiently accurate to rule out formula. A specific heat formula similarly derived vanishes at $T = 0°$K and approaches n_0k at $T = \infty$, but reaches a maximum about 10 percent above n_0k at $T = \epsilon_0/k$.

Absorption Bands in the Ultraviolet Continua of Associated Primary and Secondary Alcohols.* GLADYS A. ANSLOW AND HSI-TEH HSIEH, *Smith College.*—Absorption spectra of alcohols of various types have been obtained with a Lyman vacuum grating spectrograph, using thin cells formed between the windows of the spectrograph and hydrogen lamp, following a method initiated by Scheibe and recently employed by Platt and Klevens.[1] Propyl, butyl, amyl, hexyl, heptyl, and octyl alcohols were studied as pure liquids or as dilutions with 2–4 dimethyl pentane or isooctane. Spectrograms of the 2600–1800A region were analyzed with a photoelectric densitometer. Continuous bands appear at wave numbers which suggest their origin as the dissociation following electronic excitation of hydrogen-bridged hydroxyl groups.[2] Most prominent in the spectra of normal alcohols is strong absorption which appears to be characteristic of linear polymers. Isomeric forms, in which association is limited by steric hindrance, exhibit the strongest bands at wave numbers which agree with predictions for dimer dissociation bands.[2] Weaker bands with onsets near 51,000 cm^{-1} may result from the dissociation of unassociated hydroxyls.

* Supported by the ONR.
[1] J. R. Platt *et al.*, J. Chem. Phys. 11, 535 (1943).
[2] Anslow, Hsieh, and Shea, J. Chem. Phys. 17, 426 (1949).

Chemical Thermodynamics in Jacobian Form. F. H. CRAWFORD, *Williams College.*—The author has developed a method[1] of obtaining the general relations of thermodynamics (involving first partial derivatives) in terms of ratios of readily computable Jacobians. The method is general, permits ready change of independent variables and gives the desired derivatives directly in terms of a standard set of derivatives. When applied to chemical systems of variable composition and total mass the advantages over conventional methods become apparent. Relations given in comprehensive tables such as those of Goranson[2] can be deduced directly with a common starting point and a few explicit definitions as the only intermediate relations. To be specific, in the case of a two-component chemical system the starting point is Gibbs' expression for du, *viz.*, $dU = Tds - pdV + \mu_1dm_1 + \mu_2dm_2$ where U is the internal energy and the μ's and m's refer to specific Gibbs potentials and masses, respectively. It will be shown that a simple symmetrical fourth-order Jacobian which can be written down directly, contains not only all the derivatives in the standard set, but expresses by its symmetry the six reciprocal relations of Maxwell appropriate to the set of independent variables chosen for the system.

[1] F. H. Crawford, Am. J. Phys. 17, 1 (1949). Phys. Rev. 76, 456A (1949). Proc. Am. Acad. Arts Sci. (in press).
[2] R. W. Goranson, "Thermodynamic relations in multi-component systems," Carnegie Institution, Pub. No. 408, Washington, D. C. (1930).

Utilization of a Cathode-Ray Tube and Photo-Cell to Synthesize Integral D.C. Voltages from a Sequence of Pulses. H. P. STABLER, *Williams College.*—Feedback from a photomultiplier tube to the vertical deflection plates of a cathode-ray tube can cause the fluorescent electron beam spot to rise until it rests, partially obscured, against the edge of an opaque template.[1] If the template consists of a series of equally spaced horizontal line segments, the beam spot can remain in equilibrium at the lower edge of any line, provided that each line is broader than the spot diameter. The ends of the lines are alternately staggered right and left. Alternate right and left pulses applied to the horizontal deflection plates enable the spot to climb the ladder structure in step increments. Since the potential appearing on the vertical plates corresponds to the total number of pulses received, the device acts as a counter. A vertical line on the template serves as a recycle path and provides a carry-over pulse. The degree of resolution and speed feasible with a P5 phosphor is being investigated. With a simple two-channel input circuit and a somewhat more

complicated line pattern, stepwise potential changes can be made in either sense. This corresponds to a reversible counter. Possible servo applications are suggested.

[1] A continuous d.c. function generator employing this method was reported by McCann, Wilts, and Locanthi, Proc. I.R.E. 37, 960 (August, 1949).

Packing Fractions of W^{183} and W^{186}.* RICHARD F. WOODCOCK, HENRY E. DUCKWORTH, RICHARD S. PRESTON, AND HOWARD A. JOHNSON, *Scott Laboratory, Wesleyan University.*—The Wesleyan double-focusing mass spectrograph, which is a Dempster-type, has been used to measure the packing fraction differences ($W^{183}-Ni^{61}$) and ($W^{186}-Ni^{62}$). Triply-charged tungsten ions and singly-charged nickel ions, produced in a high frequency spark, formed the appropriate doublets at mass numbers 61 and 62. Since the magnetic field of the instrument is very constant with time, it has been possible to photograph the tungsten and nickel lines consecutively. In this way, by use of an arrangement for changing electrodes, the intensities of the doublet lines were matched by running the spark between different pairs of electrodes for different times. The packing fraction difference ($W^{183}-Ni^{61}$) was measured from seven fair doublets to be $(9.11\pm0.15)\times10^{-4}$. The packing fraction difference ($W^{186}-Ni^{62}$) was measured from eight good doublets to be $(9.15\pm0.10)\times10^{-4}$. These results, combined with Shaw's[1] recent measurement of the packing fractions of the nickel isotopes, give for W^{183} $f=(+0.36\pm0.23)\times10^{-4}$, and for W^{186} $f=(+0.14\pm0.15)\times10^{-4}$. The mass scale for the measurement was provided in the first case by the separation $W^{183}-W^{182}$, and, in the second, by the separation $W^{186}-W^{184}$. In both cases these separations were assumed to be integral. Typical spectra will be shown.

* This work has been done under contract with AEC.
[1] A. E. Shaw, "A new measurement of the packing fractions of the nickel isotopes," Phys. Rev. 75, 1011 (1949).

Packing Fraction of Pt^{198}.* HOWARD A. JOHNSON, HENRY E. DUCKWORTH, RICHARD S. PRESTON, AND RICHARD F. WOODCOCK, *Scott Laboratory, Wesleyan University.*—The scheme outlined in the previous abstract, of photographing the doublet lines consecutively in order to adjust intensities, has been used to obtain $Pt^{198}-Zn^{66}$ doublets at mass number 66. Measurement of 18 selected doublets, using the separation $Pt^{198}-Pt^{196}$ as mass scale, gave the packing fraction difference $Pt^{198}-Zn^{66}$ as $(9.61\pm0.06)\times10^{-4}$. Dempster[1] has recently given the packing fraction of Zn^{64} as -7.68×10^{-4} and Zn^{68} as -7.64×10^{-4}. If one assumes that the packing fraction of Zn^{66} is the mean of these two, the calculated value of Pt^{198} is $+1.95$. The brass which was used as a source of zinc ions also served as a source of copper ions, creating a second doublet at mass number 65. Measurement of 12 good doublets, using $Pt^{195}-Pt^{194}$ as the mass scale, gave the packing fraction difference $Pt^{195}-Cu^{65}$ as $(9.57\pm0.04)\times10^{-4}$.

* This work has been done under contract with AEC.
[1] A. J. Dempster, Phys. Rev. 74, 1225 (1948).

The Equivalent Circuit of Partially Plated Thickness-Shear Piezoelectric Resonators.* KARL S. VAN DYKE, EDWARD A. PENDLETON AND GARY D. GORDON, *Wesleyan University.*—The amplitude distribution in the fundamental mode of thickness-shear vibration of square BT-cut quartz plates is studied through measurements of the impedance of partially plated resonators. The piezoelectric coupling is changed by using different electrode arrangements which however have only secondary effects on the mechanical mode. A theoretical analysis based upon an assumed sinoidal distribution of amplitude along both principal directions of the square and zero strain at all four edges predicts to within a few percent the parameters of the equivalent circuit from the known piezoelectric constants of quartz. The use of thickness-shear plate resonators thus becomes feasible for measurement of the piezoelectric constants of new crystals. Important elements in the measuring technique are the plating and short-circuiting of those portions of the faces of the plate which are not occupied by driving electrodes and the dimensioning of the plate to be free from spurious coupled modes. Surface exploration had indicated a distribution such as is now proven although theoretical treatments of boundary conditions to date have permitted the full half-wave sine distribution along only one direction.

* The work here reported has been done as part of the research under contract between Wesleyan University and the Signal Corps.

A D.C. Magnetic Generator. A. E. BENFIELD, *Cruft Laboratory, Harvard University.*—It is well known that an alternating electrical voltage appears in a closed circuit if a magnet is passed repeatedly through it, and that no direct voltage is thereby generated. A direct voltage, however, may also be generated in such a circuit provided that part of the circuit is rigidly attached to the magnet, and rotates with the magnet as it links the circuit. In this case there is no relative motion between the magnetic field and the rotating part of the circuit, which acts, therefore, as a gap for the action of the magnetic field. If electrical contact is maintained between the moving and stationary parts of the circuit, direct current flows. Devices of this sort have been made and studied, and the values of the direct current, as measured with a galvanometer, agreed with the predictions of theory. Although, with the configuration used, the direct current was small, it is thought that the principle involved may be usefully employed in a tachometer.[1]

[1] A. E. Benfield, Rev. Sci. Inst. 20, 663 (1949).

A New Theory of Electricity. BAYARD P. PEAKES, *Northeastern University.*—In studying all the facts concerning the discovery and development of the electron, one might well develop an intelligent theory for the electric current without the use of electrons. History shows us that the electrons were practically on the road to being developed since the founding of the atomic theory and similar lines of thought. But to get electrons there must be a certain amount of residual air in the tube; under ordinary conditions, you can't get a discharge unless there is a conducting medium present. Thus, we may deduce the fact that electrons must be due to a condition imposed upon the air in the tube. The cathode rays resemble light, and this leads one to search for kinetic energy as being the true nature of electricity. After doing much research through text books, one can find this definition for electricity: it is a supersonic motiviation, of necessity a wave disturbance; and it is created and persists only where there is a contact, or potential difference, between two points in its line of propagation.